

AD/A-000 941

SOLAR COLLECTOR THERMAL POWER SYSTEM.
VOLUME II. DEVELOPMENT, FABRICATION,
AND TESTING OF FIFTEEN FOOT HEAT PIPES

Robert Richter

Xerox Corporation/Electro-Optical Systems

Prepared for:

Air Force Aero Propulsion Laboratory

November 1974

DISTRIBUTED BY:

NTIS

National Technical Information Service
U. S. DEPARTMENT OF COMMERCE

UNCLASSIFIED

SECURITY CLASSIFICATION OF THIS PAGE (When Data Entered)

REPORT DOCUMENTATION PAGE		READ INSTRUCTIONS BEFORE COMPLETING FORM
1. REPORT NUMBER AFAPL-TR-74-89-2	2. GOVT ACCESSION NO.	3. RECIPIENT'S CATALOG NUMBER AD/A-000 241
4. TITLE (and Subtitle) SOLAR COLLECTOR THERMAL POWER SYSTEM Volume II - Development, Fabrication, and Testing of Fifteen Foot Heat Pipes		5. TYPE OF REPORT & PERIOD COVERED Final 16 Aug 1971 to 28 Jun 1974
		6. PERFORMING ORG. REPORT NUMBER 4074-Final
7. AUTHOR(s) Robert Richter Xerox Corporation Electro-Optical Systems		8. CONTRACT OR GRANT NUMBER(s) F33615-72-C-1092
9. PERFORMING ORGANIZATION NAME AND ADDRESS Xerox Corporation/Electro-Optical Systems 300 North Halstead Street Pasadena, California 91107		10. PROGRAM ELEMENT, PROJECT, TASK AREA & WORK UNIT NUMBERS PE62203F Project 3145 Task 314519 Work Unit 31451940
11. CONTROLLING OFFICE NAME AND ADDRESS Air Force Aero Propulsion Laboratory/POE Wright-Patterson Air Force Base, Ohio 45433		12. REPORT DATE November 1974
		13. NUMBER OF PAGES 199
14. MONITORING AGENCY NAME & ADDRESS (if different from Controlling Office) Air Force Aero Propulsion Laboratory Wright-Patterson Air Force Base, Ohio 45433		15. SECURITY CLASS. (of this report) Unclassified
		15a. DECLASSIFICATION/DOWNGRADING SCHEDULE
16. DISTRIBUTION STATEMENT (of this Report) Approved for public release; distribution unlimited		
17. DISTRIBUTION STATEMENT (of the abstract entered in Block 20, if different from Report)		
18. SUPPLEMENTARY NOTES NATIONAL TECHNICAL INFORMATION SERVICE D D C NOV 29 1974 D		
19. KEY WORDS (Continue on reverse side if necessary and identify by block number) Thermal Space Power Heat Pipe Energy Transport Space Power System Study		
20. ABSTRACT (Continue on reverse side if necessary and identify by block number) The final Technical Report presents the work performed on the Solar Collector Thermal Power System (SCTPS) Program from 16 August 1971 to 28 June 1974. The report covers Phase I (Preliminary Technology and System Design Analysis) and Phase II (Experimental Evaluation of Component Performance) and is issued in three volumes. Volume I contains the system analysis for a solar collector thermal power system supplying thermal energy to a Vuilleumier cooler that is carried on a BMS type satellite. The analysis also investigates specific		

DD FORM 1 JAN 73 1473

EDITION OF 1 NOV 65 IS OBSOLETE

UNCLASSIFIED

SECURITY CLASSIFICATION OF THIS PAGE (When Data Entered)

UNCLASSIFIED

SECURITY CLASSIFICATION OF THIS PAGE(When Data Entered)

requirements of individual components of the power system, including the solar collector, heat pipes, and the thermal energy storage system. An extensive bibliography of pertinent heat transfer, solar collectors, and space power system reports is a part of this volume. Volume II presents the technical effort in the development of a 15-foot long primary heat pipe capable of transferring 6 kW of thermal power and its integration with the remaining components of a complete thermal train. The effort comprised the design, fabrication, and testing of the heat pipe as an individual component and the integration and testing with the secondary heat pipe, the thermal energy storage unit, and a radiation heat transfer joint. In Volume III, the basic studies and the experimental evaluation of thermal train components are collected. This includes the tests of subscale thermal energy storage capsules, the design, fabrication, and testing of the secondary heat pipe with its full scale thermal energy storage unit; the design, fabrication, and testing of subscale heat pipes for the evaluation of material compatibility; the design, fabrication, and testing of a subscale heat pipe with a cavity receiver; and a heat pipe wick study performed in support of the design of a second primary heat pipe and the subscale cavity heat pipe.

UNCLASSIFIED

SECURITY CLASSIFICATION OF THIS PAGE(When Data Entered)

FOREWORD

Volume II of this report, "Design and Experimental Evaluation of a 15 foot Primary Heat Pipe and Its Mating with Components of a Thermal Train," presents the effort of a number of individual contributors who are members of the staff of the Xerox Corporation, TRW Systems Group, and the General Electric Company. The entire effort was under the direction of R. Richter of the Xerox Corporation, a prime contractor to the U. S. Air Force Aeronautical Propulsion Laboratory. Subsections 2.1 through 2.5, except for minor modifications, were the contributions of G. L. Fleischman and R. D. Marcus of TRW. The information for Subsections 2.6 through 3.4 was provided by R. L. Hammel of TRW, while the data of Subsections 3.5 and 3.6 was provided by J. A. Vogrin of TRW. Subsections 3.7 through 3.10 and Sections IV, V and Appendix A are the technical contributions of the author.

The author acknowledges with thanks the support of the above-mentioned contributors for working as a team toward the success of the overall program.

CONTENTS

I.	INTRODUCTION	1
II.	PRELIMINARY THERMAL TRAIN STUDY	3
2.1	Introduction	3
2.2	Wicks	4
2.2.1	Conventional Bolting Cloth Solution	5
2.2.2	Arteries (Class B Wick)	7
2.2.3	Open Arteries	7
2.2.4	Temperature Drops	9
2.2.5	Primary Evaporator	9
2.2.6	Primary Condenser	10
2.2.7	Secondary Evaporator	13
2.2.8	Secondary Condenser	13
2.3	Stress Considerations	14
2.4	Start-Up From the Frozen State	16
2.5	Variable Conductance	21
2.5.1	Flat Front Analysis	22
2.5.2	TRW Gas Pipe Program	22
2.6	Preliminary Design	24
2.6.1	Materials	24
2.6.2	Primary Heat Pipe	26
2.6.3	Secondary Heat Pipe	28
2.6.4	Variable Conductance Heat Pipe (VCHP)	29
III.	DESIGN, MANUFACTURING, AND TESTING OF FIRST FIFTEEN FOOT PRIMARY HEAT PIPE	31
3.1	Introduction	31
3.2	Design Analysis	31
3.2.1	Hydrodynamic Design	31
3.2.2	Insulation Design	34
3.3	Mechanical Design	34
3.3.1	Wick Forming and Manufacture	38
3.3.2	Offset	39
3.3.3	Wick Installation and Support	39
3.4	Hardware Build-Up	41
3.5	Initial Performance Testing	49
3.5.1	Test Setup	51
3.5.2	Heat Pipe	51
3.5.3	Test Instrumentation, Readout Equipment, and Test Support Hardware	51
3.6	Water Calorimeter	55
3.6.1	Test Results	60
3.6.2	Conclusions	76
3.7	Evaluation of Initial Test Results	78
3.8	Performance Testing of First Primary Heat Pipe	80
3.8.1	Test Setup	80
3.8.2	Testing	86

CONTENTS (Contd)

3.9	Failure Analysis for First Primary Heat Pipe	98
3.9.1	Metallurgical Analysis	98
3.9.2	Stress Analysis	100
3.10	Conclusions	108
IV.	DESIGN, MANUFACTURING, AND TESTING OF SECOND PRIMARY HEAT PIPE	109
4.1	Introduction	109
4.2	Second Primary Heat Pipe Design	109
4.3	Working Fluid Fill Charge	125
4.4	Fabrication of the Second Primary Heat Pipe	138
4.5	Instrumentation, Heater Installation, Insulation and Charging with Sodium	139
4.6	Testing	151
4.6.1	Testing Without Power Transfer	151
4.6.2	Testing with Power Transfer at the Condenser	157
V.	THERMAL TRAIN	169
5.1	Introduction	169
5.2	Integration	169
5.3	Test	173
5.4	Testing	173
5.5	Conclusion	183
APPENDIX A	- FLUID FLOW IN HEMISPHERICAL RECEIVER	185
REFERENCES		189

ILLUSTRATIONS

1	Maximum Heat Pipe Performance	6
2	Maximum Heat Pipe Performance	6
3	Maximum Heat Pipe Performance	6
4	Primary Heat Pipe Performance	8
5	Primary Heat Pipe Performance	8
6	Analytical Model for Hemispherical Evaporator Flow	10
7	Wick Study for Primary Heat Pipe	11
8	Primary Heat Pipe Condenser	12
9	Secondary Heat Pipe Condenser	15
10	Heat Pipe Limits for Primary Heat Pipe Operating with Sodium as Working Fluid and Inconel Walls and Wicks	20
11	Variable Conductance Heat Pipe Performance	23
12	Thermal Power Subsystem	25
13	Performance Limits for 2.5-inch Heat Pipe	33
14	Performance Limits for 2.25-inch Heat Pipe	33
15	Internal Gas Reservoir Length versus Temperature Difference for Primary Heat Pipe Startup	35
16	Primary Heat Pipe Heat Losses and Surface Temperatures	36
17	Primary Heat Pipe	37
18	Demonstration Diametral Wick	40
19	Demonstration Elbow Sections	40
20	Demonstration Section Installed Wick	40
21	Fifteen Foot Heat Pipe Parts	43
22	Fifteen Foot Thermal Train Heat Pipe - View Toward Condenser	45
23	Fifteen Foot Thermal Train Heat Pipe - View Toward Evaporator	45
24	Fifteen Foot Primary Heat Pipe - Condenser End with TES Flange	46
25	Primary Heat Pipe Following Addition of Heaters and Insulation Forward of TES Flange	46
26	Primary Pipe with Temporary Processing Heaters on Condenser	47
27	Primary Pipe with Axial Insulation Completed	47
28	Sodium Fill System with Primary Pipe Attached	48
29	Primary Heat Pipe Evaporator Flux versus Heat Transfer Capacity	50
30	Heat Pipe Test Installation and Instrumentation	52
31	Location of Primary Heat Pipe Thermocouples and Heaters	53
32	Radiation Heat Sink for Primary Heat Pipe Testing	56
33	Condenser End of Heat Pipe with Thermocouples Installed	58
34	Condenser End of Heat Pipe with a Typical Calorimeter Radiation Shield in Place	58
35	Calorimeter Installed on Condenser End of Heat Pipe	59
36	View of Completely Insulated Calorimeter and Heat Pipe	59
37	Evaporator End of Heat Pipe with Thermocouples Installed and Heaters Partially Installed	61
38	Evaporator End of Heat Pipe with Heaters Installed	61
39	Test Support Equipment	62

ILLUSTRATIONS (Contd)

40	Test #1 (1-11-73) - Transient Startup without Inert Gas and Supplemental Heaters	65
41	Test #2 (1-12-73) - Transient Startup with Supplemental Heaters and without Inert Gas	66
42	Test #3 (2-16-73) - Transient Startup without Supplemental Heaters and Inert Gas	67
43	Test #4 (2-21-73) - Transient Startup with Inert Gas and without Supplemental Heaters	68
44	Test #5 (2-21-73) - Transient Startup with Inert Gas and without Supplemental Heaters	69
45	Test #6 (2-23-73) - Transient Startup with Inert Gas and without Supplemental Heaters	70
46	Test #7 (2-26-73) - Transient Startup with Inert Gas and without Supplemental Heaters	71
47	Test #8 (2-27-73) - Transient Startup with Inert Gas and without Supplemental Heaters	72
48	Test #9 (3-6-73) - Transient Startup with Inert Gas and without Supplemental Heaters	73
49	Test #10 (3-7-73) - Transient Startup with Inert Gas and without Supplemental Heaters	74
50	Test #11 (3-8-73) - Transient Startup with Inert Gas and without Supplemental Heaters	75
51	Heat Pipe Insulation Heat Loss	77
52	Wick Structure of First Primary Heat Pipe	81
53	Available Flow Factor $\Delta p \times K$ as a Function of the Packing Factor	82
54	Permeability and Pressure Drop in the Wick as Function of Packing Factor	83
55	Insulation Requirement for Primary Heat Pipe with and without Secondary Heaters	85
56	Thermocouple Arrangement for Testing of First Primary Heat Pipe at EOS	87
57	Heater and Insulation Arrangement for Testing of First Primary Heat Pipe at EOS	88
58	Primary Heat Pipe with Primary and Secondary Heaters Installed	89
59	Primary Heat Pipe with Secondary Heater Elements and Intermittent Insulation (Flex Min-K)	89
60	Primary Heat Pipe with Four Layers of Flex Min-K Insulation Over One Segment of the Heat Pipe	90
61	Primary Heat Pipe with Completed Four Layers Flex Min-K Insulation	90
62	Primary Heat Pipe with Four Layers Cera-Felt Insulation Over Flex Min-K Insulation	91
63	Primary Heat Pipe Shown with One Segment Fully Insulated (four layers Flex Min-K, four layers Cera-Felt and foil)	91

ILLUSTRATIONS (Contd)

64	Primary Heat Pipe Fully Insulated	92
65	Complete Test Setup of Primary Heat Pipe	92
66	Steady-State Temperatures Along First Primary Heat Pipe Under Various Power Inputs (Increasing Power)	93
67	Steady-State Temperatures Along First Primary Heat Pipe Under Various Power Conditions (Decreasing Power)	94
68	Correlation Between Input Power and Operating Temperature for First Primary Heat Pipe	95
69	Active Heat Pipe Length as Function of Power Input	95
70	Required Input Power as Function of Loss Integral	95
71	Temperature History of the First Primary Heat Pipe During Startup with a Power Input of 5.97 kW at the Evaporator	97
72	Temperature Distribution Along the First Primary Heat Pipe During Startup with a Power Input of 3.325 kW at the Evaporator	99
73	Primary Heat Pipe Appearance after Failure	101
74	Cracks in the Evaporator Section of the Primary Heat Pipe as Indicated by the Zyglo Process	102
75	Branched, Intergranular Cracking - 100X Unetched - Inconel Alloy 600	103
76	Effect of Temperature Gradients on the Pipe	104
77	Allowable Temperature Differences Along the Heat Pipe	106
78	Creep Stress of Inconel 600	107
79	Characteristics of Inconel 600 and Inconel 617	110
80	Permeability K for Standard Bolting Cloth	112
81	Pressure Drop Across a Wick Structure	113
82	Heat Pipe Design Dimensions	115
83	Safety Factor for a 2.25-inch Diameter 0.062-inch Wall Thickness Sodium Heat Pipe Operating with a Power Transfer of 6.3 kW	120
84	Safety Factor for a 2.25-inch Diameter 0.062-inch Wall Thickness Sodium Heat Pipe Operating with a Power Transfer of 6.3 kW	124
85	Permeability and Wick Characteristic of Bolting Cloth	126
86	Vapor Pressure Drop as a Function of Flow Area	127
87	Wick Design for Primary Heat Pipe	128
88	Construction Design of Diametral Wick	140
89	Wick Construction for Second Primary Heat Pipe	141
90	Diametral Wick in Section of Heat Pipe	142
91	Primary Heat Pipe with End Cap	143
92	Thermocouple Arrangement for Testing of Second Primary Heat Pipe	144
93	Heater Configuration for Primary Heat Pipes	145

ILLUSTRATIONS (Contd)

94	Primary Heat Pipe Fully Instrumented and Heaters in Place	147
95	Primary Heat Pipe Fully Instrumented and Heaters in Place	147
96	Primary Heater of Primary Heat Pipe	148
97	Insulation of Primary Heat Pipe	148
98	Second Primary Heat Pipe	149
99	Temperature Distribution Along the Primary Heat Pipe During Processing	150
100	Steady-State Temperature Distribution Along Second Primary Heat Pipe	152
101	Temperatures Along the 15-ft Heat Pipe as Function of Power Input at the Evaporator	154
102	Operating Length of Primary Heat Pipe	155
103	Temperature and Power Loss Correlation for the Two Primary Heat Pipes	156
104	Power Transfer at Condenser of Primary Heat Pipe for Varying Insulation Thickness	159
105	Tubular Heat Exchanger at Condenser Section of Second Primary Heat Pipe	161
106	Power Transfer by Radiation from Condenser Section of Primary Heat Pipe to Heat Exchanger	161
107	Temperature Distribution Along 15-Ft Long Heat Pipe for Various Power Inputs into Secondary Primary Heat Pipe with Condenser 1-1/2-inch below Evaporator Elevation	162
108	Temperature Distribution Along Primary Heat Pipe	165
109	Temperature Distribution Along Primary Heat Pipe	167
110	Secondary Heat Pipe with Thermal Energy Storage Unit	170
111	Fully Assembled Full-Scale Thermal Train of the Solar Collector Thermal Power System	171
112	Close-up View of Rotary Radiation Heat Transfer Joint and the Secondary Heat Pipe as Assembled in the Full-Scale Thermal Train of the Solar Collector Thermal Power System	172
113	Thermocouple Arrangement for Testing of Full Scale Solar Collector Thermal Power System Thermal Train	174
114	Power Losses of the Thermal Train	175
115	Temperature History of Full Scale Thermal Train	177
116	Temperature Distribution in the Thermal Train (4204 Watt Input)	178
117	Temperature Distribution in the Thermal Train (5059 Watt Input)	179
118	Temperature Distribution in the Thermal Train (6053 Watt Input)	180
119	Correlation Between Maximum Possible Radiation Power Transfer and Heater Power at the Primary Heat Pipe Evaporator	182
120	Temperature Distribution in the Thermal Train (6053 Watt Input and 2700 Watt Output)	184
121	Geometric Relations	185

TABLES

I.	Maximum Combined Stresses at 1600°F in the 4-Inch Diameter Receiver with Hemispherical End Caps	17
II.	Maximum Combined Stresses at 1600°F in Emitter Body with Hemispherical End Caps	17
III.	First Primary Heat Pipe - Comparison of Design Parameters	32
IV.	Fifteen-Foot Heat Pipe - Bill of Materials	42
V.	Radiation Heat Sink Design for Primary Heat Pipe Testing	57
VI.	Start-Up Test Summary	63
VII.	Heat Pipe Axial Transport Capability Test	64
VIII.	Parametric Study of a 2.25-Inch Diameter Heat Pipe	117
IX.	Parametric Study of a 2.25-Inch Diameter Heat Pipe	121
X.	Parametric Study for 2.5-Inch Heat Pipe Operating with Sodium	129
XI.	Parametric Study of a 2.75-Inch Heat Pipe	132
XII.	Parametric Study of a 3-Inch Diameter Heat Pipe	135
XIII.	Heat Pipe Characteristics	157
XIV.	Temperature History of Primary Heat Pipe	158
XV.	Power Losses From Primary Heat Pipe	160

SECTION I

INTRODUCTION

In Volume I of this report, the Preliminary Technology Systems Study of a solar collector thermal power system was presented. In this volume which is the second of three, the design, fabrication, and testing of a 15-foot heat pipe and its integration with the remaining components of a thermal power train are presented.

Since prior to this program no heat pipe operating anywhere close to the desired operating conditions needed for the primary heat pipe of a solar collector thermal power system had been designed, built, or tested, the entire task was initiated with a study which is presented in Section II of this volume. Following the Study the first primary heat pipe was designed using existing technological background. The design of the heat pipe differed to some degree from that which evolved from the study because allowance was made for its fabrication and testing. For proving the power carrying capacity of a 15-foot long heat pipe, it was not felt necessary to test a configuration that had two bends in its length. A straight heat pipe would also have the advantage of being easily placed into a slightly larger pipe if it should have become desirable to perform testing in a vacuum.

During the testing of the first primary heat pipe, it became quite obvious that the design of large power carrying heat pipes was not as far advanced as had been assumed at the outset of the program. After the failure of the first primary heat pipe, analytical studies confirmed that some shorter heat pipes can easily be designed and built without great stress on details while still operating with a large margin of safety. A 15-foot long heat pipe, which has to have a power transfer capacity of over 6 kW, had, however, to be designed using every nuance for optimizing performance to assure achieving the design goal. For the design of the second primary heat pipe a wick study had to be conducted which is described in Volume III of this report.

The second primary heat pipe was built and operated at the design goal. But many data were taken which would be worthwhile to have been analyzed and evaluated in separate tests for a better understanding of heat pipe design and operation. Because of the cost of a full scale 15-foot heat pipe, the reluctance of testing the heat pipe over a wide range of operating conditions and subjecting the heat pipe to severe starting conditions was great. The second primary heat pipe had to be integrated with the secondary heat pipe, which is fully described in Section VII of the third volume of this report, for operating the entire thermal train as a final confirmation of the concept of the solar collector thermal power system.

SECTION II

PRELIMINARY THERMAL TRAIN STUDY

2.1 INTRODUCTION

An initial analytical design study of a solar collector thermal power system thermal train was performed to evaluate in general the use of heat pipes in the thermal train. The particular systems studied were those depicted in Volume 1, Figure 18.

A specific objective of this study was to produce a preliminary design for the heat pipes of the thermal train which could meet the specified requirements. In accomplishing this, particular attention was given to the following features, limits and constraints:

- The entire thermal train must be capable of operating in a 1-g environment when horizontally deployed. This requires that wicks and/or arteries in the system be able to prime and operate against the hydrostatic heads equivalent to the least elevation differential in the system. This constraint, necessary for earthbound testing, has major impact on the wick designs for the various heat pipe elements.
- Consistent with the 1-g operating requirement, various wick structures were examined for feasibility and optimum performance. These included homogeneous wicks, closed arteries, and open arteries.
- The wicks must be configured within the various heat pipe elements for minimum temperature drops at their respective evaporators and condensers.
- The system must be designed for starting without failure from a state in which the heat pipes are cold and the working fluid is frozen.
- A variable conductance heat pipe might be necessary to control the temperature of the thermal train by dumping excess heat after the lithium-fluoride thermal storage material is fully charged. Specific attention was focused on maintaining the operating temperature within a control band and minimizing heat leakage from the variable conductance heat pipe when energy losses are not desired.

The results of the generalized hydrodynamic and heat transfer (temperature drop) studies are discussed in subsection 2.2. Subsection 2.3

presents the results of system stress calculations. Start-up from the frozen state is considered in subsection 2.4, and the studies on the variable conductance heat pipe are presented in subsection 2.5. Subsection 2.6 presents the synthesis of all these studies yielding a heat pipe system design which should successfully meet the specifications under both steady state and start-up conditions. Based on the results of these studies the authors (G. L. Fleischman and B. D. Marcus, TRW) concluded that the Inconel-sodium system:

- Can accommodate 6 kW input at 1600°F when level in a 1-g field.
- Can be started up at full load from the cold state when the working fluid, sodium, is frozen.*
- Will exhibit maximum temperature drops at full load of:
 - 0 to 37°F into the primary evaporator
 - 2.5°F through the coupling between primary and secondary pipes
 - 8°F out of the secondary condenser
 - ~ 0°F along the vapor flow paths
- Will operate over a temperature range of 1600°F to 1650°F as established by the Variable Conductance Heat Pipe (VCHP), with a VCHP loss of about 0.2 kW at the shut-off condition (1600°F).

2.2 WICKS

In providing wicks for the liquid return mechanism in high temperature liquid metal heat pipes it is desirable to utilize the more conventional approaches where possible. Because of the rather complex evaporator and condenser geometries for the solar collector heat pipes, the hydrodynamics study was broken into several individual parts.

First, the maximum possible heat transport capacity was mapped out for a straight pipe of various diameters and lengths with various gravitational and condenser loadings. Then the condenser and evaporator wicks were sized to minimize the overall temperature drop, taking into account that the evaporator wick must pump against the condenser and adiabatic liquid and vapor losses, as well as the gravitational load based on the lowest reference level in the system.

*Test results and additional analytical studies at a later date proved the conclusions drawn to be optimistic. (R.R.)

In order to make the necessary tradeoffs a set of design curves was generated for each component of the thermal train. Bolting cloth (fine wire screen), which is the optimum screen mesh type wick (Reference 1), was used in this tradeoff. It should be noted that equivalent metal felt wicks or sintered porous materials of equivalent or improved pumping characteristics may be substituted for the various bolting cloth sizes in the detailed design.

2.2.1 CONVENTIONAL BOLTING CLOTH SOLUTION

Figures 1 through 3 show the maximum heat transport capacity predicted by the TRW heat pipe design program for a simple circumferential bolting cloth wick in a 2.0, 2.25, and 2.50 inch o.d. tube, respectively; the working fluid is sodium at the temperatures indicated.

The curves were generated by running several tilt angles for a uniform cross section pipe of a particular length. The tilt angles translate into a loading parameter (Δp_o), which may consist of the gravitational head plus any liquid and vapor losses downstream of the section of interest. The gravitational loading may be due to horizontal operation of the heat pipe at a particular elevation above a lower point in the system (e.g., a larger diameter condenser). The minimum value of Δp_o in each figure represents the gravity head associated with the pipe diameter; i.e., horizontal operation of the given pipe on a 1-g gravitational field. The performance is presented in terms of heat transport capacity (QL_{eff}), and thus applies to any length heat pipe. In order to obtain the heat throughput in kilowatts for a particular heat pipe, one simply divides the ordinate (QL_{eff}) by the effective length defined as follows:

$$L_{eff} = \frac{L_{ev} + 2L_{ad} + L_{cond}}{2} \quad (1)$$

where

L_{ev} = evaporator length (inches)

L_{ad} = adiabatic length (inches)

L_{cond} = condenser length (inches)

It is seen that, as the wick thickness is increased for a given diameter, the maximum heat throughput increases until there is a significant vapor pressure drag due to the reduced vapor flow area. Maximum heat transport refers to the fact that these curves are based on a factor of safety of one. Thus, sufficient margin should be allowed in using the curves. In past experience with bolting cloth wicks the calculations have been somewhat conservative, so a margin of 25 to 50 percent should be sufficient.

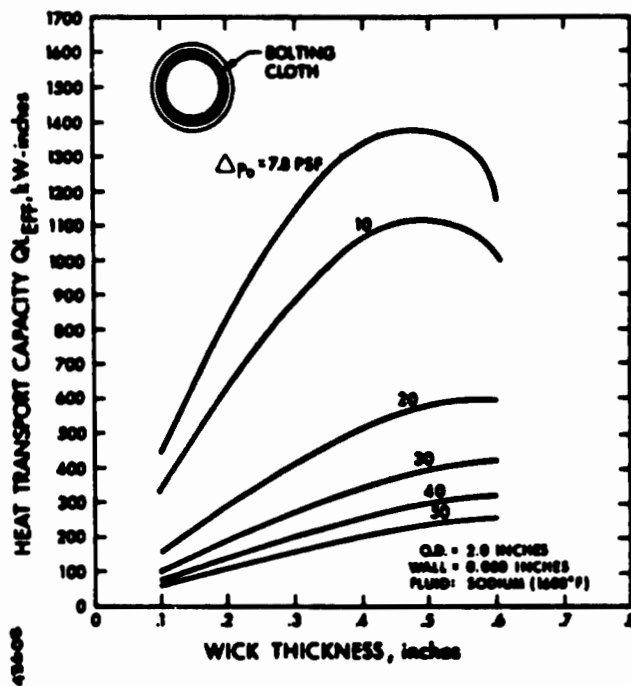


Figure 1. Maximum Heat Pipe Performance (2.0-inch outside diameter)

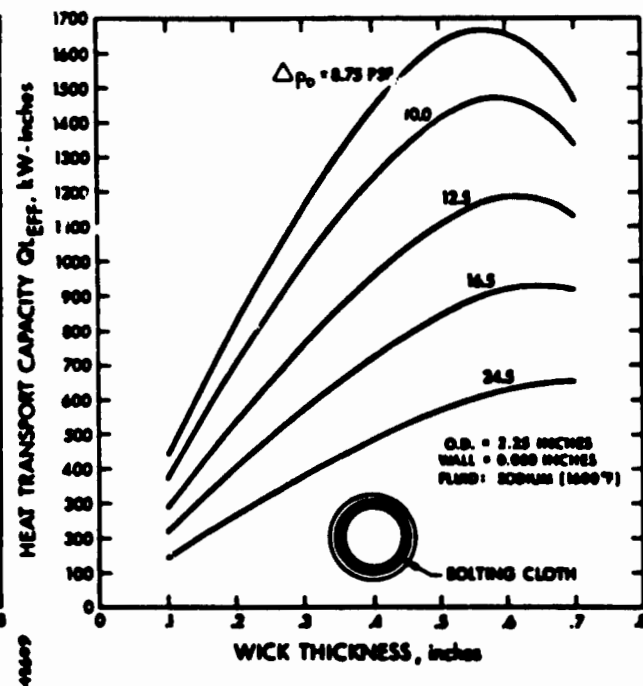


Figure 2. Maximum Heat Pipe Performance (2.25-inch outside diameter)

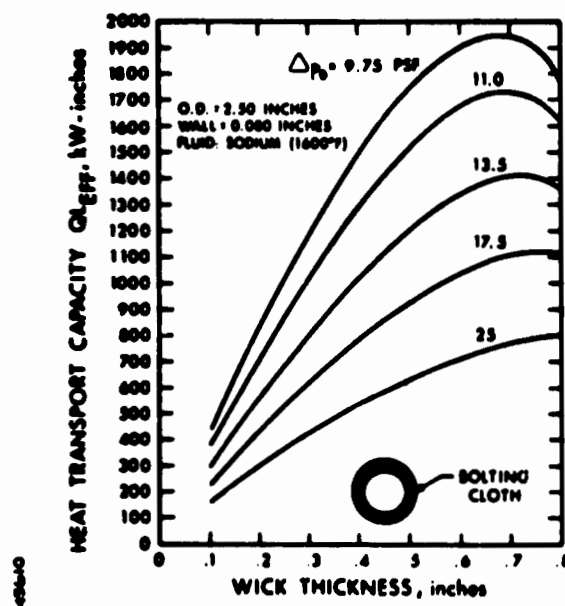


Figure 3. Maximum Heat Pipe Performance (2.5-inch outside diameter)

In summary, the effective length and Δp_0 terms are quite general and must be evaluated in each specific application. Also, it should be clear that the curves do not specify the particular bolting cloth mesh size to use for a given performance. The reason that the mesh size cannot be included on the curves is that these are optimized solutions, and each point represents a different mesh size. Thus, the curves are simply used as an indication of what may and what may not be possible, i.e., these are working curves. Once a wick thickness, pipe diameter, and length are obtained from the curves, the computer program is entered to evaluate the corresponding bolting cloth mesh size.

2.2.2 ARTERIES (Class B Wick)

A typical artery which might be considered for a fifteen foot liquid metal heat pipe is the concentric annular artery depicted in Figure 4. This is the type of artery fabricated by TRW for a fifteen foot diameter circumferential water heat pipe delivered to NASA Houston (Reference 2.)

The annular gap width must be sized so that the artery will self-prime by capillary forces in a gravitational field. Using a factor of safety of 1.5 for the priming criterion, a series of curves was generated for various pipe diameters and effective pore diameters of the artery seal for a uniform cross section and essentially horizontal operation. An effective pore diameter of 0.005 inch corresponds to number 200 mesh screen, 0.010 inch corresponds to number 100 mesh screen, etc. If the pipe diameter is too small, then the performance is vapor limited as seen in Figure 4. But if the pipe is made too large, then the liquid gap must be so small in order to self-prime that the liquid flow resistance limits the performance. This effect also restricts the artery pipe to near zero elevation because of the limit in priming. It was found, for example, that for priming of the annular artery at a 2.9 inch elevation, corresponding to the primary condenser in the solar collector heat pipe, the best performance is only about 1.5 kW for a fifteen foot heat pipe.

Although the various artery configurations appear to have exceptionally high heat transport capacity, the problems associated with sealing of the arteries, self-priming for testing in the earth gravitational field, gas and/or vapor bubbles due to high heat flux, etc., should be kept in mind. Also, artery wicks are much more susceptible to failure by wick dissolution due to mass transport and corrosion.

2.2.3 OPEN ARTERIES

One approach to avoid the sealing requirement of artery wicks is to size the gaps smaller than that required for priming, such that the gaps themselves provide the pumping head. It can be realized that more than one gap would be required to achieve high performance but this, in addition, provides some redundancy in the design.

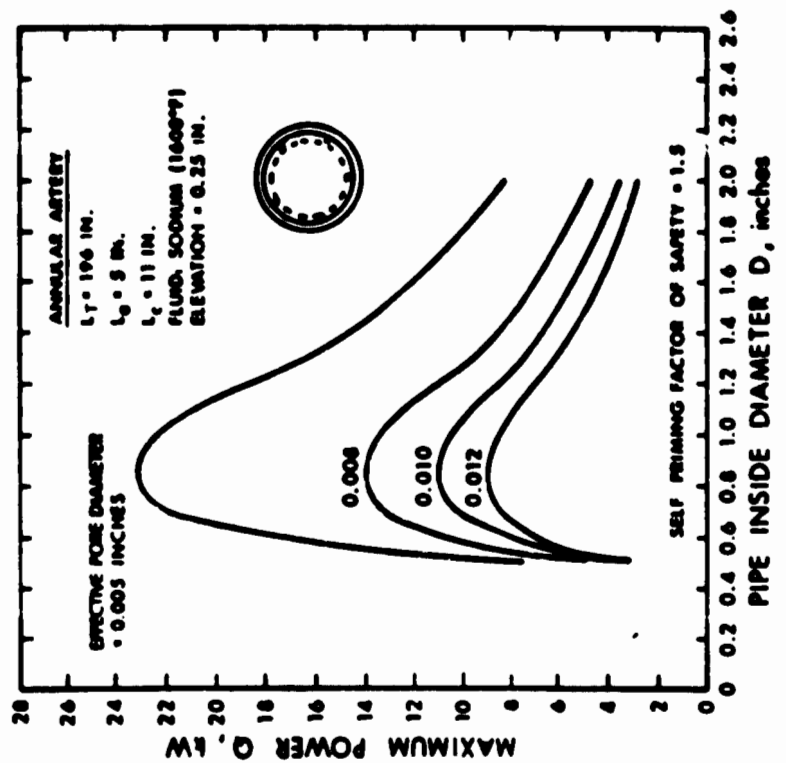


Figure 4. Primary Heat Pipe Performance

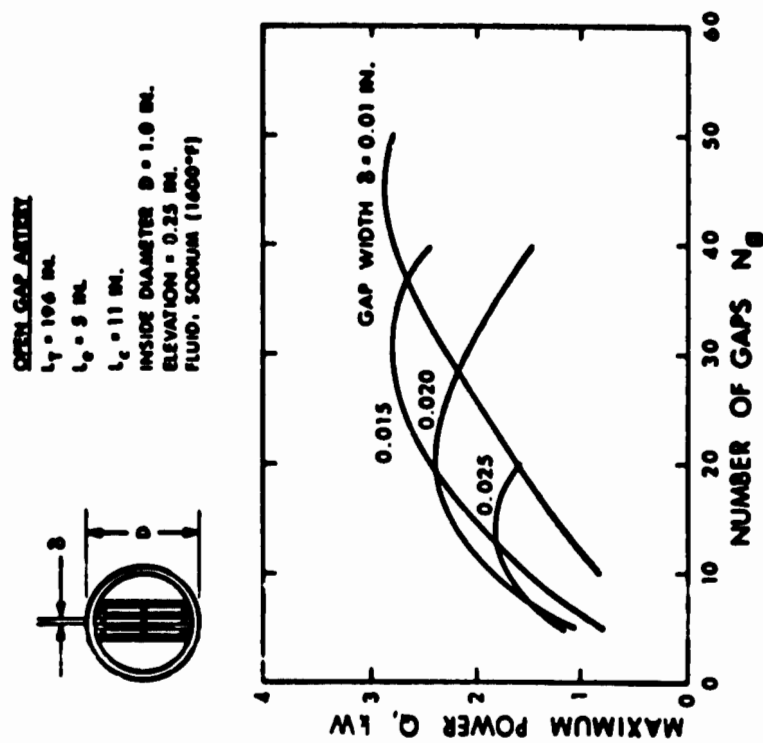


Figure 5. Primary Heat Pipe Performance

The results of an investigation of this wick for a uniform cross section heat pipe are presented in Figure 5. Again, the performance is based on essentially zero elevation, and would be severely limited by an appreciable gravity head.

The performance could be significantly improved by utilizing a series composite wick for which the gaps are wider in the condenser and adiabatic sections than in the evaporator. Also, the results in Figure 5 are for a 15 foot length heat pipe; the performance might be more attractive for shorter length heat pipes.

2.2.4 TEMPERATURE DROPS

The temperature drops associated with conducting heat into and out of heat pipes are affected by the hydrodynamic design, because the wick thickness is determined by the flow requirements and the temperature drop across the wick is directly proportional to the wick thickness.

2.2.5 PRIMARY EVAPORATOR

The primary heat pipe evaporator (receiver) was looked at rather carefully because six kilowatts has to be transferred through a 2-inch radius hemisphere (Figure 6). If planar solar radiation on the hemispherical surface, i.e., cosine heat flux distribution for which the maximum heat flux is equal to twice the average, is assumed (as illustrated in Figure 6), the following equation for the liquid flow pressure drop holds.*

$$\Delta p_l = \frac{1}{2\pi} \frac{\mu_l \dot{Q}}{\rho_l K t H_{fg}} \quad (2)$$

where

\dot{Q} = total heat input

H_{fg} = latent heat of vaporization of working fluid

μ_l = viscosity of liquid

ρ_l = density of liquid

K = wick permeability

t = wick thickness

*Deviation of Eq. 2 is presented in Appendix A.

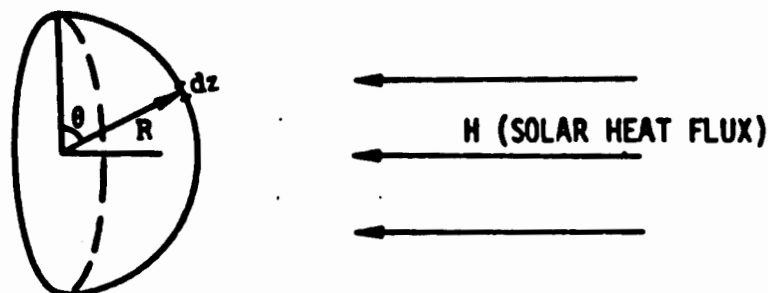


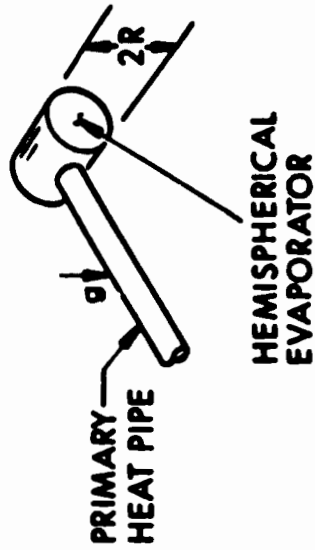
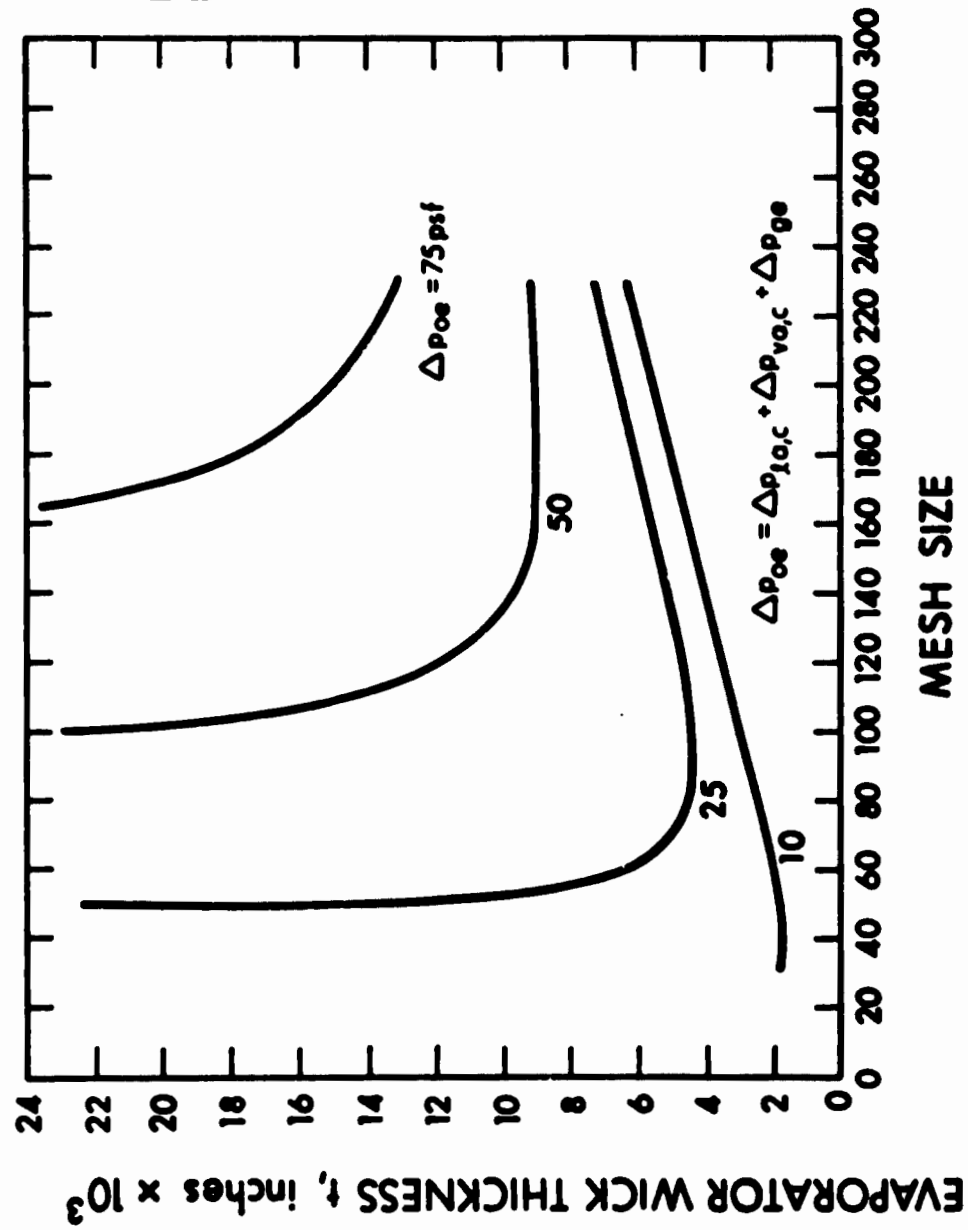
Figure 6. Analytical Model for Hemispherical Evaporator Flow

It is of interest to realize from Equation 2 that the liquid pressure drop is independent of the hemisphere radius. However, a larger radius will require a smaller pore wick, because of the need to overcome a larger gravity head. This in turn leads to a lower wick permeability and larger wick thickness. This effect is expressed in the Δp_0 loading parameter in the evaporator performance curves plotted in Figure 7 for a 6 kW heat input. Again, the Δp_0 term includes the gravity head associated with the height from the lowest point in the system (condenser) to the top of the evaporator, plus any liquid and vapor losses in the various heat pipe sections downstream of the evaporator.

Since the evaporator must pump against these losses it is not surprising that a rather fine mesh is required (approximately number 100 to number 200 mesh bolting cloth). But it was found that a rather thin wick (~ 0.010 to 0.020 inch) may be used.

2.2.6 PRIMARY CONDENSER

With a design heat load for the primary heat pipe of approximately 6 kilowatts, approximately 3.5 kW is transferred to the thermal storage canister (see Figure 8) to charge the storage material, and 2.5 kW is transferred to the secondary heat pipe. Since the pressure drop associated with the condenser must be taken into account in sizing the wick of the adiabatic and evaporator, a relation was developed for the evaluation of the liquid pressure drop in the condenser. This takes into account the flow pattern over the secondary heat pipe, storage canisters, and the return flow in the outer wick of the primary pipe. In the analysis it was assumed that a single mesh size is used for all surfaces and that the wicking on the heat transfer surfaces was of uniform thickness. The particular mesh sizes, not indicated on the curves, were based on an effective pore diameter capable of providing a capillary head equal to twice the gravitational head due to the diameter, D (rule of thumb yielding near optimum designs).



HEAT LOAD, $Q = 6 \text{ kW}$
 WICK: BOLTING CLOTH
 FLUID: SODIUM (1600°F)

Figure 7. Wick Study for Primary Heat Pipe

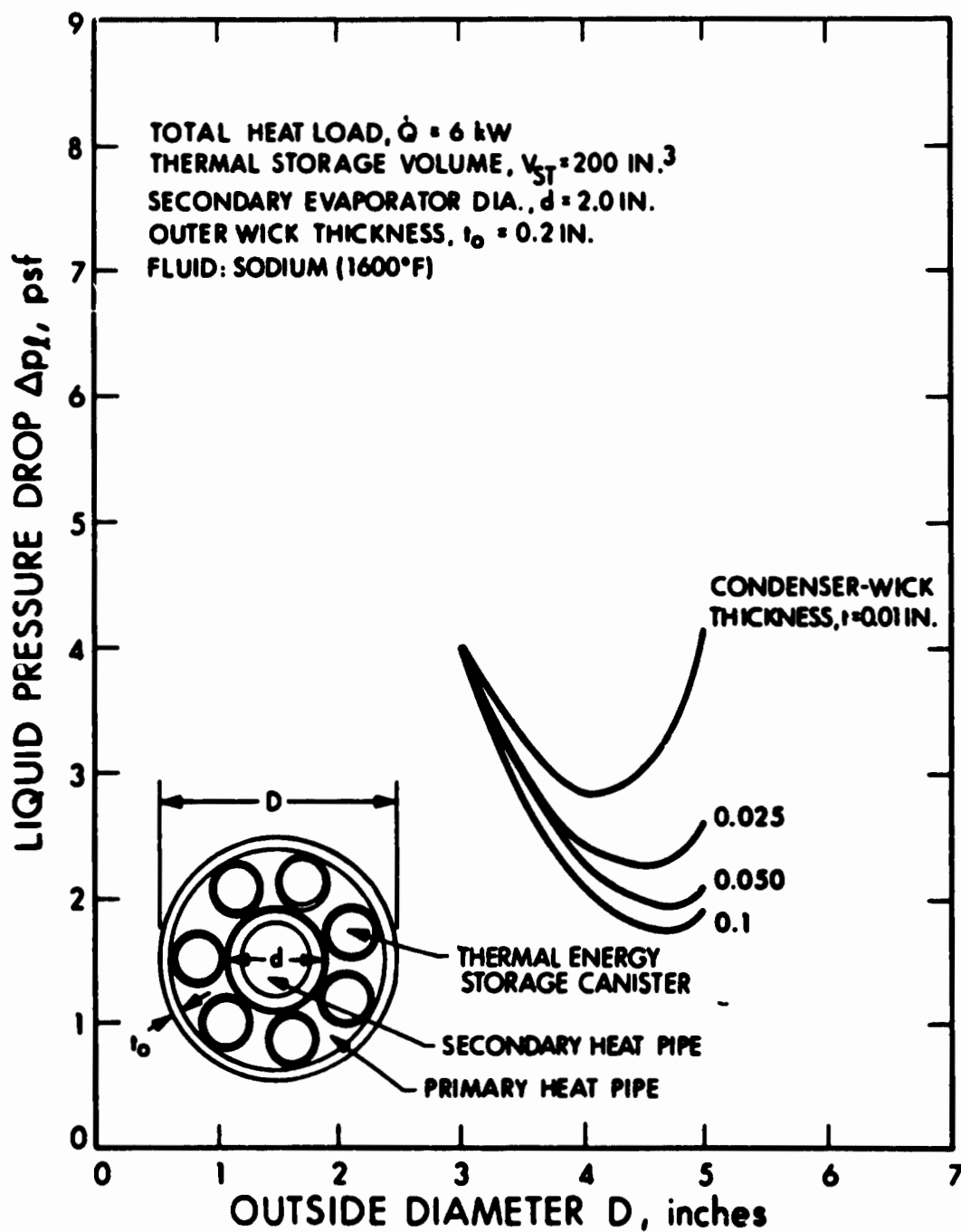


Figure 8. Primary Heat Pipe Condenser* - Solar Collector Thermal Power System

*See footnote page 13.

Figure 8 shows the results based on the above considerations for a fixed secondary heat pipe diameter of 2.0 inches.* The following additional relations are implicit in the model:

- The diameter of the thermal storage canisters is fixed by the primary and secondary heat pipe diameters

$$d_{st} \approx 0.8 (D - d)/2 \quad (3)$$

- The number of thermal storage canisters is fixed by the primary and secondary heat pipe diameters

$$N \approx \pi(D + d)/(D - d) \quad (4)$$

- The volume of thermal storage material, V , is 200 cubic inches. This determines the length of the primary condenser

$$L_c \approx \frac{4V}{\pi N d_{st}^2} \quad (5)$$

Most of the pressure drop was found to occur in the outer wick, because the canisters provide several parallel flow paths to transport the liquid over the relatively short distance from the inner secondary heat pipe surface to the outer primary heat pipe surface. For this reason, the outer wick thickness, t_o , was set at a maximum practical value of 0.20 inch for the tradeoff. This feature of the primary condenser geometry is very fortunate in that the wick thickness on all heat transfer surfaces may be made very thin, resulting in low temperature drops.

It is seen in Figure 8 that the optimum outer pipe diameter is approximately 4.5 inches. If the diameter is made smaller, then the condenser becomes too long because of the thermal storage volume requirement. If the diameter of the outer pipe is larger, the mesh must be fine to accommodate the gravity head. This increases the flow resistance in addition to a long transverse flow path across the canisters.

2.2.7 SECONDARY EVAPORATOR

The secondary evaporator length is determined by the primary condenser length. The evaporator wick will be identical to the wick in the adiabatic section of the secondary heat pipe.

2.2.8 SECONDARY CONDENSER

As in the primary heat pipe, the secondary condenser (emitter) pressure drop must be known for sizing the adiabatic and evaporator wicks.

*The final design of the experimental thermal train differed from this relative arrangement between primary and secondary heat pipe.

Thus, a similar analysis was carried out, but in this case the flow path is straightforward, since a conventional circumferential wick is utilized. The length of the emitter is subjected to the restraint that an area of 140 sq. in. is available for radiation heat transfer to the VM cooler receiver, when all but approximately 110 degrees of the outer circumference is shielded by a rotary insulation blanket as depicted in Figure 9. This requirement, then, fixes the secondary length as follows:

$$L_c = \frac{A}{\pi D} \left(\frac{360}{110} \right) \quad (6)$$

where D is the condenser diameter and A is the required radiation area (140 sq. in.).

For a 3 kW heat load, relatively low pressure losses can be obtained with wicks of the order of 0.050 to 0.10 inch thick as shown in Figure 9. Again the particular mesh size was based on a pore diameter necessary to provide a capillary head equal to twice the gravitational head due to the condenser diameter. The peculiar shape of these pressure drop curves is due to the particular bolting cloth mesh sizes available, and the fact that whereas the flow resistance increases for large diameters, the flow area also increases for a given wick thickness.

2.3 STRESS CONSIDERATIONS

In addition to the wick, the heat pipe wall contributes to the overall temperature drop at the various heat transfer surfaces.

The minimum allowable wall thickness is a function of the required strength. Although the internal pressure level at operating temperature ($\sim 1600^\circ\text{F}$) is only 12 psia, the stresses in the hemispherical receiver (primary evaporator) and the large cylindrical emitter (secondary condenser) are relatively high when the system operates in a vacuum. Because the heat flux (~ 6.1 kW over a two-inch radius hemisphere) is relatively high it is very desirable to make the receiver as thin as possible.

A TRW computer program, based on the equations in Reference 3 for thin wall pressure vessels, was utilized to establish the required wall thickness. The hoop and radial stresses in the cylinder, the maximum bending moment, radial stresses in the end cap as well as the maximum combined stresses in the end cap, and cylinder for hemispherical and flat end caps were calculated.

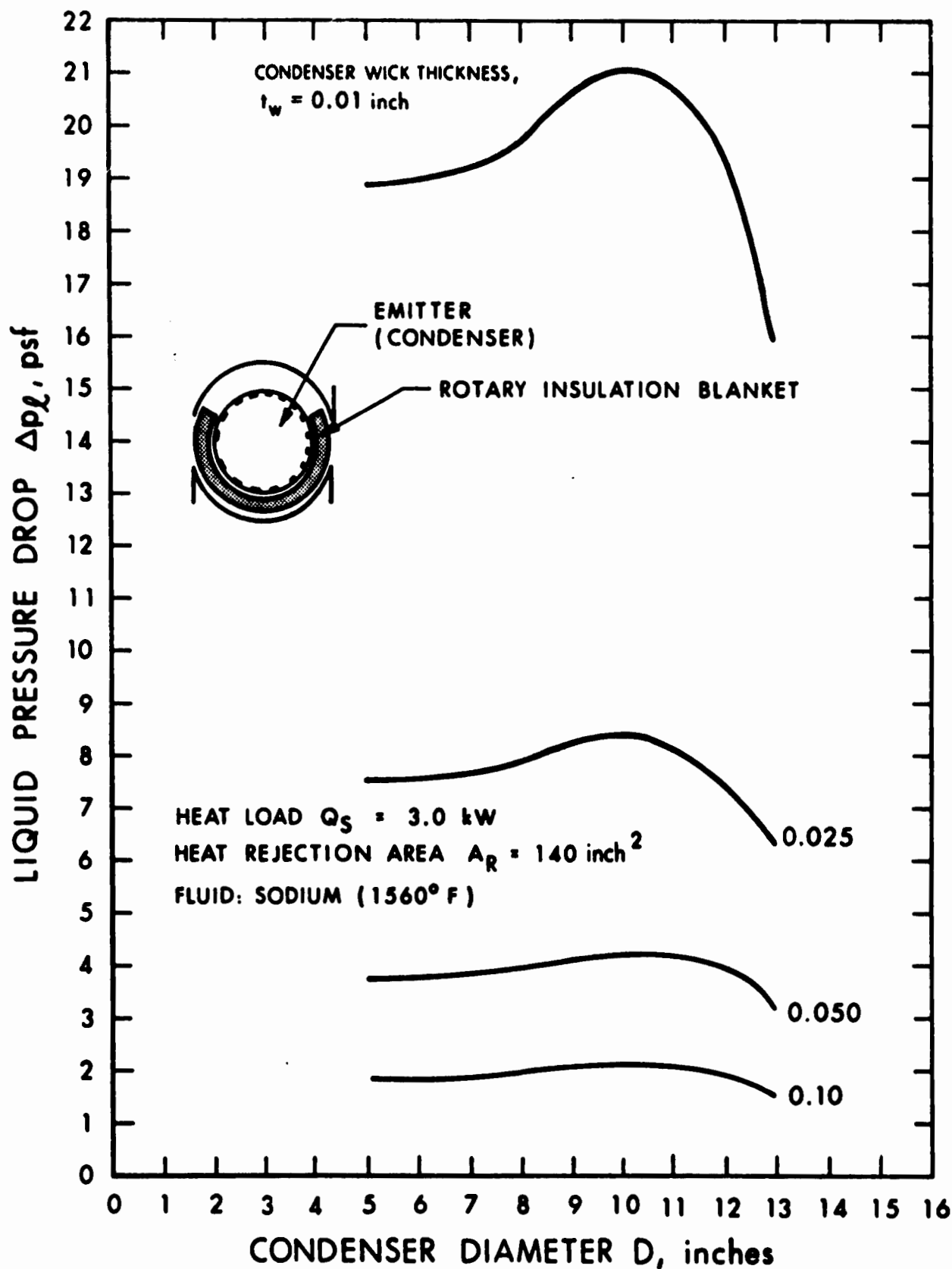


Figure 9. Secondary Heat Pipe Condenser- Solar Collector Thermal Power System

A review of the properties of Inconel 600* at 1600°F show that the yield strength is $\approx 9,000$ psi and that the stress to produce rupture in 50,000 hours is in the range of 1400 to 1700 psi (Reference 4). Since the system must survive 50,000 hours, the stress rupture value of 1400 psi was selected as the design limit.

The stresses in the receiver and emitter were calculated, and the total combined stresses were compared to the stress rupture value. Because of the high stresses which are encountered at the intersection of flat end caps and a cylinder, hemispherical or dished end caps would be required on both the receiver and emitter to reduce the end stresses. The results of the specific calculations for the 4-inch diameter receiver and the 13-inch diameter emitter as a function of end plate and cylinder wall thickness are presented in Tables I and II respectively.

Since there are uncertainties both in the material data at the operating temperature as well as in the manufacturing of the required sections, a safety factor of 2 should be used in all of the wall thickness calculations. Thus, the values shown in the tables are the calculated stresses and are one-half the design stresses.

2.4 START-UP FROM THE FROZEN STATE

The start-up of a liquid metal heat pipe from the frozen state is a complex phenomenon subject to numerous limits and failure modes. Since evaporator wick boiling will not occur with liquid metals at the superheats involved, all of the potential failure modes relate to an inability to supply liquid to the evaporator at a sufficient rate.

The most obvious difficulty is that the frozen working fluid, sodium, must first melt before it can flow through the wicks. The thermal energy required to heat the system to the appropriate melting point and melt the fluid must be provided by sodium vapor generated in the evaporator. A failure occurs if the evaporator is depleted of working fluid before sufficient fluid thaws to replenish the evaporator wick.

A second difficulty relates to the rate of energy transport from the evaporator in relation to the wick circulation capacity. The hydrodynamic capacity of liquid metal heat pipes falls off rapidly at low temperatures due to the large vapor pressure drops associated with high velocity vapor flow at low densities. If the required circulation rate exceeds the hydrodynamic limit at any point during the start-up transient, the evaporator may become dry. This would cause a hot spot and potential failure.

* This material proved not to be suitable and was replaced by Inconel 617 for a second primary heat pipe (R.R.).

TABLE I
MAXIMUM COMBINED STRESSES AT 1600°F IN THE 4-INCH DIAMETER
RECEIVER WITH HEMISPHERICAL END CAPS

<u>Wall thickness (in.)</u>	<u>End cap thickness (in.)</u>			
	<u>0.018</u>	<u>0.021</u>	<u>0.025</u>	
0.040	$\frac{610^a}{680^b}$	$\frac{625}{600}$	$\frac{650}{500}$	psi
0.050	$\frac{490}{690}$	$\frac{480^c}{570}$	$\frac{500^c}{500}$	psi
0.080	$\frac{325}{780}$	$\frac{320}{635}$	$\frac{310}{510}$	psi

TABLE II
MAXIMUM COMBINED STRESSES AT 1600°F IN EMITTER BODY
WITH HEMISPHERICAL END CAPS

<u>Wall thickness (in.)</u>	<u>End cap thickness (in.)</u>				
	<u>0.040</u>	<u>0.050</u>	<u>0.060</u>	<u>0.080</u>	
0.060	$\frac{1350^a}{1030^b}$	$\frac{1470}{800}$	$\frac{1625}{660}$		psi
0.093	$\frac{845}{980}$	$\frac{890}{810}$	$\frac{900}{680}$		psi
0.125	$\frac{650}{1030}$	$\frac{625}{780}$	$\frac{640^c}{680}$	$\frac{680}{510}$	psi
0.140	$\frac{580}{1070}$	$\frac{575}{805}$	$\frac{560^d}{655}$	$\frac{600}{500}$	psi

^a Combined cylinder stress

^b Combined end cap stress

^c Minimum acceptable solutions

^d Acceptable solutions

A related failure mode corresponds to entrainment of liquid in the vapor flow due to the high countercurrent velocities at low vapor pressures and high load. When liquid is torn from the wicks by the flowing vapor, it is prevented from returning to the evaporator. This promotes dryout conditions.*

Finally, a limit on the rate at which vapor can flow from the evaporator exists which corresponds to sonic conditions at the evaporator exit plane. This, however, is not a failure mode. It simply limits energy flow from the evaporator. If the energy input rate exceeds the sonic limit, the evaporator heats up, increasing this limit as the acoustic velocity rises with temperature. During sonic limiting conditions, the heat pipe operates with a large axial gradient, which progressively decreases as the sonic limit approaches and exceeds the rate of energy input. When the vapor pressure rises and flow velocity decreases sufficiently, the vapor approaches isothermal conditions along the entire heat pipe.

Thus, it is an acceptable condition for the heat pipe to operate along the sonic limit curve during a portion of the start-up transient. However, it is not acceptable for the circulation rate to exceed the entrainment limit nor the hydrodynamic limit at any point in the transient. Also, it must be assured that sufficient fluid thaws to provide a liquid return, prior to depleting the evaporator of working fluid when starting from a frozen state. This is particularly troublesome with very long heat pipes having small evaporators, as is the case in the current study.

The various limits discussed above are all a function of heat pipe geometry and structure. The sonic limit varies with the vapor flow area at the evaporator exit; the entrainment limit varies with the vapor area and the wick surface structure; the hydrodynamic limit varies with the vapor flow area, wick flow area, and wick properties; and the question of fluid thawing varies with the starting temperature, system heat capacity, and heat rejection characteristics. Because of this, it is not possible to present start-up calculations for the general case. Instead, calculations were performed for the specific heat pipe discussed in Section II. This heat pipe is designed to meet the specifications of the steady state and transient operating conditions for the proposed application.

Only the primary heat pipe was analyzed. Successful start-up of the primary heat pipe with the sudden application of a 6 kilowatt load implies successful start-up of the secondary pipe with the gradual application of a 2.5 kilowatt load using similar design techniques.

*This is true only if the wick surface is exposed to the vapor flow. (R.R.)

For the primary heat pipe the sonic, entrainment, and hydrodynamic limits were calculated as a function of temperature using various computer routines. The theoretical basis for these computer routines is presented in Reference 1. These limit curves are all plotted in Figure 10. It is seen that the sonic limit lies below the entrainment limit until the axial heat transport exceeds 11.5 kilowatts. Since this exceeds the design point, it is clear that the start-up transient will not suffer an entrainment-induced failure.

On the other hand, the hydrodynamic limit falls off very rapidly at low temperature and would fall below the sonic limit at about 700°F.

This suggests that, below this temperature, the liquid return rate provided by the wicking system cannot keep up with the vapor flow rate out of the evaporator. The system could suffer an evaporator dryout if maintained at this condition for a period of time.

The time for which this condition would actually prevail depends on the heat storage and rejection properties of the system downstream of the evaporator, compared with the sonic-limited heat supply as the system temperatures increase. This cannot be determined without a comprehensive transient model of the entire system which was beyond the scope of this study. Consequently, to insure successful start-ups, it is necessary to constrain the operating regime of the heat pipe to those conditions for which no failure mode limits are encountered.

This can be accomplished through introducing an appropriate quantity of noncondensable gas into the vapor core. The gas serves as a diffusion barrier preventing vapor flow from the evaporator until the evaporator vapor pressure rises high enough to compress the gas and push it downstream. The temperature and pressure at which this occurs depends on the gas inventory.

For the system under study, a noncondensable gas pressure of 6.7×10^{-3} psia will block vapor flow from the evaporator until it reaches 750°F. Since there is no vapor flow from the evaporator, it cannot dry out and thus the system is protected from a hydrodynamic failure until it begins to "turn on" at 750°F. At this temperature, however, the hydrodynamic limit exceeds the sonic limit which then replaces gas blockage as the mechanism preventing both hydrodynamic and entrainment failures until all limits exceed the input power of 6 kilowatts.

The addition of 6.7×10^{-3} psia of gas thus constrains the operating regime of the primary heat pipe to that shown by the dotted line on Figure 10. If, starting from a cold condition, 6 kilowatts is suddenly imposed on the evaporator, the evaporator will begin to heat up with minimal vapor emission, though some diffusion will occur. When it

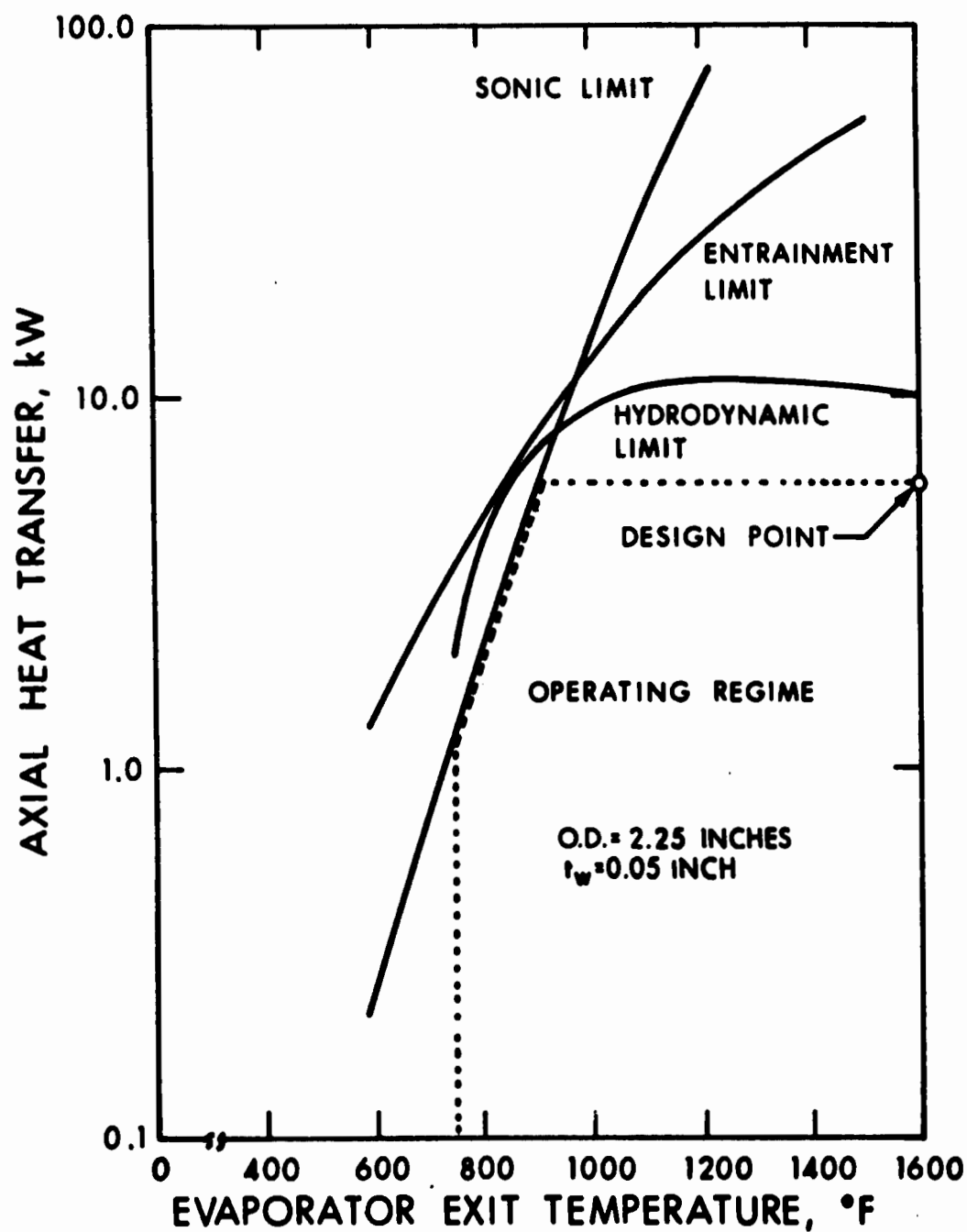


Figure 10. Heat Pipe Limits for Primary Heat Pipe Operating with Sodium as Working Fluid and Inconel Walls and Wicks

reaches 750°F, gas will be purged from the evaporator and the gas blocked region (gas-front) will begin to move down the adiabatic section at a rate dependent on the heat storage and rejection properties of the active (unblocked) section. During this process, an upper bound on the heat transport from the evaporator is provided by the sonic limit curve which protects the system from hydrodynamic or entrainment failure in the temperature regime where these are below 6 kilowatts. Once the temperature at the evaporator exit reaches 900°F, the full 6 kilowatts can flow from the evaporator which continues to heat the system and compress the gas. At the design point of 1600°F, the gas will be so compressed that it occupies only about 0.1 inch of the condenser in the thermal storage unit.

It should be emphasized that the dotted envelope shown on Figure 10 does not represent the actual operating curve during a start-up transient. Rather it represents constraints on the operating regime which have been designed into the system to assure successful start-ups. The actual operating curve will fall within this regime, starting with nearly zero axial heat transfer at 750°F evaporator temperature and ending at the design point of 6 kilowatts at 1600°F.

The addition of the noncondensable gas has a second beneficial feature. By acting as a vapor diffusion barrier which progressively moves down the pipe as temperature and vapor pressure increase, it constrains the vapor to the unblocked region. Thus, it is only necessary to thaw a little of the frozen fluid at a time as the gas front moves out, rather than the entire system simultaneously. This substantially alleviates the problem of start-up with a frozen working fluid, for it is possible to assure the return of the liquid to the evaporator while most of the working fluid in the pipe is still frozen.

Calculation of the maximum evaporator wick fluid depletion during a start-up from 0°F yielded approximately 1.5 mils for the noncondensable-gas inventory specified. This compares with an evaporator wick thickness of 20 mils, showing a substantial factor of safety in avoiding wick dryout.

2.5 VARIABLE CONDUCTANCE

The gas controlled variable conductance heat pipe attached to the primary heat pipe is to provide a heat rejection capability for the thermal energy input in excess of that required to power the VM engine, to melt the thermal storage material, and to account for the various heat losses. This excess thermal energy is expected to vary from zero to approximately 3.2 kW during a typical cycle. In addition, by appropriately sizing the gas reservoir and gas inventory the variable conductance heat pipe fixes the temperature level of the entire "thermal train."

Most of the experience to date is related to low temperature variable conductance heat pipes, but preliminary tests have indicated that the theory (Reference 5) is directly applicable to high temperature liquid metal systems. Thus, an investigation was conducted to establish a feasible temperature control range, required gas reservoir volume, and radiator design for the solar collector application. Various problem areas such as the diffusion freezeout phenomenon and heat leakage were taken into account.

2.5.1 FLAT FRONT ANALYSIS

First, a rapid survey of the effect of various sink temperatures, evaporator steady-state temperature control spans, and type of reservoir (hot or cold) was made assuming a sharp vapor-gas front. This approach assumes that the total pressure in the pipe is established by the evaporator vapor pressure, that the partial gas pressure in the off portion of the condenser is the difference between the total pressure and the vapor pressure of the working fluid at the effective sink temperatures, and that the effect of axial conduction is negligible. A cold reservoir is defined as a volume whose temperature is approximately that of the effective sink temperature, whereas the temperature of a hot reservoir corresponds to the heat pipe evaporator (Reference 5).

The results are shown in Figure 11. Some of the trends in the curves are peculiar to a high temperature liquid metal heat pipe in that the vapor pressure at the sink temperatures of interest is negligible. Providing a cold reservoir, for example, results in a significantly reduced reservoir volume requirement. Also, the reservoir volume is essentially independent of the maximum sink temperature (full-on condition). The results indicate that a $\pm 15^{\circ}\text{F}$ to $\pm 20^{\circ}\text{F}$ control span would be feasible by installing the reservoir inside the titanium support structure where the temperature will be relatively constant between 150°F and 200°F . An attempt to achieve much tighter control would require excessively large reservoirs. It should also be pointed out that the results in Figure 11 represent the vapor temperature variation of the variable conductance heat pipe itself. An additional temperature drop must be considered in conducting heat through the wick and wall of the primary heat pipe and into the variable conductance heat pipe, since it is the temperature of the primary heat pipe that is being controlled.

2.5.2 TRW GAS PIPE PROGRAM

After the reservoir location and approximate volume were established using the sharp front analysis, a heat pipe and radiator design was worked out. One difficulty encountered in sizing the radiator was that radiation fin efficiency at high temperatures is extremely low.

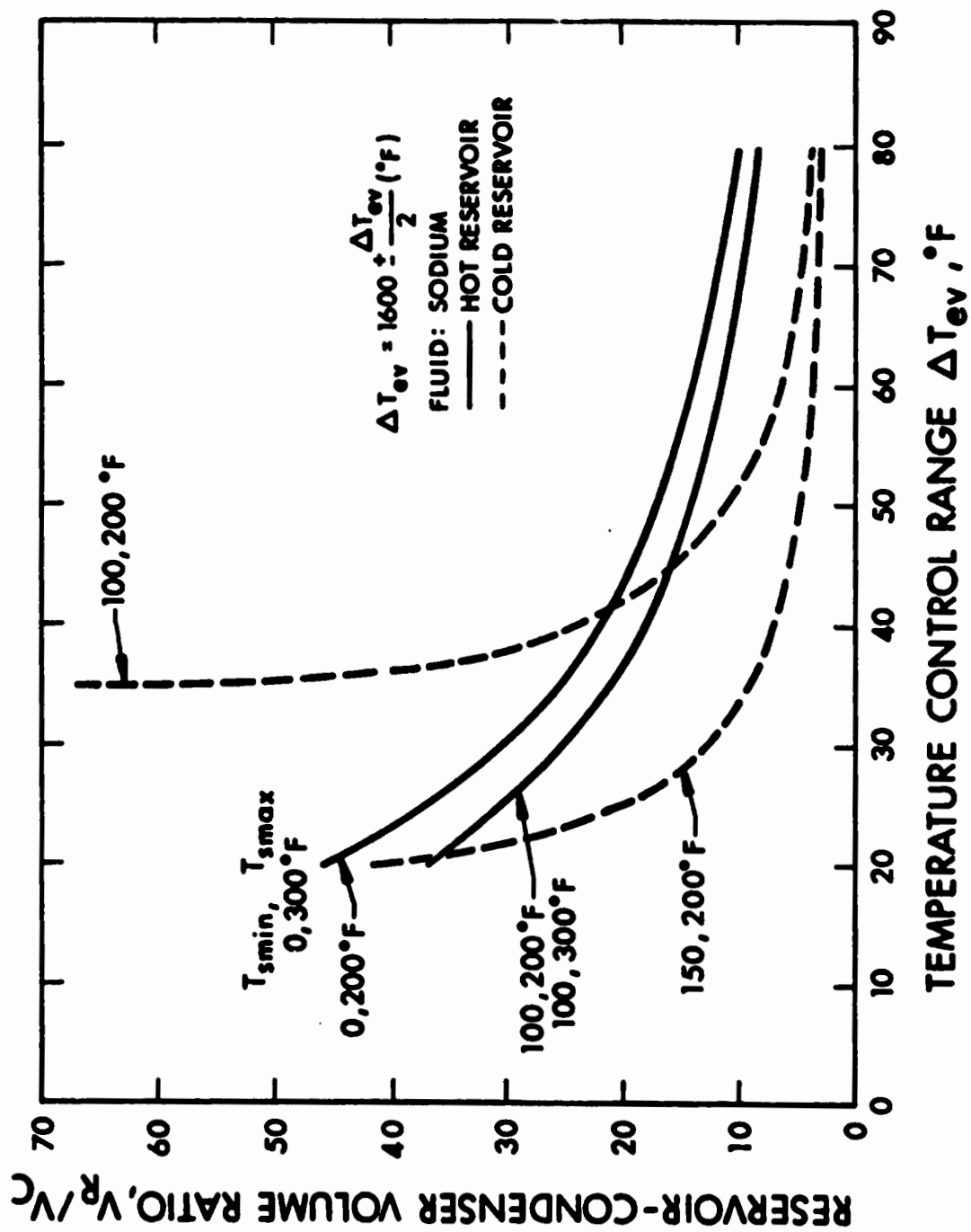


Figure 11. Variable Conductance Heat Pipe Performance

This poor fin efficiency led to a high conductivity, rather thick fin material, which in turn necessitated slotted fins (cold trap) at the end of the condenser. This is required to avoid an excessively high temperature at the reservoir feed tube entrance due to the high axial conductance (Reference 5).

Once a particular wick and pipe size were established using the principles outlined in subsection 2.2, the TRW Gaspipe Program (Reference 6) was utilized to determine the effects of heat leakage during shut down of the pipe (i.e., minimum power) and axial conduction on the temperature at the gas reservoir feed tube entrance and diffusion freezeout rate. The program also yielded a more accurate gas reservoir volume requirement.

A minimum power loss (full-off condition) of less than 0.2 kW was found feasible with a 12-inch-length adiabatic section. By providing a slotted radiator and reducing the wick thickness for a six-inch length at the end of the condenser (cold trap), the temperature at the feed tube entrance can be brought down to approximately 600°F in the full-on (3.2 kW) condition. Moreover, because of the extremely low vapor pressure of sodium at this temperature, the diffusion freezeout rate is on the order of 1 cc over a period of years. The associated radiator size is approximately 4 inches wide by 30 inches long with a reservoir-to-condenser volume requirement on the order of 4.5. This ratio is somewhat less than indicated in Figure 11 ($V_R/V_C = 9.5$). One reason for this is that the sink temperature which the condenser "sees" is actually somewhat higher than the reservoir temperature for the location chosen (inside the titanium support structure) in contrast with the flat front analysis which assumed them equal.

2.6 PRELIMINARY DESIGN

Based on the material discussed in Subsections 2.2 through 2.5 a preliminary design for the thermal train heat pipes evolved. The primary concern was to establish a set of heat pipe diameters, lengths, and wick structures, which yields a system that fulfills the general requirements of the thermal train subsystem. Careful attention to maximizing capacity and reliability while minimizing system temperature drops yielded an attractive system design which offered acceptable performance, long life, and relative ease of manufacture. This system is shown in Figure 12.

2.6.1 MATERIALS

Sodium was selected as the working fluid. In the required operating temperature range, sodium offers superior hydrostatic and hydrodynamic performance at acceptable pressure levels. Also, it appears compatible with the preferred materials of construction.



With Inconel 600 selected for the wick and wall materials, the effect of wall thickness on stress and heat transfer in a conservative sense was evaluated. Substitution of columbium alloys in place of Inconel 600 at 1600°F would, in all cases, satisfy the limits established for Inconel 600 because of their greater strength and higher conductivities. The converse would not be true. No attempt to resolve the long-term operational capability between sodium and Inconel 600 was made in this preliminary design effort. Many benefits of Inconel 600 utilization include:

- a. Ready availability
- b. Oxidation resistance
- c. Modest raw materials cost
- d. Properties consistent with atmospheric processing during heat pipe fabrication
- e. Properties consistent with survival in case of loss of vacuum during high temperature system tests
- f. Flexibility in fabrication and welding

Dependent upon the size of the heat pipe hardware, a large differential exists between the fabrication and test costs of an Inconel 600 type system and a refractory metal system. Specific long-term service constraints of Inconel-type heat pipe materials include:

- a. Sublimation rate of chromium, the highest vapor pressure alloy element of Inconel.
- b. Mass transport processes between sodium and Inconel alloy elements.

With regard to chromium sublimation, the upper free surface limit (assuming no diffusion limit in the alloy) approaches 3×10^{-5} cm/year at 1600°F. Use of cladding or coating techniques can reduce this value. TRW experience with Inconel/sodium heat pipe systems up to 2200°F service temperatures includes satisfactory performance for many hundreds of hours with no indication of mass transport failures. However, because of the dependence of this type of failure on both the chemistry of the specific sodium/heat pipe materials and circulation rates, extrapolation of data between various tests and designs is not readily accomplished.

2.6.2 PRIMARY HEAT PIPE

Based on the background presented in the previous subsections of this report, a thermal train was specified and sized which included all essential components, primary heat pipe, secondary heat pipe, and thermal energy.

2.6.2.1 Condenser

Referring to subsection 2.2, Figure 8, the optimum primary condenser diameter would be approximately 4.5 inches i.d. A slightly smaller diameter, however, was chosen to reduce the gravitational loading on the evaporator and adiabatic wicks. This diameter requires a wick structure on all the surfaces made of 70 mesh bolting cloth.

Equations 3, 4, and 5 when used to establish the thermal storage system geometry for a 2-inch o.d. secondary heat pipe with 0.050-inch wicks on its outer surface and those of the canisters, yields:

Number of canisters	8
Diameter of canisters	0.9 inch
Length of canisters	35 inches

A wick thickness of 0.20 inch must be used for the outer surface of the primary pipe condenser as specified in Figure 8.

The temperature drop associated with 2.5 kW heat transfer through the primary wick is $\approx 0.7^{\circ}\text{F}$. This value is low because of the low heat flux in combination with the thin (50 mil) wicks.

2.6.2.2 Adiabatic Section

Because the final system will require a 90 degree bend in the heat pipe and to minimize the temperature drop between the primary heat pipe and the variable conductance heat pipe, a coaxial bolting cloth wick, illustrated in Figure 12 was suggested. This type of wick is easier to fabricate and not as easily damaged in bending as circumferential wicks or arteries. Moreover, a homogenous wick as opposed to arteries renders the system less susceptible to failure by means of wick erosion or corrosion.

For sizing the wick, the effective length and loading (Δp_0) must be known. The curves in subsection 2.2 are valid for coaxial and circumferential wicks, if the relative areas are maintained. The total length of the primary heat pipe is 90 inches including the 35-inch condenser. Thus, the effective length of the adiabatic section is 55 inches. The vapor pressure drop in the condenser is negligible. Therefore, the loading parameter (Δp_0) is the sum of the liquid pressure drop, Figure 8, corresponding to the above dimensions, plus the gravitational head from the bottom of the condenser to the top of the heat pipe. Referring to Figure 2 for a 2.25 inch o.d. tube, $\Delta p \approx 17.0$ psf, and a heat transport capacity of approximately 550 kW-inches is obtained for a reasonable wick thickness of 0.3 inch. This is equivalent to a 1.5-inch diameter coaxial wick. Dividing by the effective length, the power transfer capacity is

$$\dot{Q} = \frac{550}{55} = 11.0 \text{ kW}$$

This is more than enough capacity for the 6.1 kW heat load having a factor of safety ≈ 1.8 . A #60 mesh bolting cloth was assumed in the calculations for the above conditions.

2.6.2.3 Evaporator

Though Equation 2 proved the evaporator flow losses to be independent of the evaporator diameter, the total pressure drop Δp_o term is dependent on its diameter. For a 2.0-inch radius hemisphere using 60 mesh bolting cloth in the adiabatic section the total pressure drop is more than 50 psf. Using a 165 mesh bolting cloth, or the equivalent, yields a wick thickness of only 0.020 inch, including a factor of safety of 2.0.

Based on the stress calculations in subsection 2.3, a hemisphere wall of 0.020 inch to 0.025 is required; the cylinder should be 0.050 inch thick (Table I). (Note that making the cylinder wall too thick may increase the stresses in the thin wall end cap.) If the minimum value is used, then the temperature drop associated with the evaporator varies from 0°F at the base to 37°F at the center of the hemisphere. If a larger temperature differential can be allowed, a slightly thicker wall is recommended.

It is only necessary to provide a thin wick over the hemispherical heat transfer surface. The wick in the opposite surface and the cylindrical walls can be thicker to act as a fluid reservoir during start-up and to provide low flow resistance in distributing fluid around the hemisphere.

2.6.3 SECONDARY HEAT PIPE

2.6.3.1 Condenser

Because a large diameter secondary heat pipe condenser (emitter) imposes a significant gravitational loading on the adiabatic and evaporator section wicks, the diameter was reduced to 10 inches for the system studied. For a radiation area of 140 square inches the condenser had to be 15 inches in length. As in the primary condenser, the diameter and heat load fixes the mesh size and thickness. Referring to Figure 9, a 0.10-inch-thick wick was selected to minimize the liquid pressure drop. This corresponds to 145 mesh bolting cloth for the wick material.

The smaller diameter condenser also reduces the severe stress limitation on the wall thickness. For the present design, a 0.125-inch wall thickness (Table II) was selected, leading to an overall temperature drop of 8°F through the emitter wick and wall.

2.6.3.2 Adiabatic Section and Evaporator

The same type of coaxial wick used in the primary heat pipe is also recommended for the secondary heat pipe. However, the mesh size and diameter will differ. Also, the secondary adiabatic wick will extend into the 35-inch evaporator length. Since the total length of the secondary heat pipe is 90 inches, excluding the condenser, the effective length is calculated from Equation 1 as follows:

$$L_{\text{eff}} = \frac{35 + 2(55)}{2} = 72.5 \text{ in.}$$

The loading parameter, Δp_o , is due to the condenser liquid pressure drop obtained from Figure 9 and the gravitational head from the bottom of the condenser to the top of the heat pipe. Thus, entering Figure 1 for a 2.0 inch o.d. tube, and $\Delta p_o \approx 27$ psf, a heat transport capacity of 275 kW-inches is obtained for a 0.3-inch wick. This is equivalent to a 1.4 inch diameter coaxial wick. Dividing by the effective length, the power transfer capacity is

$$\dot{Q} = \frac{275}{72.5} = 3.8 \text{ kW}$$

This represents a factor of safety of ≈ 1.5 . Optimization for the above dimensions yielded a bolting cloth of 105 mesh for the secondary coaxial wick.

The temperature drop between the primary heat pipe and the secondary heat pipe is simply due to the 0.05-inch wall and two layers of No. 105 mesh screen (or circumferential grooves) on the wall. This corresponds to $\approx 1.7^\circ\text{F}$ for a 2.5 kW heat load.

2.6.4 VARIABLE CONDUCTANCE HEAT PIPE (VCHP)

The VCHP was discussed in some detail in subsection 2.5. Since the VCHP was not a part of the thermal train itself, a general hydrodynamic (QL_{eff}) curve was not necessary. A circumferential bolting cloth wick, as shown in Figure 12, is adequate for this heat pipe. Calculations yielded a 0.2-inch-thick wick of 50 mesh bolting cloth with a factor of safety of about 2.0. By using several transfer wicks a very thin wick may be used over the evaporator heat transfer surface. The temperature drop through the wick and wall between the primary and variable conductance heat pipes varies from zero in the full-off case to approximately 15°F in the full-on case. Although this temperature drop is small, it illustrates the need for a common wall. Clamping the VCHP to the primary heat pipe would result in an excessive thermal contact resistance.

As mentioned in subsection 2.5, the rather low radiation fin efficiency at high temperatures causes some difficulty in the radiator design. A nickel-clad copper radiator with slotted fins to reduce axial conduction was assumed in the calculation. By providing a 12-inch insulated adiabatic section, the heat leak in the full-off condition was calculated to be less than 0.2 kW.

The results of the TRW Gas Pipe Program indicated a gas reservoir volume of 25 cubic inches for a temperature variation of 35°F in the VCHP vapor temperature. Slightly better control might be achieved with a larger reservoir, but the design is reaching the point of diminishing return. The variation in wall temperature drop must be added to that of the vapor temperature, yielding an overall control range of 50°F .

The amount of gas inventory fixes the operating temperature of the system. In the VCHP a 2.4×10^{-5} lb-moles of nitrogen will yield a primary heat pipe control range of 1600°F to 1650°F , which assures a temperature above that of the thermal storage material fusion point.

SECTION III

DESIGN, MANUFACTURING, AND TESTING OF FIRST FIFTEEN FOOT PRIMARY HEAT PIPE

3.1 INTRODUCTION

This section describes the design, fabrication and testing of the first 15-foot primary heat pipe, capable of delivering 6 kW at 1600°F, which can be integrated with a thermal energy storage unit described in Section VII of Volume III of this report.

In Section II a preliminary design of a Thermal Train Subsystem was analytically evolved which needed experimental verification. The initial design appeared inappropriate for the experimental phase because of its complexity. A simpler demonstration design was laid out with which the fabrication and assembly methods for wicks and structures of a full-scale heat pipe could be established. The general guidelines for the 15-foot primary heat pipe were:

- a. Fifteen-foot running length
- b. Constant diameter cross section
- c. Composite or homogeneous wick structure
- d. 6 kW of power at 1600°F delivered

3.2 DESIGN ANALYSIS

3.2.1 HYDRODYNAMIC DESIGN

Detailed hydrodynamic designs were performed for two 1600°F sodium 15-foot 6 kW heat pipes. These designs are summarized in Table III. Figures 13 and 14 show the calculated performance limits for the two 15-foot heat pipes with 2.50 and 2.25-inch diameters, respectively. The limits are plotted as functions of the evaporator exit temperature. The design for the two 15-foot pipes specifies a composite homogeneous diametral wick for the return flow of the working fluid. This wick design calls for a 38-mesh bolting cloth which encloses a thin section of 60-mesh screen. The 60-mesh screen, identified as the "wet finger," serves to maintain sodium in the evaporator during start-up and through significant volume change due to expansion and contraction.

The volume change of sodium between room temperature and 1600°F is approximately 21 percent. The required fill is based upon the liquid volume required at the operating temperature 1600°F, thus during shutdown with a single mesh size, the contraction could conceivably be concentrated at the evaporator end. Use of a smaller 60 mesh bolting cloth

TABLE III

FIRST PRIMARY HEAT PIPE
COMPARISON OF DESIGN PARAMETERS

	<u>First-Primary</u>		<u>Comments</u>	
HEAT PIPE				
Tube o.d. (inch)	2.50	2.25	2.50 o.d. tube considered for better start-up	
Wall (inch)	0.0625	0.0625		
Length (inch)	180	180		
Evaporator Length (inch)	24	24		
Condenser Length (inch)	37.5	37.5		
WICK				
Diametral Wick				
Width (inch)	1.1	1.1	Primary wick includes 0.1 inch wide "wet finger" for start-up made of 60-mesh bolting cloth	
Cross Section Area (inch ²)	2.4	2.1		
Mesh (Bolting Cloth)	38	38		
Circumferential Wick				
Number of layers	2	2		
Mesh	60	60	Includes insulation loss	
Wire diameter (inch)	0.007	0.007		
OPERATING CONDITIONS				
Temperature (°F)	1600	1600		Based on tube o.d.
Power Input (watts)	8000	8000		
Evaporator Heat Input Flux (watts/inch ²)	42	47.2	Based on power input	
Condenser Heat Flux (watts/inch ²)	31	22.6		
Axial Mass Transport Flux (lb/hour-inch ²)	6.0	8.0		
INSULATION				
Number of layers	3	3	J-M Flex Min-K (0.375 inch layers)	
Heat Loss (watts/feet)	110	100		

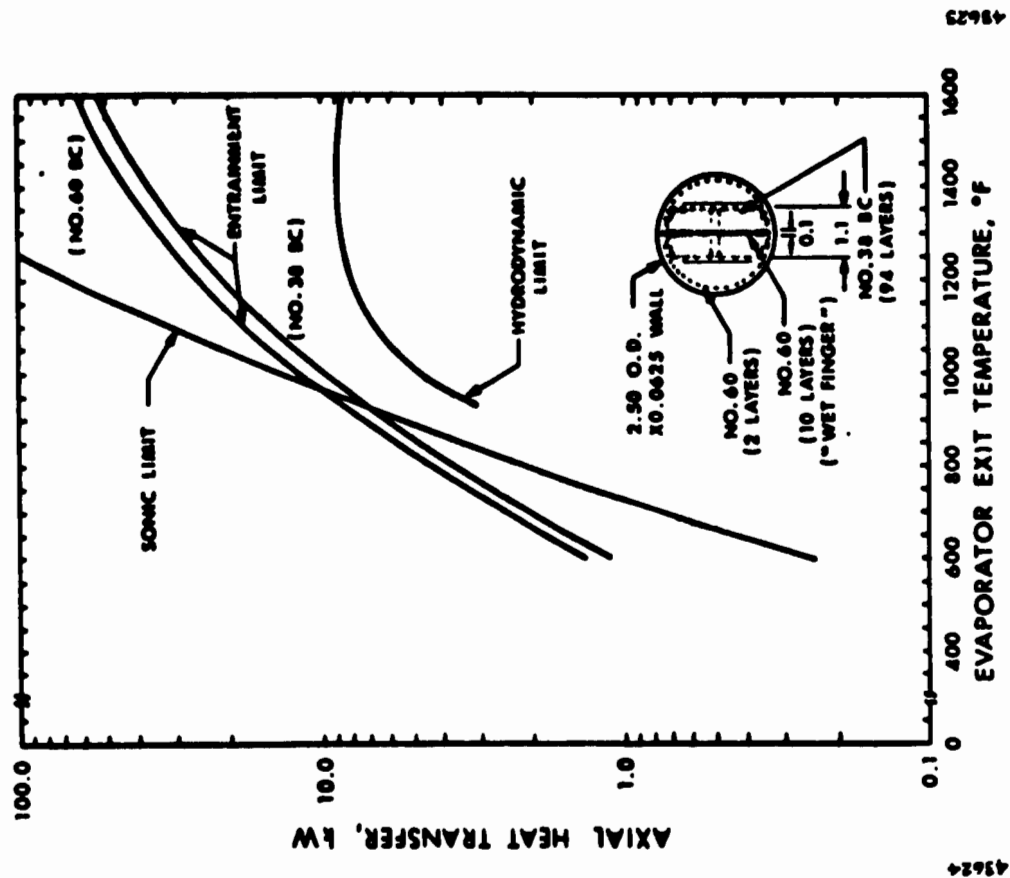


Figure 13. Performance Limits for 2.5-inch Heat Pipe

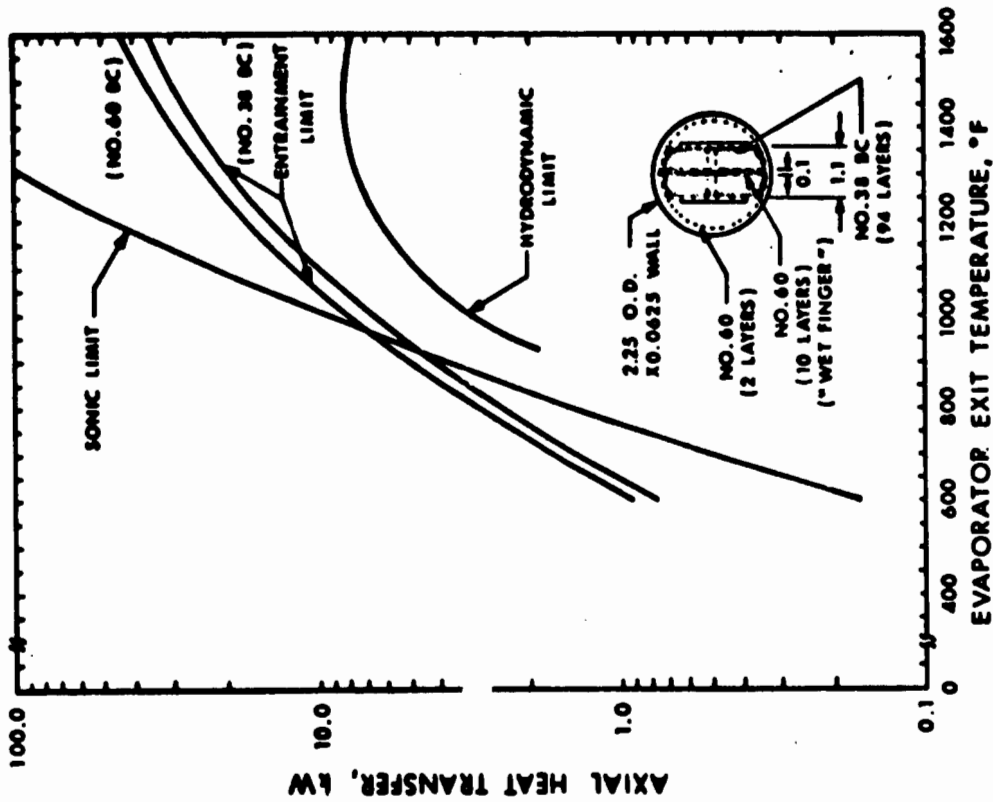


Figure 14. Performance Limits for 2.25-inch Heat Pipe

structure along the diametral length guarantees that it will contain sodium by drawing from the 38 mesh bolting cloth as required.

Theoretically, the 2.5-inch diameter heat pipe provides a higher steady-state limit than the 2.25-inch pipe at the operating point of 1600°F, and significantly higher capacities at lower temperatures. Neither steady-state sonic nor entrainment limit either design. Transient start-up curves could not be modeled for these pipes. For that reason, some concern had to be given as to how much power can be applied in the frozen start-up. Methods which individually or in combination could assure correct start-up include:

- a. Start-up at a reduced power, i.e., < 2 kW
- b. Use of an inert gas to control the rate of vapor front growth during the start-up transient
- c. Use of supplemental start-up heaters along the heat pipe

All three options were available for testing the 15-foot heat pipe so that design and operational criteria of both steady-state and transient performance could be established. Start-up at reduced power implies, in space application, either off-pointing of the collector or shuttering the receiver, or both. Use of an inert gas requires containment of the inert gas during steady-state heat pipe operation after start-up has been achieved. In this case, the location of gas reservoirs, (internal or external) must be considered. Figure 15 illustrates a calculated internal gas reservoir length if the gas could be contained internally at the condenser end. It is immediately apparent that the temperature difference between the primary heat pipe and the secondary heat pipe, resulting from the use of gas, would profoundly influence the gas reservoir volume. This curve further shows the impracticality of containing a full inventory of start-up gas in an internal reservoir when the primary condenser is well clamped to a secondary system.

3.2.2 INSULATION DESIGN

In addition to the detailed hydrodynamic design, insulation losses were calculated for the proposed in-air testing as shown in Figure 16. The hydrodynamic design has to account for these losses. For the in-air tests, the primary pipe is therefore designed with an 8 kW capacity delivering 6 kW at the condenser.

3.3 MECHANICAL DESIGN

The mechanical design of the primary pipe is shown in Figure 17. One full-scale unit was manufactured per this configuration. The pipe was constructed of three 5-foot sections of 2.25-inch o.d. Inconel 600 tube that are girt-welded. A single diametral wick structure, 1.1 inches wide, runs the length of the tube and terminates 6 inches from the condenser end. A flange with a fill tube for later integration with a

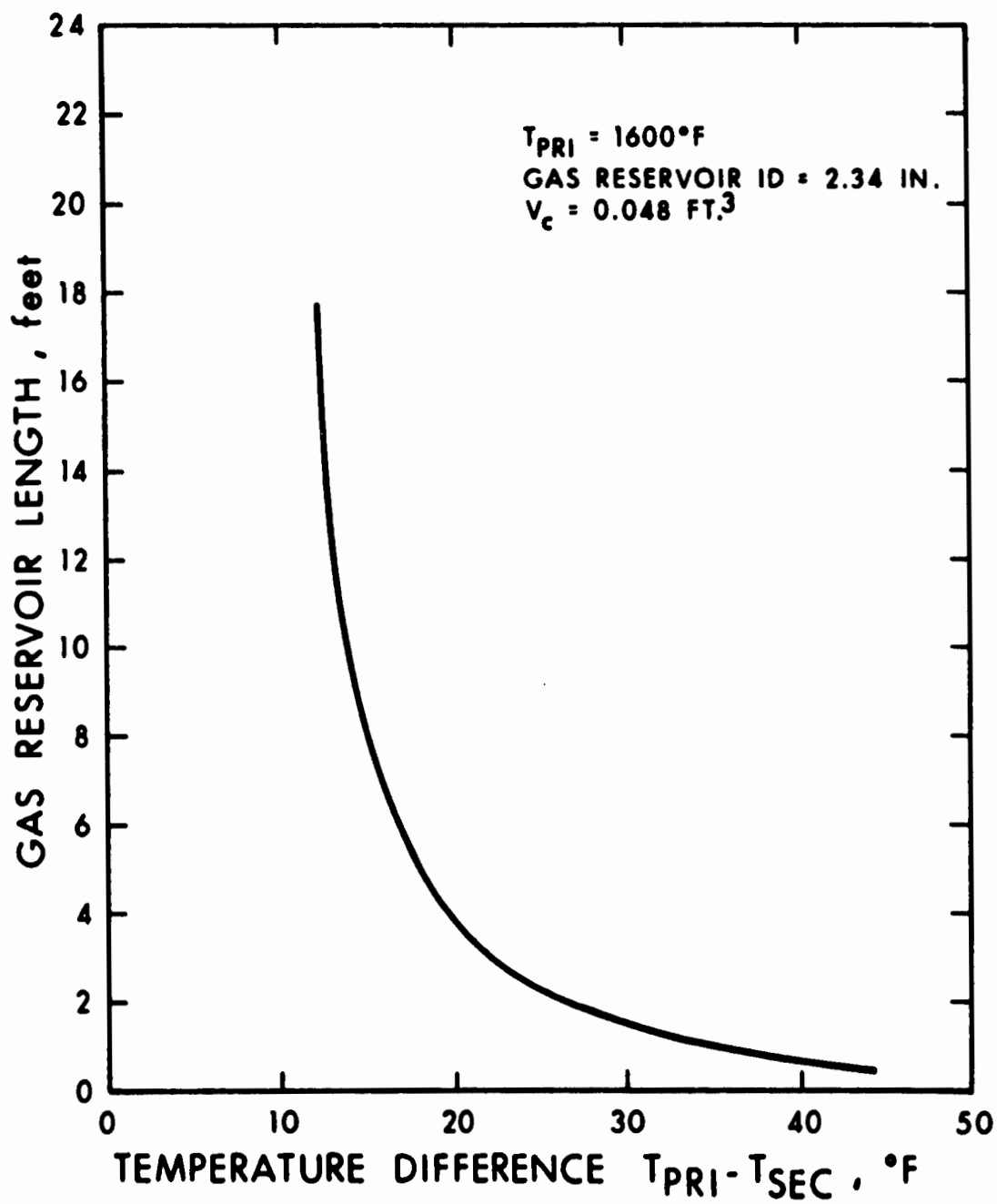
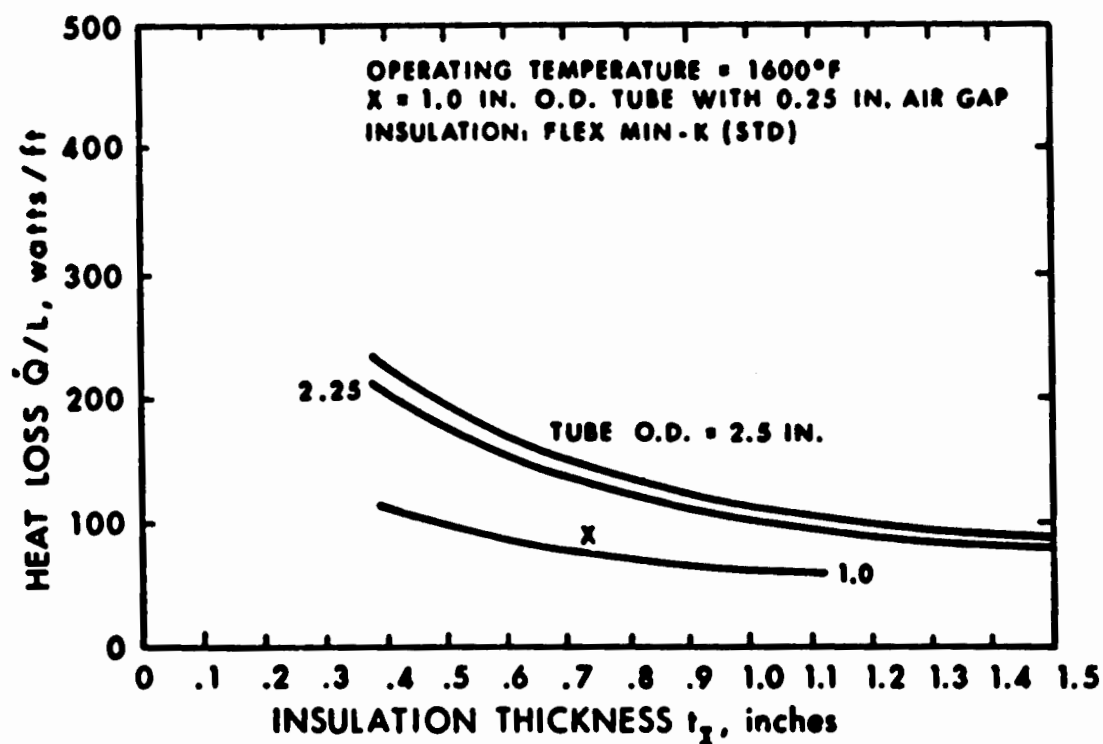
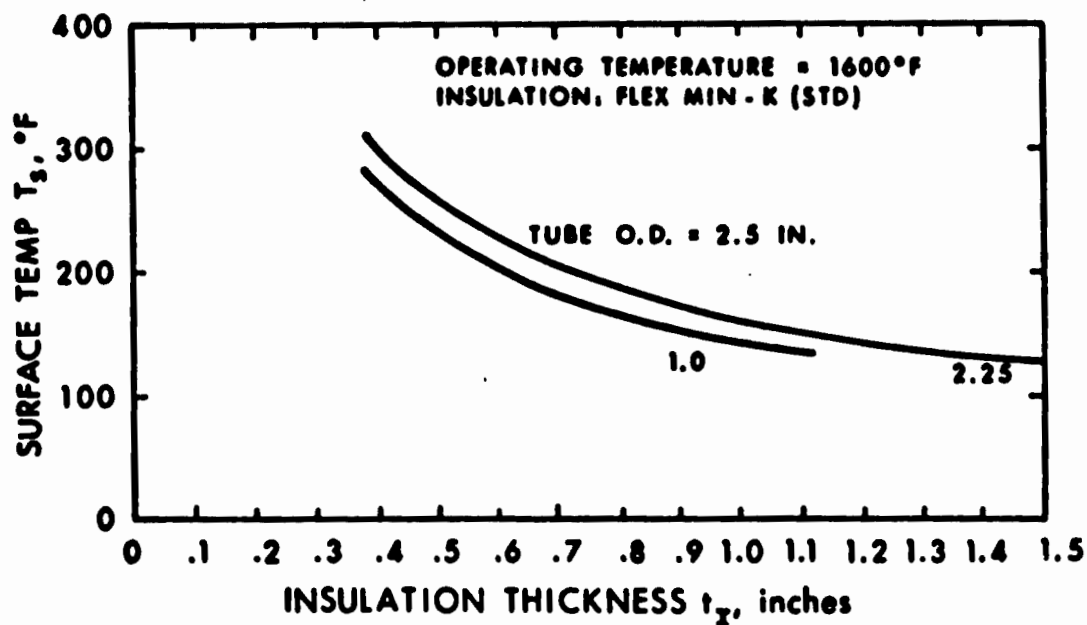


Figure 15. Internal Gas Reservoir Length versus Temperature Difference for Primary Heat Pipe Startup

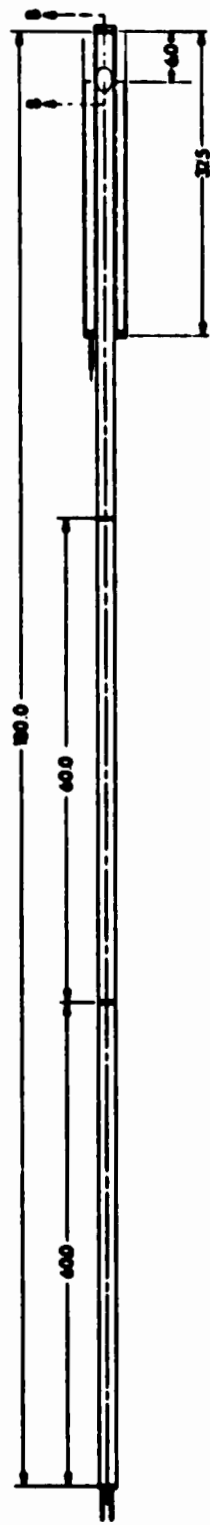


(a) Heat Losses



(b) Surface Temperatures

Figure 16. Primary Heat Pipe Heat Losses and Surface Temperatures



37

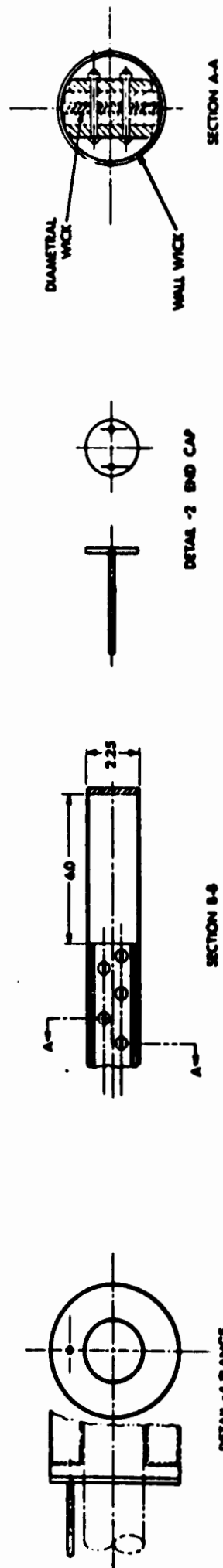


Figure 17. Primary Heat Pipe

Thermal Energy Storage System is located 37.5 inches from the condenser end. The evaporator end is closed with an end cap which is provided with two fill tubes. A double wrap of 60 mesh nickel screen is placed around the inner circumference of each 5-foot tube section. The diametral wick structure is built up from 94 layers of folded 38 mesh Inconel bolting cloth. A 0.1-inch thick 60 mesh (10 layers) nickel screen (the "wet finger") is located along the core of the diametral wick. The diametral wick is held together by Inconel 600 bolts between two 0.025-inch Inconel straps. A 2-foot long by 0.001-inch thick zirconium foil is located in a center fold at the evaporator end of the diametral wick structure to serve as an oxygen getter.

Several manufacturing concepts were evaluated which are briefly reviewed. Key manufacturing design and developmental areas included:

- a. Method of wick forming and manufacture
- b. Use of mitre or bent wicks and tubes for effecting the heat pipe offset required in the spacecraft
- c. Modular concepts
- d. Wick installation methods
- e. Wick support methods

Clearly, a strong interplay between each of the above exists in evolving the final hardware design. Though the 15-foot heat pipe design in this phase embodied certain simplifying features, which an ultimate thermal train subsystem heat pipe will not permit, it provided a mechanism for establishing the appropriate full-scale hardware manufacturing technology. Further, it provided a test unit which can ultimately be used to perform testing on a long, high-powered liquid metal heat pipe with a thermal energy storage unit.

3.3.1 WICK FORMING AND MANUFACTURE

Only two forms of wick materials appeared practical for a 15-foot wick system, screen materials and porous metal felts. Both require extensive shaping or lay-up to achieve the final wick dimensional cross sections. From the screen material, long sheets or strips must be formed or cut by stamping or die operations. Metal felts might possibly be fabricated to achieve a final cross section during manufacture; an alternate consists of laying up strips. With either screen or felt materials, the cross-section will be partially dictated by the manufacturing method selected and the design solution to off-setting the evaporator from the condenser. Metal felts were not available in the length or material of interest. Likewise bias-cut screen was limited to 48-inch wide stock. Thus, the approach concentrated on was wick design which could be formed from 15-foot wide screen material and thus avoid joints in the wick structure.

Both bolting cloth and conventional screen weaves were found available in stainless steel, nickel, and Inconel materials.

Several practice methods of lay-up were performed with screens to establish forming methods. Cutting or die operations were found unnecessary when folding methods were demonstrated to be consistent with both handling and tolerance requirements. Diametral-type folded structures were capable of conforming to 60-degree bend dimensions prior to tightening of connectors holding the structure together (see Figure 18).

3.3.2 OFFSET

The pipe and wick structure can be offset by joints or by bending. Bending appeared attractive in contrast to joints only in that it reduced the number of welds required on the pipe itself. Bending of the pipe presumes the wick structure can be designed and fabricated in such a manner as to permit bending of the thick wicks. These wick designs had previously involved use of bias-cut screen and/or placement of the wick structure along the neutral bend axis. The entire wick structure would be fabricated prior to installation in the heat pipe tube and the bending operation.

Joints would allow both shorter sections of pipe and wick structure to be independently fabricated. However, a design permitting the joining of the wick structure as well as the pipe would be required. A significant development effort would be required for developing a method of wick connection.

Development of a method for forming long diametral wick structures, which would conform to 60-degree offset bends, leads to examination of a means for providing the tube offset. It was found that Inconel tubes of the size of interest (short of a mill run) were available only as rolled, welded, and drawn tubes of 6-foot lengths. This suggested the use of elbows which would allow transition between straight sections and permit easy installation of the wick. As shown in Figure 19, demonstration tube bends of 2-inch o.d. stainless steel were made. The contemplated design called for axial slitting the bent tube sections to form a split elbow to be placed over the wick structure already installed into straight tube sections.

3.3.3 WICK INSTALLATION AND SUPPORT

Wick installation involved insertion of a single continuous preformed wick structure into the tubing. Furthermore, the wick design complexity and its method of support were expected to strongly interact with the wick installation method.

Wick support methods which were considered included continuous or semi-continuous radial rails and structural skins or direct contact between the wick material and the tube wall. Either the tube wall itself must



Figure 18. Demonstration Diametral Wick



Figure 19. Demonstration Elbow Sections

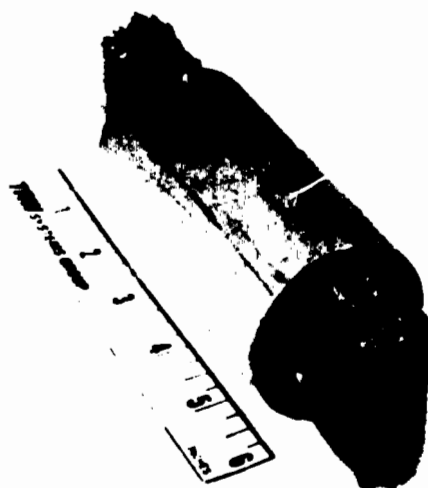


Figure 20. Demonstration Section Installed Wick

006559

be deformed to provide a final interference or the wick structure must provide a method of locking the support(s) in place. Where bends occur, methods different from those used in straight sections were considered. These included:

- a. Warping the tube along one axis and installing the wick structure to effect an interference fit upon release of the tube
- b. Drawing the tube over the wick structure to reduce the tube diameter
- c. Some form of eccentric design which would lock the wick in place upon rotation

The final method selected for the installation of the fully formed 15-foot long diametral wick was to compression warp the individual 5-foot tube sections normal to the diametral dimension to allow drawing the structure through the tube. Release of the tube compression provided an interference fit (see Figure 20) to establish both the structural support and capillary communication with the wall wick. Both drawing or lock designs involved disadvantages, the first in contamination and the latter in complexity.

3.4 HARDWARE BUILD-UP

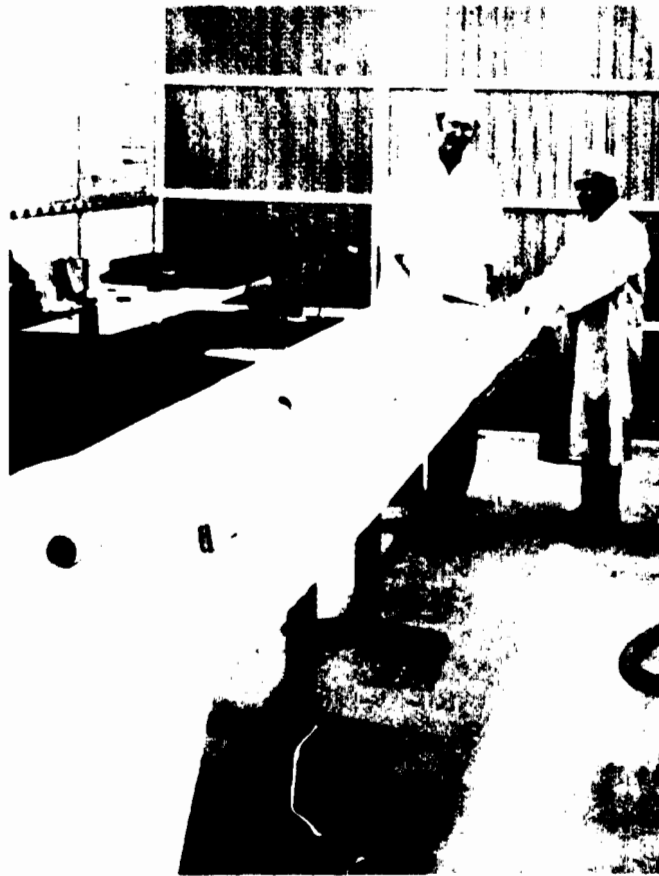
In addition to the physical structure of the heat pipe itself, a number of elements supporting the hardware build-up for process and fill, and ultimate testing were incorporated. These are summarized in Table IV and described in the assembly sequence.

All parts were fabricated according to print. Final cleaning of the parts prior to assembly was per TRW Specification PR-2-2K, level 1. Cleaning of the tube sections both prior to and following installation of the circumferential wick was made. The diametral wick structure was final-cleaned prior to installation and tightening of the Inconel bolts. Figure 21 shows the major parts prior to assembly. Installation of the diametral wick was effected by compression of the individual 5-foot tube sections to allow drawing the wick structure through the tube. The end caps, TES flange, and tube girt joints were inert gas welded. All welds were dye penetrant and x-ray inspected. Following addition of two Nupro high temperature valves (SS4-TW-STE-HT) to the fill tubes, the structure was helium leak checked.

The unit was then prepared for process and fill by addition of thermocouple instrumentation, start-up and process heaters, and insulation. Twelve thermocouples were attached along the 15-foot length using Inconel tabs spot-welded to the tube wall. The sensing tips were torch brazed to the tube wall using 82-Au-18-Ni braze. The sensing points were located on the vapor core 90 degrees from the diametral wick axis, alternating

TABLE IV
FIFTEEN-FOOT HEAT PIPE
BILL OF MATERIALS

<u>Item</u>	<u>Type/Size</u>	<u>Material</u>
Diametral Wick	38-mesh bolting cloth 0.0065 inch wire diameter	Inconel 600
Wet Finger and Circumferential Wick	60-mesh screen 0.007 inch wire diameter	Nickel 200
Diametral Wick Retainer	Sheet 0.025 inch thick	Inconel 600
Diametral Wick Connectors	6-32 NC round head screw and nut	Inconel 600
Getter	Foil 0.001 inch thick	Zirconium
Tube	2.250 inch o.d. by 0.063 inch wall	Inconel 600
End Caps and Flange	Sheet 0.250 inch thick	Inconel 600
Fill Tubes	0.250 inch o.d. by 0.035 inch wall	Inconel 600
Heat Pipe Fluid	Bulk	MSA High Purity Sodium
Start and Processing Heaters	Semicylindrical heaters Model 50242, Type 2718-KSP	Lindberg Hevi Duty
Thermocouples	CR-A1 1063K6E, CR-A1 1063K12E	Sheathed Inconel 600
Braze Material	Rod	82%Au-18%Ni
Valves	Nupro SS-4TG	Satellite Tip
Insulation	Sheet 36 by 36 by 3/8 72 by 36 by 3/8	J-M Flex-Min-K



006560

Figure 21. Fifteen Foot Heat Pipe Parts

from side-to-side. Thermocouple 1 which was located at the evaporator end and thermocouple 12 which was located at the condenser end were removed prior to testing. Thermocouples 2 through 11 were located along the adiabatic section which extended 2 feet from the evaporator end to the TES flange. Ten 1200-watt half cylinder heaters (Lindberg Model 50242 Type 2718-KSP, each 18 inches in length) were placed along the bottom half of the heat pipe. Two units at the condenser end and two units at the evaporator end were removed prior to testing. A triple wrap of 3/8-inch J-M Flex-Min-K insulation was added all along the tube.

Circumferential joints in the insulation were made at the TES flange and 2 feet from the evaporator end to effect later reconfigurations with minimum insulation impact. Figures 22 through 28 show the unit at various stages of preparation and fill.

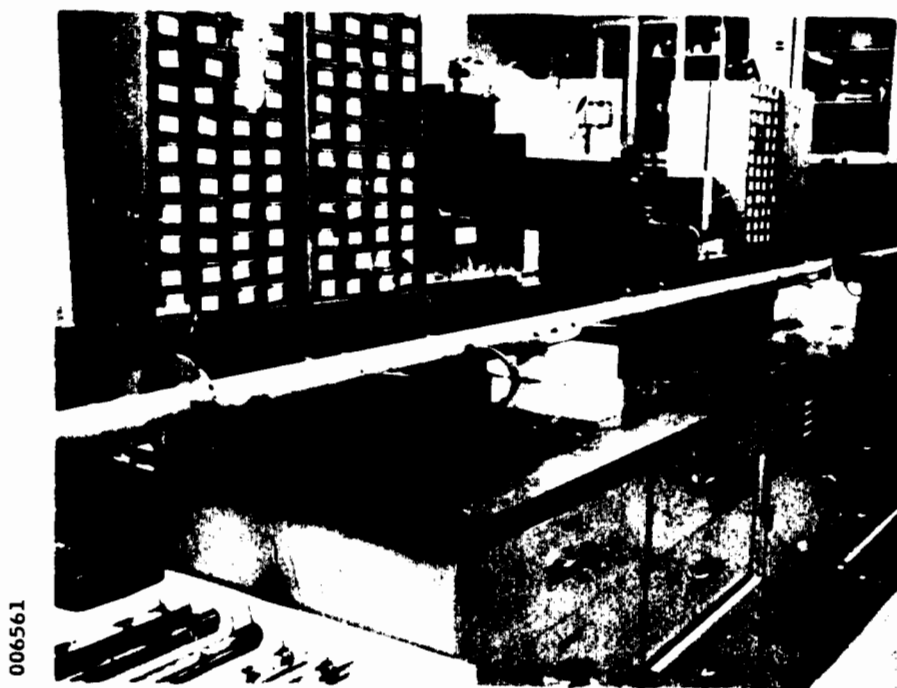
Figure 22 views the unit from the evaporator end and shows the thermocouples along the heat pipe structure. Figure 23 is from the TES flange looking toward the evaporator. Figure 24 is from the condenser end and shows the balance used to weigh the structure. The dry unit (no sodium fill) with valves and thermocouples weighed 64.75 pounds. In Figure 25, heaters and insulation have been added forward of the TES flange. Figure 26 shows the two heaters mounted on the condenser and Figure 27 shows completion of the insulation. The unit ready for sodium fill following vacuum bake-out is shown in Figure 28.

The weight of the system including heaters and insulation was 122.93 pounds, the major contribution coming from the heaters. Prior to fill, the unit was thermal vacuum baked as a preconditioning step for cleaning the internal surfaces. Vacuum was established by manifolding the two fill valves to a liquid nitrogen trapped oil diffusion pumped vacuum system. Upon heat-up, using the processing heaters, significant outgassing occurred at 600°F which took several hours to eliminate. The temperature was then raised to 1200° and held for several hours without further evidence of any significant degassing. After connection to the fill system, 8.5 pounds of sodium was transferred into the pipe from a primary sodium source. The fill was accomplished at 300°F using argon as a drive gas to move the sodium. The initial transfer was to a secondary reservoir which was volumetrically calibrated. The sodium was subsequently transferred into the pipe from the secondary volume.

The pipe was operated in the reflux mode using the integral heaters to self-process the pipe. Initial venting to vacuum while cold and subsequent burping to vacuum at temperature removed the residual drive gas (argon). Self-processing up to 1500°F was imposed.



Figure 22. Fifteen Foot Thermal Train Heat Pipe -
View Toward Condenser



006561

Figure 23. Fifteen Foot Thermal Train Heat Pipe -
View Toward Evaporator

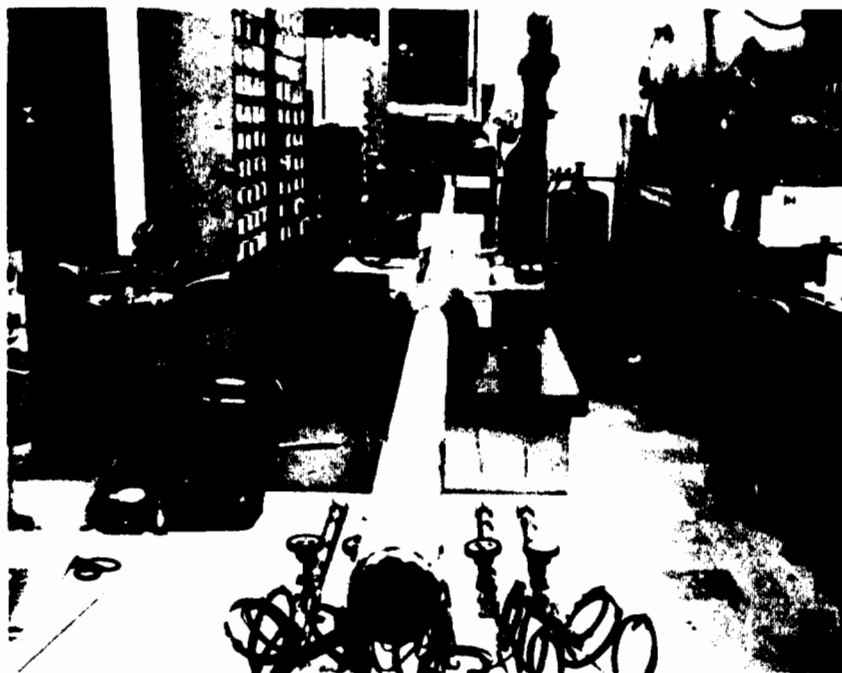


Figure 24. Fifteen Foot Primary Heat Pipe -
Condenser End with TES Flange

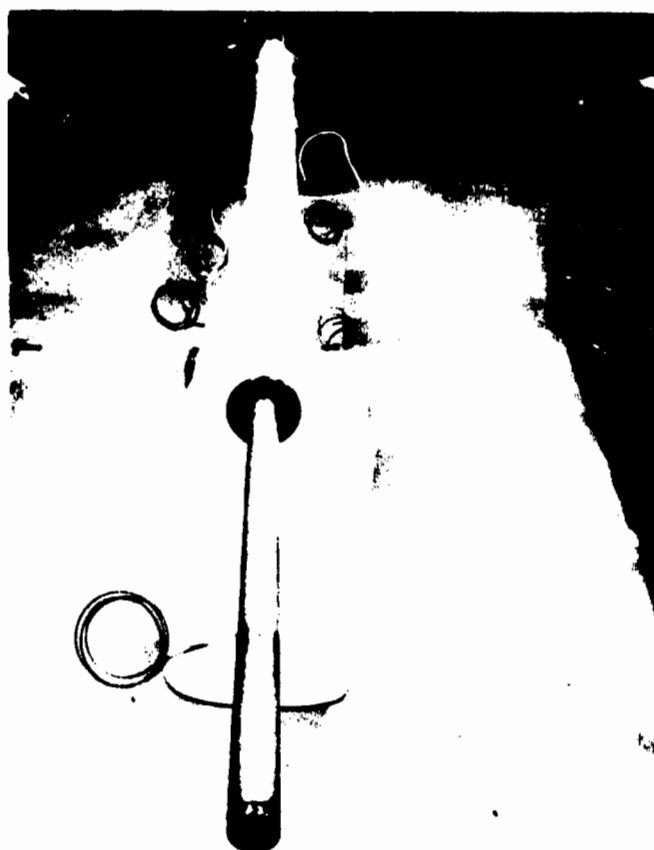


Figure 25. Primary Heat Pipe Following Addition of
Heaters and Insulation Forward of TES
Flange

006562



Figure 27. Primary Pipe with Axial Insulation Completed

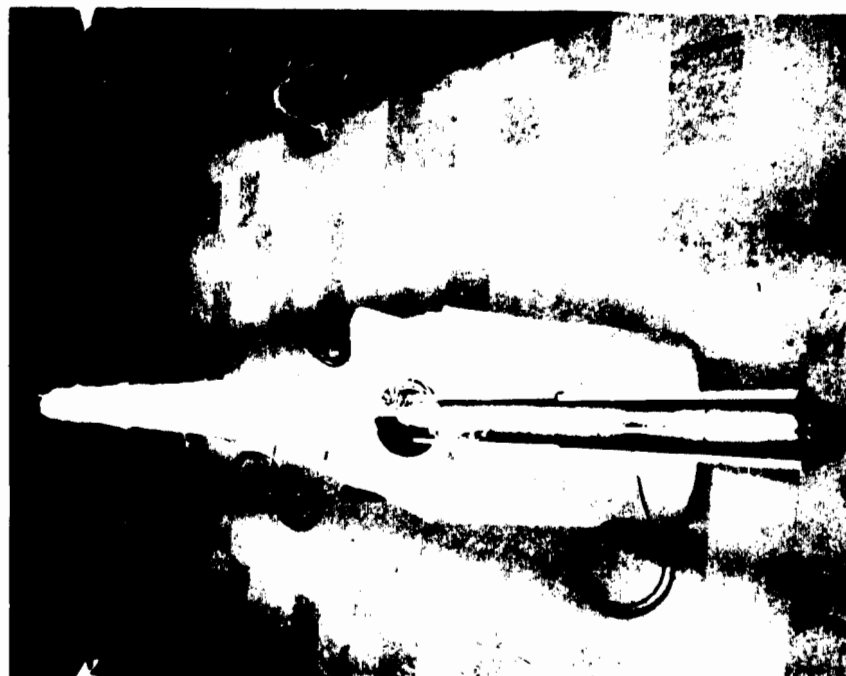


Figure 26. Primary Pipe with Temporary Processing Heaters on Condenser

00563



Figure 28. Sodium Fill System with Primary Pipe Attached

It was observed that vapor pressure losses did not permit isothermal operation below 1000°F, the steady-state temperature achieved with ≈ 1000 watts input by the two condenser heaters. With 2050 watts applied to these heaters, the pipe was isothermal above 1000°F and equilibrated around 1500°F. These results indicated that the insulation design performed as expected. The ≈ 1.5 -inch axial length increase due to thermal expansion is readily apparent at temperature.

With the fill completed the primary heat pipe was ready for steady-state heat transfer tests and transient start-up studies. Use of an inert gas to assist in start-up was to be evaluated. Initial testing was to be performed with a 24-inch long evaporator using an 8 kW heater. This evaporator length was consistent with the design analysis of Table III and Figures 14 and 29. The steady-state performance limits for the wick design of Figure 14 as function of evaporator flux were analyzed (see Figure 29). It can be seen that the heat pipe capacity decreases rapidly with increasing evaporator flux.

The calculated hydrodynamic performance limits shown in Figures 14 and 29 considered no benefit from the arterial passage ways which existed between the diametral wick and tube wall. The calculated inventory to satisfy the internal void volume required 8.2 pounds of sodium at 1600°F. A modest overfill of 0.3 pound was selected to derive some benefit from fillets. During steady-state heat pipe mode operations, all excess fluid winds up in the condenser, thus offering no real capacity increase (unless the unit is operated as a refluxer). Under serious overfill conditions, significant condenser heat transfer area blockage could occur.

3.5 INITIAL PERFORMANCE TESTING

After filling and processing of the first primary heat pipe, initial performance testing was undertaken by the designers and builders of the heat pipe. The tests were to confirm the power transfer capability of 6 kW at 1600°F, and to optimize the inert gas fill for start-up of the heat pipe from the frozen state. Methods of transient start-up that were investigated included:

- Start-up with reduced power input, i.e., ≤ 2 kW
 - Use of supplemental heaters along the adiabatic section of the heat pipe
 - Use of an inert gas to control the rate of vapor front growth during the start-up transient.
-

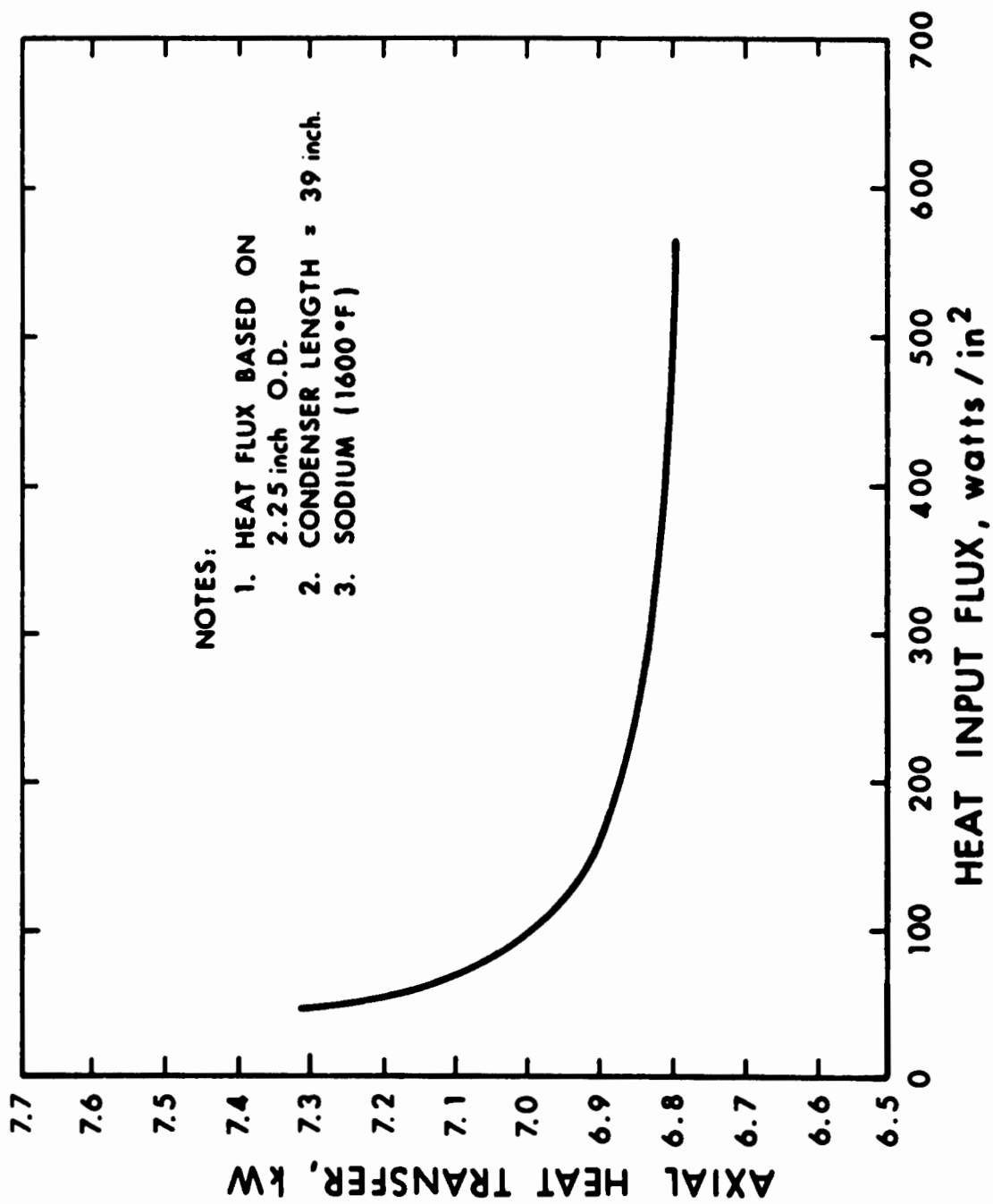


Figure 29. Primary Heat Pipe Evaporator Flux versus Heat Transfer Capacity

3.5.1 TEST SETUP

The objective of the initial testing, on the 15-foot primary heat pipe of the EOS Thermal Train Subsystem, was to determine the heat pipe power transfer capability, along with transient tests to establish the heat pipe start-up capability.

The tests were performed at TRW in the ATD Heat Pipe Laboratory, Building R1, Room 2015. The laboratory environment was maintained at $75 \pm 5^\circ\text{F}$, with the test specimen heavily insulated to limit heat loss to the surrounding environment. Cooling capability for the specimen was provided from the laboratory water supply at $70 \pm 10^\circ\text{F}$.

3.5.2 HEAT PIPE

The heat pipe is divided into three sections (see Figure 30). The evaporatory (24 inches in length), the condenser (37.5 inches in length) and the adiabatic section (118.5 inches in length). For testing ni-chrome heaters were located along the evaporator and the adiabatic sections and were insulated with J-M Flex-Min-K insulation. A water calorimeter was located at the condenser section to remove and measure the power that was transferred by the heat pipe.

3.5.3 TEST INSTRUMENTATION, READOUT EQUIPMENT, AND TEST SUPPORT HARDWARE

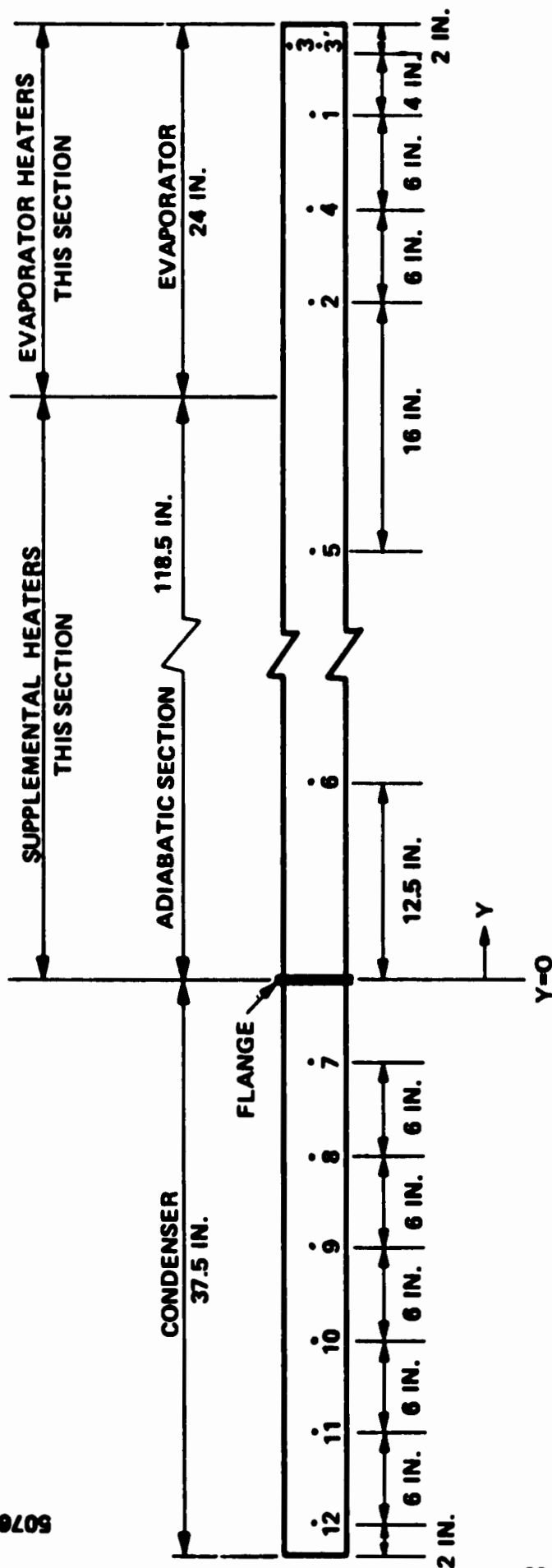
The following test instrumentation and readout equipment were employed:

a. Thermocouples

- (1) #1063K12E and #1063K16E chromel-alumel thermocouples sheathed with Inconel 600: 12 required and located as shown in Figure 31 Thermocouples #1 through #12.
- (2) Copper constantan thermocouples: 3 required and located as shown in Figure 30, Thermocouples #13 through #15
- (3) Claude S. Gordon copper constantan grounded sheathed thermocouples (0.063 inch sheath diameter) and fittings for measuring coolant temperature. Minimum immersion depth of 2 to 3 inches: 4 required as shown in Figure 30, Thermocouples #16 through #19.



Figure 30. Heat Pipe Test Installation and Instrumentation



NOTES:

- NUMERICAL I. D.'S ON HEAT PIPE CORRESPOND TO RECORDER & DATA SHEET THERMOCOUPLE I. D. NUMBERS
- T.C. NO.'S 1 AND 2 ARE LOCATED ON THE EVAPORATOR HEATERS, ALL OTHER THERMOCOUPLES ARE LOCATED ON THE HEAT PIPE. I. D. NO.3' IS LOCATION OF THE HIGH TEMPERATURE CUTOFF DEVICE THERMOCOUPLE
- HEAT PIPE THERMOCOUPLES ARE LOCATED CIRCUMFERENTIALLY AS FOLLOWS

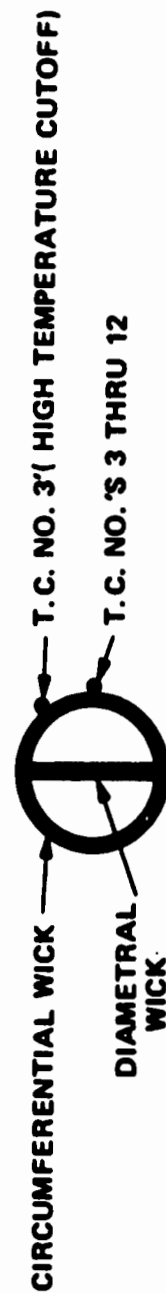


Figure 31. Location of Primary Heat Pipe Thermocouples and Heaters

b. Electrical Heaters

- (1) Evaporator: Five (5) 48-inch long, 2100 watt VULCAN ni-chrome heaters sheathed in Inconel, rated at 120 volts and 20 amps.
- (2) Adiabatic section (supplemental heaters): Six (6) 15-inch long, 1200-watt Lindberg Heavy Duty Ni-Chrome half cylinder heaters, Model #50242, Type 2718-KSP. Heaters are placed along bottom half of heat pipe.

c. Heater Power Sources

- (1) Evaporator heater circuit: Five (5) 110 volt, 20 ampere variacs.
- (2) Supplemental heater circuit: 3-phase balanced circuit with 120 volt, 12 ampere variac.

d. Temperature Control

- (1) Temperature limit on evaporator: Honeywell Versaguard Model #R7161, Type K, 0 - 2000°F range.
- (2) Temperature on calorimeter: Kistler Model #510N 185 A195, opens at 195 ±5°F, closes at 185 ±5°F.

e. Temperature Recording

- (1) One (1) - 12 point chromel-alumel recorder: 100°F to 1800°F range for monitoring thermocouples #1 through #12.
- (2) One (1) - 12 point copper-constantan recorder: 50°F to 200°F range for monitoring thermocouples #13 through #15.
- (3) Speedomax H single point recorder for measuring temperature differential between thermocouples #16 and #18, 2 and 5 mV full scale capability.
- (4) Potentiometer for reading temperature differential between thermocouples #17 and #19 and between thermocouples #16 and #18.

f. Flow Measurement

- (1) Dwyer Rate Master Flowmeter, Model #RMC142SSV, 0.2 to 2.2 gal/min.
- (2) Fischer and Porter Company, Model 10C1505 turbine flow meter.
- (3) Pressure regulator and pressure gauge (100 psi, 5 psi increments).

g. Power Measurement

- (1) One (1) 15 ampere ammeter, (supplemental heaters).
- (2) Five (5) 20 ampere ammeters (evaporator heaters).

3.5 WATER CALORIMETER

The basic design of the water calorimeter which acts as a radiation heat sink is illustrated in Figure 32. The design considers several radiation heat transfer shields with high emissivity surfaces and a single conduction heat shield. The radiation emissivity of the radiation heat shields was to be better than 0.6, and was achieved by the wet hydrogen oxidation process. Depending on the desired total heat transfer, shields with varying amounts of cutouts were used. The conduction heat shield had a 0.375-inch thick layer of J-M-Flex-Min-K insulation. For achieving a broad range of heat transfer while keeping the condenser section of the primary heat pipe at the design temperature under all heat transfer conditions, a total of eight (8) heat shields were to be used as shown in Table V. Thus, the power transfer could be varied by approximately 1.2 kW in the power regime of 5 to 10 kW and by approximately 0.6 kW in the power regime of 1 to 5 kW.

Additional adjustment in the heat transfer, e.g., ≤ 10 percent was to be attainable by adjusting the coolant flow rate.

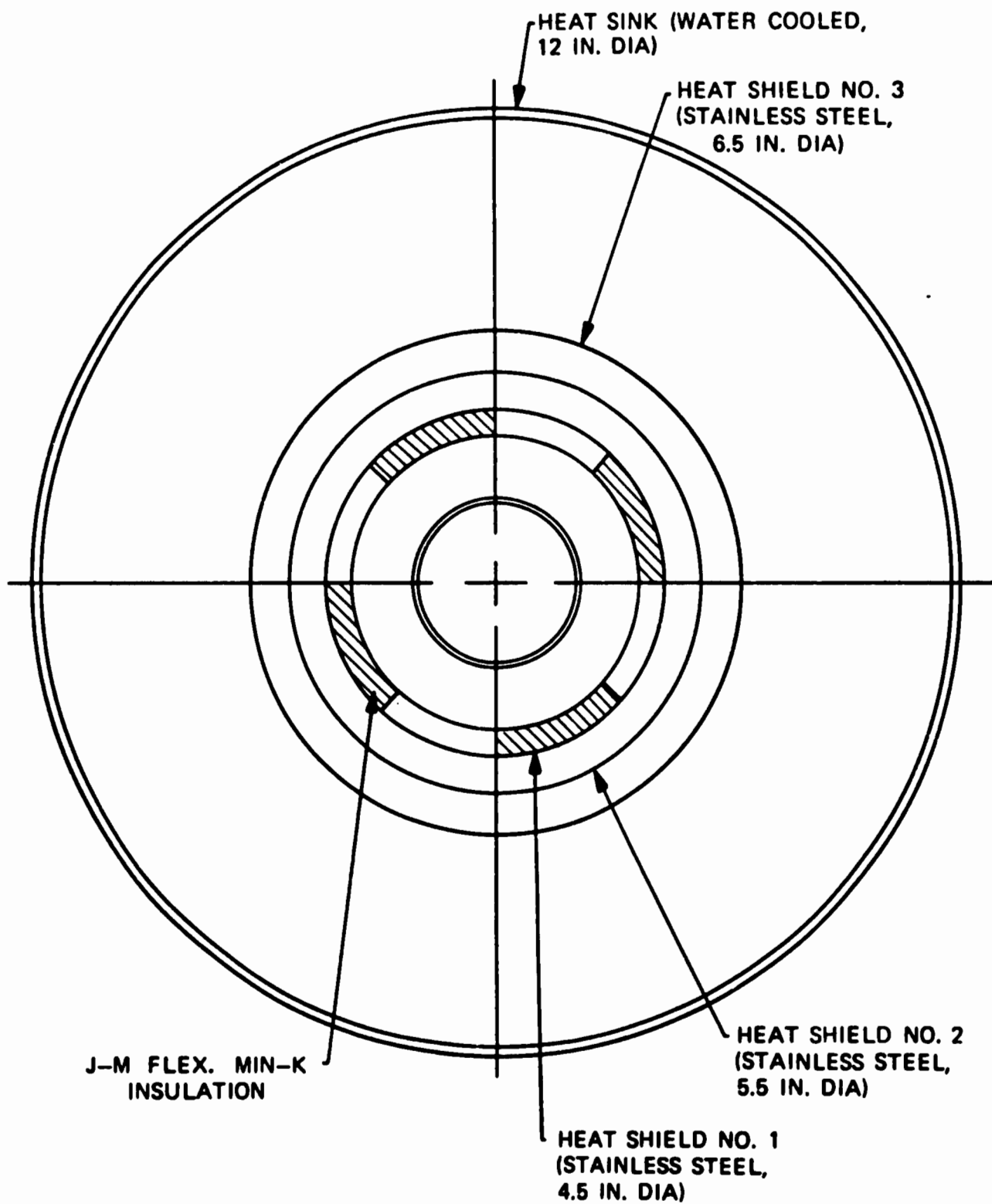


Figure 32. Radiation Heat Sink for Primary Heat Pipe Testing

TABLE V

RADIATION HEAT SINK DESIGN FOR PRIMARY HEAT PIPE TESTING

<u>Radiation Shield (#2 or #3)</u>	<u>Conduction Shield (#1)</u>	<u>Nominal Power (kW)</u>
Neither	No	10.5
#2-1 (80% cutout)	No	9.3
#2-2 (60% cutout)	No	8.1
#2-3 (40% cutout)	No	6.9
#2-4 (20% cutout)	No	5.6
#2-5 (0% cutout)	No	4.4
Neither	Yes	5.2
#2-1	Yes	4.6
#2-2	Yes	4.0
#2-3	Yes	3.4
#2-4	Yes	2.8
#2-5	Yes	2.2
#2-5, #3-1 (50% cutout)	Yes	1.8
#2-5, #3-2 (0% cutout)	Yes	1.3

The condenser end of the heat pipe is shown in Figure 33 with thermocouples installed (spot welded) prior to the installation of the calorimeter. A typical calorimeter radiation shield is shown in Figure 34. The water cooled calorimeter is shown installed in Figure 35. The calorimeter consists of a 12 inch o.d., 0.05-inch wall copper calorimeter shell wrapped with 3/4 o.d. copper cooling coils brazed to the shell. The calorimeter is painted on the inside with Cat-a-lac flat black paint to enhance radiation heat transfer with the heat pipe and with the radiation shields. The completed calorimeter installation is shown in Figure 36. The calorimeter was insulated on the exterior with foam insulation. A removable insulated end cap was installed on the near end of the calorimeter. This cap allowed for easy changing of the calorimeter radiation shields during testing when it was desirable to have a different radiative heat transfer coupling between the heat pipe and the calorimeter copper shell.

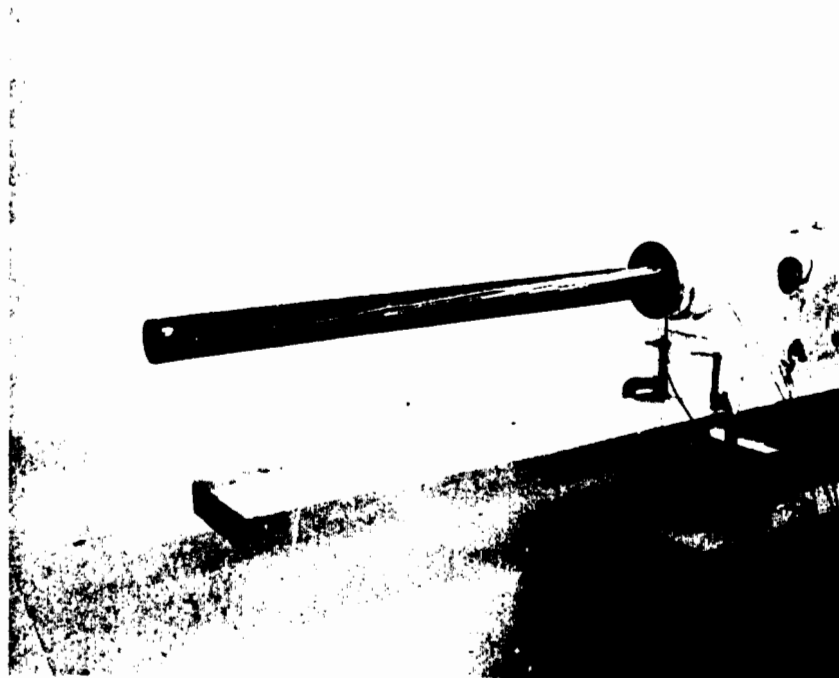


Figure 33. Condenser End of Heat Pipe with Thermocouples Installed

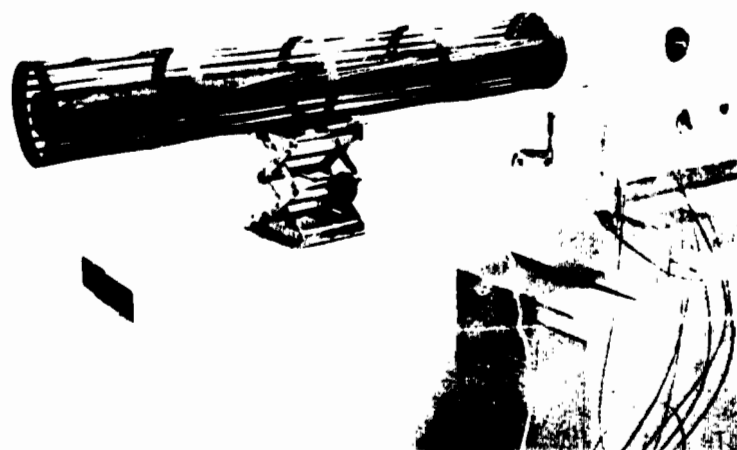


Figure 34. Condenser End of Heat Pipe with a Typical Calorimeter Radiation Shield in Place

007117

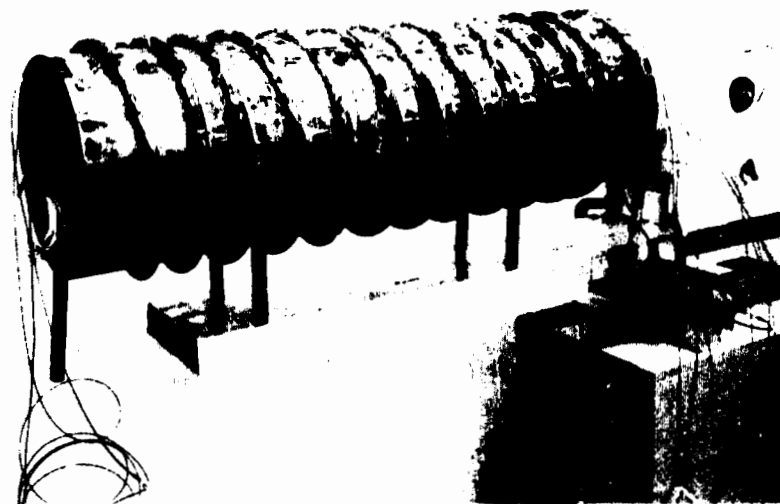


Figure 35. Calorimeter Installed on Condenser
End of Heat Pipe



007118

Figure 36. View of Completely Insulated Calorimeter
and Heat Pipe

The thermocouples for the evaporator heater and the evaporator are shown installed in Figure 37. These thermocouples were spot welded to the heat pipe and the heaters at the specific locations are shown in Figure 31. The evaporator heaters are shown completely installed in Figure 38.

The completed heat pipe assembly with all insulation and test hardware installed is shown in Figure 36. The external readout equipment, temperature recorders, flow meter digital counter, variacs, voltmeter, and ammeters are shown in Figure 39.

3.6.1 TEST RESULTS

The results of the initial tests are summarized in Table VI (start-up tests) and Table VII (axial transport capability tests). The transient temperature data taken are provided in Figures 40 through 50 for the locations shown in Figure 31. The tests provided the following pertinent information:

a. Thermal Time Constant:

The thermal time constant of the system is very large. Approximately 7 hours were required to raise the total heat pipe from room temperature to a temperature sufficiently above the sodium melt temperature (300°F) using ≈ 1.5 kW of heat at the evaporator (refer to Test #7, Figure 46).

b. Transient Start-Up:

- (1) Transient start-up could not be achieved with evaporator power levels of 1.5 and 2.0 kW as indicated in Table VI and in Figures 40 and 42 for Tests #1 and #3. These tests were performed on the heat pipe without the aid of supplemental heat or an inert gas addition.
- (2) Transient start-up was successfully achieved using 3.2 kW* of supplemental power as indicated in Figure 41 for Test #2. This test was performed without inert gas.
- (3) Transient start-up was successfully achieved using an inert gas (1.3×10^{-6} lb-mole of argon) at an evaporator power input of 1.5 kW but not at 2.0 kW (refer to Tests #4 through #8 shown in Figures 43 through 47 and Table VI), when the sodium fill was 8.48 lb. This sodium fill is the calculated required fill at 1600°F (1.3×10^{-6} lb-mole of argon), and would fill the last 6 inches of the condenser at an operating temperature of 1600°F.

*The limit of the supplemental power source was 3.2 kW.

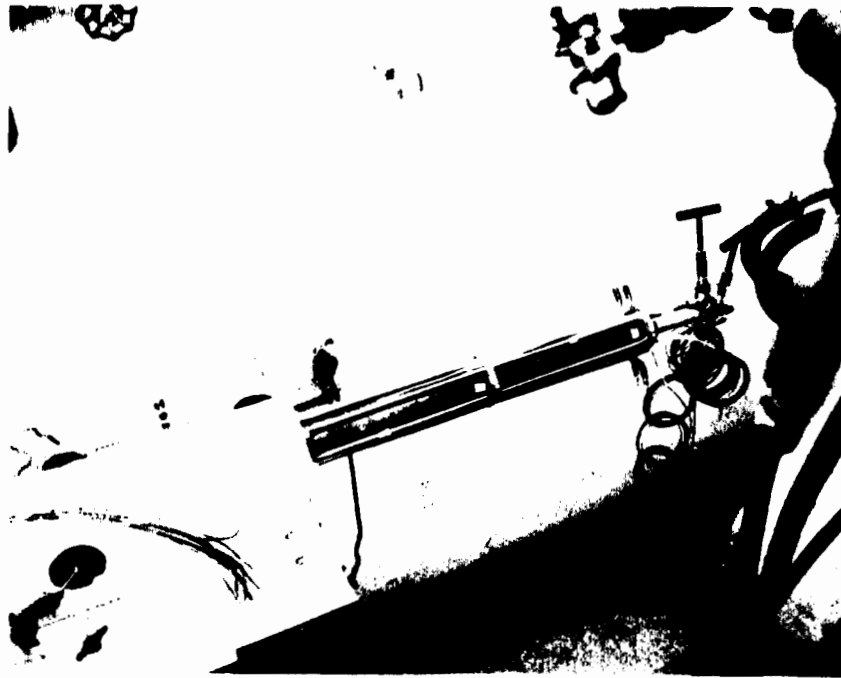


Figure 37. Evaporator End of Heat Pipe with Thermocouples Installed and Heaters Partially Installed

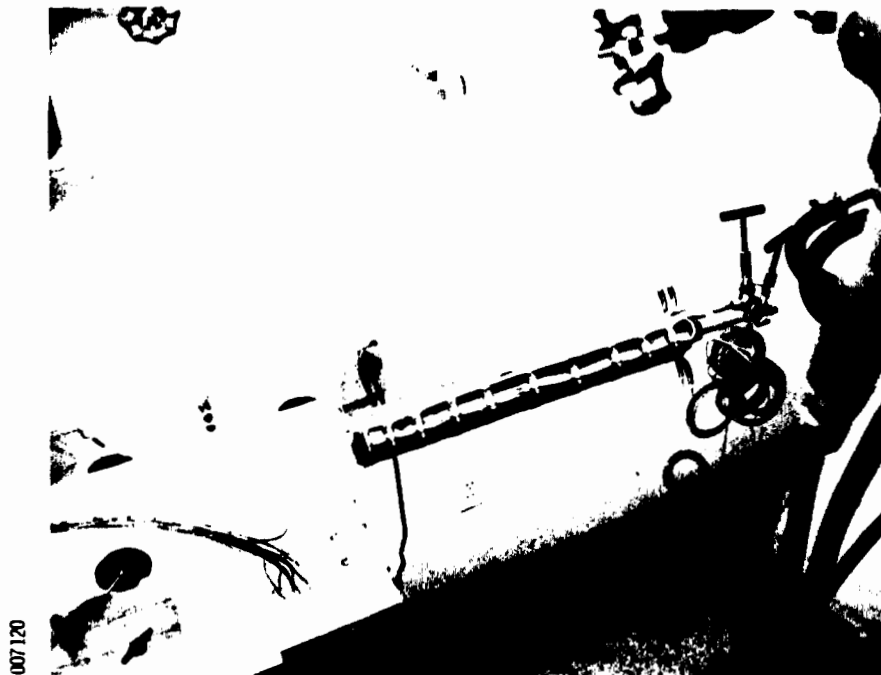


Figure 38. Evaporator End of Heat Pipe with Heaters Installed



Figure 39. Test Support Equipment

TABLE VI

START-UP TEST SUMMARY

TEST #	TYPE OF START-UP		START-UP EVAPORATOR HEATER POWER (KW)	START-UP SUPPLEMENTAL HEATER POWER (KW)	EVAPORATOR ELEVATION (IN)	CALORIMETER STATUS	AMOUNT OF SODIUM (LBS)	AMOUNT OF INERT GAS LB-MOLE	SEE FIGURE #	COMMENTS
	WITH INERT GAS	WITH SUPPL. HEAT								
1	NO	NO	2	0	3/8 (a)	(b)	8.48	0	1	START-UP UNSUCCESSFUL
2	NO	YES	0	3.2	3/8 (a)	(c)	8.48	0	2	SUCCESSFUL START-UP
3	NO	NO	1.0/1.5(d)	0	LEVEL	INSULATED	8.48	0	3	START-UP UNSUCCESSFUL
4	YES	NO	2	0	LEVEL	INSULATED	8.48	1.3×10^{-6}	4	START-UP UNSUCCESSFUL
5	YES	NO	2	0	LEVEL	INSULATED	8.48	1.3×10^{-6}	5	START-UP UNSUCCESSFUL
6	YES	NO	1.5	0	LEVEL	INSULATED	8.48	1.3×10^{-6}	6	SUCCESSFUL START-UP
7	YES	NO	1.5	0	LEVEL	INSULATED	8.48	1.3×10^{-6}	7	SUCCESSFUL START-UP
8	YES	NO	2.0	0	LEVEL	INSULATED	8.48	1.3×10^{-6}	8	START-UP UNSUCCESSFUL
9	YES	NO	2.0	0	LEVEL	(c)	8.67	1.3×10^{-6}	9	START-UP UNSUCCESSFUL
10	YES	NO	2.0	0	LEVEL	(c)	8.85	1.3×10^{-6}	10	SUCCESSFUL START-UP
11	YES	NO	2.17	0	LEVEL	(c)	8.85	1.3×10^{-6}	11	SUCCESSFUL START-UP

(a) EVAPORATOR ELEVATED ABOVE CONDENSER

(b) SET TO DELIVER ≈ 7.5 KW TO CALORIMETER AT $\approx 1525^\circ\text{F}$ (c) SET TO DELIVER ≈ 5 KW TO CALORIMETER AT $\approx 1525^\circ\text{F}$

(d) EVAPORATOR POWER INCREASED TO 1.5 KW AFTER 6 HOURS

TABLE VII
HEAT PIPE AXIAL TRANSPORT CAPABILITY TEST

TEST #	AMOUNT OF SODIUM (LBS)	AMOUNT OF INERT GAS (LB-HOLE)	EVAPORATOR HEATER POWER (KW)	SUPPLEMENTAL HEATER POWER (KW)	EVAPORATOR ELEVATION (IN)	HEAT PIPE TEMPERATURE (°F)	ENERGY DELIVERED TO CALORIMETER (KW)	LOSSES THROUGH INSULATION (KW)	SEE FIGURE #
2	8.48	0	4.9-5.3 (b)	2.2	3/8	1525-1550	4.96	2.14 (c)	2
2	8.48	0	4.9-5.3 (b)	2.2	1/8	1525-1550	4.96	2.14 (c)	2
2	8.48	0	5.3-5.8 (d)	2.2	REFLUX	1525-1550	(e)	(e)	2
9	8.67	1.3x10 ⁻⁶	5.0-5.5 (f)	2.1	LEVEL	1500	4.7	2.4 (g)	9
10	8.85	1.3x10 ⁻⁶	5.0-5.5 (f)	2.1	LEVEL	1500	4.85	2.25 (g)	10

(a) USED AS GUARD HEATERS TO SUPPLEMENT INSULATION LOSSES

(b) BURNDOUT AT 5.3 KW

(c) STEADY STATE DATA BASED ON 4.9 KW AT EVAPORATOR

(d) BURNDOUT AT 5.8 KW

(e) STEADY STATE CONDITIONS NOT ACHIEVED

(f) BURNDOUT AT 5.5 KW

(g) STEADY STATE DATA BASED ON 5.0 KW AT EVAPORATOR

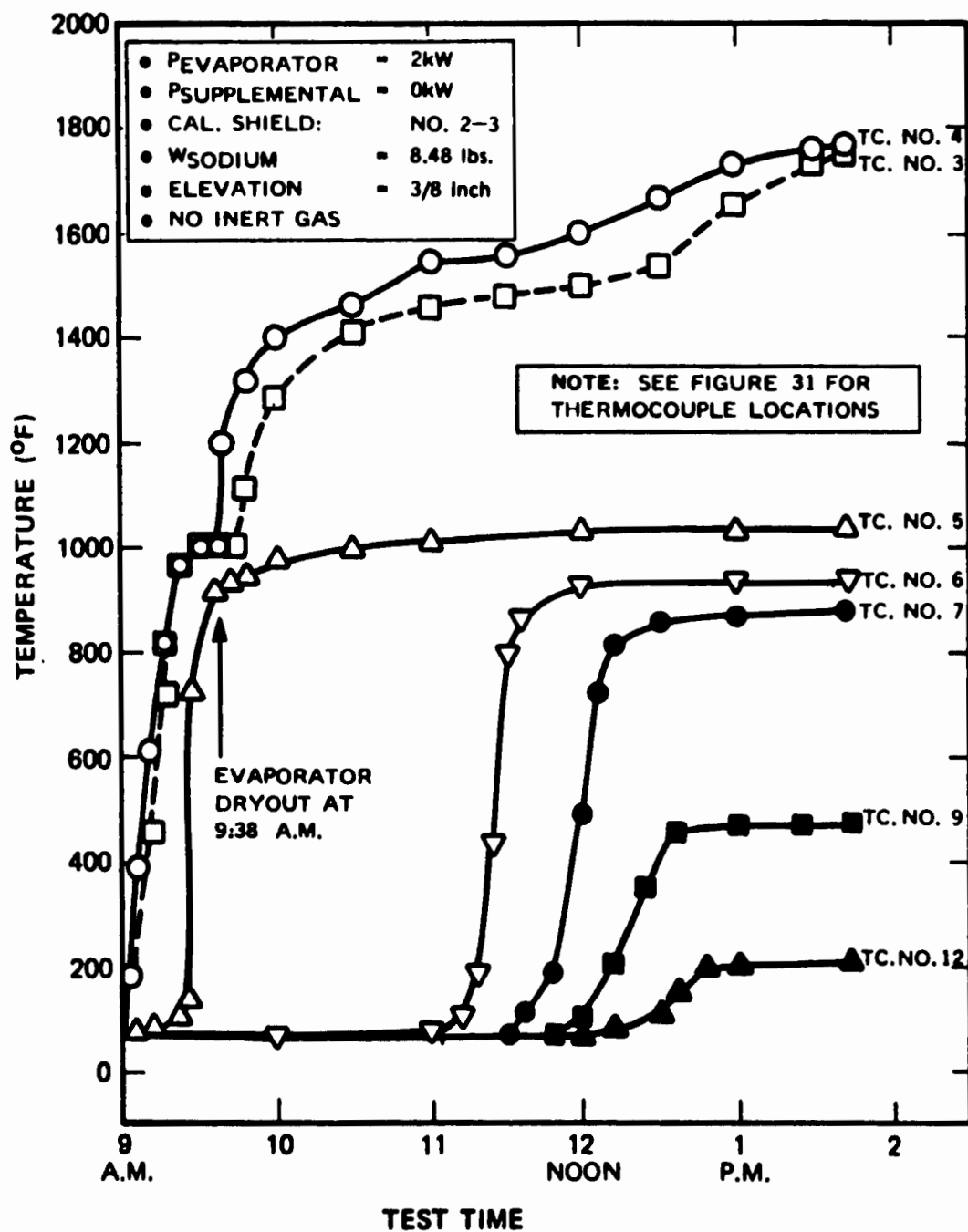


Figure 40. Test #1 (1-11-73) - Transient Startup Without Inert Gas and Supplemental Heaters

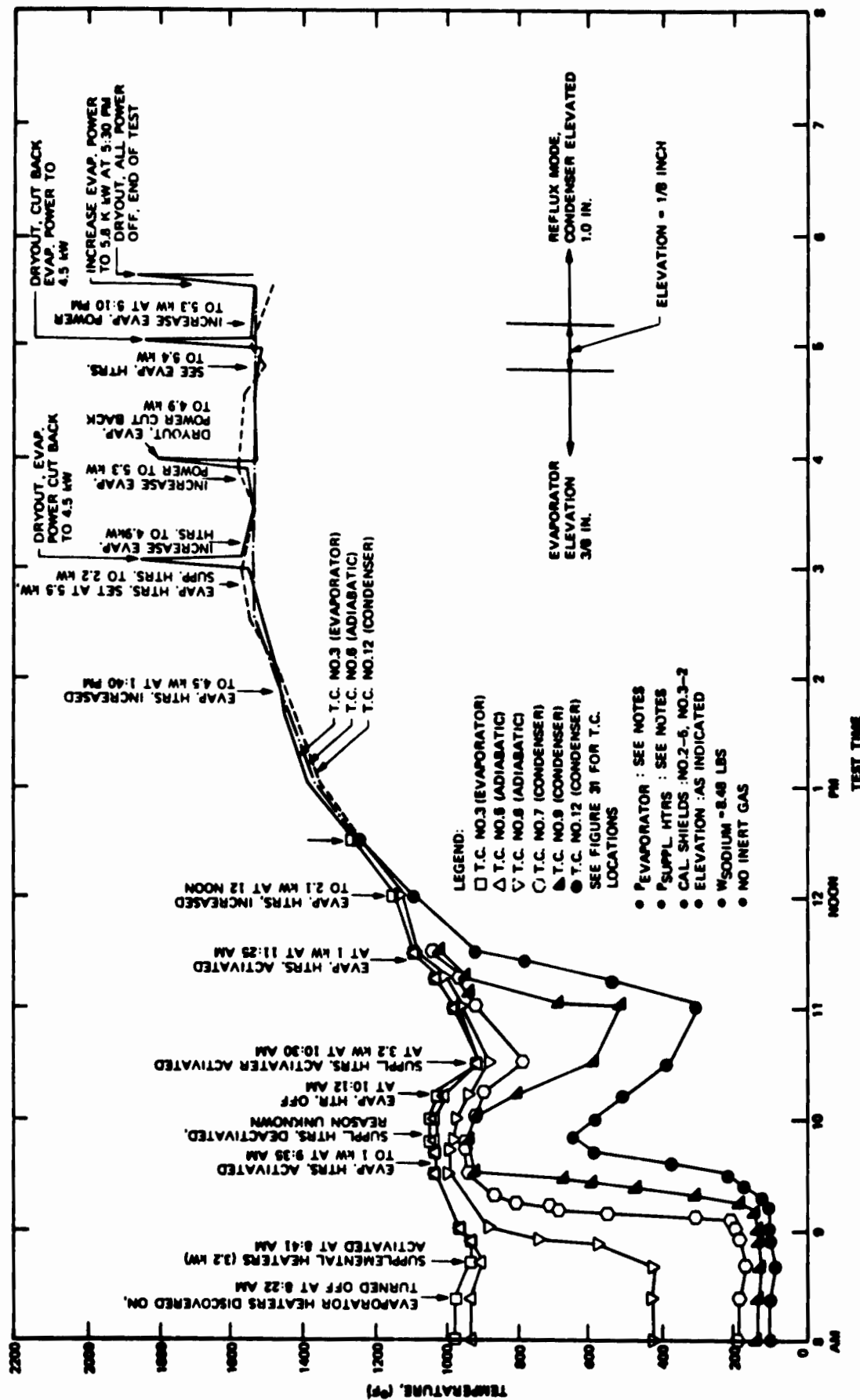


Figure 41. Test #2 (1-12-73) - Transient Startup With Supplemental Heaters and Without Inert Gas

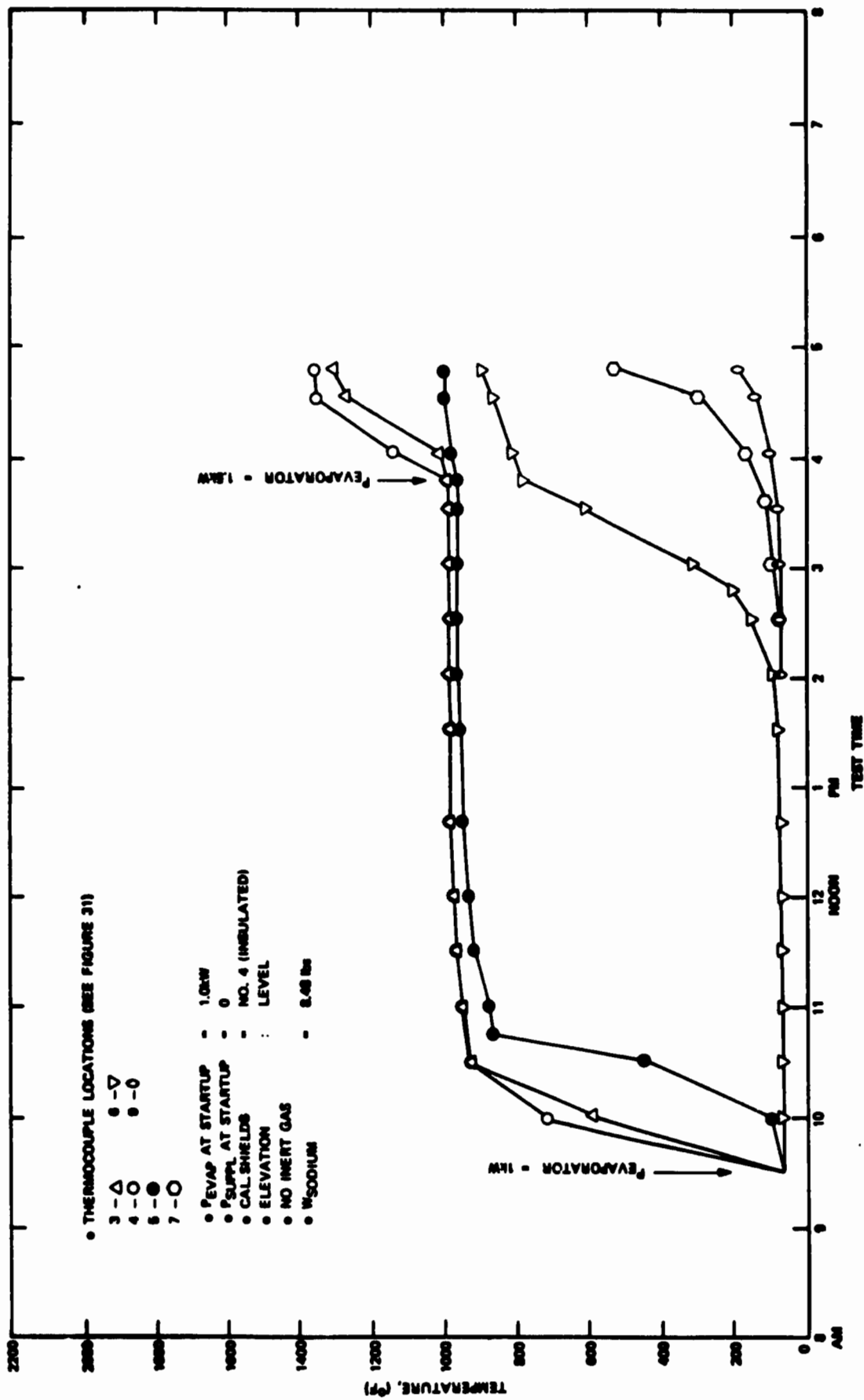


Figure 42. Test #3 (2-16-73) - Transient Startup Without Supplemental Heaters and Inert Gas

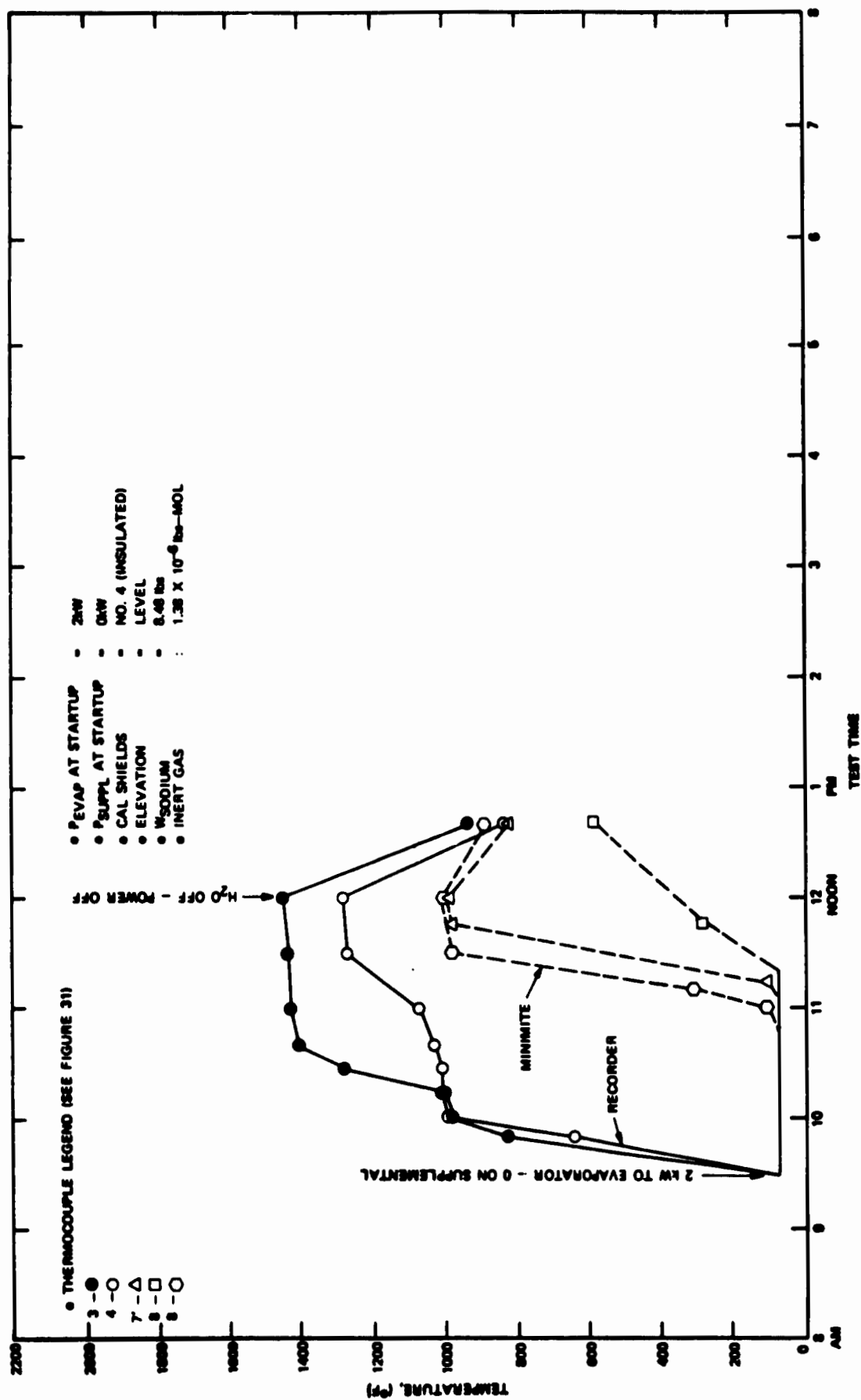


Figure 43. Test #4 (2-21-73) - Transient Startup With Inert Gas and Without Supplemental Heaters

Figure 44. Test #5 (2-21-73) - Transient Startup with Inert Gas and Without Supplemental Heaters

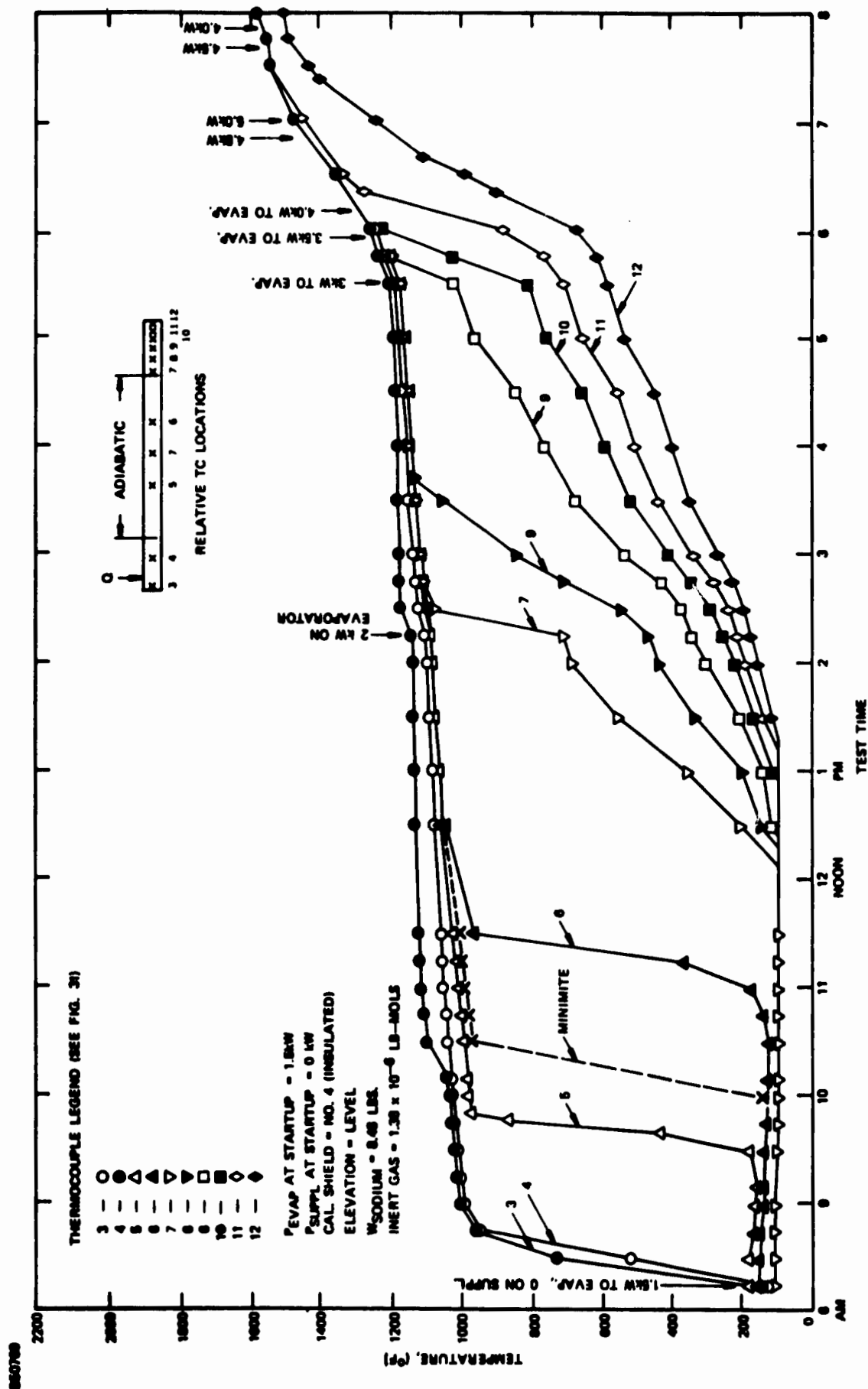


Figure 45. Test #6 (2-23-73) - Transient Startup With Inert Gas and Without Supplemental Heaters

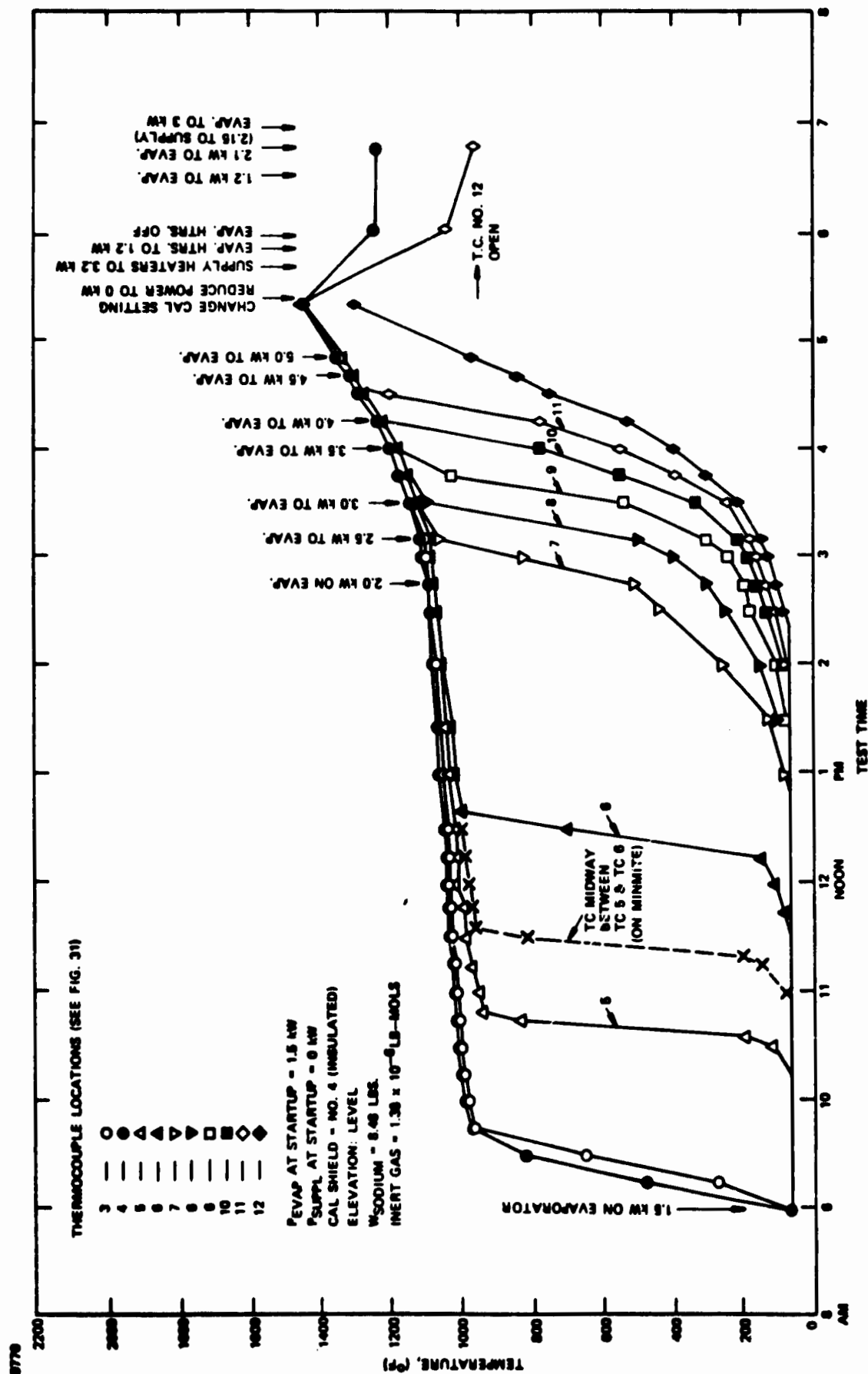


Figure 46. Test #7 (2-26-73) - Transient Startup With Inert Gas and Without Supplemental Heaters

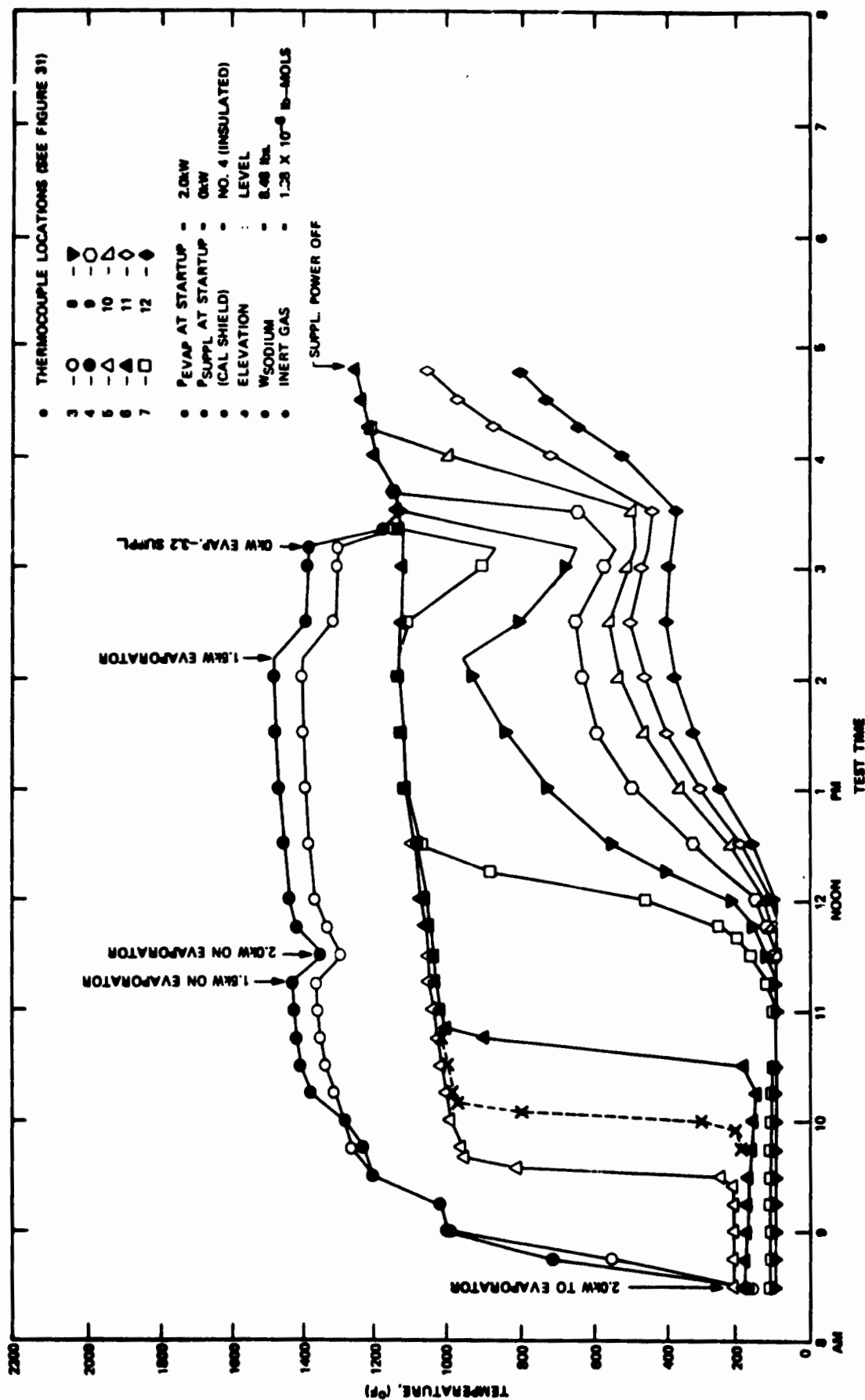


Figure 47. Test #8 (2-27-73) - Transient Startup with Inert Gas and Without Supplemental Heaters

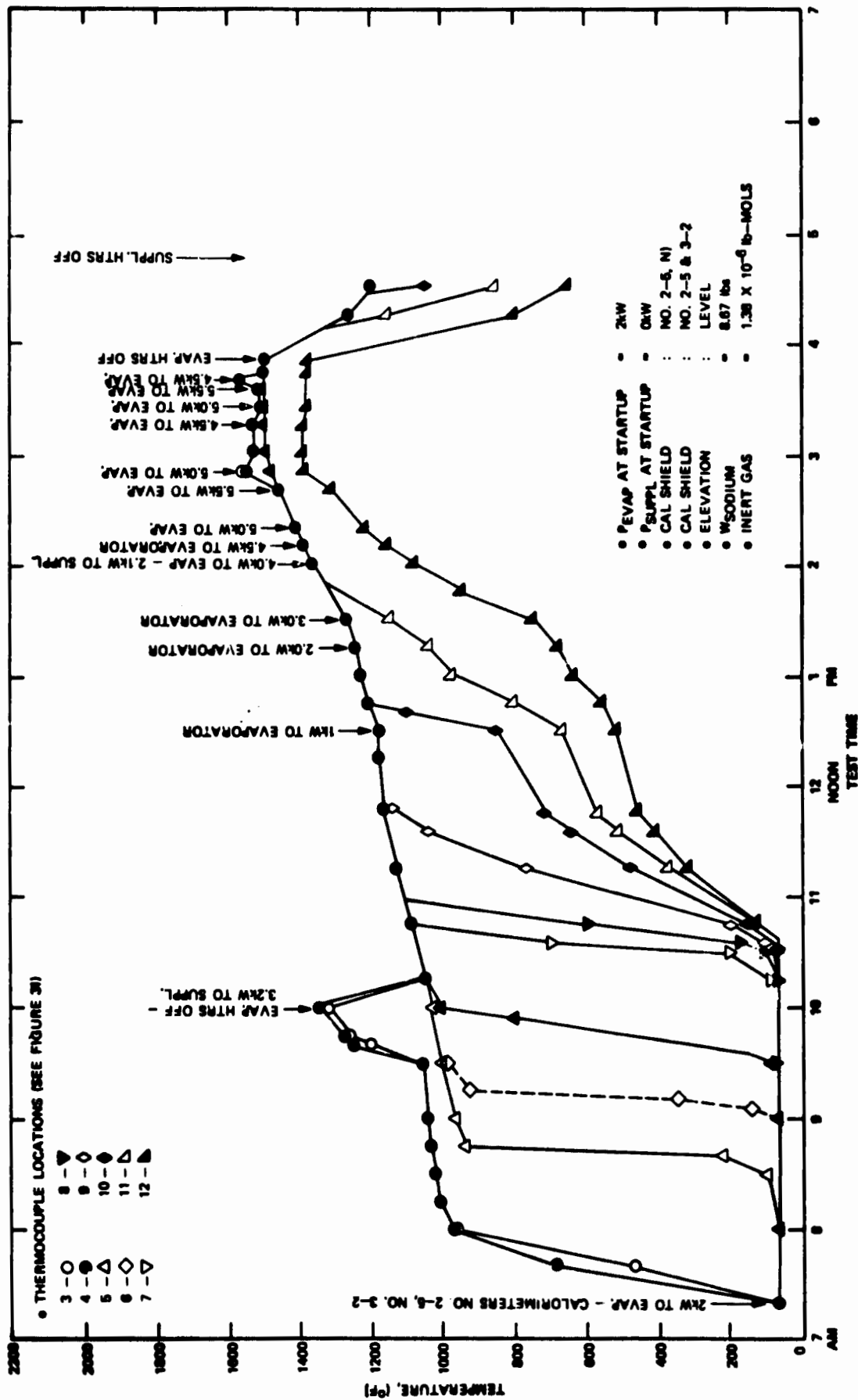


Figure 48. Test #9 (3-6-73) - Transient Startup with Inert Gas and Without Supplemental Heaters

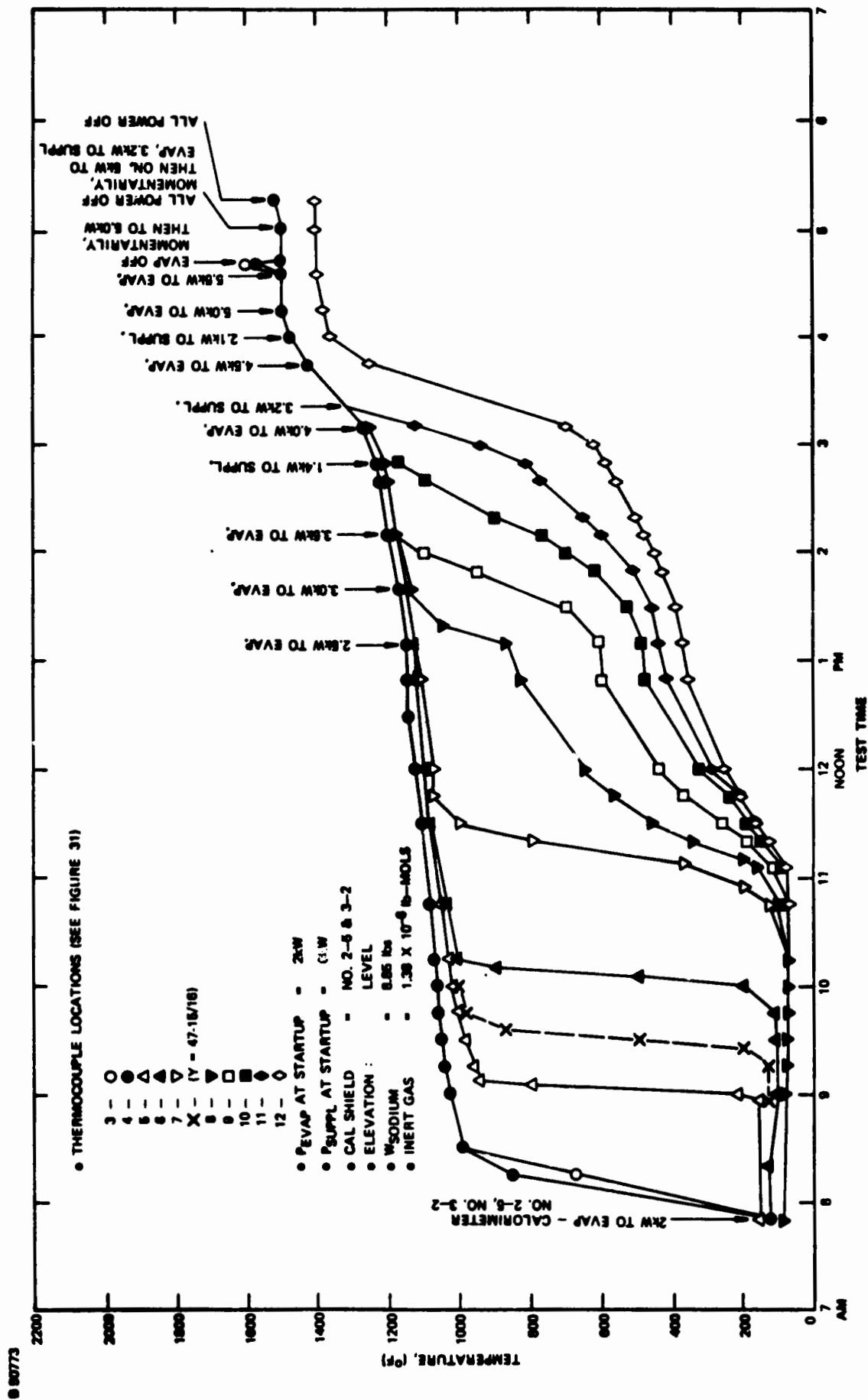


Figure 49. Test #10 (3-7-73) - Transient Startup with Inert Gas and Without Supplemental Heaters

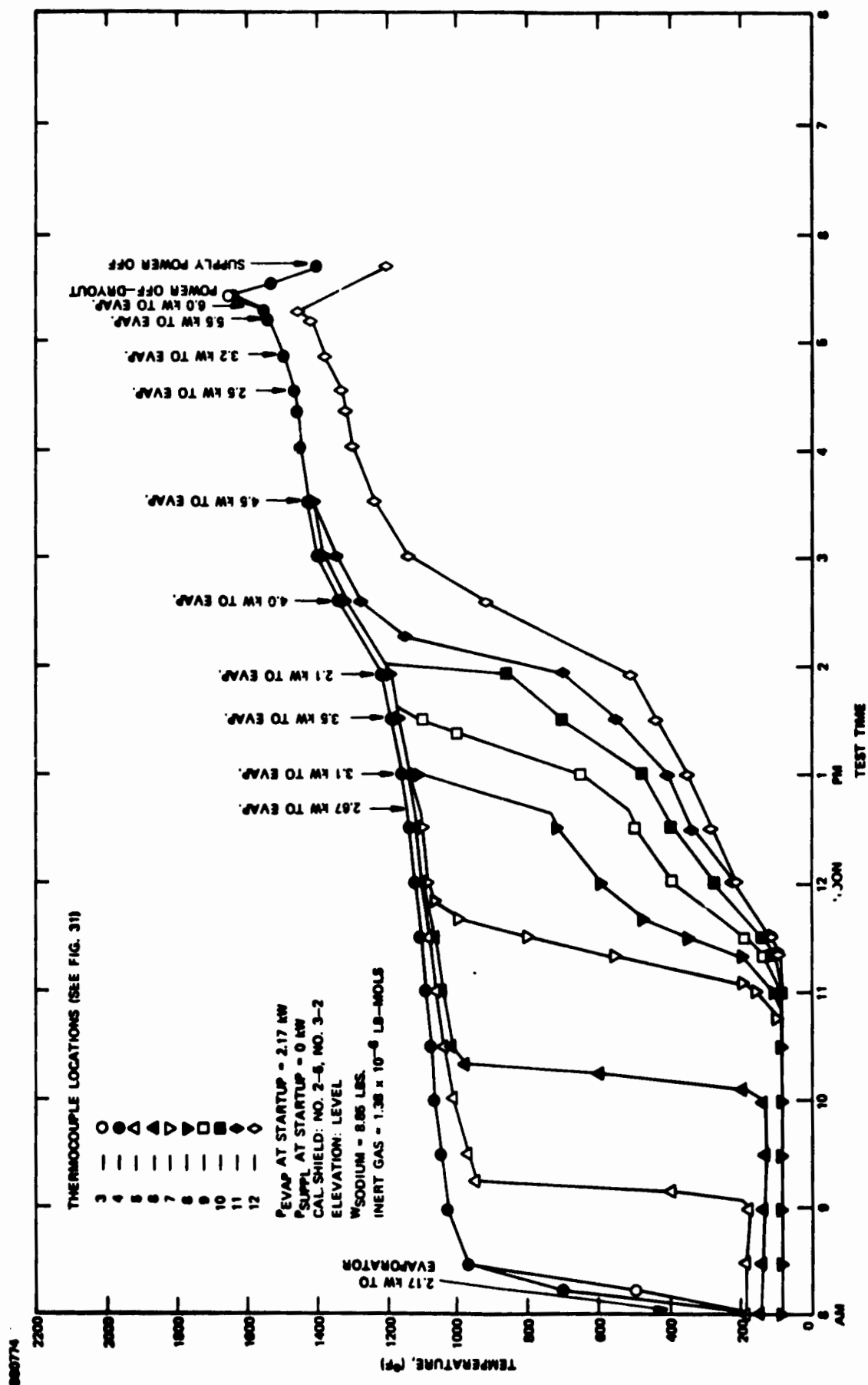


Figure 50. Test #11 (3-8-73) - Transient Startup with Inert Gas and Without Supplemental Heaters

- (4) Transient start-up could not be achieved using an inert gas (1.3×10^{-6} lb-mole of argon) at 2 kW when the sodium fill was increased to 8.67 lb. (refer to Test #9, Figure 48 and Table VI).
- (5) Transient start-up was achieved using an inert gas (1.3×10^{-6} lb-mole of argon) at 2 kW when the sodium fill was increased to 8.85 lb. (refer to Tests #10 and #11 in Figures 49 and 50 and Table VI).

c. Heat Pipe Capacity Tests:

- (1) The results of heat pipe capacity tests are shown in Table VII. The heat pipe capacity was determined to be between 4.9 and 5.3 kW for a level heat pipe at about 1500 to 1550°F. The data indicate that the capacity is relatively insensitive to evaporator elevations between zero and 3/8 inch. A slight increase of approximately 0.5 kW was observed for the reflux mode of operation. An operating temperature of 1600°F was not achievable due to calorimeter adjustment limitations. However, the capacity is not expected to change significantly at 1600°F due to the flatness of the hydrodynamic limit curve as illustrated in Figure 14. The measured capacity of 4.9 to 5.3 kW is less than the predicted capacity of 7.2 kW at 1600°F based on the calculated hydrodynamic limit as shown in Figure 14.
- (2) The heat losses through the insulation were approximately 65 percent greater than had been anticipated based on pretest calculations (see Figure 51). During capacity testing, the system heat losses were balanced using the supplemental heaters as guard heaters.
- (3) The sodium fill was increased to 8.85 lb. (see Tests #9 and #10 in Table VII) in the anticipation that increased capacity could be achieved by filling the fillets and gaps. However, the increased fill did not increase the measured heat pipe capacity.

3.6.2 CONCLUSIONS*

- Transient start-ups at evaporator power levels of 1.5 to 2 kW are achievable using an inert gas. (Parametric evaluation of gas pressure, however, was not undertaken).
- Transient start-ups can be accelerated if supplemental heat is used to melt the sodium uniformly along the heat pipe length.

*Conclusions were stated by the designers (TRW) of the first primary heat pipe.

50763

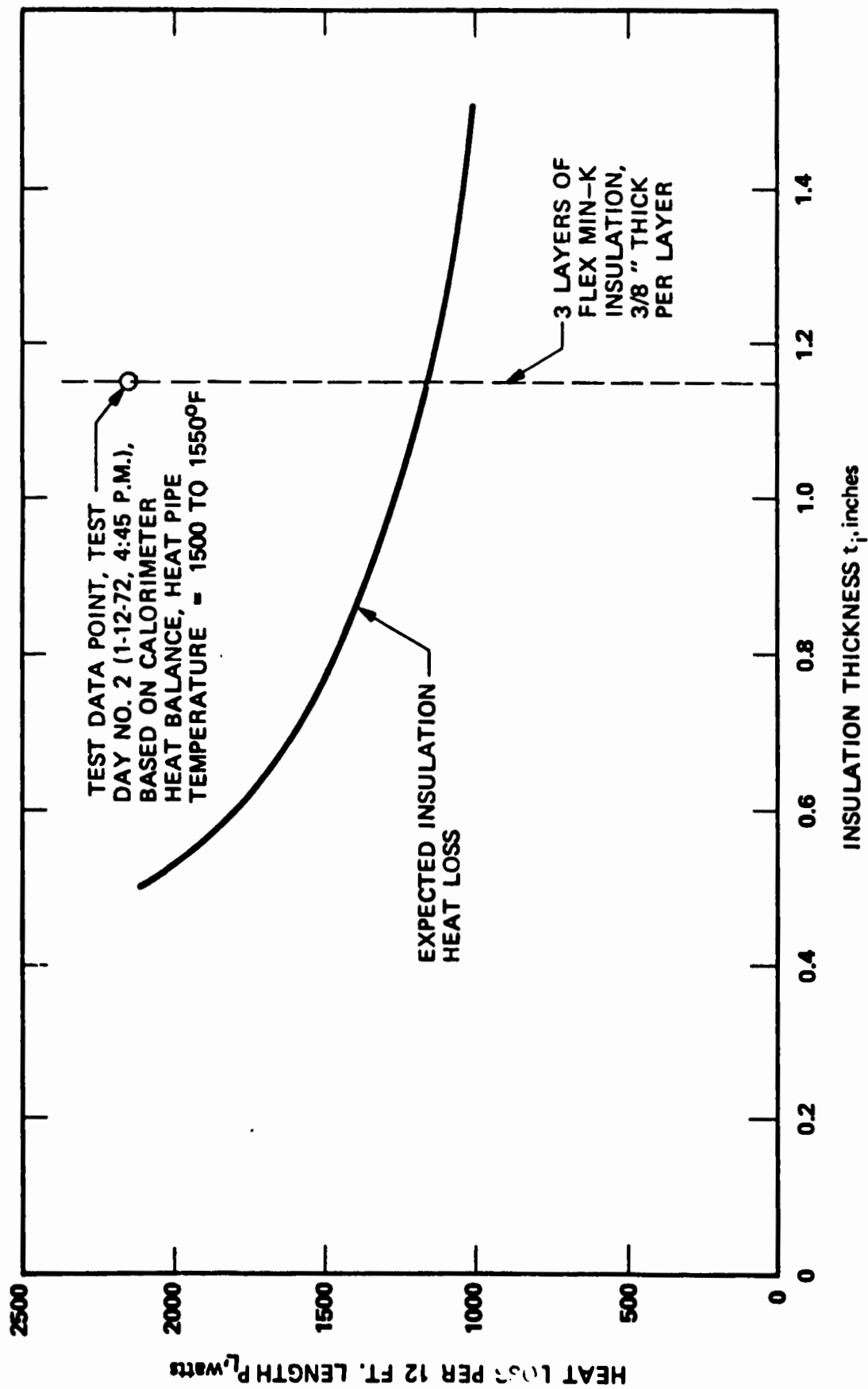


Figure 51. Heat Pipe Insulation Heat Loss

- Transient start-ups are limited by the heat pipe hydrodynamic limit, i.e., after start-up is achieved at 1.5 to 2.0 kW of power, full evaporator power cannot be applied, as axial transport capability is still limited as a function of temperature by the hydrodynamic limit.
- This heat pipe configuration appears to be limited to 5 kW at 1500 to 1600°F. Potential means of increasing capacity are to increase wick porosity and/or to utilize a larger diameter pipe. Other considerations include the use of a shorter heat pipe (e.g., reduced adiabatic section length).

3.7 EVALUATION OF INITIAL TEST RESULTS

Prior to continuing initial testing of the primary heat pipe at EOS, it was attempted to shed some light on the rather large discrepancy between the predicted power transfer capacity of more than 8 kW, and the apparent capacity of only 4.9 kW. This was done so that testing could be pursued according to the changed requirements of the first primary heat pipe.

For the primary heat pipe, the following design and operating data are pertinent:

Operating Temperature, T	1558°F
Design Power Transfer, P	6 kW
Operating Fluid	Sodium
Latent Heat of Evaporization, H_{fg}	4.4×10^3 joules/g
Liquid Density at Operating Temperature, ρ_l	0.748 g/cm^3
Liquid Viscosity at Operating Temperature, μ_l	$1.64 \times 10^{-3} \text{ dyn-sec/cm}^2$
Surface Tension at Operating Temperature, γ	116.8 dyn/cm
Vapor Density at Operating Temperature and Corresponding Vapor Pressure, ρ_v	$1.95 \times 10^{-4} \text{ g/cm}^3$
Viscosity of Sodium Vapor at Operating Temperature, μ_v	$2.245 \times 10^{-4} \text{ dyn-sec/cm}^2$
Cross-sectional Area Occupied by Wick Structure, A_{ws}	14.83 cm^2

Cross-sectional Vapor Flow Area, A_{vf}	7.094 cm ²
Effective Hydraulic Diameter of the Vapor Flow Area, D_H	1.4918 cm

Based on the above stated operating and design values for the primary heat pipe, the effective Reynolds number for the vapor flow at full design power can be calculated to be

$$N_{Re} = 1.3 \times 10^3$$

This would indicate a laminar flow of the vapor with a friction factor $f = 0.049$ as calculated from

$$f = 64/N_{Re}$$

The pressure drop of the vapor traversing the entire length of the heat pipe is found to be

$$\Delta p_{vf} = 1,429 \text{ dyn/cm}^2$$

If the flow cross-sectional area is incorrectly assumed to consist of one singular tubular cross-section, as was done in the original computer calculations, then the hydraulic diameter is about 3 cm and the Reynold's number is better than 2500. With these values, a pressure drop of only about 720 dyn/cm² can be calculated for the vapor flow, which is only one-half of the actual pressure drop.

Since the heat pipe is being operated in the gravitational field of 1-g, the effect of the diameter of the heat pipe has to be considered. The sodium condensed at the condenser can flow back to the evaporator through the entire wick structure only if it has been pumped up to the wick structure which lies above the lowest point of the internal structure of the pipe. For raising the sodium over the entire internal diameter, a suction pressure of

$$\Delta p_h = \rho D_1 g$$

is required, which is equal to

$$\Delta p_h = 3,708 \text{ dyn/cm}^2$$

This is about twice the pressure drop due to the vapor flow.

The main wick structure, as indicated in Figure 52, is made up of 94 layers of 38 mesh bolting cloth and 20 layers of 60 Mesh 0.007-inch diameter wire screen. The wick would have a total thickness of 1.502 inch with a packing factor of 1, i.e., the individual layers of the wick structure would not nest in each other. Since the final thickness of the wick was only 1.130 inch, the nesting factor is $\eta = 0.75233$. The nesting factor is quite often incorrectly equated with the packing factor, which is quite different as will be shown later. The active wick flow area, i.e., the cross-sectional area that is made up only of the wicking material, is $A_{wf} = 14.27232 \text{ cm}^2$. Based on the flow area, A_{wf} , the mass flow rate, \dot{W} , the length of the heat pipe, L , and the materials properties of the fluid, the required flow factor $\Delta p \times K$ can be calculated to be 0.096 dyn.

In Figure 53, the available flow factor $\Delta p \times K$ is plotted against the packing factor for various assumed conditions. The curves of the graph make it quite clear that the available flow factor of the primary heat pipe wick was considerably below the required flow factor for transferring 6 kW of power in the primary heat pipe. Thus, the reported power transfer capacity of only 4.9 kW* was not surprising at all. Even with a packing factor of 1, the power capacity would have been marginal.

In Figure 54, the effect of the packing factor on the pressure drop in the wick is presented. This figure indicates clearly the criticality of the construction of the wick. If the wick has been compressed to 0.75 of the nominal thickness, i.e., the wick has been assembled with a nesting factor of 0.75, the effective packing factor is considerably smaller than 0.75. This can be appreciated when considering that the wick volume has been decreased by compressing the wick structure only in the direction which is perpendicular to the flow. Therefore, the flow area has actually been decreased by a factor of 0.75^3 , i.e., 0.422. It is thus more appropriate to use the latter factor as the packing factor in the calculation of the permeability K . This consideration seemed to have been well born out by the large discrepancy between the predicted power transfer capacity of the primary heat pipe and the measured one. (See also Section IX, Volume III)

3.8 PERFORMANCE TESTING OF FIRST PRIMARY HEAT PIPE

3.8.1 TEST SETUP

After the initial testing of the first primary heat pipe by the designers and builders, general performance tests were to be conducted by Xerox/EOS prior to its mating with the secondary heat pipe. The performance tests were to include repeated start-ups for establishing thermal transient behavior, taking temperature measurements along the heat pipe and

*The deficiency of the insulation of the heat pipe suggested the power transfer to have been considerably less than 4.9 kW. (R.R.)

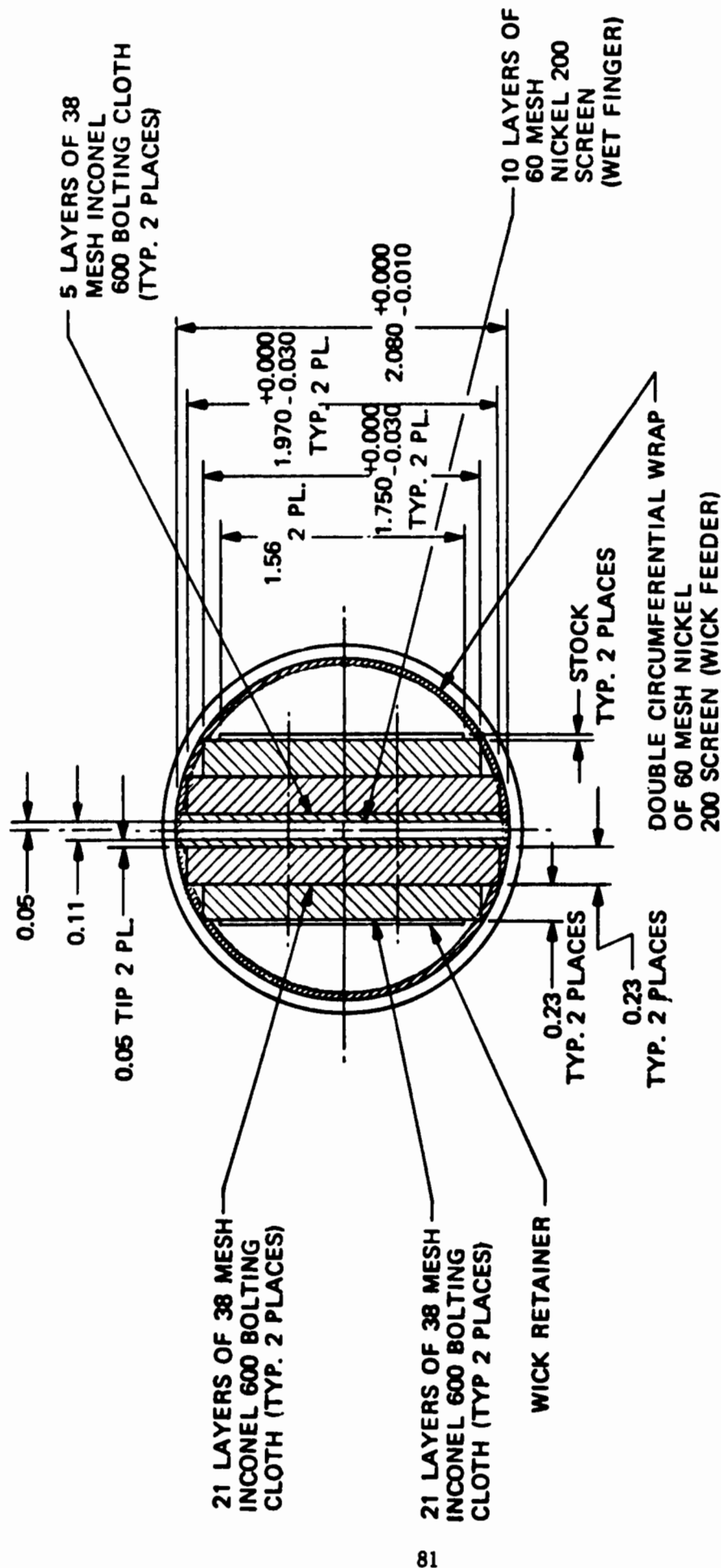


Figure 52. Wick Structure of First Primary Heat Pipe

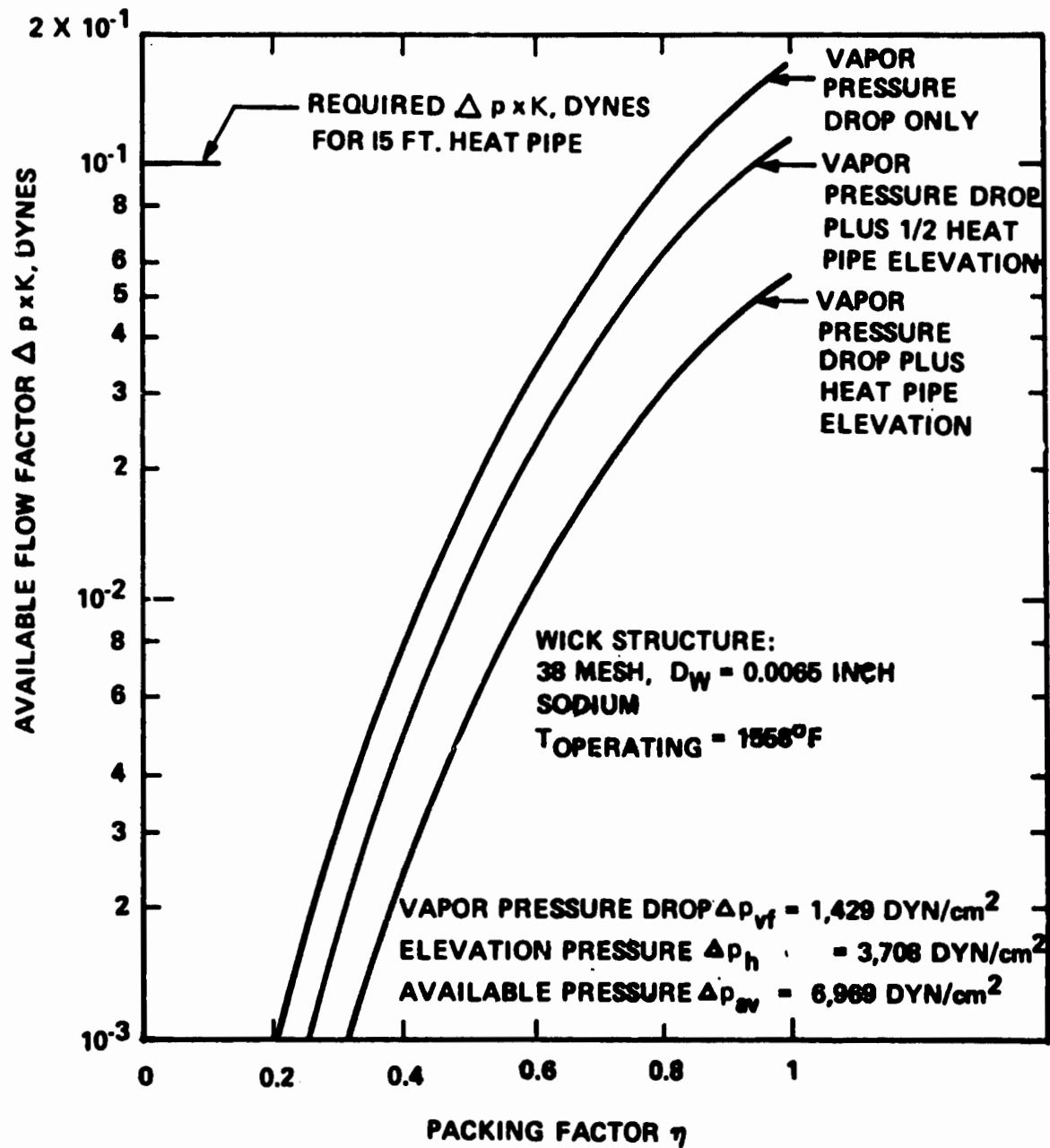


Figure 53. Available Flow Factor $\Delta p \times K$ as a Function of the Packing Factor

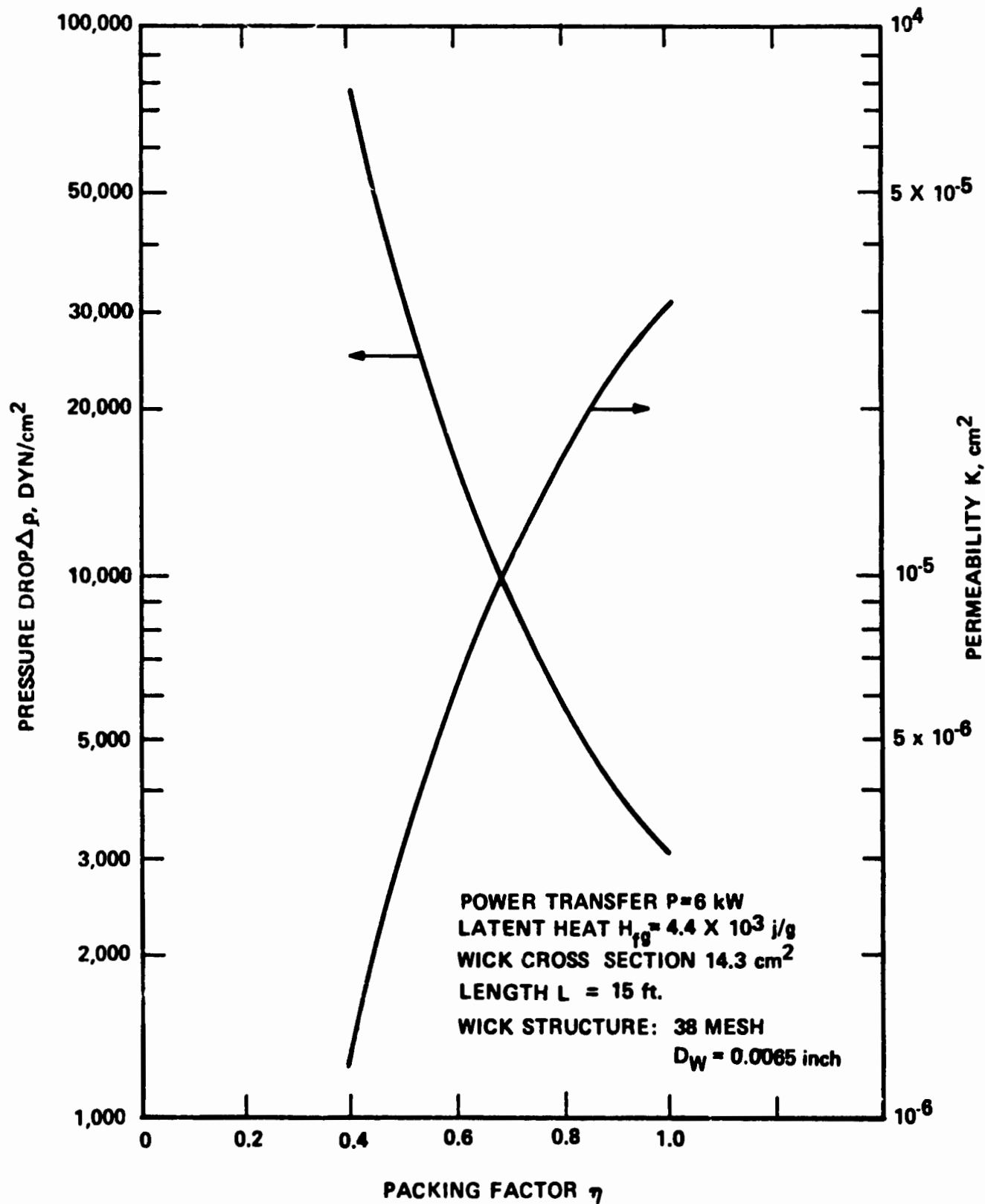


Figure 54. Permeability and Pressure Drop in the Wick as Function of Packing Factor

correlating them against input power and time, operating the pipe at various power inputs to determine the temperature distribution along the heat pipe, and permitting cool down at various rates.

When the program for the initial testing of the primary heat pipe was laid out, it was established that the total heat losses from the evaporator section and the adiabatic section of the heat pipe should not exceed 20 percent of the power input of the primary heater at the evaporator, i.e., the heat losses should be less than 1.2 kW. In Figure 55, the calculated heat losses from a 12-foot long section of the heat pipe (condenser section not included) are presented when the heat pipe is operated at the nominal operating temperature of 1558°F in an ambient temperature of about 70°F. According to these calculations, the insulation thickness when using Flex Min-K insulation material has to be at least 3 inches. This calculation assumes that none of the heaters increase the effective heat pipe diameter, i.e., that the insulation is wrapped directly around the heat pipe. When the increase in the effective heat pipe diameter, due to the secondary heaters, was considered then the insulation thickness had to be at least 4 inches thick to maintain the heat losses below 20 percent at the power input. Heat transfer calculations made by TRW indicated that an insulation thickness of only three 3/8-inch thick Flex Min-K layers would satisfy the insulation requirement. (Subsection 3.6) Heat balance calculations made by TRW and based on data taken during the initial testing of the primary heat pipe indicated, that heat losses of more than 2.1 kW occurred when the heat pipe temperature was still below the operating temperature, i.e., between 1500 and 1550°F.

The initial tests of the first primary heat pipe seemed to indicate that the power transfer capacity of the first primary heat pipe was less than 4.9 kW. This was only slightly more than half the capacity that had been predicted. (Subsection 3.2.) No explanation for the measured low power transfer capacity was presented. Furthermore, a relatively high amount of secondary heater power was required for starting the heat pipe. This could be explained by the high thermal energy losses from the heat pipe due to insufficient insulation.

Because of these deviations it was felt that prior to the actual completion of the initial testing of the first primary heat pipe at EOS, the insulation should be improved to achieve more realistic start-up conditions and to establish the correct secondary power required for operational testing of the heat pipe.

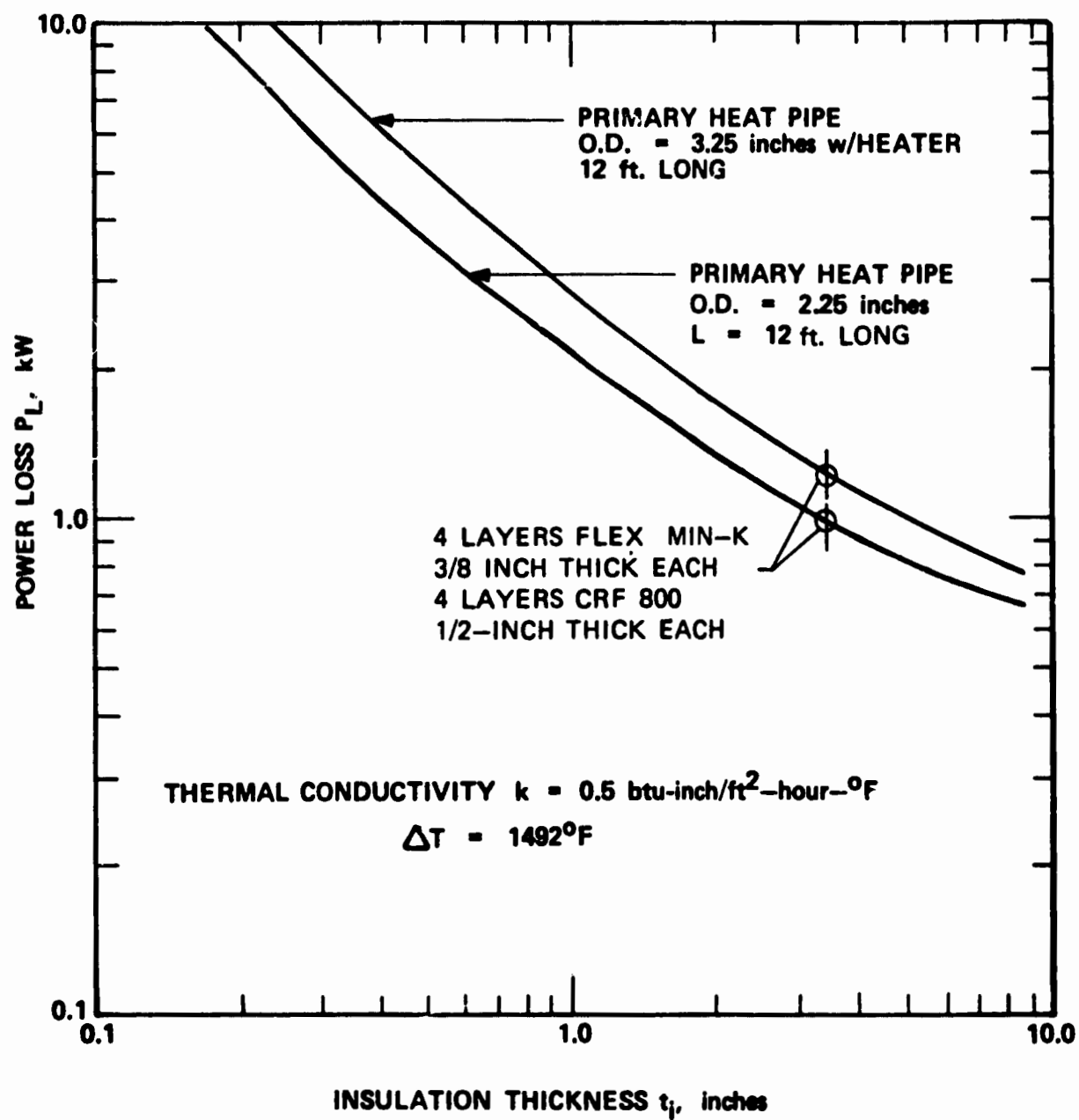


Figure 55. Insulation Requirement for Primary Heat Pipe with and without Secondary Heaters

Upon transfer of the primary heat pipe from TRW to EOS, the heat pipe was stripped of all insulation and the secondary heater elements. The two thermocouples along the adiabatic section of the heat pipe were also removed. Thirteen new thermocouples were located along the adiabatic section of the heat pipe as shown in Figure 56. The secondary heater was arranged in five double elements, each double element enclosing the heat pipe entirely as shown in Figures 57 and 58. First, insulation was wrapped around the heat pipe in sections which were not covered by the secondary heater elements as is shown in Figure 59. Then four 3/8-inch thick layers of Flex Min-K insulation as indicated in Figure 55 were applied in 36-inch length sections. A typical section of insulation is shown in Figure 60. In Figure 61, the heat pipe is shown wrapped entirely with the flexible Min-K insulation material. Over the Flex Min-K material, four 1/2-inch thick layers of Cera-Felt RF 800 were wrapped as shown in Figure 62. The insulation was completed with one layer of aluminum foil as shown in Figure 63. The fully insulated primary heat pipe is shown in position in Figure 64.

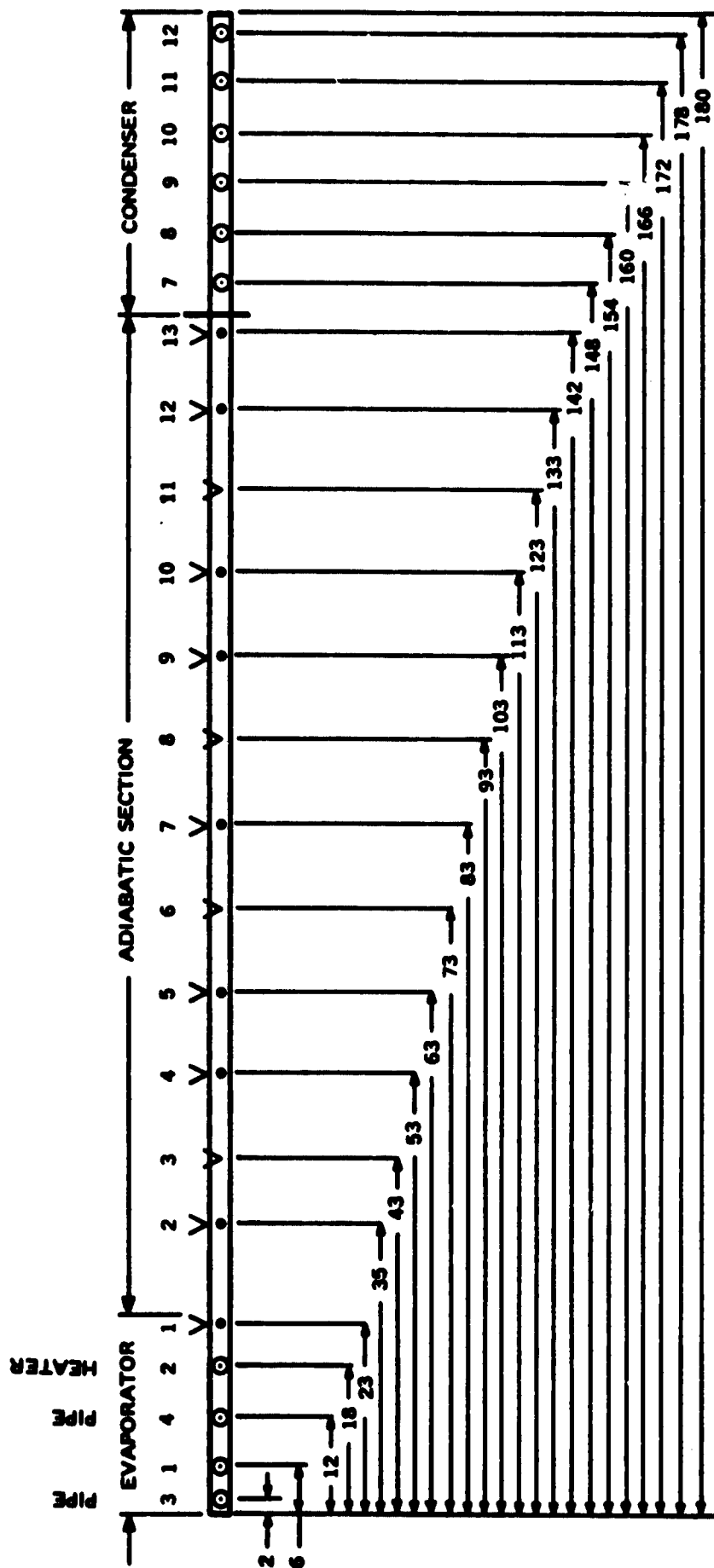
The set up for testing of the first primary heat pipe at Xerox/EOS is shown in Figure 65. The primary heater at the evaporator section of the heat pipe, which consisted of five individual elements, was controlled through two variacs. One variac controlled four of the elements while the other variac controlled the remaining element. The secondary heater consisting of the ten elements, was controlled by a single 25 ampere variac.

3.8.2 TESTING

Because of the change in the insulation, the need of which was explained above, the initial testing of the heat pipe had to be repeated.

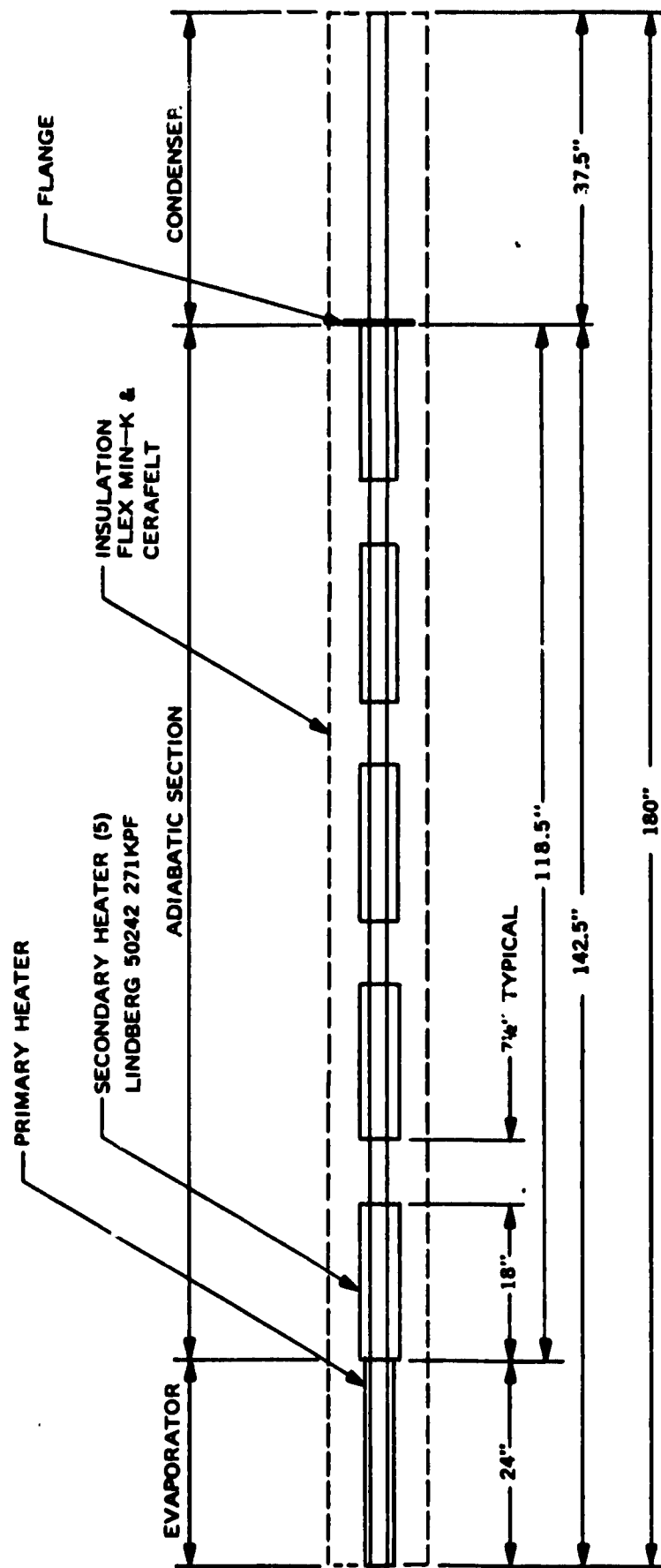
3.8.2.1 Steady State

In Figures 66 and 67, the temperatures at steady state are shown for various power inputs at the evaporator of the primary heat pipe. The data of Figure 68 were obtained while increasing the power from 0.323 kW to 1.494 kW in steps taking data when all temperatures appeared to have reached steady state. Steady-state conditions were normally only achieved after 48 hours had elapsed from the time of power adjustment. In Figure 69, the data obtained while decreasing the power input to the evaporator are shown. It was attempted to duplicate the input power settings used during the test of the increasing power input to determine whether the temperature distribution along the heat pipe is a function of the approach to the steady-state condition. The test results seemed to indicate that the same steady-state conditions were achieved regardless of whether the primary heat pipe had been hotter or colder prior to



V EOS THERMOCOUPLE
 O TRW THERMOCOUPLE

Figure 56. Thermocouple Arrangement for Testing of First Primary Heat Pipe at EOS



EVAPORATOR AND ADIABATIC SECTION	CONDENSER	INSULATION:
4 LAYERS	1 LAYER	FLEXIBLE MIN-K 3/8 inch THICK
4 LAYERS	7 LAYERS	CERA-FELT CRF 800 1/2 inch THICK

Figure 57. Heater and Insulation Arrangement for Testing of First Primary Heat Pipe at EOS



Figure 58. Primary Heat Pipe with Primary and Secondary Heaters Installed



Figure 59. Primary Heat Pipe with Secondary Heater Elements and Intermittent Insulation (Flex Min-K)

006715

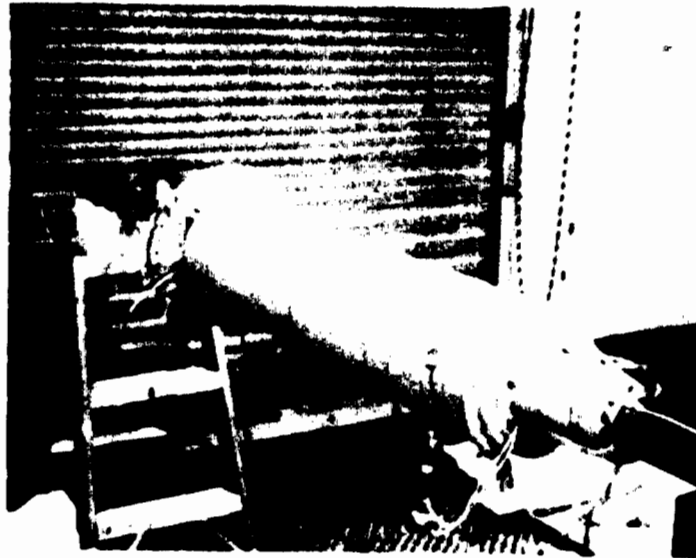


Figure 60. Primary Heat Pipe with Four Layers of Flex Min-K Insulation Over One Segment of the Heat Pipe

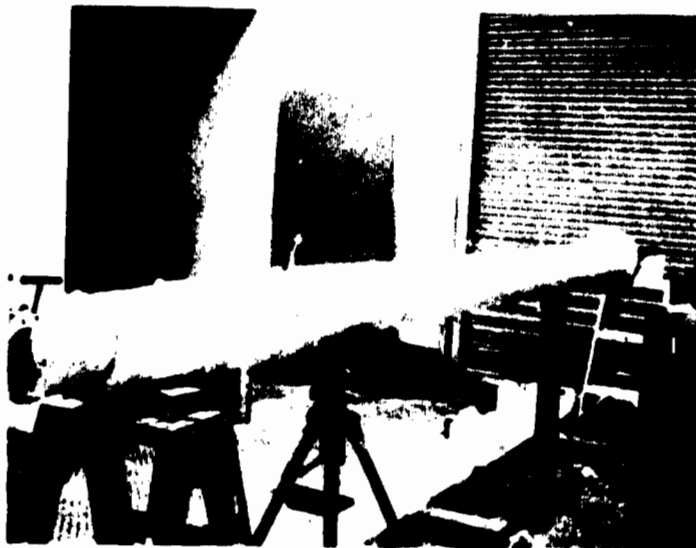


Figure 61. Primary Heat Pipe with Completed Four Layers Flex Min-K Insulation



Figure 62. Primary Heat Pipe with Four Layers
Cera-Felt Insulation Over Flex
Min-K Insulation

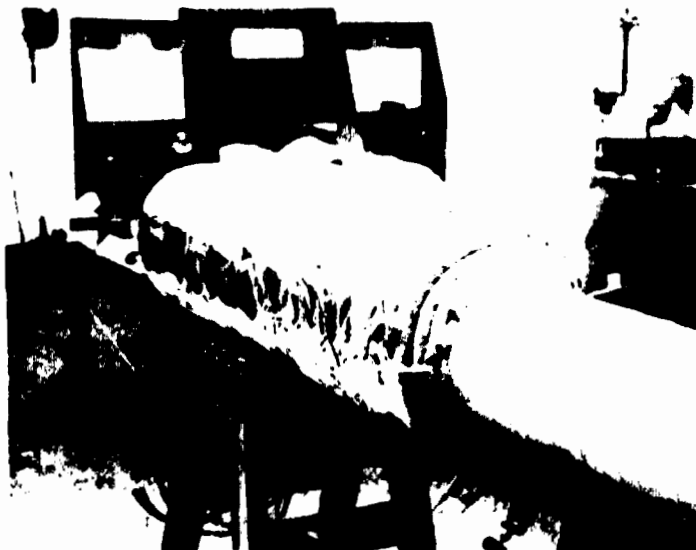


Figure 63. Primary Heat Pipe Shown with One
Segment Fully Insulated (four
layers Flex Min-K, four layers
Cera-Felt and foil)

006718

006719

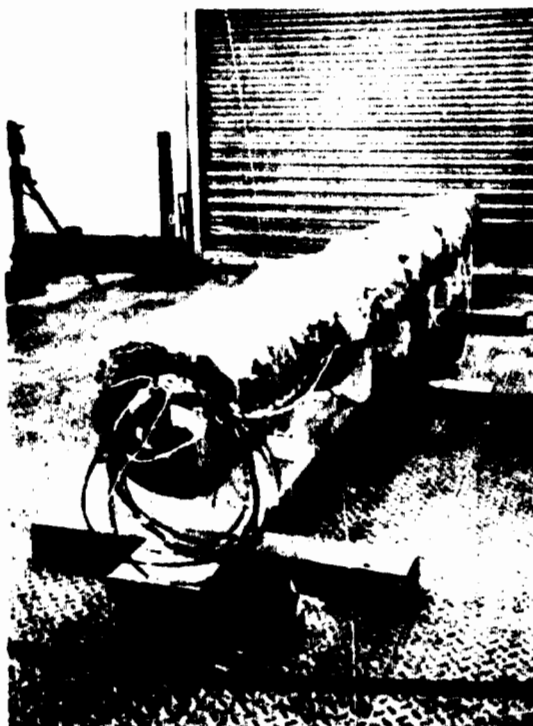


Figure 64. Primary Heat Pipe Fully Insulated

006721



Figure 65. Complete Test Setup of Primary Heat Pipe

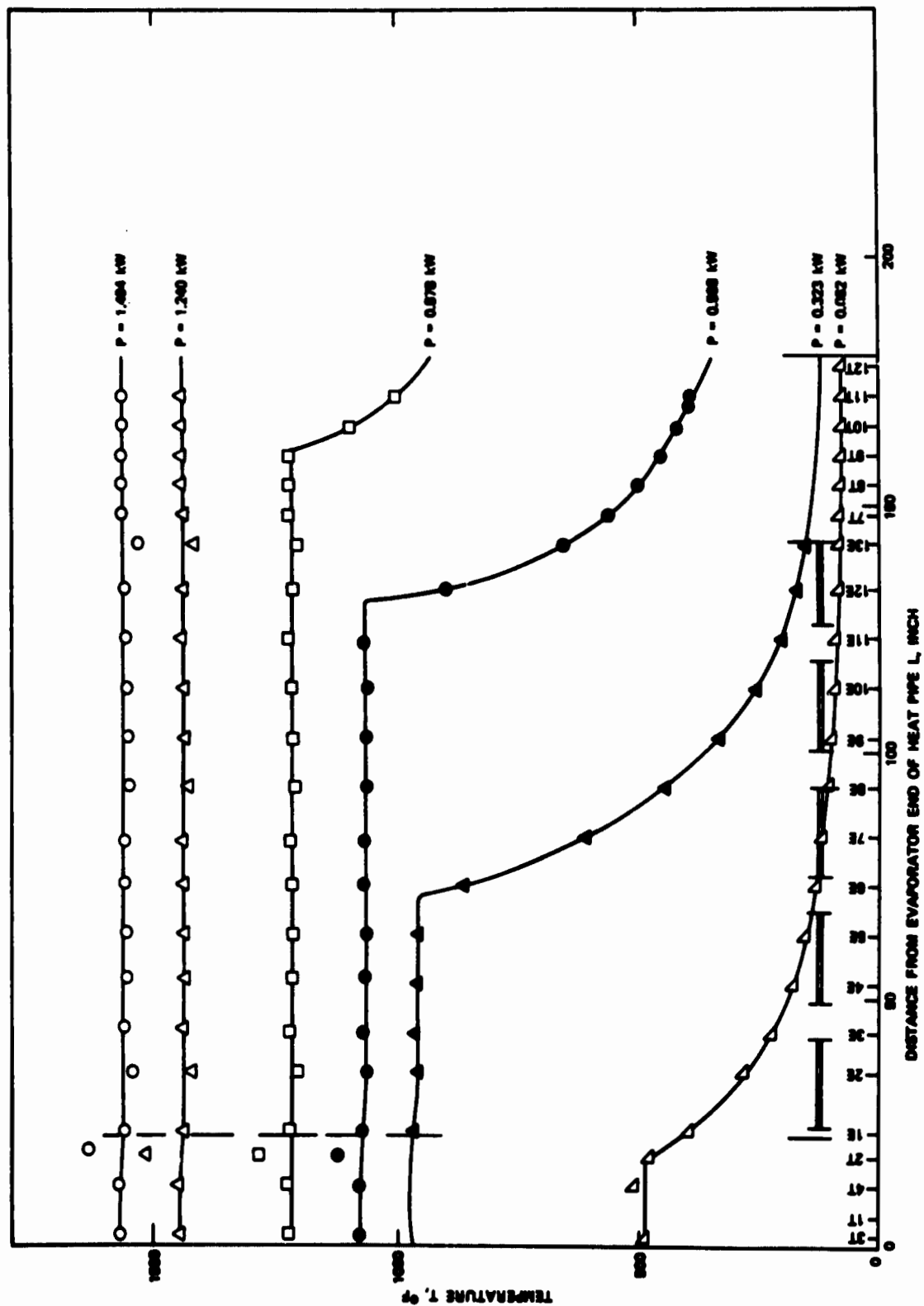


Figure 66. Steady-State Temperatures along First Primary Heat Pipe under Various Power Inputs (Increasing Power)

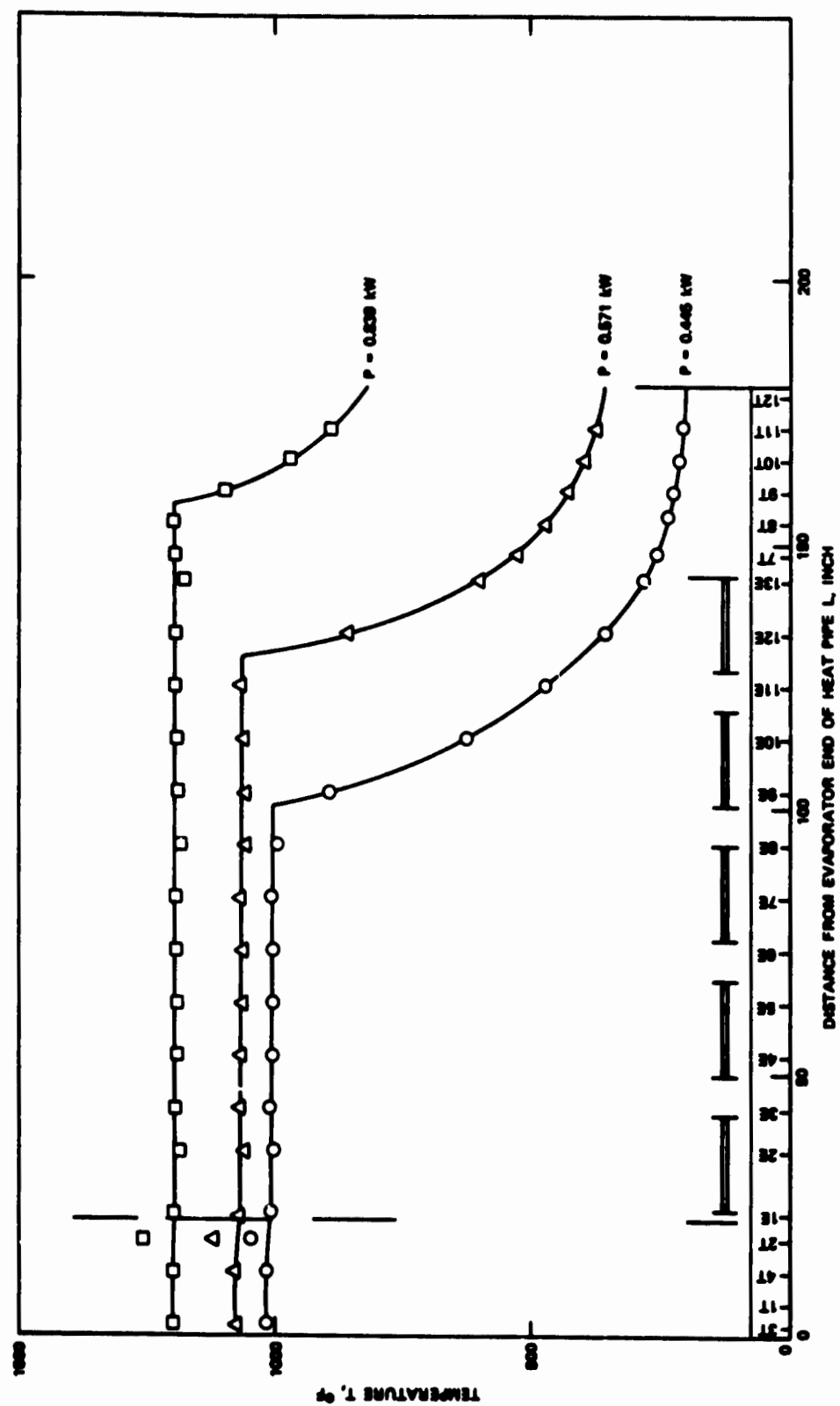


Figure 67. Steady-State Temperatures Along First Primary Heat Pipe Under Various Power Conditions (Decreasing Power)

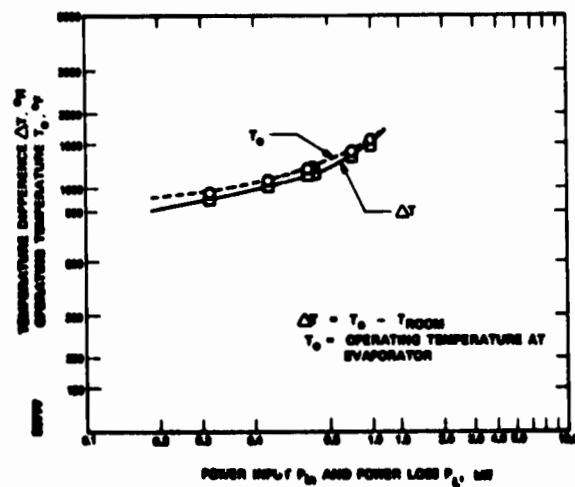


Figure 68. Correlation Between Input Power and Operating Temperature for First Primary Heat Pipe

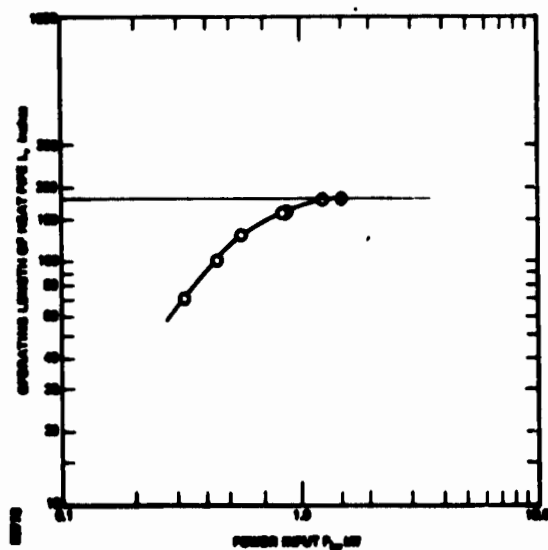


Figure 69. Active Heat Pipe Length as Function of Power Input.

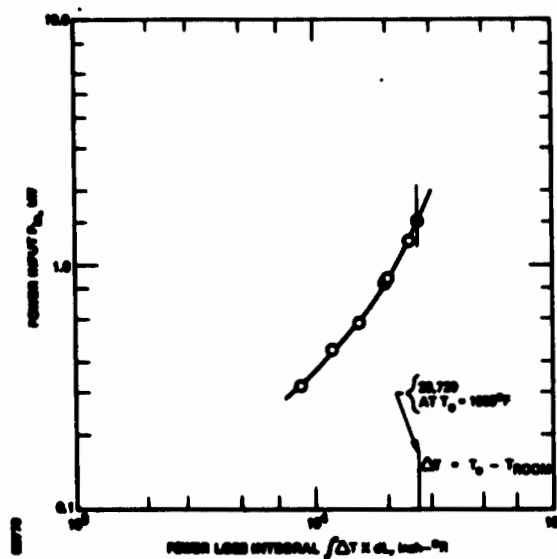


Figure 70. Required Input Power as Function of Loss Integral

to the power change. At the tested power inputs, the temperature at the evaporator was only about 10°R higher than at the active adiabatic section. Since these tests were run with a fully insulated condenser section, power input was equal to the losses from the entire heat pipe including the condenser section at operating temperature.

In Figure 68, a correlation is given between the power input (power loss) and the operating temperature of the active section of the heat pipe. The operating length of the heat pipe versus the power input is presented in Figure 69. All data points fall on the same curve regardless of whether the points were taken from the increasing input power tests or the decreasing input power tests. Finally, the power input is correlated in Figure 70 with the loss integral $\int_0^L \Delta T \times dL$, where $\Delta T = T_o - T_{room}$. The values were obtained by tracing the results presented in Figures 66 and 67 with a planimeter.

The losses from the entire primary heat pipe, including the condenser section, are 1490 watts at the operating temperature of 1558°F. The losses sustained along the evaporator and the adiabatic section (12-foot length) alone were found by rationing to be 1190 watts. This compared with the predicted losses of 1220 watts.

3.8.2.2 Transient Start-Up Tests

After verifying the heat losses from the heat pipe, start-up tests were conducted. These tests were to establish the behavior of the heat pipe under transient conditions by applying to the evaporator section of the primary heat pipe a given power and then recording the temperature response of the thermocouples along the heat pipe as was shown in Figure 56.

A total of three start ups were completed prior to failure of the first primary heat pipe. In two cases, the start up was initiated with a primary heat pipe at room temperature, and in one case, at a slightly elevated temperature at the evaporator. The temporal temperature distribution, during the start up with a power input at the evaporator of 2.579 kW, is shown in Figure 71. During the test, the temperatures appeared to increase steadily showing no abnormal or erratic discontinuities. The reduction of the data, however, as shown in Figure 71, give a more detailed account of the start up history. The temperatures seem to indicate that the evaporator wall wick at location 2T and 4T was dry almost from the very beginning of the start up. The temperatures measured at these two locations behaved distinctly differently from those temperatures that indicated heat pipe action or initial heat pipe action and a later dry out of the wick at their locations. The temperature history at location 3T indicated that up to 46 minutes the location operated in the heat pipe mode.

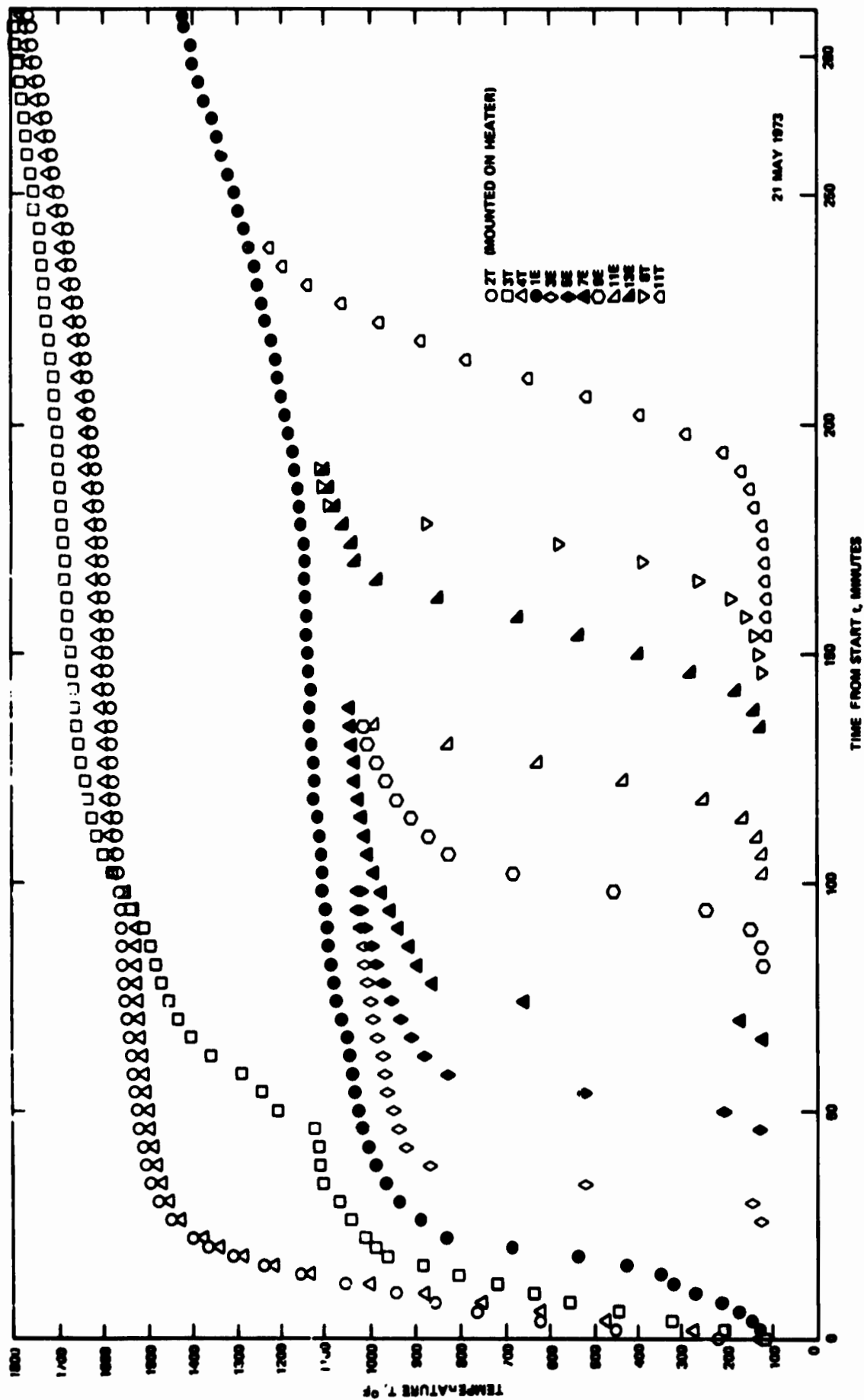


Figure 71. Temperature History of the First Primary Heat Pipe During Startup with a Power Input of 2.597 kW at the Evaporator

The sharp discontinuity in the temperature rise after 46 minutes must be interpreted as a loss of working fluid in the wall wick. This discontinuity could not be readily observed on the recording chart, and thus the dry out was not recognized during the test. After 194 minutes of operation, all temperatures measured were above the melting temperature of the working fluid (sodium), which is 208°F. No recovery of the initial dry length of the primary heat pipe, nor of the section that had gone dry about 48 minutes after the start up, can be detected from the data. This occurred despite the fact that the heat pipe became fully operational.

The data of the start-up test which was conducted with a power input of 3.325 kW are presented in Figure 72. The results are very similar to those of Figure 71. Again, the wick section in the area where the temperatures were measured by thermocouples 3T and 4T apparently went dry after 36 and 54 minutes of operation respectively. No recovery of the wick sections that went dry during the start up occurred, though prior to the conclusion of the test the entire heat pipe was well above the melting temperature of the sodium and the lowest temperature measured on the outside surface of the primary heat pipe was above 300°F. The test was terminated when thermocouples 3T and 4T had reached a temperature of 1800°F.

It was already pointed out that the diametral wick as built, was marginal for transferring 6 kW of thermal power over the entire length of the heat pipe. The calculations presented in Subsection 3.7 and Figure 53 suggested a power transfer capacity of about 3 kW for a packing factor of 0.75; the maximum possible for the present wick structure. Based on the fabrication, the actual packing factor was considerably lower. The transient test data appeared to point out that probably the drying out of the wick at the evaporator was caused by an undercharge of sodium. Each start-up test was initiated after a uniform cooling down of the entire heat pipe with a loss of only 1.54 kW at the operating temperature and with considerably lower losses at the lower temperatures encountered during the cool down. Thus, prior to each test the entire wick should have regained its charge if sufficient sodium had been in the pipe.

At the end of the last test (i.e., at the time all temperatures had reached the operating temperature of the heat pipe), an apparent failure of the primary heater occurred which later was found to have been caused by the failure of the heat pipe.

3.9 FAILURE ANALYSIS FOR FIRST PRIMARY HEAT PIPE

3.9.1 METALLURGICAL ANALYSIS

After the failure of the first primary heat pipe, the insulation and the heaters were removed from the evaporator section of the heat pipe. Two large elongated holes were immediately visible from which sodium

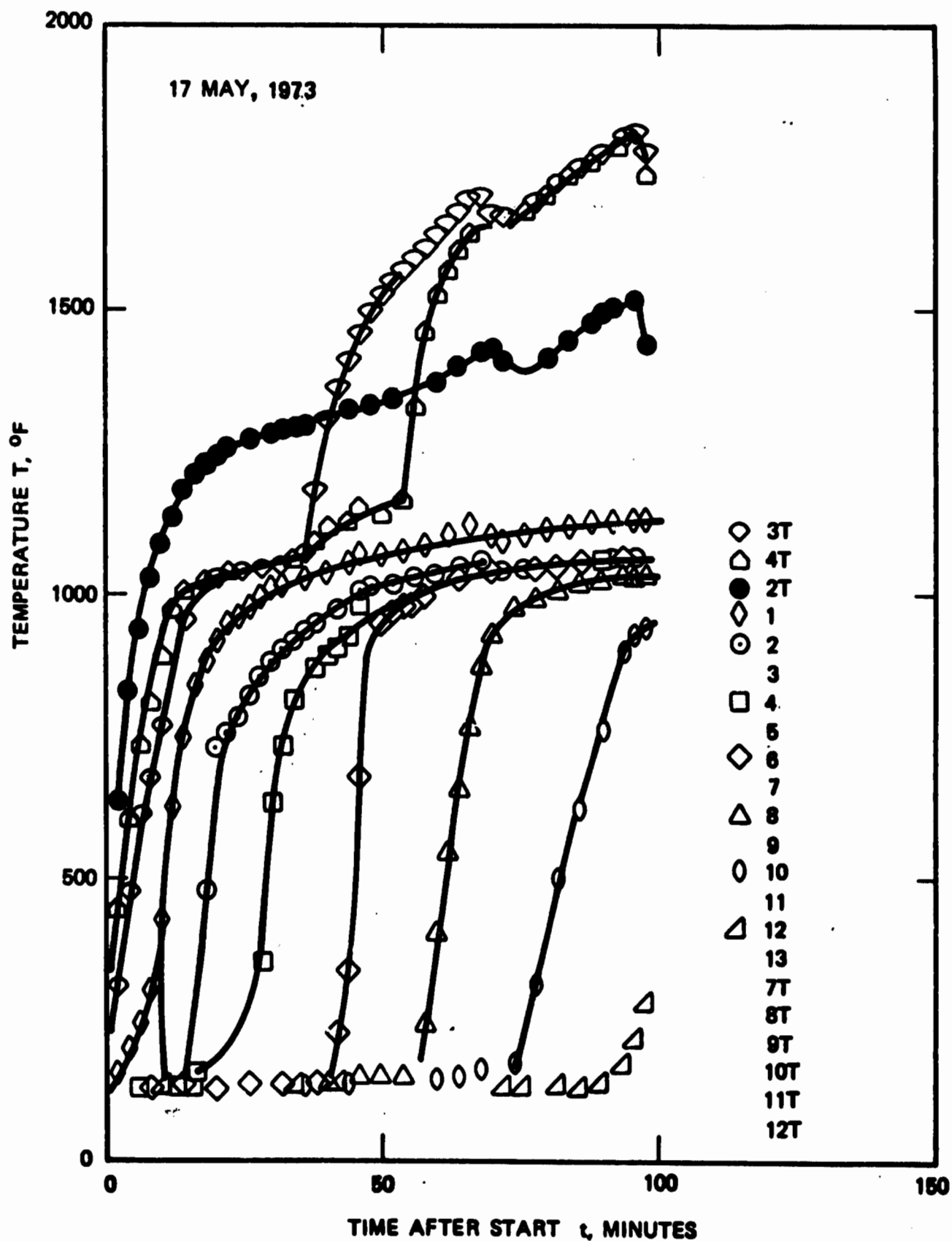


Figure 72. Temperature Distribution Along the First Primary Heat Pipe During Startup With a Power Input of 3.325 kW at the Evaporator

hydroxide appeared to ooze out (See Figure 73). The heat pipe was discharged and cleaned for further inspection. The evaporator section of the heat pipe was acid cleaned and submitted for an analysis by the Zyglo process. The results of the Zyglo Test are shown in Figure 76.

It was difficult to obtain a photographic record of the appearance of the heat pipe section under the black light by which cracks and imperfections of the material are made to show up. The cracks which were visible by the inspection process were, therefore, painted with a red color and the section of the heat pipe was then photographed (Figure 74). All cracks run circumferentially. Except for one long crack which is located 180 degrees apart from the crack furthest away from the end of the evaporator section, all cracks were located on one side of the heat pipe. This side was opposite of the weld. No cracks were found on the remaining section of the heat pipe. It was clear that the large elevated holes were due to the attack of the Inconel 600 material by the hot sodium hydroxide which was formed between the sodium and the moisture of the air when the sodium was escaping through the initial cracks. The evaporator section of the heat pipe was shipped to International Nickel Company for further analysis.

The analysis by the International Nickel Company* confirmed that the mode of failure was related to an intergranular attack on the material which led to branched, intergranular cracking as indicated in Figure 75. The appearance of these cracks is typical for those resulting from a caustic stress corrosion cracking mechanism. The predominant cracking was observed to be in a circumferential direction, implicating a longitudinal tensile stress. The implied longitudinal tensile stress seemed to indicate that the failure was caused by thermal stresses that were the result of the temperature gradients measured along the evaporator section of the heat pipe as was indicated by the data shown in Figures 40 through 50 and Figures 71 and 72.

3.9.2 STRESS ANALYSIS

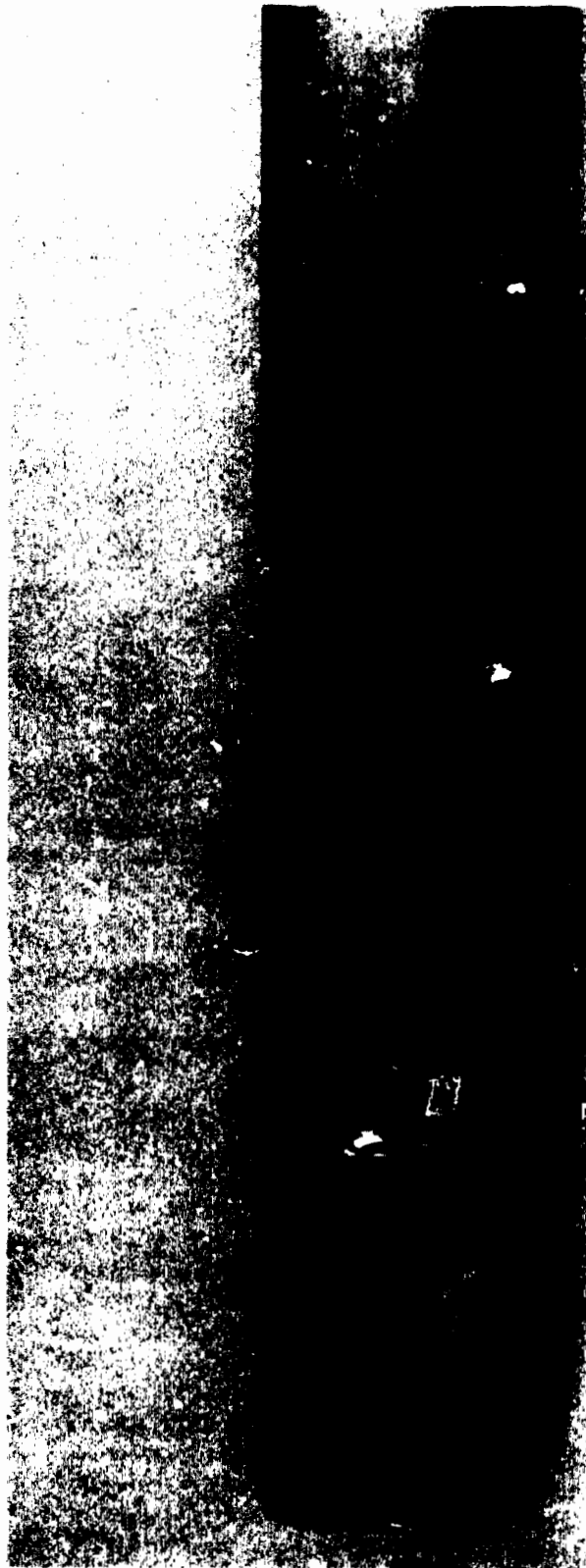
At the measured temperature gradients the heat pipe will vary in diameter over a very short length as indicated in Figure 76.

*T. F. Lembke, Huntington Alloy Products Division, The International Nickel Company, Inc., Huntington, W. Va. (September 17, 1973).



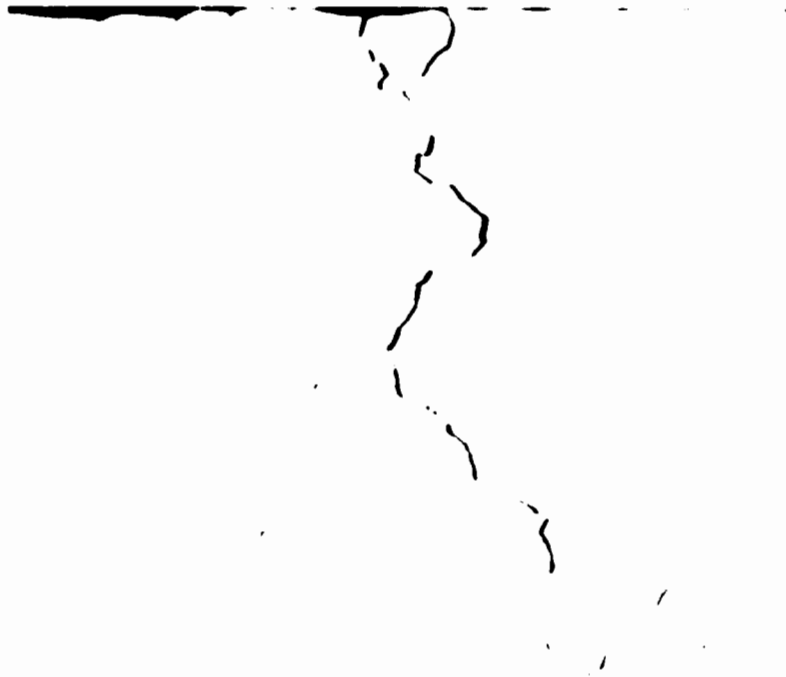
57363

Figure 73. Primary Heat Pipe Appearance after Failure



77310

Figure 74. Cracks in the Evaporator Section of the Primary Heat Pipe
as Indicated by the Zygo Process



007121

Figure 75. Branched, Intergranular Cracking - 100X
Unetched - Iconel Alloy 600
Electro-Optical Company

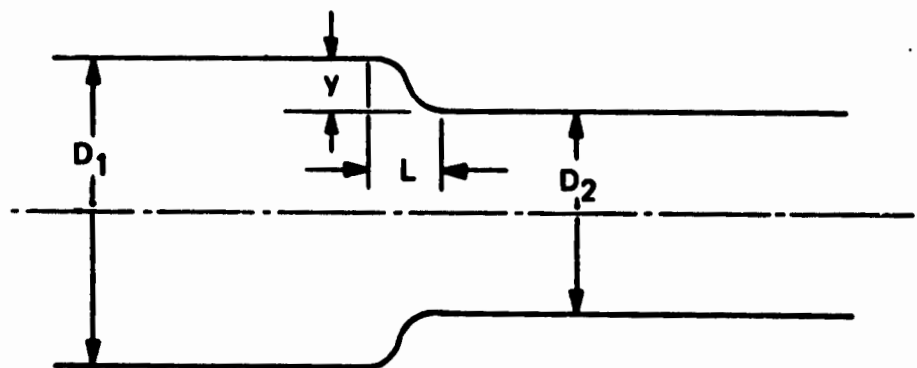


Figure 76. Effect of Temperature Gradients on the Pipe

A plate analysis can closely predict the stresses in a thin wall pipe. For a plate, the relation between deflection y and the moment M can be derived to be

$$y = \frac{M(1-\nu^2)}{2EI} \left[\frac{4}{3}x - \frac{2}{3}\frac{x^2}{L} - \frac{2}{3}L \right] \left(x + \frac{L}{2} \right) \quad (7)$$

where

- M Moment
- E Young's Module
- ν Poisson's Ratio
- I Moment of Inertia

The maximum moment M will be located at the two ends of the transition section between the larger and the smaller heat pipe diameters, i.e., at $x = 0$ and $x = L$.

The deflection y corresponds to half the difference in the two diameters and is given by

$$y = \frac{\alpha D \Delta T}{2} \quad (8)$$

where

α Coefficient of thermal expansion

ΔT Temperature difference

With the stress expressed by

$$\sigma = \frac{Mc}{I} \quad (9)$$

where

I/c Modulus of cross section

the maximum stress can be expressed by using relations 7 and 8 as a function of the measured temperature difference ΔT and the distance L between the thermocouples. With

$$E = 31 \times 10^6 \text{ psi}$$

$$\alpha = 6.4 \times 10^{-6}/^{\circ}\text{F}$$

the maximum temperature difference ΔT_M along a length L can be found for an allowable stress σ_a to be

$$\Delta T_M = \frac{L^2 \sigma_a}{46,357} \quad (10)$$

In Figure 77, this correlation is plotted with the allowable stresses taken equal to the creep stress indicated for various operating temperatures and shown in Figure 78. The creep strength is normally defined as the stress which causes 0.01 percent creep in 10,000 hours.

Temperatures were measured every 6 inches apart along the evaporator section (see Figure 56). The correlations of Figure 77 indicate that (at an operating temperature of 1800°F) the temperature difference between adjoining thermocouples cannot exceed 225°F without causing the stresses to exceed the creep stress at that temperature. The data shown in Figures 71 and 72 indicate that the creep stress was very much exceeded due to the considerably higher temperature. Similar and even larger temperature differences were experienced during the preliminary testing at TRW. (Refer to Subsection 3.1, Figures 40 through 50.)

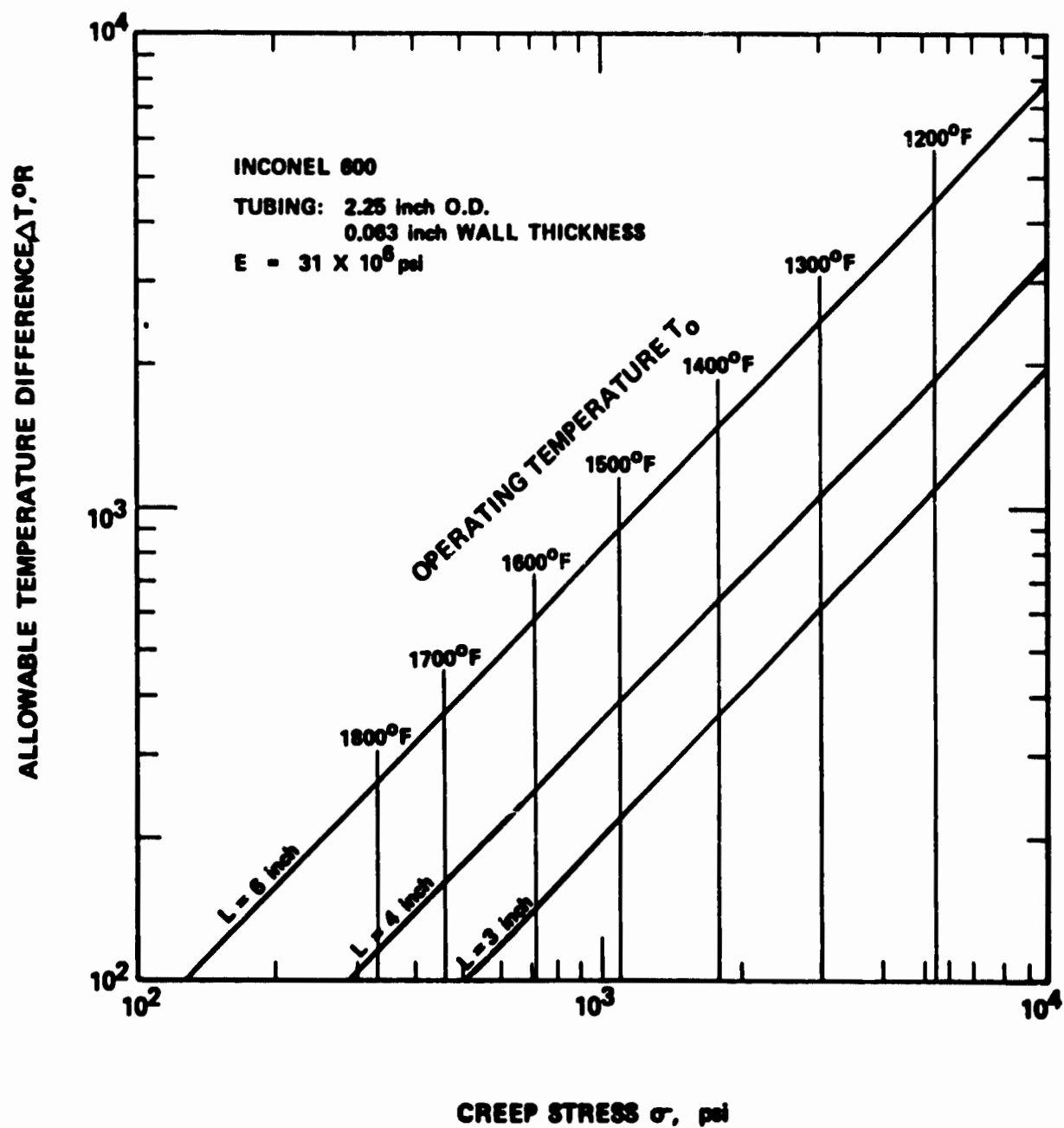


Figure 77. Allowable Temperature Differences Along the Heat Pipe

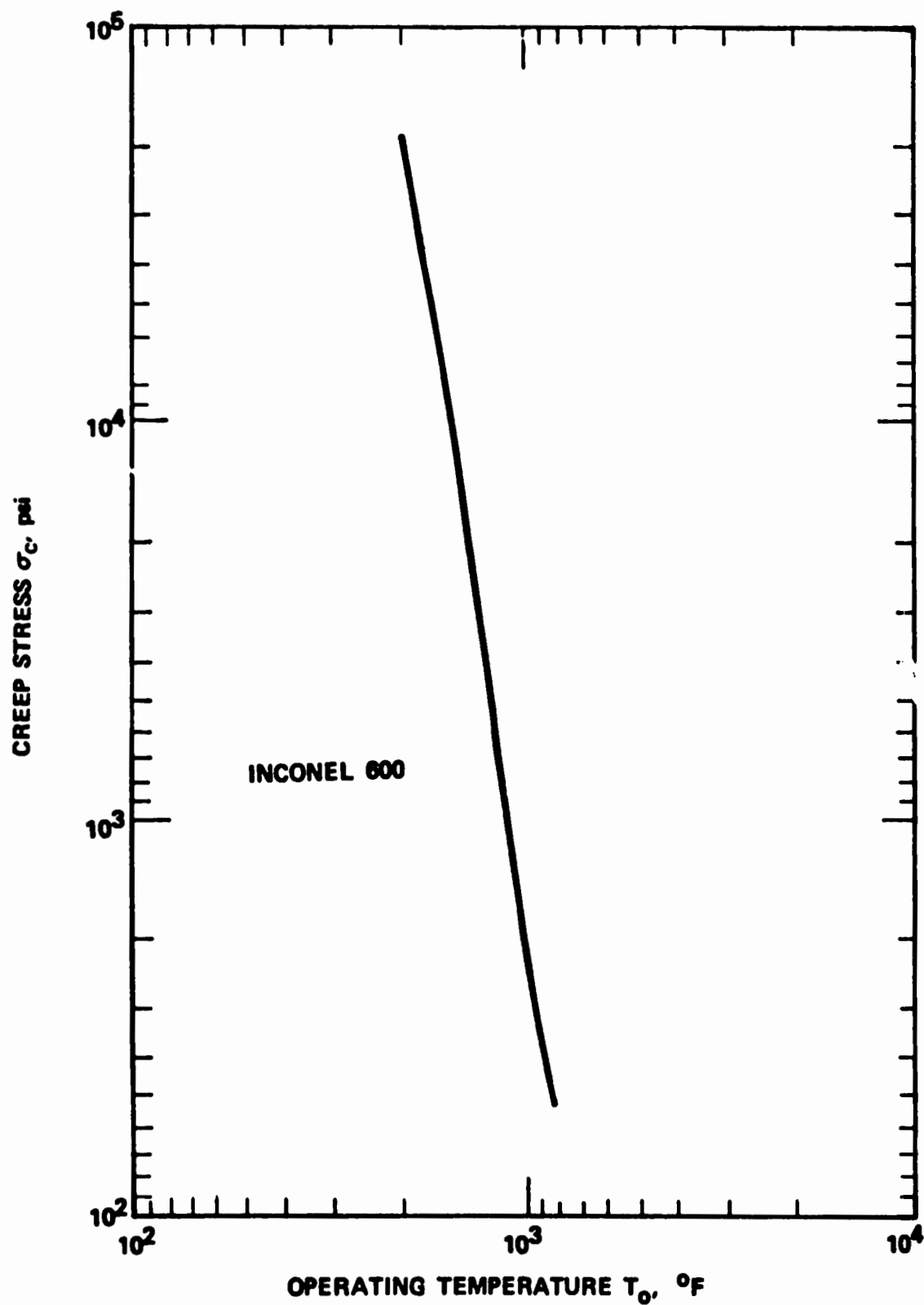


Figure 78. Creep Stress of Inconel 600

3.10 CONCLUSIONS

The failure analysis of the first primary heat pipe provided a fairly good understanding of the operational behavior of the first primary heat pipe and the cause for its final failure. All test data confirmed that the first primary heat pipe did not have the power transfer capacity for which it had been designed.

Apparently, the evaluation of the wick as a conduit for returning the working fluid from the condenser to the evaporator was not well understood, otherwise the construction of the diametral wick could not have been permitted to be so different from the construction that was assumed in the analysis. Furthermore, the effect of the vapor flow area on the pressure drop of the vapor was not fully evaluated in the design calculations. In the computer program, a circular flow area was assumed while in the final design, the flow area consisted of two passages separated by the diametral wick. The actual flow passage proved to present to the vapor flow twice the pressure drop than the assumed circular flow passage.

During the initial testing, the detrimental effect of large temperature gradients were not recognized. The heat pipe was repeatedly exposed to thermal stress conditions which finally led to the failure of the first primary heat pipe.

The results of the initial testing of the first primary heat pipe pointed out that prior to designing of another high power heat pipe, a better understanding of the characteristic of wicks made of bolting cloth had to be obtained. The failure analysis made it quite clear that testing of the heat pipe has to be conducted in such a fashion that large thermal gradients along the heat pipe are avoided. This shed a new light on the transient start-up and added a new parameter to the start-up limits of a heat pipe.

SECTION IV

DESIGN, MANUFACTURING, AND TESTING OF SECOND PRIMARY HEAT PIPE

4.1 INTRODUCTION

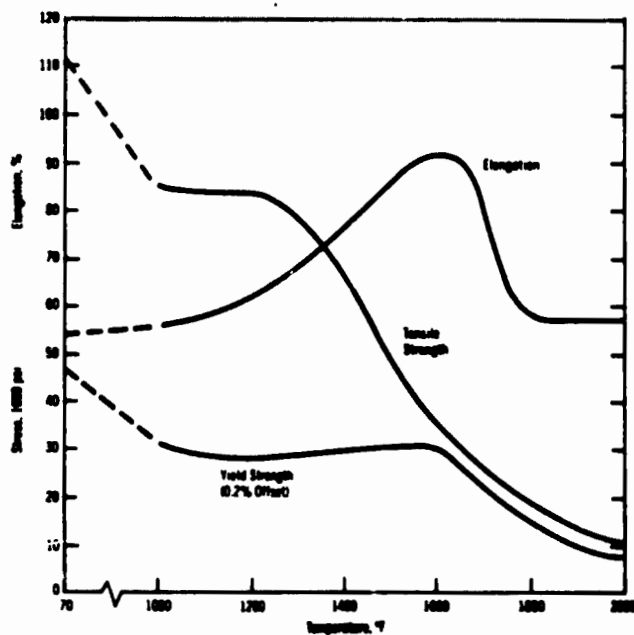
After the failure of the first primary heat pipe, it was decided to build a second primary heat pipe. The failure analysis had provided enough confidence that the cause for the failure was well understood and that a second heat pipe could be designed that could achieve the desired performance. It was, however, felt that prior to the design of the second primary heat pipe, it was imperative to obtain a better understanding of the characteristic of the wick structure made of layers of bolting cloth. The test data seemed to have indicated that the correlation for the permeability of the wick structure as used in the design of the first heat pipe was not predicting well the performance of the wick structure in the primary heat pipe.

Since the failure of the first primary heat pipe was definitely traced to longitudinal stresses caused by large temperature differentials along the heat pipe, it seemed advisable to build the second primary heat pipe of a material that had a higher creep strength than Inconel 600 at the operating temperature and thus would be less susceptible to the temperature differentials that might not be avoidable during start up of the primary heat pipe.

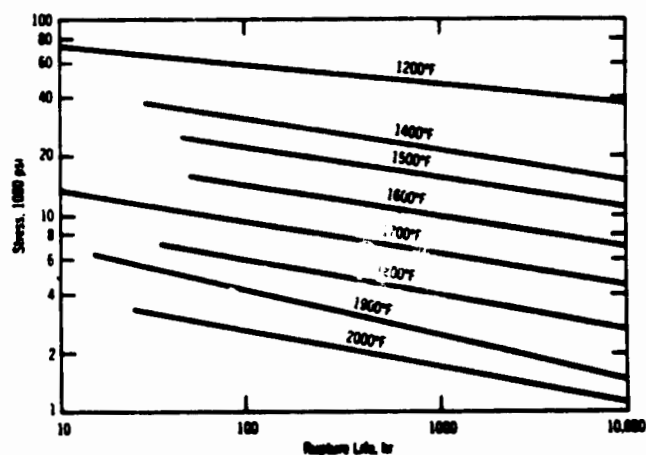
It was also decided that, if at all possible, the outer dimension of the second primary heat pipe should remain the same as that of the first primary heat pipe so that after successful testing of the heat pipe it could be mated with the secondary heat pipe which had been tested and found to perform according to design. After consultation with the vendor of the Inconel material, the new Inconel 617 alloy appeared to have the preferred characteristic creep strength without having apparent disadvantages over Inconel 600. The vendor recommended initially the readily available alloy Inconel 800 which has been used extensively for sodium heat pipes but at considerably lower operating temperatures. The alloy was found to have actually a lower creep strength at the design operating temperature and was therefore felt unsuitable for the application. In Figure 79, the creep strength of Inconel 600 and Inconel 617 are compared.

4.2 SECOND PRIMARY HEAT PIPE DESIGN

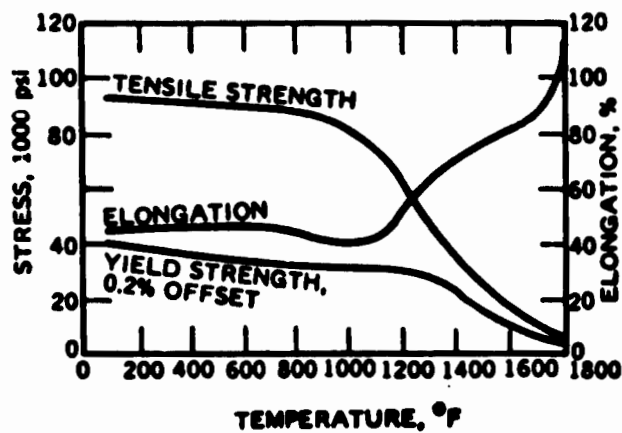
After the completion of the experimental wick study which is presented in Volume III, Section IX, of this report, the design of the second primary heat pipe was initiated. A computer program was developed which permitted studying all pertinent parameters as they affect heat pipe operation.



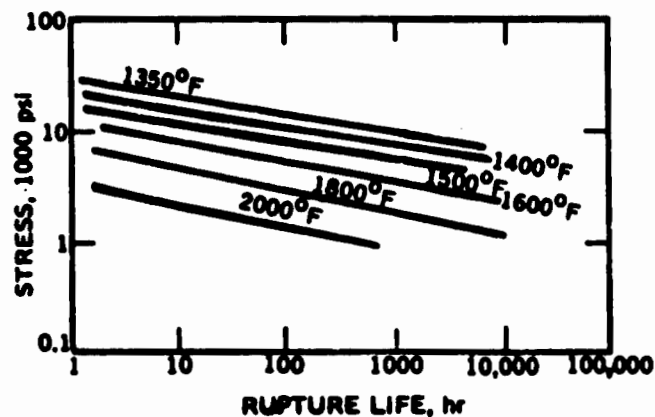
High-Temperature Tensile Properties of Inconel Alloy 617



Rupture Strength of Solution-Annealed Inconel Alloy 617



High-Temperature Tensile Properties of Inconel Alloy 600



Rupture Properties of Solution-Annealed Inconel Alloy 600

Figure 79. Characteristics of Inconel 600 and Inconel 617
(Taken from information provided by The International Nickel Company, Huntington Alloy Division)

The major parameters which affect the power transfer capacity of a heat pipe are:

- a. Heat pipe diameter
- b. Wick flow area
- c. Wick configuration
- d. Mesh size
- e. Wire diameter
- f. Wick construction

For the second primary heat pipe, the outer diameter was fixed by the interface with the secondary heat pipe. The secondary heat pipe was built with an internal diameter that permitted mating with the first primary heat pipe which had an external diameter of 2.25 inches. The design of the second primary heat pipe was therefore restricted to an outside diameter of 2.25 inches. Nevertheless, calculations were also carried out for heat pipes with larger diameters to determine the effect of a larger diameter on the overall design and power transfer capacity of the heat pipe.

The wick study, conducted in support of the heat pipe design, confirmed that the permeability of wicks made of bolting cloth, which had been used in the design of the first primary heat pipe, was not predicted correctly by the correlations of Reference 1. The results of the wick study, as they were applicable to the second primary heat pipe design, could be summarized as follows:

- a. For the bolting cloth, used in the first primary heat pipe design, the calculated permeability was only one-half of the actual. (See Figure 80.)
- b. The permeability decreases approximately by a factor of four when the wick made of bolting cloth is compressed to 0.75 times its nominal thickness. (See Figure 81.)
- c. The error in the calculated permeability, in combination with the change of permeability due to the unaccounted for variation in the manufacturing process (i.e., compressing the wick to 0.75 times its nominal thickness) resulted in an actual wick permeability of only about half the permeability on which the design of the first primary heat pipe had been based.

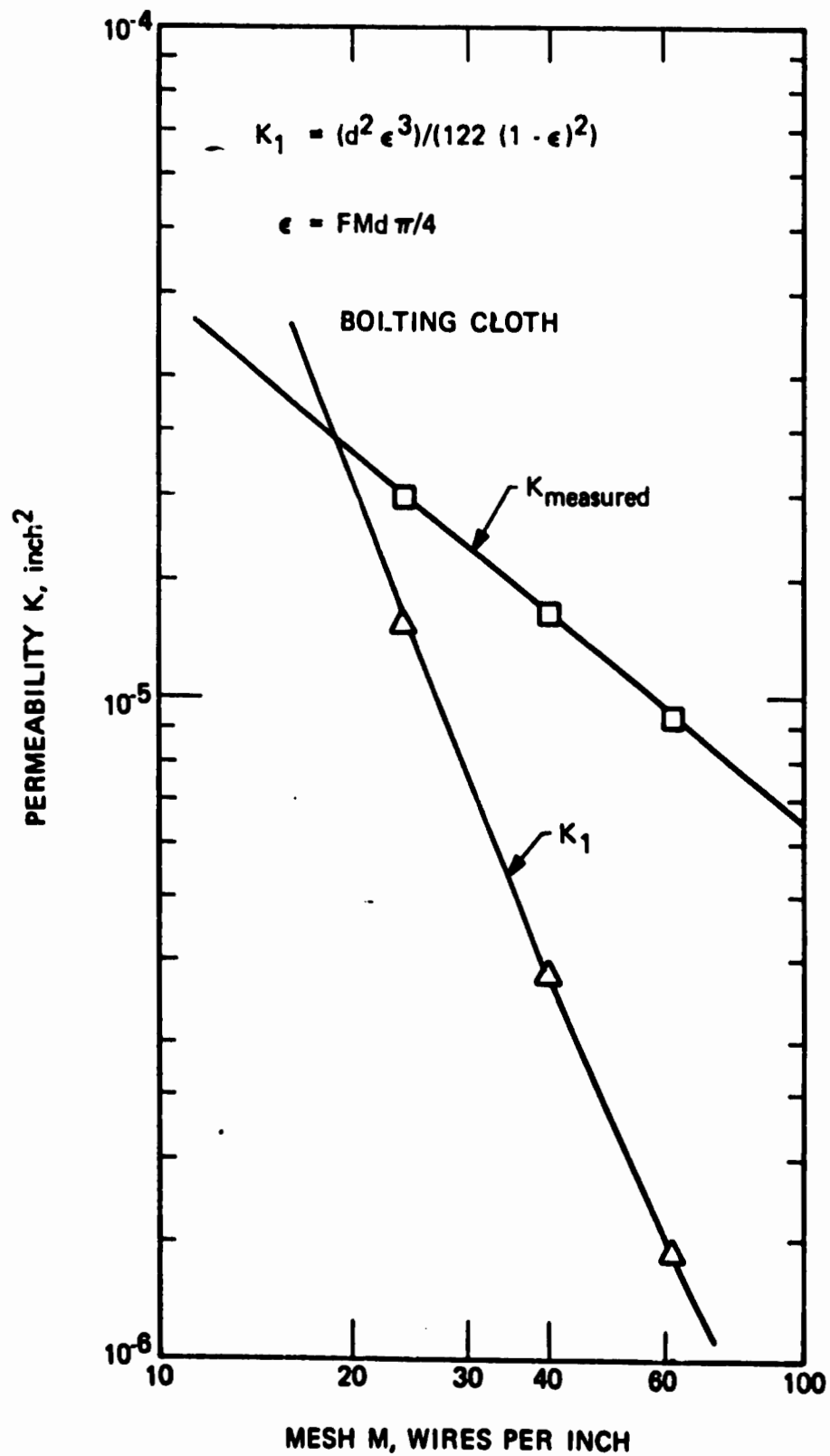


Figure 80. Permeability K for Standard Bolting Cloth

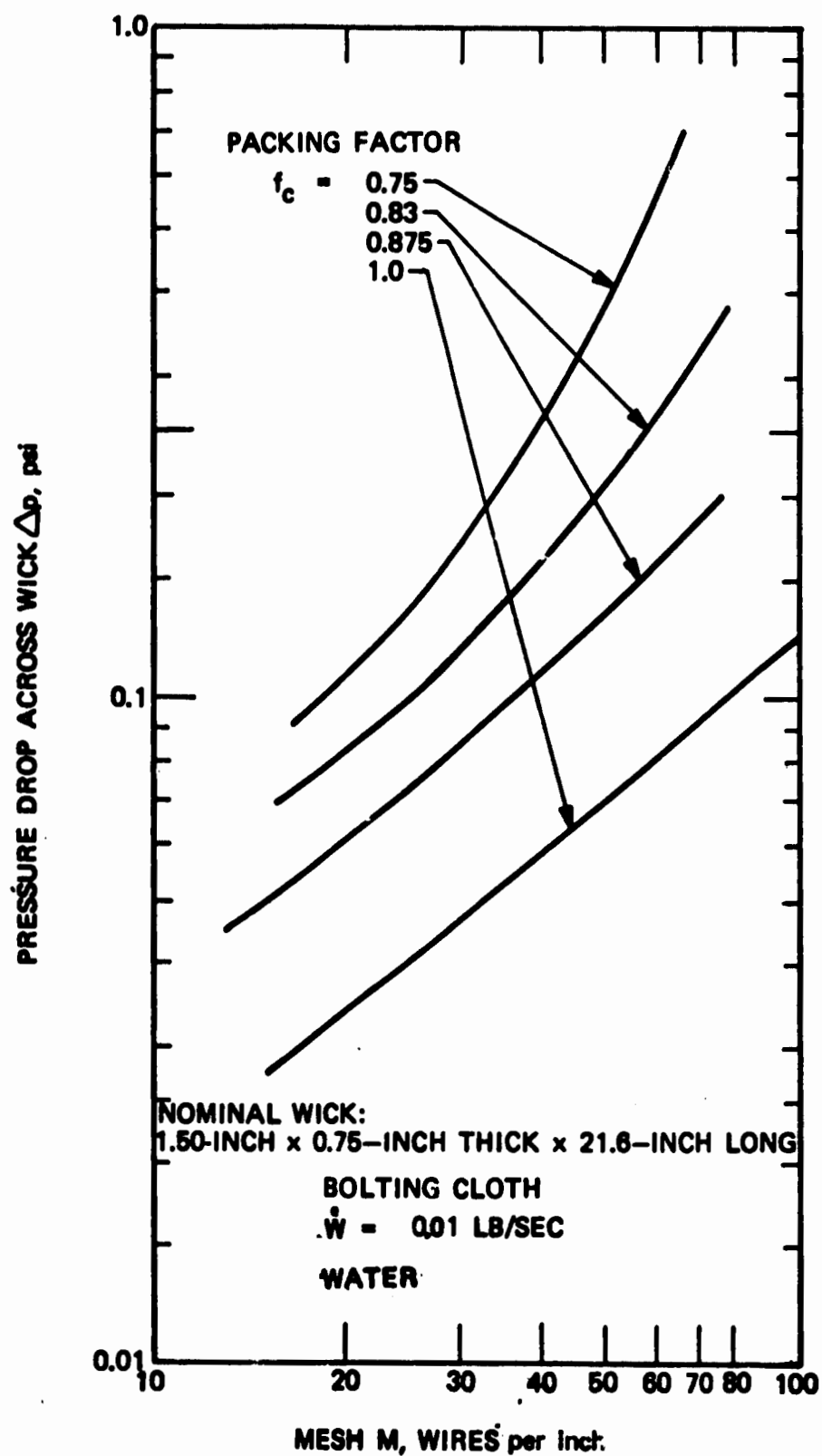


Figure 81. Pressure Drop Across a Wick Structure

50844

Furthermore, the analytical study confirmed that the configuration of the wick had a considerable effect on the performance of the heat pipe. In the design of the first primary heat pipe, the analytical model assumed a wall wick leaving a single flow path of circular cross-sectional area for the vapor flow. The construction of the heat pipe, however, employed a diametrical wick which provided two separate flow paths for the vapor flow. This construction, which was in variance from the analytical model used for the design, resulted in a considerably higher pressure drop of the vapor flow than had been established by the analysis.

The heat pipe analysis and the computer program, based on that analysis which was used for the design of the second primary heat pipe, took all design constraints into account and permitted evaluation of the permeability based on the data measured in the wick study. The computer output is headed by the invariables provided as input data, the working fluid, the operating temperature, the power capacity, the outer heat pipe diameter, the wall thickness, the total heat pipe length and the wall wick thickness. Following the input data are the properties of the working fluid which are also supplied as input data. The parametric study was performed by varying the angle ϕ as shown in Figure 82. Based on the three parameters, the dimensions of the heat pipe, the wall wick thickness and this angle, the elevation pressure, i.e., the suction pressure required for raising to and maintaining at the height of the heat pipe, the working fluid at the operating temperature, the wick thickness, t_w , the wick area, the vapor flow area, the ratio between these two areas, the sonic velocity of the vapor at the operating temperature and pressure and the actual vapor velocity in the vapor flow area when the heat pipe operates at full power transfer are calculated. The computer program automatically terminates the calculation when the calculated required flow velocity exceeds the sonic velocity as the flow velocity cannot exceed sonic flow in the heat pipe.

The second variable in the parametric study was the bolting cloth which is determined by its mesh and by its wire diameter.

The program can calculate the permeability of the bolting cloth by three correlations; the analytical correlation which was developed with the wick study, but which appears to calculate a permeability too low as based on the experimental results

$$K = \frac{d\epsilon^3}{16 \times (1 + \epsilon)^2} \text{ inch}^2$$

where

$$\epsilon = Md \pi/4$$

$$M \quad \text{Mesh, inch}^{-1}$$

$$d \quad \text{wire diameter, inch}$$

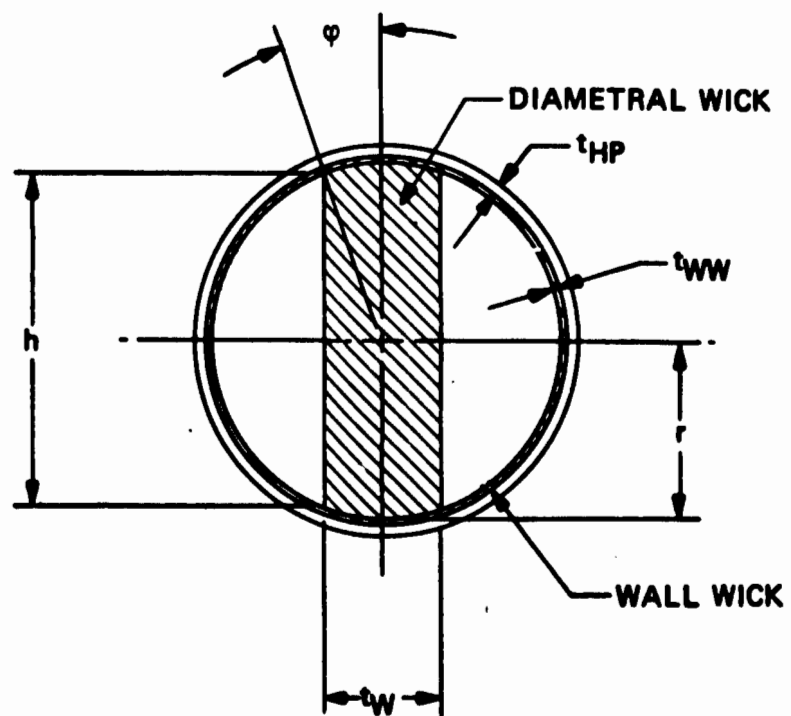


Figure 82. Heat Pipe Design Dimensions

50843

the semiempirical correlation which is presented in Reference 1 and uses an analytically derived relation with a correction factor

$$K = \frac{\epsilon^3 d^2}{122(1-\epsilon)^2} \text{ in}^2$$

and the experimentally determined correlation for bolting cloth

$$K = 2.51 \times 10^{-4} M^{-0.797} \text{ in}^2 = 1.62 \times 10^{-3} M^{-0.797} \text{ cm}^2$$

The permeability correlation used in the calculation is indicated in the heading of the computer output. The third column of the computer output presents the suction, i.e., the capillary force available for moving the liquid sodium through the wick and raising it to the height of the heat pipe. This value is entirely a function of the mesh size and the wire diameter of the bolting cloth for a given working fluid. The fifth column presents the pressure drop of the liquid sodium when it flows at the required rate for transferring the stated power from the evaporator to the condenser of the heat pipe. The pressure drop of the vapor flow is shown in column six. The total pressure drop associated with the operation of the heat pipe at the required power transfer and at the 1-g gravity of the laboratory is printed out in column seven. The difference between the suction and the total pressure difference divided by the total pressure is presented in percentage in column eight as safety factor. For the heat pipe to operate with the required power transfer the safety factor has to be greater than zero.

Table VIII presents the computer output for calculations made with the permeability correlation which was employed in the design of the first primary heat pipe. For all conditions the safety factor shown in column eight is negative, indicating that for the assumed permeability correlation no design could have satisfied the power transfer requirements of 6.3 kW. In Figure 83, the results are plotted to show, in graphical form, that the lowest negative safety factor of -22.5 is obtained with a wick that uses a 40 mesh bolting cloth and is 2.7 cm wide.

The actual wick was 2.845 cm wide and used a bolting cloth of 38 mesh. In Table IX, the results of the calculations are presented which used the experimentally determined permeability. With the permeabilities determined by the experimental wick study, safety factors well above zero can be found for many design configurations. This presumes naturally that the wick is built without compression, i.e., with a packing factor of unity. This corresponds to a wick thickness equal to the nominal thickness because the multilayer wick has not been compressed. The results are plotted in Figure 84.

TABLE VIII

PARAMETRIC STUDY OF A 2.25-INCH DIAMETER HEAT PIPE
(USING SEMIANALYTICAL PERMEABILITY)

HEAT PIPE PROGRAM HP2 K=1 13 NOVEMBER 1973

$$K = \frac{r^3 d^4}{122 (1-e)^4}$$

PROGRAM 4074-341-001

PARAMETRIC STUDY 12 DECEMBER 1973

WORKING FLUID SODIUM 22.991 GRAM/MOL
 OPERATING TEMPERATURE 1556. DEG.F
 POWER 6300.00 WATT
 HEAT PIPE DIAMETER 2.250 INCH WALL THICKNESS .0620 INCH
 WICK LENGTH 160.000 INCH WALL WICK THICKNESS .0440 INCH

PROPERTIES							
				FLUID		VAPOR	
LATENT HEAT, JOULES/G				.440E 04			
SURFACE TENSION, G/SEC2				.124E 03			
THERMAL CONDUCTIVITY, WATT/CM-DEG.K				.540E 00			
VISCOSITY, G/SEC-CM				.164E-02		.225E-03	
SPECIFIC GRAVITY, G/SEC3				.748E 00		.195E-03	
SPECIFIC HEAT, JOULES/G						.208E 02	
PARTIAL PRESSURE, DYN/CM2						.950E 01	
WICK THICKNESS 1.340 CM				ELEVATION PRESSURE 3800.24		DYN/CM2	
ANGLE 15.00 DEG		AREA RATIO .4833		SONIC VELOCITY		64218.6 CM/SEC	
WICK AREA 6.857 CM2		VAPOR AREA 14.189 CM2		VELOCITY		517.503 CM/SEC	
MESH WIRE		PERMEABILITY	SUCTION DELP W	DELP V	DELP T	SAFETY	
IN-1, INCH		CM2	DYN/CM2	DYN/CM2	DYN/CM2	PERC.	
20	.0090	.120E-03	3368.	1743.	293.	5636.	-42.29
30	.0065	.510E-04	5147.	4098.	293.	8191.	-37.17
40	.0065	.236E-04	7465.	8882.	293.	12974.	-42.46
50	.0055	.144E-04	9524.	14554.	293.	18647.	-46.92
60	.0045	.101E-04	11351.	20626.	293.	24719.	-54.06
70	.0037	.772E-05	13046.	27114.	293.	31207.	-56.20
80	.0037	.525E-05	15693.	39879.	293.	43972.	-64.31
90	.0035	.389E-05	18145.	53745.	293.	57838.	-68.63
WICK THICKNESS 1.770 CM				ELEVATION PRESSURE 3800.24		DYN/CM2	
ANGLE 20.00 DEG		AREA RATIO .7447		SONIC VELOCITY		64218.6 CM/SEC	
WICK AREA 8.983 CM2		VAPOR AREA 12.063 CM2		VELOCITY		608.699 CM/SEC	
MESH WIRE		PERMEABILITY	SUCTION DELP W	DELP V	DELP T	SAFETY	
IN-1, INCH		CM2	DYN/CM2	DYN/CM2	DYN/CM2	PERC.	
20	.0090	.120E-03	3368.	1331.	430.	5561.	-39.43
30	.0065	.510E-04	5147.	3129.	430.	7359.	-30.06
40	.0065	.236E-04	7465.	6780.	430.	11010.	-32.20
50	.0055	.144E-04	9524.	11110.	430.	15340.	-37.91
60	.0045	.101E-04	11351.	15745.	430.	19975.	-43.18
70	.0037	.772E-05	13046.	20698.	430.	24928.	-47.67
80	.0037	.525E-05	15693.	30442.	430.	34672.	-54.74
90	.0035	.389E-05	18145.	41026.	430.	45256.	-59.91

TABLE VIII

PARAMETRIC STUDY OF A 2.25-INCH DIAMETER HEAT PIPE
(USING SEMIANALYTICAL PERMEABILITY) (Contd)

WICK THICKNESS 2.188 CM ELEVATION PRESSURE 3800.24 DYN/CM²
ANGLE 25.00 DEG AREA RATIO 1.0904 SONIC VELOCITY 64218.6 CM/SEC
WICK AREA 10.976 CM² VAPOR AREA 1.18 CM² VELOCITY 729.31 CM/SEC

MESH WIRE IN-1, INCH	PERMEABILITY CM ²	SUCTION DELP W DYN/CM ²	DELP V DYN/CM ²	DELP T DYN/CM ²	SAFETY PERC.		
20	.0090	.120E-03	3368.	1089.	659.	5548.	-39.29
30	.0065	.510E-04	5147.	2560.	659.	7020.	-26.68
40	.0065	.236E-04	7465.	5546.	659.	10007.	-25.41
50	.0055	.144E-04	9524.	9091.	659.	13551.	-29.71
60	.0045	.101E-04	11351.	12864.	659.	17343.	-34.55
70	.0037	.772E-05	13046.	16937.	659.	21396.	-39.03
80	.0037	.525E-05	15693.	24910.	659.	29369.	-46.57
90	.0035	.389E-05	18145.	33571.	659.	36030.	-52.29

WICK THICKNESS 2.586 CM ELEVATION PRESSURE 3800.24 DYN/CM²
ANGLE 30.00 DEG AREA RATIO 1.5575 SONIC VELOCITY 64218.6 CM/SEC
WICK AREA 12.617 CM² VAPOR AREA 8.229 CM² VELOCITY 892.295 CM/SEC

MESH WIRE IN-1, INCH	PERMEABILITY CM ²	SUCTION DELP W DYN/CM ²	DELP V DYN/CM ²	DELP T DYN/CM ²	SAFETY PERC.		
20	.0090	.120E-03	3368.	933.	1061.	5794.	-41.67
30	.0065	.510E-04	5147.	2193.	1061.	7054.	-27.04
40	.0065	.236E-04	7465.	4752.	1061.	9613.	-22.35
50	.0055	.144E-04	9524.	7787.	1061.	12648.	-24.70
60	.0045	.101E-04	11351.	11035.	1061.	15897.	-28.60
70	.0037	.772E-05	13046.	14506.	1061.	19368.	-32.64
80	.0037	.525E-05	15693.	21336.	1061.	26197.	-40.09
90	.0035	.389E-05	18145.	28754.	1061.	33616.	-46.02

WICK THICKNESS 2.969 CM ELEVATION PRESSURE 3800.24 DYN/CM²
ANGLE 35.00 DEG AREA RATIO 2.2052 SONIC VELOCITY 64218.6 CM/SEC
WICK AREA 14.486 CM² VAPOR AREA 6.566 CM² VELOCITY 1118.244 CM/SEC

MESH WIRE IN-1, INCH	PERMEABILITY CM ²	SUCTION DELP W DYN/CM ²	DELP V DYN/CM ²	DELP T DYN/CM ²	SAFETY PERC.		
20	.0090	.120E-03	3368.	826.	1806.	6432.	-47.63
30	.0065	.510E-04	5147.	1941.	1806.	7547.	-31.81
40	.0065	.236E-04	7465.	4206.	1806.	9813.	-23.92
50	.0055	.144E-04	9524.	6892.	1806.	12499.	-23.80
60	.0045	.101E-04	11351.	9768.	1806.	15375.	-26.17
70	.0037	.772E-05	13046.	12841.	1806.	18447.	-29.28
80	.0037	.525E-05	15693.	18886.	1806.	24492.	-35.92
90	.0035	.389E-05	18145.	25452.	1806.	31059.	-41.58

TABLE VIII

PARAMETRIC STUDY OF A 2.25-INCH DIAMETER HEAT PIPE
(USING SEMIANALYTICAL PERMEABILITY) (Contd)

WICK THICKNESS 3.327 CM ELEVATION PRESSURE 3600.24 DYN/CM²
 ANGLE 40.00 DEG AREA RATIO 3.1306 SONIC VELOCITY 64218.6 CM/SEC
 WICK AREA 15.951 CM² VAPOR AREA 5.095 CM² VELOCITY 1441.205 CM/SEC

MESH WIRE PERMEABILITY SUCTION DELP W DELP V DELP T SAFETY
 IN-1, INCH CM² DYN/CM² DYN/CM² DYN/CM² DYN/CM² PERC.

20	.0090	.120E-03	3368.	749.	3281.	7830.	-56.96
30	.0065	.510E-04	5147.	1702.	3281.	8843.	-41.80
40	.0065	.236E-04	7465.	3818.	3281.	10699.	-31.51
50	.0055	.144E-04	9524.	6257.	3281.	13336.	-28.59
60	.0045	.101E-04	11351.	8867.	3281.	15948.	-26.63
70	.0037	.772E-05	13046.	11656.	3281.	18737.	-30.37
80	.0037	.525E-05	15693.	17143.	3281.	24224.	-35.22
90	.0035	.389E-05	18145.	23104.	3281.	30185.	-39.89

WICK THICKNESS 3.660 CM ELEVATION PRESSURE 3600.24 DYN/CM²
 ANGLE 45.00 DEG AREA RATIO 4.5038 SONIC VELOCITY 64218.6 CM/SEC
 WICK AREA 17.222 CM² VAPOR AREA 3.824 CM² VELOCITY 1920.233 CM/SEC

MESH WIRE PERMEABILITY SUCTION DELP W DELP V DELP T SAFETY
 IN-1, INCH CM² DYN/CM² DYN/CM² DYN/CM² DYN/CM² PERC.

20	.0090	.120E-03	3368.	694.	6437.	10931.	-69.19
30	.0065	.510E-04	5147.	1632.	6437.	11869.	-56.64
40	.0065	.236E-04	7465.	3536.	6437.	13773.	-45.80
50	.0055	.144E-04	9524.	5795.	6437.	16032.	-40.59
60	.0045	.101E-04	11351.	8213.	6437.	18450.	-38.48
70	.0037	.772E-05	13046.	10796.	6437.	21033.	-37.97
80	.0037	.525E-05	15693.	15878.	6437.	26115.	-39.91
90	.0035	.389E-05	18145.	21399.	6437.	31636.	-42.65

WICK THICKNESS 3.965 CM ELEVATION PRESSURE 3600.24 DYN/CM²
 ANGLE 50.00 DEG AREA RATIO 6.6353 SONIC VELOCITY 64218.6 CM/SEC
 WICK AREA 16.269 CM² VAPOR AREA 2.756 CM² VELOCITY 2663.865 CM/SEC

MESH WIRE PERMEABILITY SUCTION DELP W DELP V DELP T SAFETY
 IN-1, INCH CM² DYN/CM² DYN/CM² DYN/CM² DYN/CM² PERC.

20	.0090	.120E-03	3368.	654.	23898.	28351.	-88.12
30	.0065	.510E-04	5147.	1537.	23898.	29234.	-82.40
40	.0065	.236E-04	7465.	3330.	23898.	31028.	-75.94
50	.0055	.144E-04	9524.	5457.	23898.	33155.	-71.27
60	.0045	.101E-04	11351.	7733.	23898.	35431.	-67.96
70	.0037	.772E-05	13046.	10166.	23898.	37864.	-65.54
80	.0037	.525E-05	15693.	14951.	23898.	42649.	-63.20
90	.0035	.389E-05	18145.	20150.	23898.	47848.	-62.08

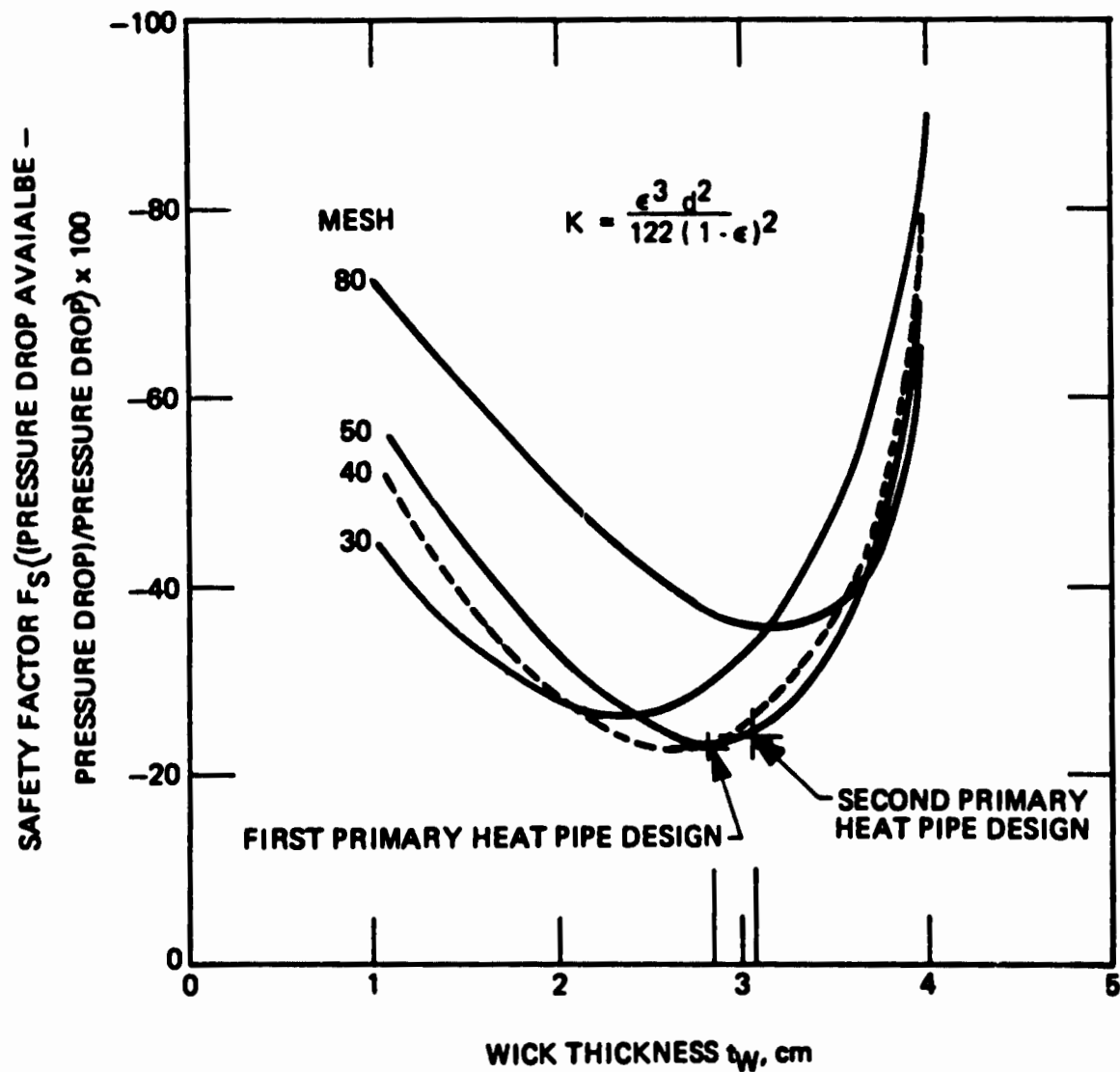


Figure 83. Safety Factor for a 2.25-inch Diameter 0.062-inch Wall Thickness Sodium Heat Pipe Operating with a Power Transfer of 6.3 kW

TABLE IX

PARAMETRIC STUDY OF A 2.25-INCH DIAMETER HEAT PIPE
(USING EXPERIMENTALLY DETERMINED PERMEABILITY)

HEAT PIPE PROGRAM HP3 K=1.62x10-3 IN-797 CM2

PROGRAM 4074-341-001
PARAMETRIC STUDY 12 DECEMBER 1973

WORKING FLUID SODIUM 22.991 GRAM/MOL
OPERATING TEMPERATURE 1556. DEG.F
POWER 6300.00 WATT
HEAT PIPE DIAMETER 2.250 INCH WALL THICKNESS .0620 INCH
WICK LENGTH 160.000 INCH WALL WICK THICKNESS

PROPERTIES	FLUID	VAPOR
LATENT HEAT, JOULES/G	.440E 04	
SURFACE TENSION, G/SEC2	.124E 03	
THERMAL CONDUCTIVITY, WATT/CM-DEG.K	.540E 00	
VISCOSITY, G/SEC-CM	.164E-02	.225E-03
SPECIFIC GRAVITY, G/SEC3	.748E 00	.195E-03
SPECIFIC HEAT, JOULES/G		.206E 02
PARTIAL PRESSURE, DYN/CM2		.950E 01

WICK THICKNESS 1.340 CM ELEVATION PRESSURE 3800.24 DYN/CM2
ANGLE 15.00 DEG AREA RATIO .4833 SONIC VELOCITY 64218.00 CM/SEC
WICK AREA 6.657 CM2 VAPOR AREA 1.169 CM2 C. Y. 2.1000 CM/SEC

MESH	WIRE	PERMEABILITY	SUCTION DELP	W DELP	V DELP	T DELP	SAFETY
IN-1, INCH		CM2	DYN/CM2	DYN/CM2	DYN/CM2	DYN/CM2	PERC.
20	.0090	.146E-03	3368.	1410.	293.	5502.	-38.79
30	.0065	.107E-03	5147.	1947.	293.	6040.	-14.79
40	.0065	.854E-04	7465.	2449.	293.	6542.	14.11
50	.0055	.715E-04	9524.	2926.	293.	7019.	35.69
60	.0045	.618E-04	11351.	3364.	293.	7477.	51.62
70	.0037	.547E-04	13046.	3626.	293.	7919.	64.74
80	.0037	.492E-04	15693.	4256.	293.	8349.	67.97
90	.0035	.448E-04	18145.	4675.	293.	8768.	106.95

WICK THICKNESS 1.770 CM ELEVATION PRESSURE 3600.24 DYN/CM2
ANGLE 20.00 DEG AREA RATIO .7447 SONIC VELOCITY 64218.6 CM/SEC
WICK AREA 8.983 CM2 VAPOR AREA 12.063 CM2 VELOCITY 608.699 CM/SEC

MESH	WIRE	PERMEABILITY	SUCTION DELP	W DELP	V DELP	T DELP	SAFETY
IN-1, INCH		CM2	DYN/CM2	DYN/CM2	DYN/CM2	DYN/CM2	PERC.
20	.0090	.146E-03	3368.	1076.	430.	5306.	-36.52
30	.0065	.107E-03	5147.	1486.	430.	5717.	-9.97
40	.0065	.854E-04	7465.	1870.	430.	6100.	22.38
50	.0055	.715E-04	9524.	2234.	430.	6464.	47.35
60	.0045	.618E-04	11351.	2583.	430.	6813.	66.60
70	.0037	.547E-04	13046.	2921.	430.	7151.	82.44
80	.0037	.492E-04	15693.	3249.	430.	7479.	109.84
90	.0035	.448E-04	18145.	3568.	430.	7799.	132.67

TABLE IX

PARAMETRIC STUDY OF A 2.25-INCH DIAMETER HEAT PIPE
(USING EXPERIMENTALLY DETERMINED PERMEABILITY) (Contd)

WICK THICKNESS 2.188 CM ELEVATION PRESSURE 3800.24 DYN/CM²
 ANGLE 25.00 DEG AREA RATIO 1.0904 SONIC VELOCITY 64218.6 CM/SEC
 WICK AREA 10.976 CM² VAPOR AREA 10.066 CM² VELOCITY 729.311 CM/SEC

MESH WIRE	PERMEABILITY	SUCTION DELP	W	DELP V	DELP T	SAFETY	
IN-1, INCH	CM ²	DYN/CM ²	DYN/CM ²	DYN/CM ²	DYN/CM ²	PERC.	
20	.0090	.148E-03	3368.	860.	659.	5340.	-36.92
30	.0065	.107E-03	5147.	1216.	659.	5676.	-9.33
40	.0065	.854E-04	7465.	1530.	659.	5669.	24.64
50	.0055	.715E-04	9524.	1826.	659.	6287.	51.49
60	.0045	.618E-04	11351.	2114.	659.	6573.	72.69
70	.0037	.547E-04	13046.	2390.	659.	6849.	90.47
80	.0037	.492E-04	15693.	2656.	659.	7118.	120.48
90	.0035	.448E-04	18145.	2920.	659.	7380.	145.86

WICK THICKNESS 2.568 CM ELEVATION PRESSURE 3800.24 DYN/CM²
 ANGLE 30.00 DEG AREA RATIO 1.5575 SONIC VELOCITY 64218.6 CM/SEC
 WICK AREA 12.617 CM² VAPOR AREA 8.229 CM² VELOCITY 892.295 CM/SEC

MESH WIRE	PERMEABILITY	SUCTION DELP	W	DELP V	DELP T	SAFETY	
IN-1, INCH	CM ²	DYN/CM ²	DYN/CM ²	DYN/CM ²	DYN/CM ²	PERC.	
20	.0090	.148E-03	3368.	754.	1061.	5616.	-40.02
30	.0065	.107E-03	5147.	1042.	1061.	5903.	-12.62
40	.0065	.854E-04	7465.	1310.	1061.	6172.	20.95
50	.0055	.715E-04	9524.	1565.	1061.	6427.	46.19
60	.0045	.618E-04	11351.	1810.	1061.	6672.	70.13
70	.0037	.547E-04	13046.	2047.	1061.	6909.	88.84
80	.0037	.492E-04	15693.	2277.	1061.	7138.	119.64
90	.0035	.448E-04	18145.	2501.	1061.	7363.	146.45

WICK THICKNESS 2.969 CM ELEVATION PRESSURE 3800.24 DYN/CM²
 ANGLE 35.00 DEG AREA RATIO 2.2052 SONIC VELOCITY 64218.6 CM/SEC
 WICK AREA 14.480 CM² VAPOR AREA 6.566 CM² VELOCITY 1118.244 CM/SEC

MESH WIRE	PERMEABILITY	SUCTION DELP	W	DELP V	DELP T	SAFETY	
IN-1, INCH	CM ²	DYN/CM ²	DYN/CM ²	DYN/CM ²	DYN/CM ²	PERC.	
20	.0090	.148E-03	3368.	668.	1806.	6274.	-46.31
30	.0065	.107E-03	5147.	922.	1806.	6529.	-21.17
40	.0065	.854E-04	7465.	1160.	1806.	6766.	10.32
50	.0055	.715E-04	9524.	1386.	1806.	6992.	36.21
60	.0045	.618E-04	11351.	1602.	1806.	7209.	57.46
70	.0037	.547E-04	13046.	1812.	1806.	7418.	75.86
80	.0037	.492E-04	15693.	2015.	1806.	7622.	105.90
90	.0035	.448E-04	18145.	2214.	1806.	7820.	132.02

TABLE IX

PARAMETRIC STUDY OF A 2.25-INCH DIAMETER HEAT PIPE
(USING EXPERIMENTALLY DETERMINED PERMEABILITY) (Contd)

WICK THICKNESS 3.327 CM ELEVATION PRESSURE 3800.24 DYN/CM²
ANGLE 40.00 DEG AREA RATIO 3.1306 SONIC VELOCITY 64218.6 CM/SEC
WICK AREA 15.921 CM² VAPOR AREA 5.095 CM² VELOCITY 1441.205 CM/SEC

MESH WIRE PERMEABILITY SUCTION DELP * DELP V DELP T SAFETY
IN-1, INCH CM² DYN/CM² DYN/CM² DYN/CM² DYN/CM² PERC.

20	.0090	.146E-03	3366.	606.	3261.	7687.	-56.18
30	.0065	.107E-03	5147.	837.	3261.	7916.	-35.00
40	.0065	.654E-04	7465.	1053.	3261.	6134.	-8.22
50	.0055	.715E-04	9524.	1258.	3261.	6339.	14.22
60	.0045	.618E-04	11351.	1455.	3261.	6535.	32.98
70	.0037	.547E-04	13046.	1645.	3261.	6726.	49.51
80	.0037	.492E-04	15693.	1829.	3261.	6910.	76.12
90	.0035	.448E-04	18145.	2010.	3261.	9090.	99.60

WICK THICKNESS 3.660 CM ELEVATION PRESSURE 3800.24 DYN/CM²
ANGLE 45.00 DEG AREA RATIO 4.5038 SONIC VELOCITY 64218.6 CM/SEC
WICK AREA 17.222 CM² VAPOR AREA 3.824 CM² VELOCITY 1920.233 CM/SEC

MESH WIRE PERMEABILITY SUCTION DELP * DELP V DELP T SAFETY
IN-1, INCH CM² DYN/CM² DYN/CM² DYN/CM² DYN/CM² PERC.

20	.0090	.148E-03	3368.	561.	6437.	10798.	-66.61
30	.0065	.107E-03	5147.	775.	6437.	11012.	-53.27
40	.0065	.654E-04	7465.	975.	6437.	11212.	-33.42
50	.0055	.715E-04	9524.	1165.	6437.	11402.	-16.47
60	.0045	.618E-04	11351.	1347.	6437.	11584.	-2.02
70	.0037	.547E-04	13046.	1523.	6437.	11760.	10.93
80	.0037	.492E-04	15693.	1694.	6437.	11932.	31.53
90	.0035	.448E-04	18145.	1861.	6437.	12098.	49.98

WICK THICKNESS 3.965 CM ELEVATION PRESSURE 3800.24 DYN/CM²
ANGLE 50.00 DEG AREA RATIO 6.6353 SONIC VELOCITY 64218.6 CM/SEC
WICK AREA 16.289 CM² VAPOR AREA 2.756 CM² VELOCITY 2663.865 CM/SEC

MESH WIRE PERMEABILITY SUCTION DELP * DELP V DELP T SAFETY
IN-1, INCH CM² DYN/CM² DYN/CM² DYN/CM² DYN/CM² PERC.

20	.0090	.146E-03	3368.	526.	23898.	28226.	-84.07
30	.0065	.107E-03	5147.	730.	23898.	28428.	-81.90
40	.0065	.654E-04	7465.	918.	23898.	28616.	-73.91
50	.0055	.715E-04	9524.	1097.	23898.	28795.	-66.92
60	.0045	.618E-04	11351.	1269.	23898.	28966.	-60.81
70	.0037	.547E-04	13046.	1434.	23898.	29132.	-55.22
80	.0037	.492E-04	15693.	1596.	23898.	29293.	-46.43
90	.0035	.448E-04	18145.	1753.	23898.	29451.	-38.39

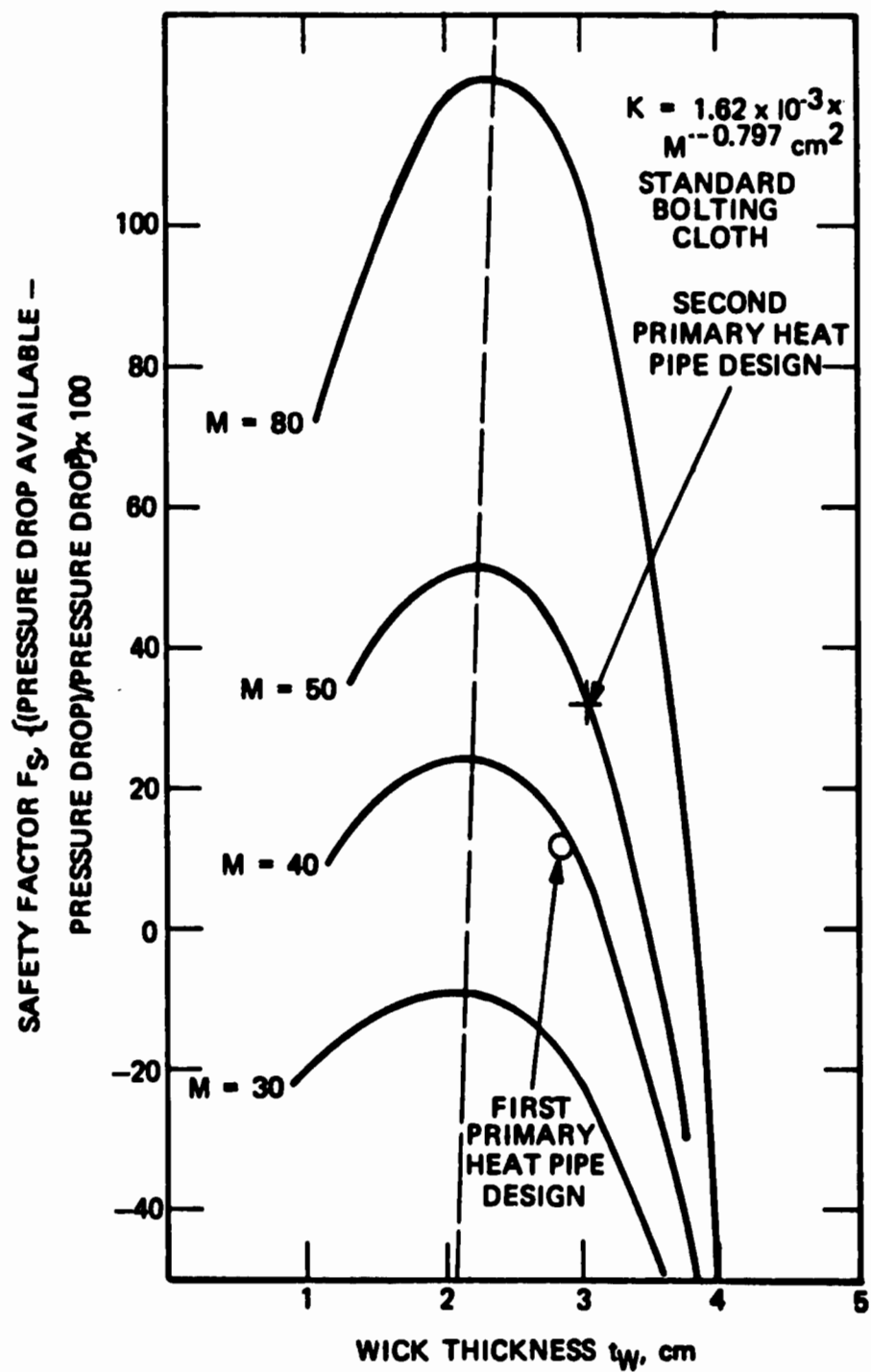


Figure 84. Safety Factor for a 2.25-inch Diameter 0.062-inch Wall Thickness Sodium Heat Pipe Operating with a Power Transfer of 6.3 kW

The results of the calculations based on the semi-analytically determined permeability, which are plotted in Figure 83, would indicate that the best design would consist of a wick 2.7 cm wide with a 40 Mesh bolting cloth. This design would not quite satisfy the requirements. The safety factor is negative, though least negative of all other possible combinations. The results of the calculations using the experimentally determined correlation between permeability and bolting cloth which are plotted in Figure 84 would have called for a wick of about 2.3 cm width and a bolting cloth of the largest mesh.

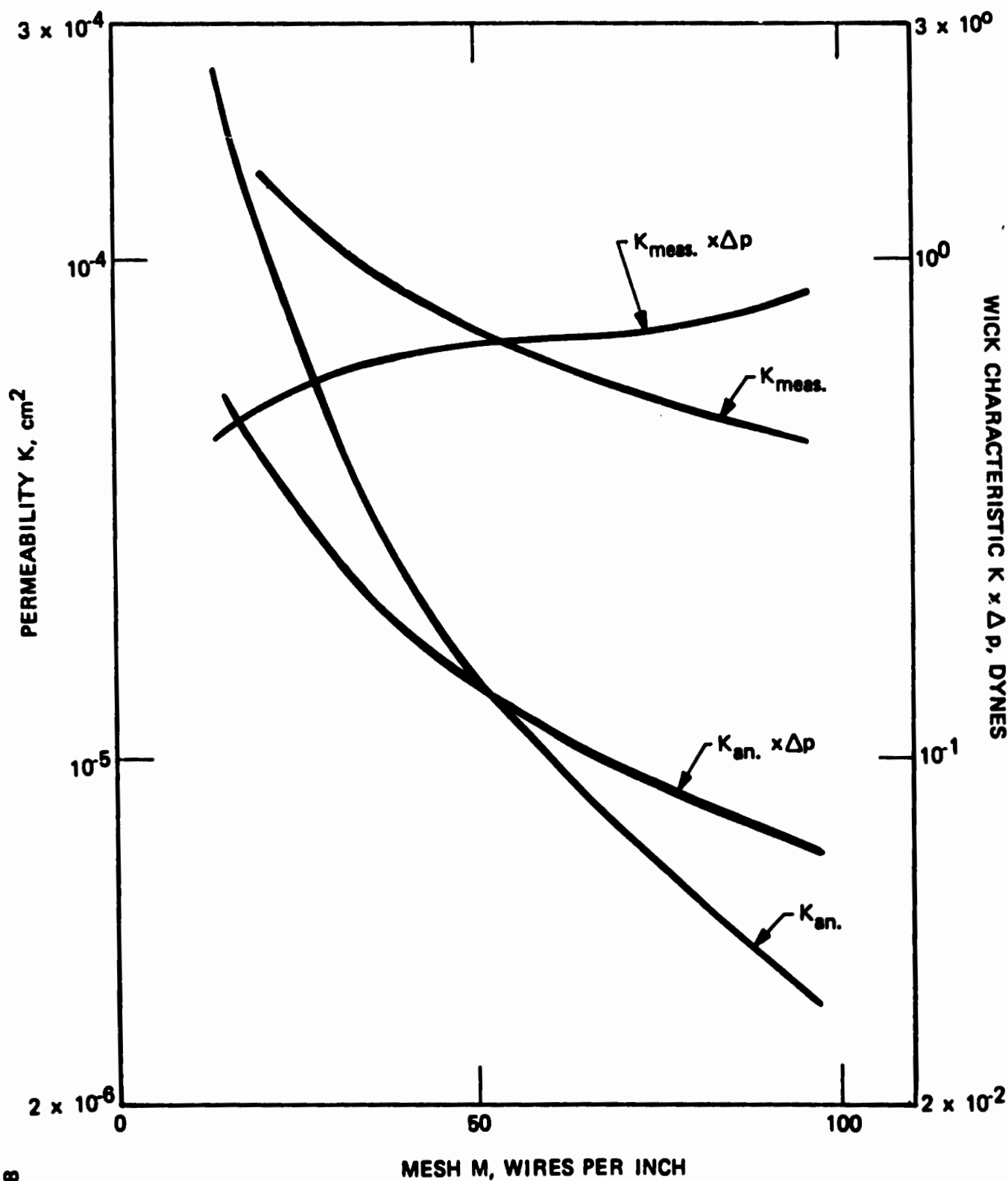
The measured as well as the analytically determined permeability decreases with increasing mesh value. The product of the capillary force and the permeability which determines the capacity of the wick, however, increases with mesh size for the measured permeability while it decreases for the analytically determined permeability. This is shown in Figure 85.

When the results plotted in Figure 84 are analyzed it is found that on the ascending side of the curves (positive slope) the safety factor improves due to the increasing flow area of the wick with a corresponding decrease in the vapor flow area with little detrimental effect. On the descending side of the curves (negative slope) the safety factor decreases because with the decreasing vapor flow area the pressure drop of the vapor flow rapidly increases without much decrease of the pressure drop in the wick. This is shown in Figure 86. The design that was chosen for the second primary heat pipe uses a bolting cloth of 50 mesh and has a width of 3.07 cm. With this design, the pressure drop in the vapor flow passage is still relatively low while at the same time the wick has a large flow area. This should minimize the effect of possible variations in the permeability of the wick structure which might be experienced in the full size wick. The final wick design for the second primary heat pipe is shown in Figure 87.

A parametric study of the effect of the heat pipe diameter on the power transfer capacity of the primary heat pipe was made using the permeability correlation used in the design of the first heat pipe. The results are presented in Tables X through XII. If the permeability correlation were accepted as valid, the primary heat pipe should have been designed with a minimum diameter of slightly more than 2.8 inches.

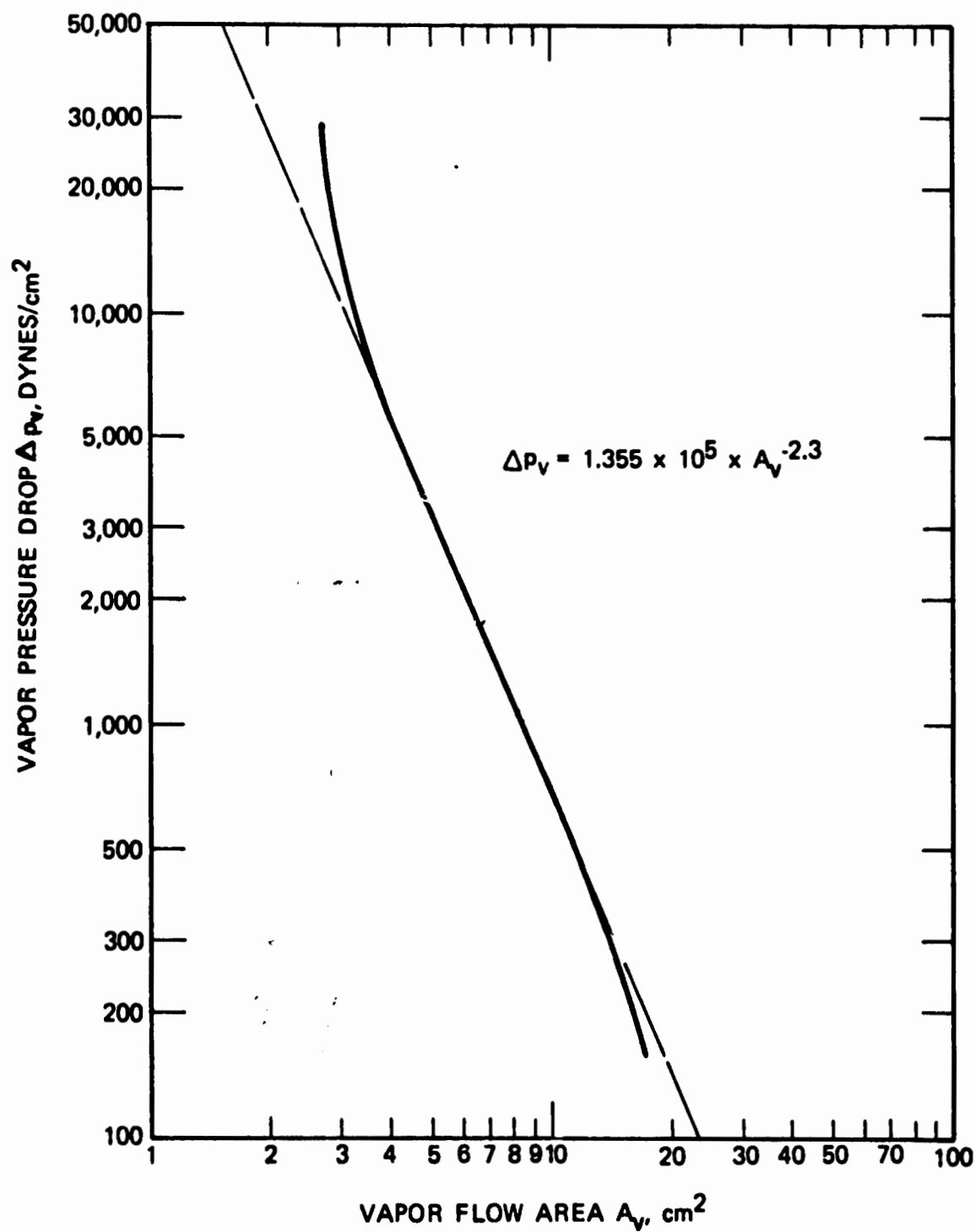
4.3 WORKING FLUID FILL CHARGE

With the design of the wick structure established, the amount of working fluid for charging the heat pipe had to be determined. With 22 layers per section and five sections, the wick width was 1.21 inch. The internal diameter for the diametral wick was 2.082 inch and equal to the external diameter of the heat pipe minus the double wall thickness of 0.062 inch and twice the wall wick thickness of 0.022 inch. The wick



50848

Figure 85. Permeability and Wick Characteristic of Bolting Cloth ($K_{\text{meas.}}$ Measured Permeability, $K_{\text{an.}}$ Semianalytically Derived Permeability)



50849

Figure 86. Vapor Pressure Drop as a Function of Flow Area

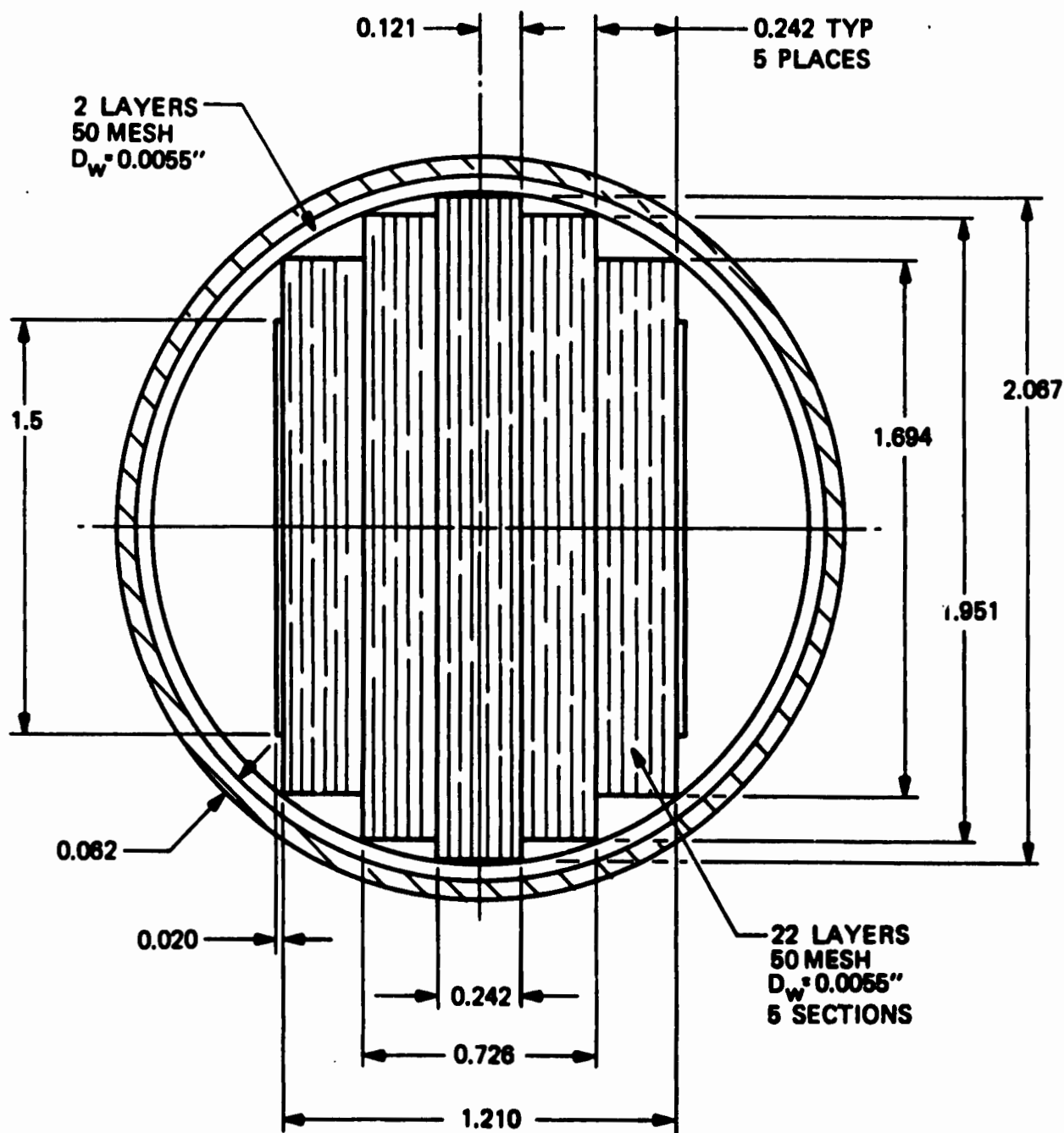


Figure 87. Wick Design for Primary Heat Pipe

TABLE X

PARAMETRIC STUDY FOR 2.5-INCH HEAT PIPE OPERATING WITH SODIUM

HEAT PIPE PROGRAM HP2 K=1 13 NOVEMBER 1973

$$K = \frac{\epsilon^3 d^2}{122(1-\epsilon)^2}$$

PROGRAM 4074-341-001
PARAMETRIC STUDY 12 DECEMBER 1973

WORKING FLUID SODIUM 22.991 GRAM/MOL
 OPERATING TEMPERATURE 1558. DEG.F
 POWER 6300.00 WATT
 HEAT PIPE DIAMETER 2.500 INCH WALL THICKNESS .0620 INCH
 WICK LENGTH 180.000 INCH WALL WICK THICKNESS .0440 INCH

PROPERTIES		FLUID	VAPOR
LATENT HEAT, JOULES/G		.440E 04	
SURFACE TENSION, G/SEC2		.124E 03	
THERMAL CONDUCTIVITY, WATT/CM-DEG.K		.540E 00	
VISCOSITY, G/SEC-CM		.164E-02	.225E-03
SPECIFIC GRAVITY, G/SEC3		.748E 00	.195E-03
SPECIFIC HEAT, JOULES/G			.208E 02
PARTIAL PRESSURE, DYN/CM2			.950E 01
WICK THICKNESS 1.504 CM ELEVATION PRESSURE 4266.41 DYN/CM2			
ANGLE 15.00 DEG AREA RATIO .4833 SONIC VELOCITY 64218.6 CM/SEC			
WICK AREA 8.643 CM2 VAPOR AREA 17.883 CM2 VELOCITY 410.590 CM/SEC			
MESH WIRE	PERMEABILITY	SUCTION DELP W	DELP V DELP T SAFETY
IN-1, INCH	CM2	DYN/CM2 DYN/CM2	DYN/CM2 DYN/CM2 PERC.
20 .0090	.120E-03	3368. 1383.	184. 5834. -42.26
30 .0065	.510E-04	5147. 3252.	184. 7702. -33.18
40 .0065	.236E-04	7465. 7047.	184. 11497. -35.07
50 .0055	.144E-04	9524. 11547.	184. 15996. -40.47
60 .0045	.101E-04	11351. 16365.	184. 20816. -45.47
70 .0037	.772E-05	13046. 21513.	184. 25963. -49.75
80 .0037	.525E-05	15693. 31640.	184. 36091. -56.52
90 .0035	.389E-05	18145. 42641.	184. 47092. -61.47
WICK THICKNESS 1.988 CM ELEVATION PRESSURE 4266.41 DYN/CM2			
ANGLE 20.00 DEG AREA RATIO .7447 SONIC VELOCITY 64218.6 CM/SEC			
WICK AREA 11.322 CM2 VAPOR AREA 15.204 CM2 VELOCITY 482.946 CM/SEC			
MESH WIRE	PERMEABILITY	SUCTION DELP W	DELP V DELP T SAFETY
IN-1, INCH	CM2	DYN/CM2 DYN/CM2	DYN/CM2 DYN/CM2 PERC.
20 .0090	.120E-03	3368. 1056.	271. 5593. -39.77
30 .0065	.510E-04	5147. 2482.	271. 7019. -26.68
40 .0065	.236E-04	7465. 5379.	271. 9916. -24.72
50 .0055	.144E-04	9524. 8815.	271. 13352. -28.67
60 .0045	.101E-04	11351. 12492.	271. 17029. -33.35
70 .0037	.772E-05	13046. 16422.	271. 20959. -37.75
80 .0037	.525E-05	15693. 24153.	271. 28690. -45.30
90 .0035	.389E-05	18145. 32550.	271. 37088. -51.08

TABLE X

PARAMETRIC STUDY FOR 2.5-INCH HEAT PIPE OPERATING WITH SODIUM (Contd)

WICK THICKNESS 2.456 CM ELEVATION PRESSURE 4266.41 DYN/CM²
 ANGLE 25.00 DEG AREA RATIO 1.0904 SONIC VELOCITY 64218.6 CM/SEC
 WICK AREA 13.536 CM² VAPOR AREA 12.690 CM² VELOCITY 578.640 CM/SEC

MESH WIRE PERMEABILITY SUCTION DELP W DELP V DELP T SAFETY
 IN-1, INCH CM² DYN/CM² DYN/CM² DYN/CM² DYN/CM² PERC.

20	.0090	.120E-03	3368.	864.	415.	5545.	-39.26
30	.0065	.510E-04	5147.	2031.	415.	6713.	-23.33
40	.0065	.236E-04	7465.	4402.	415.	9083.	-17.81
50	.0055	.144E-04	9524.	7213.	415.	11894.	-19.93
60	.0045	.101E-04	11351.	10222.	415.	14904.	-23.84
70	.0037	.772E-05	13046.	13438.	415.	18119.	-28.00
80	.0037	.525E-05	15693.	19763.	415.	24445.	-35.80
90	.0035	.389E-05	18145.	26635.	415.	31317.	-42.06

WICK THICKNESS 2.906 CM ELEVATION PRESSURE 4266.41 DYN/CM²
 ANGLE 30.00 DEG AREA RATIO 1.5575 SONIC VELOCITY 64218.6 CM/SEC
 WICK AREA 16.154 CM² VAPOR AREA 10.372 CM² VELOCITY 707.952 CM/SEC

MESH WIRE PERMEABILITY SUCTION DELP W DELP V DELP T SAFETY
 IN-1, INCH CM² DYN/CM² DYN/CM² DYN/CM² DYN/CM² PERC.

20	.0090	.120E-03	3368.	740.	668.	5674.	-40.64
30	.0065	.510E-04	5147.	1740.	668.	6674.	-22.69
40	.0065	.236E-04	7465.	3770.	668.	8705.	-14.24
50	.0055	.144E-04	9524.	6178.	668.	11112.	-14.29
60	.0045	.101E-04	11351.	8755.	668.	13690.	-17.09
70	.0037	.772E-05	13046.	11510.	668.	16444.	-20.66
80	.0037	.525E-05	15693.	16928.	668.	21862.	-28.22
90	.0035	.389E-05	18145.	22814.	668.	27748.	-34.61

WICK THICKNESS 3.333 CM ELEVATION PRESSURE 4266.41 DYN/CM²
 ANGLE 35.00 DEG AREA RATIO 2.2051 SONIC VELOCITY 64218.6 CM/SEC
 WICK AREA 16.250 CM² VAPOR AREA 8.276 CM² VELOCITY 887.221 CM/SEC

MESH WIRE PERMEABILITY SUCTION DELP W DELP V DELP T SAFETY
 IN-1, INCH CM² DYN/CM² DYN/CM² DYN/CM² DYN/CM² PERC.

20	.0090	.120E-03	3368.	655.	1137.	6058.	-44.40
30	.0065	.510E-04	5147.	1540.	1137.	6943.	-25.88
40	.0065	.236E-04	7465.	3377.	1137.	8741.	-14.59
50	.0055	.144E-04	9524.	5469.	1137.	10872.	-12.40
60	.0045	.101E-04	11351.	7750.	1137.	13154.	-13.71
70	.0037	.772E-05	13046.	10188.	1137.	15591.	-16.32
80	.0037	.525E-05	15693.	14984.	1137.	20387.	-23.02
90	.0035	.389E-05	18145.	20194.	1137.	25597.	-29.11

TABLE X

PARAMETRIC STUDY FOR 2.5-INCH HEAT PIPE OPERATING WITH SODIUM (Contd)

WICK THICKNESS 3.736 CM ELEVATION PRESSURE 4266.41 DYN/CM²
 ANGLE 40.00 DEG AREA RATIO 3.1308 SONIC VELOCITY 64218.6 CM/SEC
 WICK AREA 20.104 CM² VAPOR AREA 6.421 CM² VELOCITY 1143.458 CM/SEC

MESH WIRE PERMEABILITY SUCTION DELP W DELP V DELP T SAFETY
 IN-1, INCH CM² DYN/CM² DYN/CM² DYN/CM² DYN/CM² PERC.

20	.0095	.120E-03	3366.	595.	2065.	6926.	-51.37
30	.0065	.510E-04	5147.	1398.	2065.	7729.	-33.41
40	.0065	.236E-04	7465.	3029.	2065.	9361.	-20.25
50	.0055	.144E-04	9524.	4964.	2065.	11296.	-15.68
60	.0045	.101E-04	11351.	7035.	2065.	13367.	-15.08
70	.0037	.772E-05	13046.	9248.	2065.	15580.	-16.26
80	.0037	.525E-05	15693.	13602.	2065.	19933.	-21.27
90	.0035	.389E-05	18145.	18331.	2065.	24663.	-26.43

WICK THICKNESS 4.109 CM ELEVATION PRESSURE 4266.41 DYN/CM²
 ANGLE 45.00 DEG AREA RATIO 4.5038 SONIC VELOCITY 64218.6 CM/SEC
 WICK AREA 21.706 CM² VAPOR AREA 4.02 CM² VELOCITY 1923.52 CM/SEC

MESH WIRE PERMEABILITY SUCTION DELP W DELP V DELP T SAFETY
 IN-1, INCH CM² DYN/CM² DYN/CM² DYN/CM² DYN/CM² PERC.

20	.0090	.120E-03	3368.	551.	4052.	8669.	-62.02
30	.0065	.510E-04	5147.	1295.	4052.	9613.	-46.46
40	.0065	.236E-04	7465.	2806.	4052.	11124.	-32.89
50	.0055	.144E-04	9524.	4598.	4052.	12916.	-26.26
60	.0045	.101E-04	11351.	6516.	4052.	14834.	-23.46
70	.0037	.772E-05	13046.	8566.	4052.	16884.	-22.73
80	.0037	.525E-05	15693.	12598.	4052.	20916.	-24.97
90	.0035	.389E-05	18145.	16976.	4052.	25297.	-28.27

WICK THICKNESS 4.452 CM ELEVATION PRESSURE 4266.41 DYN/CM²
 ANGLE 50.00 DEG AREA RATIO 6.6352 SONIC VELOCITY 64218.6 CM/SEC
 WICK AREA 23.052 CM² VAPOR AREA 3.474 CM² VELOCITY 2113.521 CM/SEC

MESH WIRE PERMEABILITY SUCTION DELP W DELP V DELP T SAFETY
 IN-1, INCH CM² DYN/CM² DYN/CM² DYN/CM² DYN/CM² PERC.

20	.0090	.120E-03	3368.	519.	8732.	13517.	-75.08
30	.0065	.510E-04	5147.	1219.	8732.	14217.	-63.80
40	.0065	.236E-04	7465.	2642.	8732.	15640.	-52.27
50	.0055	.144E-04	9524.	4329.	8732.	17328.	-45.03
60	.0045	.101E-04	11351.	6136.	8732.	19134.	-40.68
70	.0037	.772E-05	13046.	8066.	8732.	21064.	-38.06
80	.0037	.525E-05	15693.	11863.	8732.	24861.	-36.68
90	.0035	.389E-05	18145.	15987.	8732.	28986.	-37.40

TABLE X1

PARAMETRIC STUDY OF A 2.75-INCH HEAT PIPE

PROGRAM 4074-341-001
PARAMETRIC STUDY 12 DECEMBER 1973

WORKING FLUID SODIUM 22.991 GRAM/MOL
OPERATING TEMPERATURE 1556. DEG.F
POWER 6300.00 WATT
HEAT PIPE DIAMETER 2.750 INCH WALL THICKNESS .0620 INCH
WICK LENGTH 180.000 INCH WALL WICK THICKNESS .0440 INCH

PROPERTIES		FLUID	VAPOR
LATENT HEAT, JOULES/G		.440E 04	
SURFACE TENSION, G/SEC2		.124E 03	
THERMAL CONDUCTIVITY, WATT/CM-DEG.K		.540E 00	
VISCOSITY, G/SEC-CM		.164E-02	.225E-03
SPECIFIC GRAVITY, G/SEC3		.748E 00	.195E-03
SPECIFIC HEAT, JOULES/G			.205E 02
PARTIAL PRESSURE, DYN/CM2			.950E 01
WICK THICKNESS 1.666 CM	ELEVATION PRESSURE	4732.58 DYN/CM2	
ANGLE 15.00 DEG	AREA RATIO .4633	SONIC VELOCITY	64218.6 CM/SEC
WICK AREA 10.635 CM2	VAPOR AREA 22.005 CM2	VELOCITY	333.686 CM/SEC
MESH WIRE PERMEABILITY SUCTION DELP W DELP V DELP T SAFETY			
IN-1, INCH CM2 DYN/CM2 DYN/CM2 DYN/CM2 DYN/CM2 PERC.			
20 .0090 .120E-03 3368. 1124. 122. 5978. -43.66			
30 .0065 .510E-04 5147. 2643. 122. 7497. -31.35			
40 .0065 .236E-04 7465. 5727. 122. 10581. -29.45			
50 .0055 .144E-04 9524. 9385. 122. 14239. -33.11			
60 .0045 .101E-04 11351. 13300. 122. 18154. -37.48			
70 .0037 .772E-05 13046. 17463. 122. 22334. -			
80 .0037 .525E-05 15693. 25714. 122. 30568. -48.66			
90 .0035 .389E-05 18145. 34654. 122. 39509. -54.07			
WICK THICKNESS 2.205 CM	ELEVATION PRESSURE	4732.58 DYN/CM2	
ANGLE 20.00 DEG	AREA RATIO .7447	SONIC VELOCITY	64218.6 CM/SEC
WICK AREA 13.931 CM2	VAPOR AREA 18.708 CM2	VELOCITY	392.489 CM/SEC
MESH WIRE PERMEABILITY SUCTION DELP W DELP V DELP T SAFETY			
IN-1, INCH CM2 DYN/CM2 DYN/CM2 DYN/CM2 DYN/CM2 PERC.			
20 .0090 .120E-03 3368. 858. 179. 5769. -41.62			
30 .0065 .510E-04 5147. 2017. 179. 6929. -25.72			
40 .0065 .236E-04 7465. 4372. 179. 9283. -19.58			
50 .0055 .144E-04 9524. 7164. 179. 12075. -21.12			
60 .0045 .101E-04 11351. 10152. 179. 15064. -24.65			
70 .0037 .772E-05 13046. 13346. 179. 18257. -28.54			
80 .0037 .525E-05 15693. 19629. 179. 24540. -36.05			
90 .0035 .389E-05 18145. 26454. 179. 31365. -42.15			

TABLE XI

PARAMETRIC STUDY OF A 2.75-INCH HEAT PIPE (Contd)

WICK THICKNESS 2.724 CM ELEVATION PRESSURE 4732.58 DYN/CM²
 ANGLE 25.00 DEG AREA RATIO 1.0904 SONIC VELOCITY 64218.6 CM/SEC
 WICK AREA 17.025 CM² VAPOR AREA 15.614 CM² VELOCITY 470.259 CM/SEC

MESH WIRE PERMEABILITY SUCTION DELP # DELP V DELP T SAFETY
 IN-1, INCH CM² DYN/CM² DYN/CM² DYN/CM² DYN/CM² PERC.

20	.0090	.120E-03	3368.	702.	274.	5709.	-41.00
30	.0065	.510E-04	5147.	1651.	274.	6657.	-22.69
40	.0065	.236E-04	7465.	3577.	274.	6584.	-13.04
50	.0055	.144E-04	9524.	5862.	274.	10869.	+12.37
60	.0045	.101E-04	11351.	8308.	274.	13314.	-14.75
70	.0037	.772E-05	13046.	10921.	274.	15927.	-18.69
80	.0037	.525E-05	15693.	16062.	274.	21068.	-25.51
90	.0035	.389E-05	16145.	21646.	274.	26653.	-31.92

WICK THICKNESS 3.223 CM ELEVATION PRESSURE 4732.58 DYN/CM²
 ANGLE 30.00 DEG AREA RATIO 1.5575 SONIC VELOCITY 64218.6 CM/SEC
 WICK AREA 19.877 CM² VAPOR AREA 12.762 CM² VELOCITY 575.351 CM/SEC

MESH WIRE PERMEABILITY SUCTION DELP # DELP V DELP T SAFETY
 IN-1, INCH CM² DYN/CM² DYN/CM² DYN/CM² DYN/CM² PERC.

20	.0090	.120E-03	3368.	601.	441.	5775.	-41.66
30	.0065	.510E-04	5147.	1414.	441.	6588.	-21.67
40	.0065	.236E-04	7465.	3064.	441.	6238.	-9.3E
50	.0055	.144E-04	9524.	5021.	441.	10195.	-6.56
60	.0045	.101E-04	11351.	7116.	441.	12289.	-7.64
70	.0037	.772E-05	13046.	9354.	441.	14528.	-10.20
80	.0037	.525E-05	15693.	13757.	441.	18931.	-17.10
90	.0035	.389E-05	16145.	18541.	441.	23714.	-23.49

WICK THICKNESS 3.698 CM ELEVATION PRESSURE 4732.58 DYN/CM²
 ANGLE 35.00 DEG AREA RATIO 2.2051 SONIC VELOCITY 64218.6 CM/SEC
 WICK AREA 22.456 CM² VAPOR AREA 10.183 CM² VELOCITY 721.042 CM/SEC

MESH WIRE PERMEABILITY SUCTION DELP # DELP V DELP T SAFETY
 IN-1, INCH CM² DYN/CM² DYN/CM² DYN/CM² DYN/CM² PERC.

20	.0090	.120E-03	3368.	532.	751.	6016.	-44.01
30	.0065	.510E-04	5147.	1251.	751.	6735.	-23.58
40	.0065	.236E-04	7465.	2712.	751.	8196.	-8.92
50	.0055	.144E-04	9524.	4444.	751.	9200.	-4.07
60	.0045	.101E-04	11351.	6298.	751.	11782.	-3.46
70	.0037	.772E-05	13046.	8280.	751.	13763.	-5.21
80	.0037	.525E-05	15693.	12177.	751.	17661.	-11.14
90	.0035	.389E-05	16145.	16412.	751.	21895.	-17.13

TABLE XI

PARAMETRIC STUDY OF A 2.75-INCH HEAT PIPE (Contd)

WICK THICKNESS 4.144 CM ELEVATION PRESSURE 4732.58 DYN/CM²
 ANGLE 40.00 DEG AREA RATIO 3.1368 SONIC VELOCITY 64218.6 CM/SEC
 WICK AREA 24.736 CM² VAPOR AREA 7.901 CM² VELOCITY 929.286 CM/SEC

MESH WIRE PERMEABILITY SUCTION DELP W DELP V DELP T SAFETY
 IN-1, INCH CM² DYN/CM² DYN/CM² DYN/CM² DYN/CM² PERC.

20	.0090	.120E-03	3366.	463.	1364.	6580.	-48.61
30	.0065	.510E-04	5147.	1136.	1364.	7233.	-26.84
40	.0065	.236E-04	7465.	2462.	1364.	8556.	-12.78
50	.0055	.144E-04	9224.	4034.	1364.	10131.	-5.59
60	.0045	.101E-04	11351.	5717.	1364.	11614.	-3.92
70	.0037	.772E-05	13046.	7516.	1364.	13612.	-4.16
80	.0037	.525E-05	15693.	11054.	1364.	17151.	-8.50
90	.0035	.369E-05	16145.	14896.	1364.	20994.	-13.57

WICK THICKNESS 4.556 CM ELEVATION PRESSURE 4732.58 DYN/CM²
 ANGLE 45.00 DEG AREA RATIO 4.5036 SONIC VELOCITY 64218.6 CM/SEC
 WICK AREA 26.709 CM² VAPOR AREA 5.930 CM² VELOCITY 1238.166 CM/SEC

MESH WIRE PERMEABILITY SUCTION DELP W DELP V DELP T SAFETY
 IN-1, INCH CM² DYN/CM² DYN/CM² DYN/CM² DYN/CM² PERC.

20	.0090	.120E-03	3368.	446.	2676.	7856.	-57.13
30	.0065	.510E-04	5147.	1052.	2676.	8461.	-39.17
40	.0065	.236E-04	7465.	2280.	2676.	9649.	-22.95
50	.0055	.144E-04	9224.	3737.	2676.	11145.	-14.55
60	.0045	.101E-04	11351.	5295.	2676.	12704.	-10.65
70	.0037	.772E-05	13046.	6961.	2676.	14370.	-9.21
80	.0037	.525E-05	15693.	10238.	2676.	17647.	-11.07
90	.0035	.369E-05	16145.	13796.	2676.	21207.	-14.44

WICK THICKNESS 4.938 CM ELEVATION PRESSURE 4732.58 DYN/CM²
 ANGLE 50.00 DEG AREA RATIO 6.6353 SONIC VELOCITY 64218.6 CM/SEC
 WICK AREA 28.364 CM² VAPOR AREA 4.275 CM² VELOCITY 1717.657 CM/SEC

MESH WIRE PERMEABILITY SUCTION DELP W DELP V DELP T SAFETY
 IN-1, INCH CM² DYN/CM² DYN/CM² DYN/CM² DYN/CM² PERC.

20	.0090	.120E-03	3368.	421.	5767.	10921.	-69.16
30	.0065	.510E-04	5147.	991.	5767.	11491.	-55.21
40	.0065	.236E-04	7465.	2147.	5767.	12647.	-40.97
50	.0055	.144E-04	9224.	3516.	5767.	14018.	-32.06
60	.0045	.101E-04	11351.	4986.	5767.	15486.	-26.70
70	.0037	.772E-05	13046.	6555.	5767.	17055.	-23.50
80	.0037	.525E-05	15693.	9641.	5767.	20141.	-22.08
90	.0035	.369E-05	16145.	12993.	5767.	23493.	-22.76

TABLE XII

PARAMETRIC STUDY OF A 3-INCH DIAMETER HEAT PIPE

PROGRAM 4074-341-001
PARAMETRIC STUDY 12 DECEMBER 1973

WORKING FLUID SODIUM 22.951 GRAM/MOL
OPERATING TEMPERATURE 1556. DEG.F
POWER 6300.00 WATT
HEAT PIPE DIAMETER 3.000 INCH WALL THICKNESS .0620 INCH
WICK LENGTH 180.000 INCH WALL WICK THICKNESS .0440 INCH

PROPERTIES		FLUID	VAPOR
LATENT HEAT, JOULES/G		.440E 04	
SURFACE TENSION, G/SEC2		.124E 03	
THERMAL CONDUCTIVITY, WATT/CM-DEG.K		.540E 00	
VISCOSITY, G/SEC-CM		.164E-02	.225E-03
SPECIFIC GRAVITY, G/SEC3		.748E 00	.195E-03
SPECIFIC HEAT, JOULES/G			.206E 02
PARTIAL PRESSURE, DYN/CM2			.950E 01
WICK THICKNESS 1.833 CM ELEVATION PRESSURE 5198.76 DYN/CM2			
ANGLE 15.00 DEG AREA RATIO .4833 SONIC VELOCITY 64218.6 CM/SEC			
WICK AREA 12.633 CM2 VAPOR AREA 26.553 CM2 VELOCITY 276.525 CM/SEC			
MESH WIRE PERMEABILITY SUCTION DELP W DELP V DELP T SAFETY			
IN-1, INCH CM2 DYN/CM2 DYN/CM2 DYN/CM2 DYN/CM2 PERC.			
20 .0090 .120E-03 3368. 932. 84. 6214. -45.79			
30 .0065 .510E-04 5147. 2190. 84. 7472. -31.12			
40 .0065 .236E-04 7465. 4746. 84. 10028. -25.56			
50 .0055 .144E-04 9524. 7777. 84. 13059. -27.07			
60 .0045 .101E-04 11351. 11022. 84. 16304. -30.38			
70 .0037 .772E-05 13046. 14488. 84. 19771. -34.01			
80 .0037 .525E-05 15693. 21309. 84. 26591. -40.98			
90 .0035 .389E-05 18145. 28716. 84. 34001. -46.63			
WICK THICKNESS 2.422 CM ELEVATION PRESSURE 5196.76 DYN/CM2			
ANGLE 20.00 DEG AREA RATIO .7447 SONIC VELOCITY 64218.6 CM/SEC			
WICK AREA 16.611 CM2 VAPOR AREA 22.575 CM2 VELOCITY 325.256 CM/SEC			
MESH WIRE PERMEABILITY SUCTION DELP W DELP V DELP T SAFETY			
IN-1, INCH CM2 DYN/CM2 DYN/CM2 DYN/CM2 DYN/CM2 PERC.			
20 .0090 .120E-03 3368. 711. 123. 6033. -44.16			
30 .0065 .510E-04 5147. 1672. 123. 6993. -26.41			
40 .0065 .236E-04 7465. 3623. 123. 8944. -16.54			
50 .0055 .144E-04 9524. 5937. 123. 11258. -15.40			
60 .0045 .101E-04 11351. 8413. 123. 13735. -17.36			
70 .0037 .772E-05 13046. 11060. 123. 16381. -20.36			
80 .0037 .525E-05 15693. 16266. 123. 21588. -27.30			
90 .0035 .389E-05 18145. 21922. 123. 27244. -33.40			

TABLE XII

PARAMETRIC STUDY OF A 3-INCH DIAMETER HEAT PIPE (Contd)

WICK THICKNESS 2.993 CM ELEVATION PRESSURE 5198.76 DYN/CM²
 ANGLE 25.00 DEG AREA RATIO 1.0904 SONIC VELOCITY 64218.6 CM/SEC
 WICK AREA 20.544 CM² VAPOR AREA 16.842 CM² VELOCITY 389.703 CM/SEC

MESH WIRE PERMEABILITY SUCTION DELP W DELP V DELP T SAFETY
 IN-1, INCH CM² DYN/CM² DYN/CM² DYN/CM² DYN/CM² PERC.

20	.0090	.120E-03	3368.	582.	188.	5969.	-43.57
30	.0065	.510E-04	5147.	1366.	188.	6755.	-23.81
40	.0065	.236E-04	7465.	2964.	188.	6351.	-10.61
50	.0055	.144E-04	9524.	4856.	188.	10245.	-7.03
60	.0045	.101E-04	11351.	6884.	188.	12271.	-7.50
70	.0037	.772E-05	13046.	9070.	188.	14437.	-9.63
80	.0037	.525E-05	15693.	13310.	188.	18697.	-16.07
90	.0035	.369E-05	18145.	17938.	188.	23325.	-22.21

WICK THICKNESS 3.541 CM ELEVATION PRESSURE 5198.76 DYN/CM²
 ANGLE 30.00 DEG AREA RATIO 1.555 SONIC VELOCITY 64218.6 CM/SEC
 WICK AREA 23.986 CM² VAPOR AREA 15.400 CM² VELOCITY 476.793 CM/SEC

MESH WIRE PERMEABILITY SUCTION DELP W DELP V DELP T SAFETY
 IN-1, INCH CM² DYN/CM² DYN/CM² DYN/CM² DYN/CM² PERC.

20	.0090	.120E-03	3368.	498.	303.	6000.	-43.86
30	.0065	.510E-04	5147.	1172.	303.	6673.	-22.86
40	.0065	.236E-04	7465.	2539.	303.	6041.	-7.16
50	.0055	.144E-04	9524.	4161.	303.	9663.	-1.43
60	.0045	.101E-04	11351.	5897.	303.	11398.	-.42
70	.0037	.772E-05	13046.	7751.	303.	13253.	-1.56
80	.0037	.525E-05	15693.	11401.	303.	16902.	-7.15
90	.0035	.389E-05	18145.	15365.	303.	20866.	-13.04

WICK THICKNESS 4.062 CM ELEVATION PRESSURE 5198.76 DYN/CM²
 ANGLE 35.00 DEG AREA RATIO 2.2051 SONIC VELOCITY 64218.6 CM/SEC
 WICK AREA 27.098 CM² VAPOR AREA 12.288 CM² VELOCITY 597.528 CM/SEC

MESH WIRE PERMEABILITY SUCTION DELP W DELP V DELP T SAFETY
 IN-1, INCH CM² DYN/CM² DYN/CM² DYN/CM² DYN/CM² PERC.

20	.0090	.120E-03	3368.	441.	516.	6156.	-45.28
30	.0065	.510E-04	5147.	1037.	516.	6752.	-23.77
40	.0065	.236E-04	7465.	2248.	516.	7962.	-6.24
50	.0055	.144E-04	9524.	3683.	516.	9397.	1.35
60	.0045	.101E-04	11351.	5220.	516.	10934.	3.61
70	.0037	.772E-05	13046.	6861.	516.	12576.	3.74
80	.0037	.525E-05	15693.	10091.	516.	15806.	-.71
90	.0035	.389E-05	18145.	13600.	516.	19315.	-6.06

TABLE XII

PARAMETRIC STUDY OF A 3-INCH DIAMETER HEAT PIPE (Contd)

WICK THICKNESS 4.552 CM ELEVATION PRESSURE 5198.76 DYN/CM²
 ANGLE 40.00 DEG AREA RATIO 3.130P SONIC VELOCITY 64218.6 CM/SEC
 WICK AREA 29.851 CM² VAPOR AREA 9.535 CM² VELOCITY 770.100 CM/SEC

MESH WIRE PERMEABILITY SUCTION DELP W DELP V DELP T SAFETY
 IN-1, INCH CM² DYN/CM² DYN/CM² DYN/CM² DYN/CM² PERC.

20	.0090	.120E-03	3368.	400.	937.	6536.	-48.46
30	.0065	.510E-04	5147.	941.	937.	7077.	-27.28
40	.0065	.236E-04	7465.	2040.	937.	5176.	-8.69
50	.0055	.144E-04	9524.	3343.	937.	9475.	.46
60	.0045	.101E-04	11351.	4736.	937.	10874.	4.39
70	.0037	.772E-05	13046.	6228.	937.	12364.	5.52
80	.0037	.525E-05	15693.	9160.	937.	15296.	2.60
90	.0035	.389E-05	18145.	12346.	937.	18481.	-1.62

WICK THICKNESS 5.007 CM ELEVATION PRESSURE 5198.76 DYN/CM²
 ANGLE 45.00 DEG AREA RATIO 4.503K SONIC VELOCITY 64218.6 CM/SEC
 WICK AREA 32.230 CM² VAPOR AREA 7.156 CM² VELOCITY 1076.068 CM/SEC

MESH WIRE PERMEABILITY SUCTION DELP W DELP V DELP T SAFETY
 IN-1, INCH CM² DYN/CM² DYN/CM² DYN/CM² DYN/CM² PERC.

20	.0090	.120E-03	3368.	371.	1838.	7408.	-54.53
30	.0065	.510E-04	5147.	672.	1838.	7909.	-34.92
40	.0065	.236E-04	7465.	1890.	1838.	8926.	-16.37
50	.0055	.144E-04	9524.	3096.	1838.	10133.	-6.01
60	.0045	.101E-04	11351.	4388.	1838.	11425.	-.65
70	.0037	.772E-05	13046.	5769.	1838.	12805.	1.88
80	.0037	.525E-05	15693.	8484.	1838.	15521.	1.11
90	.0035	.389E-05	18145.	11435.	1838.	18471.	-1.77

WICK THICKNESS 5.425 CM ELEVATION PRESSURE 5198.76 DYN/CM²
 ANGLE 50.00 DEG AREA RATIO 6.6352 SONIC VELOCITY 64218.6 CM/SEC
 WICK AREA 34.221 CM² VAPOR AREA 5.158 CM² VELOCITY 1423.420 CM/SEC

MESH WIRE PERMEABILITY SUCTION DELP W DELP V DELP T SAFETY
 IN-1, INCH CM² DYN/CM² DYN/CM² DYN/CM² DYN/CM² PERC.

20	.0090	.120E-03	3368.	349.	3961.	9509.	-64.58
30	.0065	.510E-04	5147.	821.	3961.	9980.	-46.43
40	.0065	.236E-04	7465.	1779.	3961.	10939.	-31.76
50	.0055	.144E-04	9524.	2916.	3961.	12075.	-21.13
60	.0045	.101E-04	11351.	4132.	3961.	13292.	-14.60
70	.0037	.772E-05	13046.	5432.	3961.	14591.	-10.59
80	.0037	.525E-05	15693.	7989.	3961.	17149.	-8.49
90	.0035	.389E-05	18145.	10767.	3961.	19927.	-8.94

flow area was therefore 15.277 cm^2 . The density of the wick structure was calculated from

$$\delta = 1 - \pi d M/4$$

where

δ = density

d = wire diameter, 0.0055 inch

M = Mesh, number of wires per inch

$$\delta = 0.784125$$

The total volume of the diametral wick was $6,984.6 \text{ cm}^3$, while the total volume of the wall wick was 412.5 cm^3 and the volumes of the wicks on the end caps was 0.075 cm^3 each. The total wick structure in the heat pipe had, therefore, a volume of $7,397.25 \text{ cm}^3$. The free space for the working fluid was

$$V_{TS} = 0.784125 \times 7,397.25 = 5,800.37 \text{ cm}^3$$

For a sodium density of 0.8705 g/cm^3 at 350°F , this volume corresponded to 5,049.2 grams or 11.122 lb. This amount of sodium was considerably larger than the charge of the first primary heat pipe which was only 8.48 lb initially and was later increased to 8.85 lb.

For the initial fill of the heat pipe, it was stipulated that the entire wick structure shall be saturated with the working fluid at or near the freezing temperature of the working fluid. This would prevent the wick structure from ever being dry anywhere in the heat pipe, and especially in the evaporator section, at the time of start up of the heat pipe. If experimentally it should become obvious that the heat pipe had been overfilled, sodium could be withdrawn from the heat pipe relatively easier than added at a later date. Addition of sodium would require the entire fill setup while withdrawal could be achieved by simply venting the heat pipe to a calibrated volume.

4.4 FABRICATION OF THE SECOND PRIMARY HEAT PIPE

The fabrication of the second primary heat pipe followed basically the same pattern as that of the first primary heat pipe. The heat pipe wall was built from three 5-foot long sections. Each section was rolled to an outside diameter of 2.25 inch from 0.065-inch thick sheet stock of Inconel 617 alloy. This work was performed by the same vendor who rolled the sections of the first primary heat pipe. Prior to shipment the sections were fully inspected by the dye process and radiographically. When the

sections came to Verox/EOS they were cleaned by process C-19 (Code 12705). Two layers of 50 mesh bolting cloth were placed into each section. Two additional layers were placed in the evaporator section which was to be 20 inches long.

The diametral wick was fabricated according to the wick design shown in Figure 87. Each of the five sections of the wick were formed in a single length by folding bolting cloth into 22 layers. The five sections and the two end shims were then bolted together with nickel plated stainless steel screws and nuts in the pattern shown in Figure 88. Considerable care was taken to maintain the width of the wick and not to compress the bolting cloth to less than 1.210 inch. In Figure 89 the wick is shown as fabricated.

Each 5-foot section of the heat pipe wall was pulled over the wick individually (Figure 90). The three sections were then welded together in an inert gas atmosphere and the two end caps (Figure 91) welded to the pipe after being covered with screen material. All welds were inspected for soundness and full weld penetration. The heat pipe was evacuated and helium leak checked. The heat pipe remained evacuated for 2 days to assure that all weld joints were vacuum tight.

4.5 INSTRUMENTATION, HEATER INSTALLATION, INSULATION AND CHARGING WITH SODIUM

With the basic fabrication of the heat pipe completed, the following was initiated: the build up of the heat pipe instrumentation, installation of the primary heater units and the secondary heater units, the insulation of the heat pipe, and the charging of the heat pipe with the working fluid, sodium.

A total of 30 Chromel-Alumel refrasil sheathed thermocouples were attached to the heat pipe by tabs which were spot welded to the heat pipe at locations shown in Figure 92. At the evaporator, two thermocouples covered each location. This was a precautionary measure taken to assure that even after failure of one of the thermocouples in that area it would still be possible to monitor the temperature.

The primary heater comprised three heater elements consisting of a Calrod Tubular Inconel sheathed heater (General Electric Company 5D878G2) with a rating of 3,000 watt at 240 volt. The total length of each element was 164 inches with an effective heating length of 150 inches. All three elements were coiled parallel over a 2-inch diameter tube to assure that the inner diameter of the heater when placed over the heat pipe would make tight contact with the 2.25-inch diameter. The primary heater construction is shown in Figure 93 where it is compared with the primary heater figuration of the first primary heat pipe.

50840

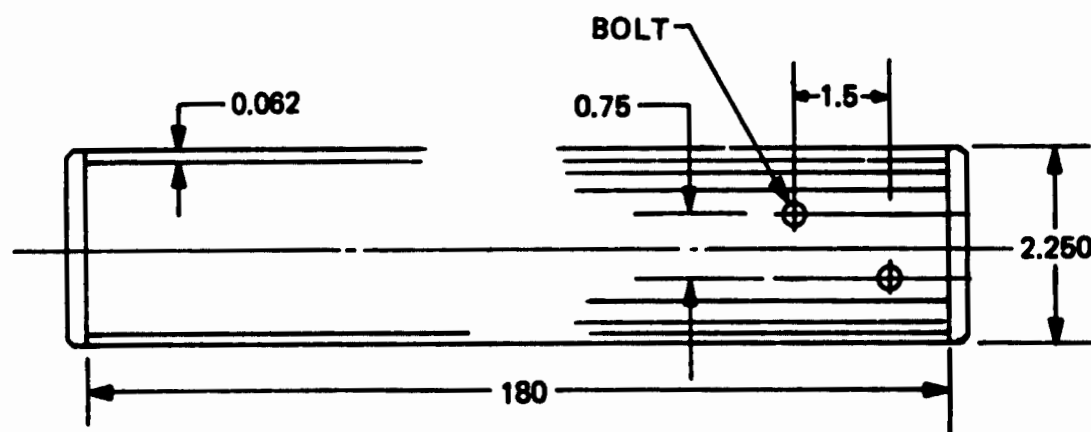


Figure 88. Construction Design of Diametral Wick

50840



Figure 89. Wick Construction for Second Primary Heat Pipe

17425

17426

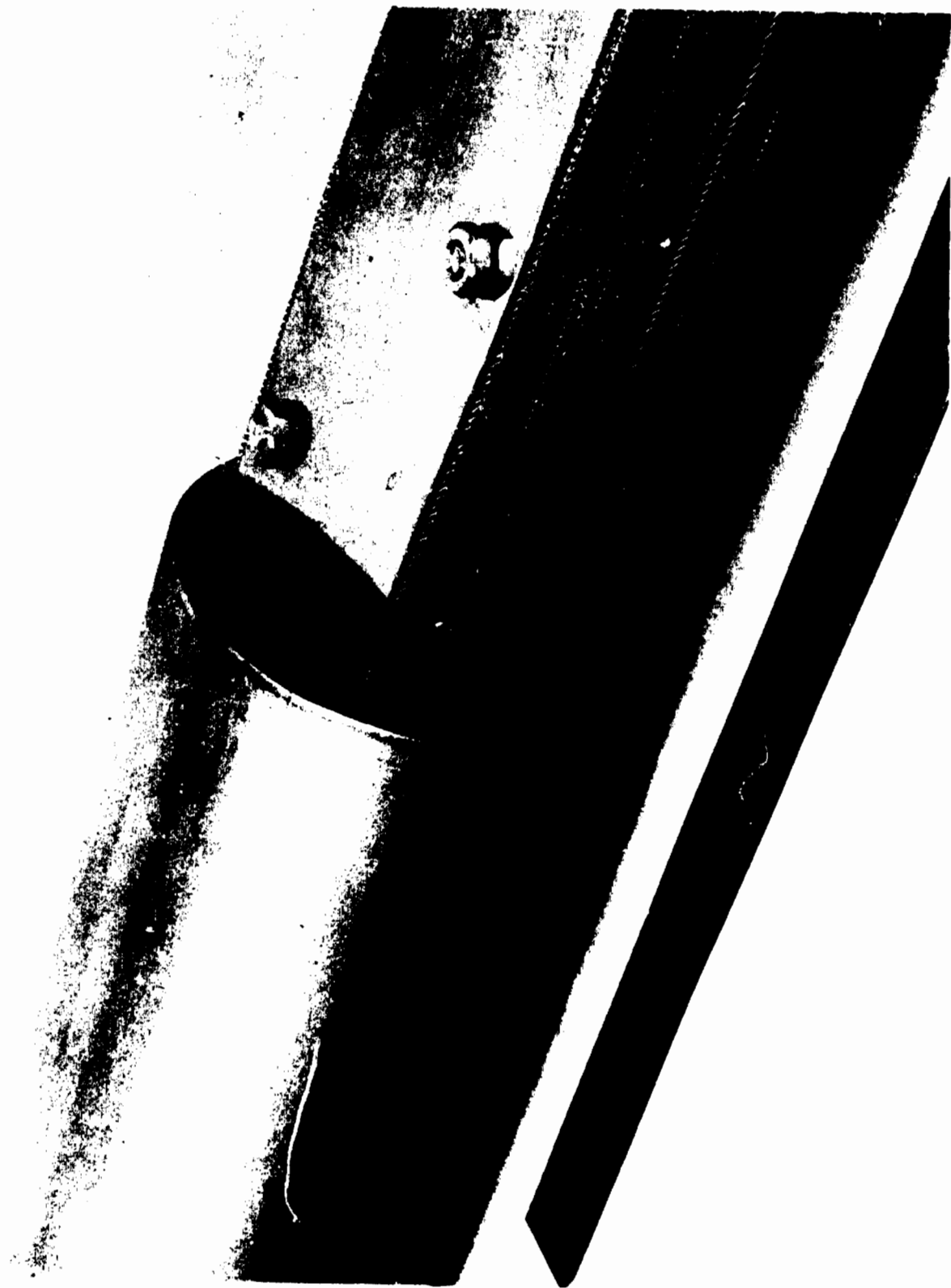
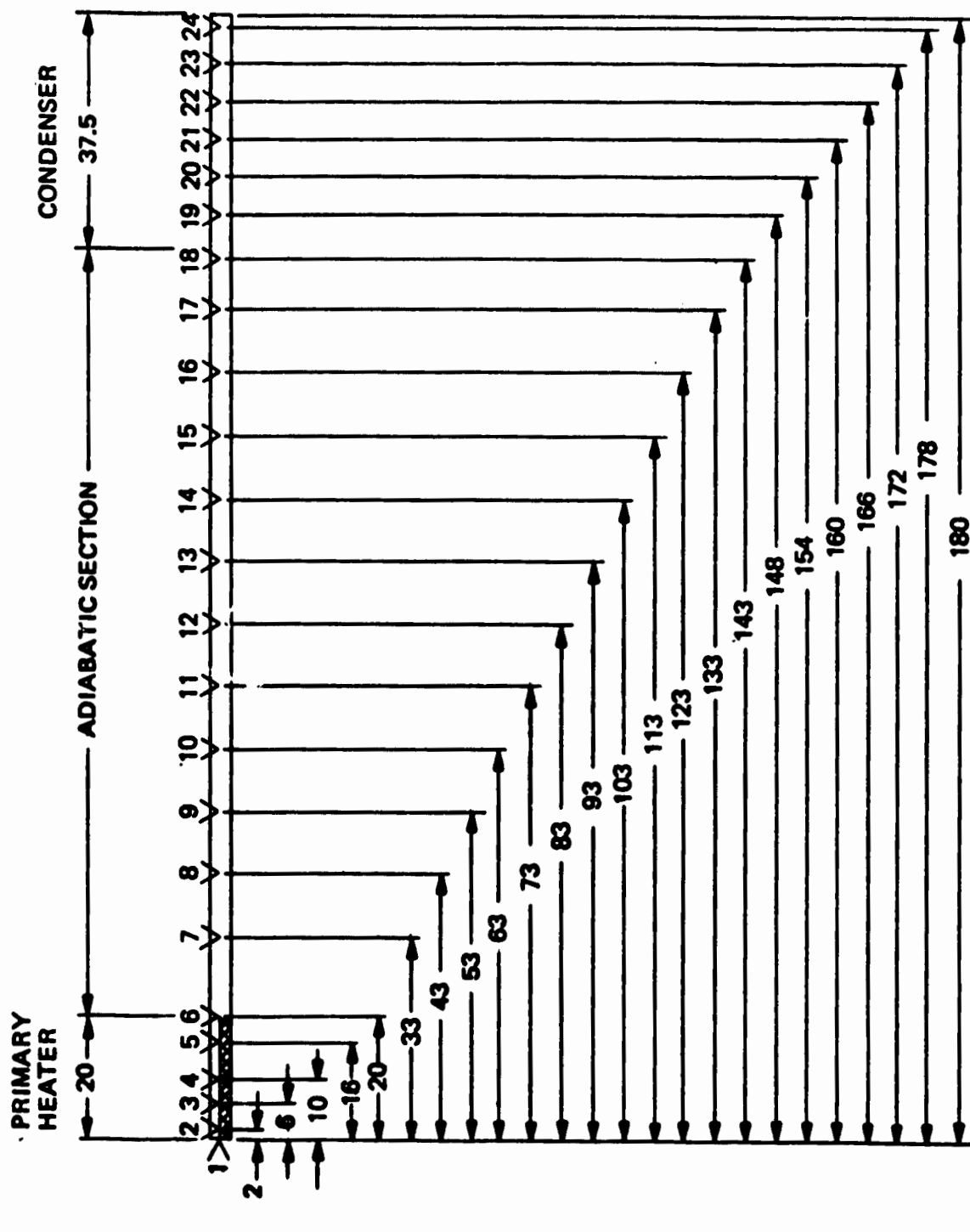


Figure 90. Diametral Wick in Section of Heat Pipe



17426

Figure 91. Primary Heat Pipe with End Cap



THERMOCOUPLES NO. 2 THROUGH NO. 6 EACH HAS A SPARE (B)

Figure 92. Thermocouple Arrangement for Testing of Second Primary Heat Pipe

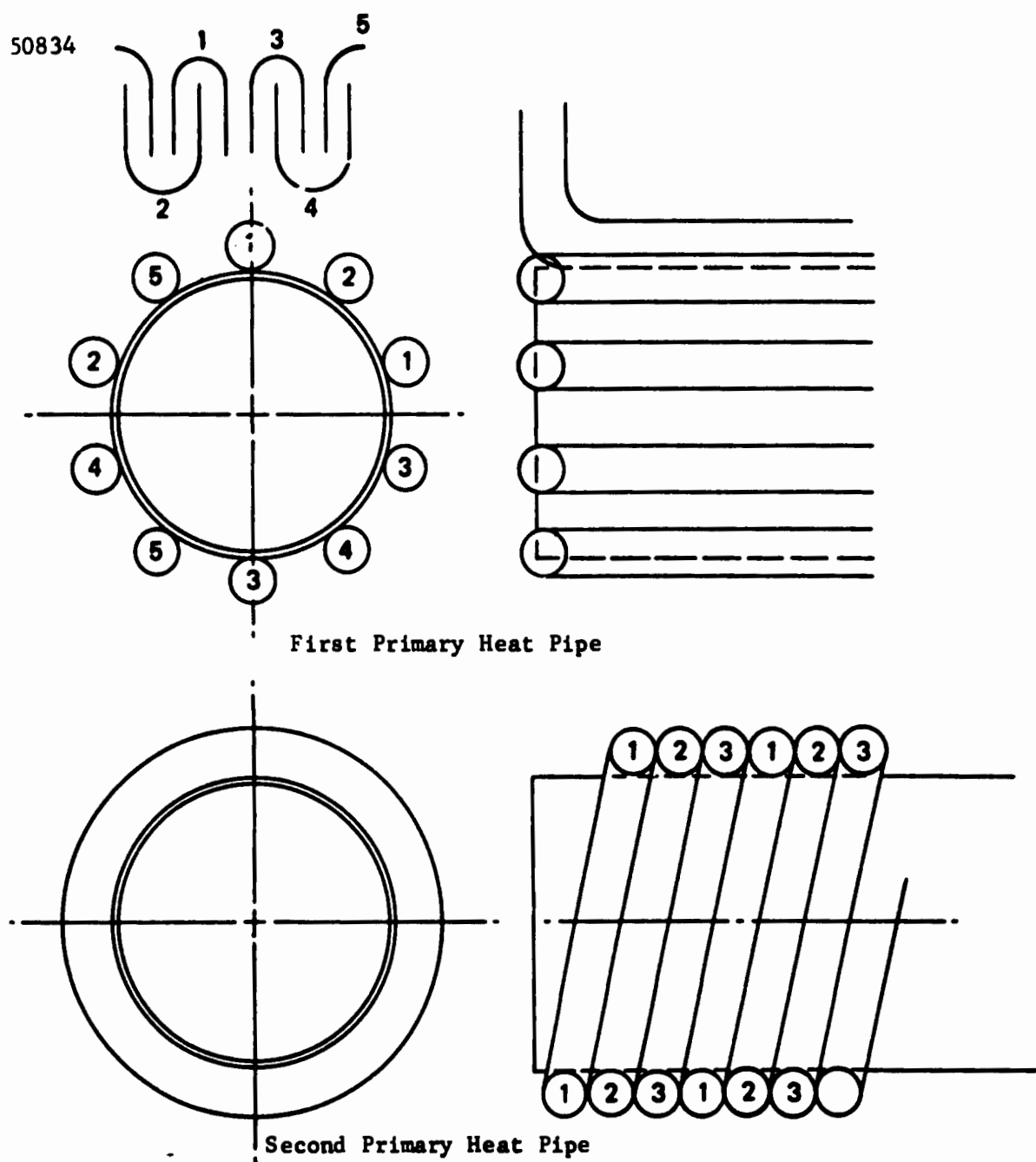


Figure 93. Heater Configuration for Primary Heat Pipes

There are several distinct differences between the test setup of the first primary heat pipe and the second primary heat pipe. The primary heater of the first primary heat pipe consisted of five separate heaters. Each heater was bent into the shape of a hairpin and placed along the evaporator length of the heat pipe. The heaters had an outside diameter of 3/8 inch. Thus, effectively only $(10 \times 3/8) / (2.25 \times 3.14) \times 100 = 49$ percent of the condenser surface was directly exposed to the heaters.

The heater of the second primary heat pipe was placed over the evaporator section of the heat pipe without gaps between the individual windings except where thermocouples were located, thus providing 100 percent coverage. The secondary heater consisted of two units of the same tubular heater as used for the primary heater. The two units were placed along the adiabatic section of the heat pipe 180 degrees apart from each other. The size of the two heater elements was so small that they did not increase the effective heat pipe diameter. This contrasted with the shell heaters which were used with the first primary heat pipe. They increased the effective heat pipe diameter to 3.25 inches and thereby increased the losses from the heat pipe by about 25 percent. (See Figure 55.) The fully instrumented heat pipe with the primary heater and the secondary heater is shown in Figures 94 and 95 and a close-up of the primary heater is shown in Figure 96.

The entire heat pipe was covered with four layers of 3/8-inch thick flexible Min-K insulation, which were overlaid with four layers of 1/2-inch thick Cerafelt 800 insulation. The insulation was completed with one layer of aluminum foil. The insulation is shown in Figure 97, while the fully insulated heat pipe is shown in Figure 98.

Charging the heat pipe with sodium was initiated by heating the heat pipe uniformly to approximately 320°F. A sodium fill of 11 pounds, 2 ounces \pm 12 ounces was specified. Prior to filling, the entire heat pipe and its support, consisting of an aluminum channel and fire bricks, was placed on a scale. The initial weight of the heat pipe with its support was 282 pounds and 8 ounces. The final weight was 294 pounds. The amount of sodium added during the fill was thus 11 pounds and 8 ounces which was well within the specified fill weight.

The heat pipe was processed for 1 day keeping the heaters at a power input sufficient to maintain all parts of the heat pipe above the melting temperature of sodium. The temperature distribution of the heat pipe under those conditions is shown in Figure 99.

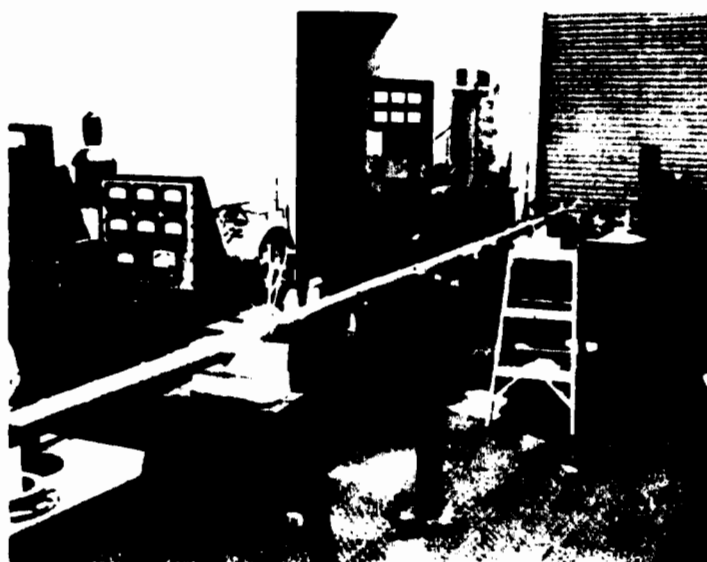
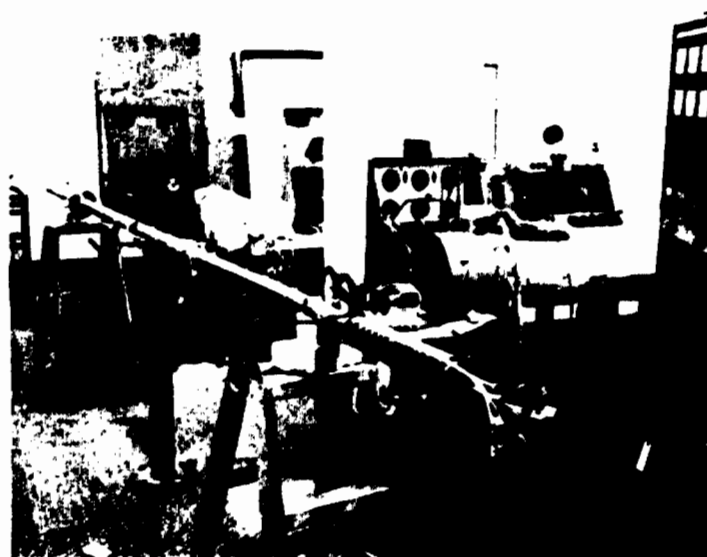


Figure 94. Primary Heat Pipe Fully Instrumented and Heaters in Place (view from condenser end)



007122

Figure 95. Primary Heat Pipe Fully Instrumented and Heaters in Place (view from evaporator end)

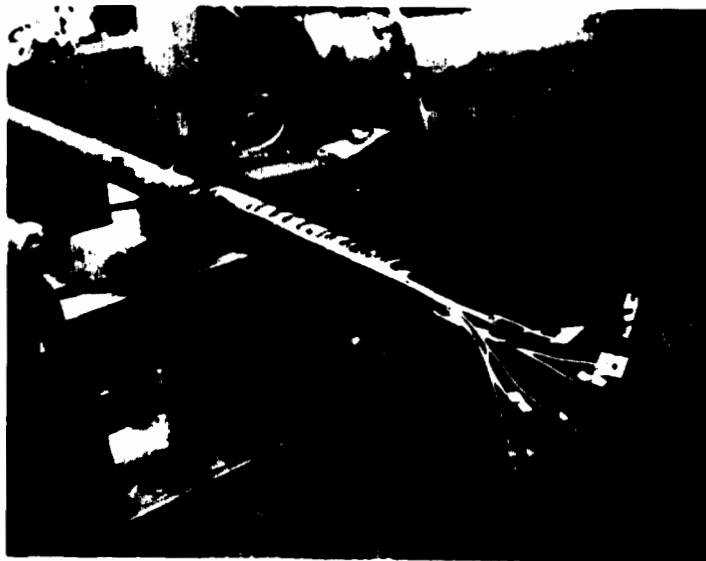


Figure 96. Primary Heat of Primary Heat Pipe
(three 3000 watt Calrad Units
parallel wound)



Figure 97. Insulation of Primary Heat Pipe
(flexible Min-K and Cerafelt)

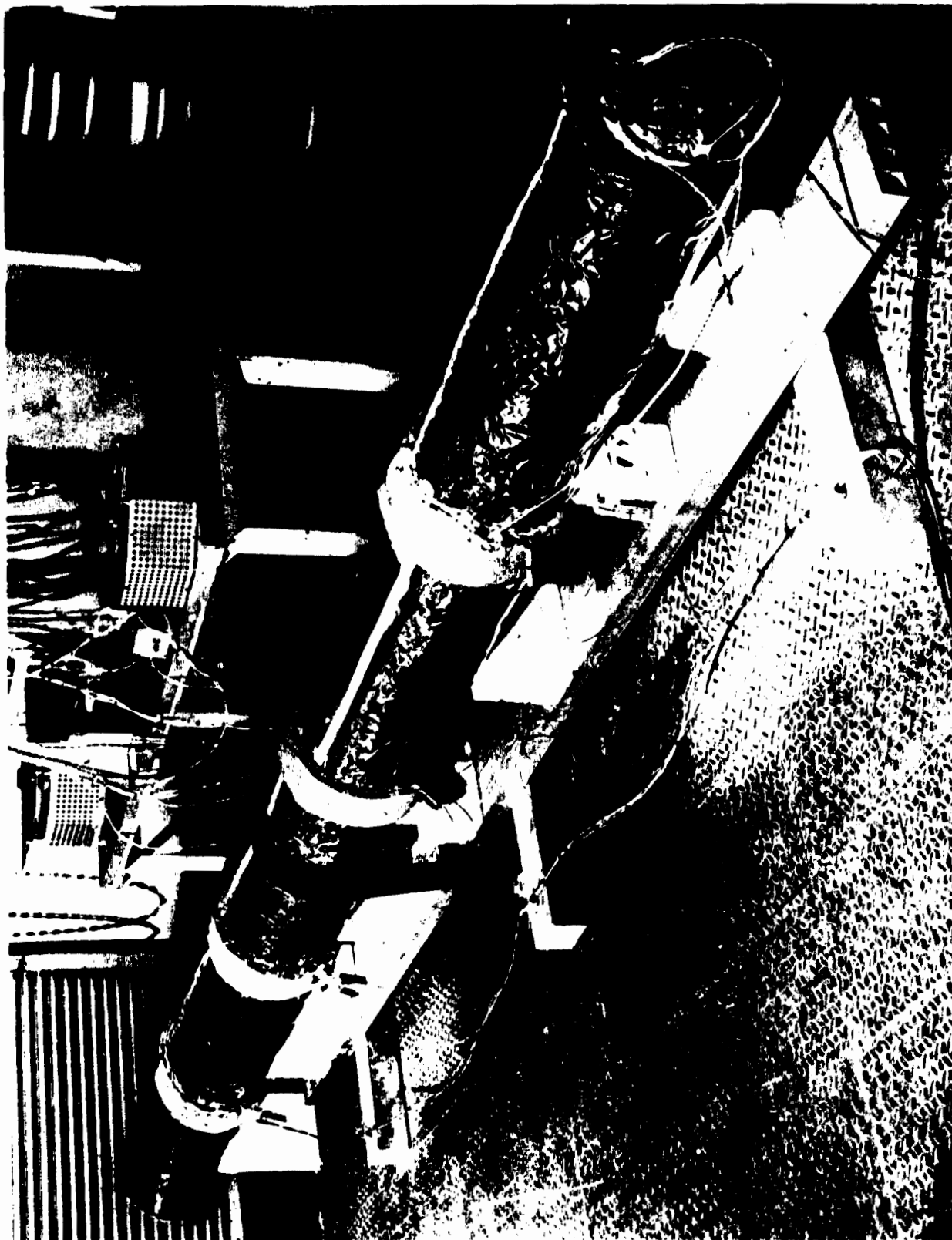
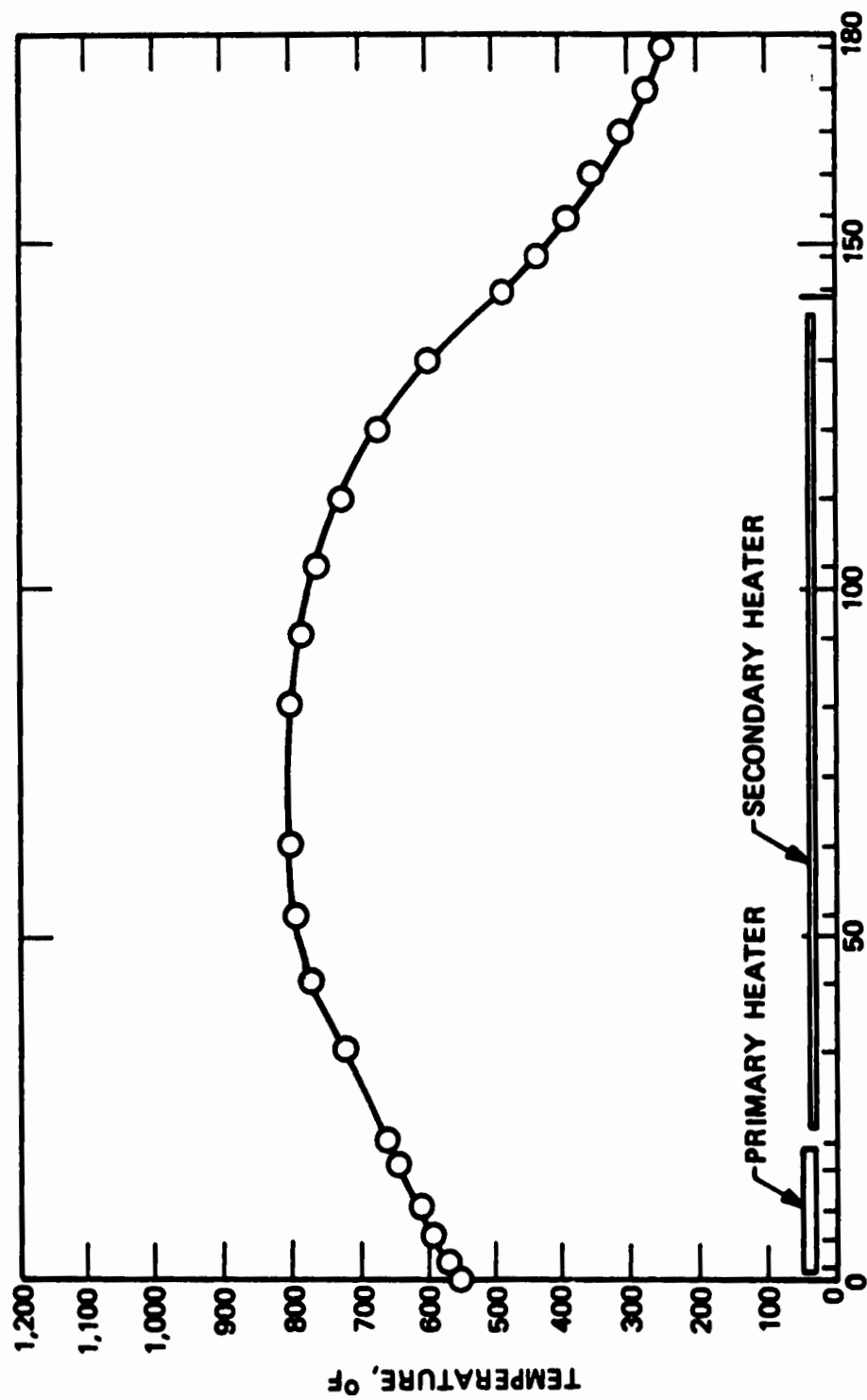


Figure 98. Second Primary Heat Pipe

57363



DISTANCE FROM EVAPORATOR END OF HEAT PIPE L, INCH

Figure 99. Temperature Distribution Along the Primary Heat Pipe During Processing

4.6 TESTING

After processing, testing of the second primary heat pipe was initiated. Similar to the approach taken by EOS for testing of the first primary heat pipe, the power to the primary heat pipe was increased in steps permitting the heat pipe to reach steady-state temperature conditions along its entire length. (All data presented for the second primary heat pipe can be compared with data presented in Subsections 3.6 and 3.8 of this volume for the first primary heat pipe). As shown in Figure 93, the location of the thermocouples along the heat pipe and the three sections of the heat pipe -- evaporator, adiabatic section, and condenser -- can be readily seen.

As stated before, there were several distinct differences between the test setup of the first primary heat pipe and the second primary heat pipe. The primary heater of the first primary heat pipe consisted of five separate heaters covering effectively only 49 percent of the condenser surface. The thermocouples at the evaporator section were placed between the heaters, thus measuring the heat pipe temperature. The primary heater of the second heat pipe consisted of three heaters tightly wound in parallel. No gaps were left between the heaters, thereby heating the evaporator uniformly. Despite the fact that the thermocouples were placed against the heat pipe, the thermocouples in the evaporator section #2 through #5, would see the heaters which had to be considerably hotter than the heat pipe to permit radiation and conduction heat transfer from the heater to the heat pipe. Only thermocouple #1, which was attached to the end flange of the heat pipe, measured the heat pipe temperature at the evaporator.

The primary heater had an effective hot resistance of 6.09 ohms.

While for the first primary heat pipe, five shell heaters were used along the adiabatic section as auxiliary heaters, the second primary heat pipe employed only two 3/8 inch diameter heaters. Since the thermocouples are all placed 90 degrees apart from the two heaters, the correct temperatures were measured along the adiabatic section of the heat pipe. Even during operation of the two auxiliary heaters the use of the Calrod units for the second heat pipe decreased the heat losses from the heat pipe by about 25 percent.

4.6.1 TESTING WITHOUT POWER TRANSFER

The testing of the second primary heat pipe was initiated by obtaining the temperature distribution and power losses under various power input conditions. In Figure 100 the temperature distribution along the heat pipe for increasing power inputs of the primary heater at the evaporator section are shown. These temperature distributions can be compared with the temperature distributions of the first heat pipe, which were presented

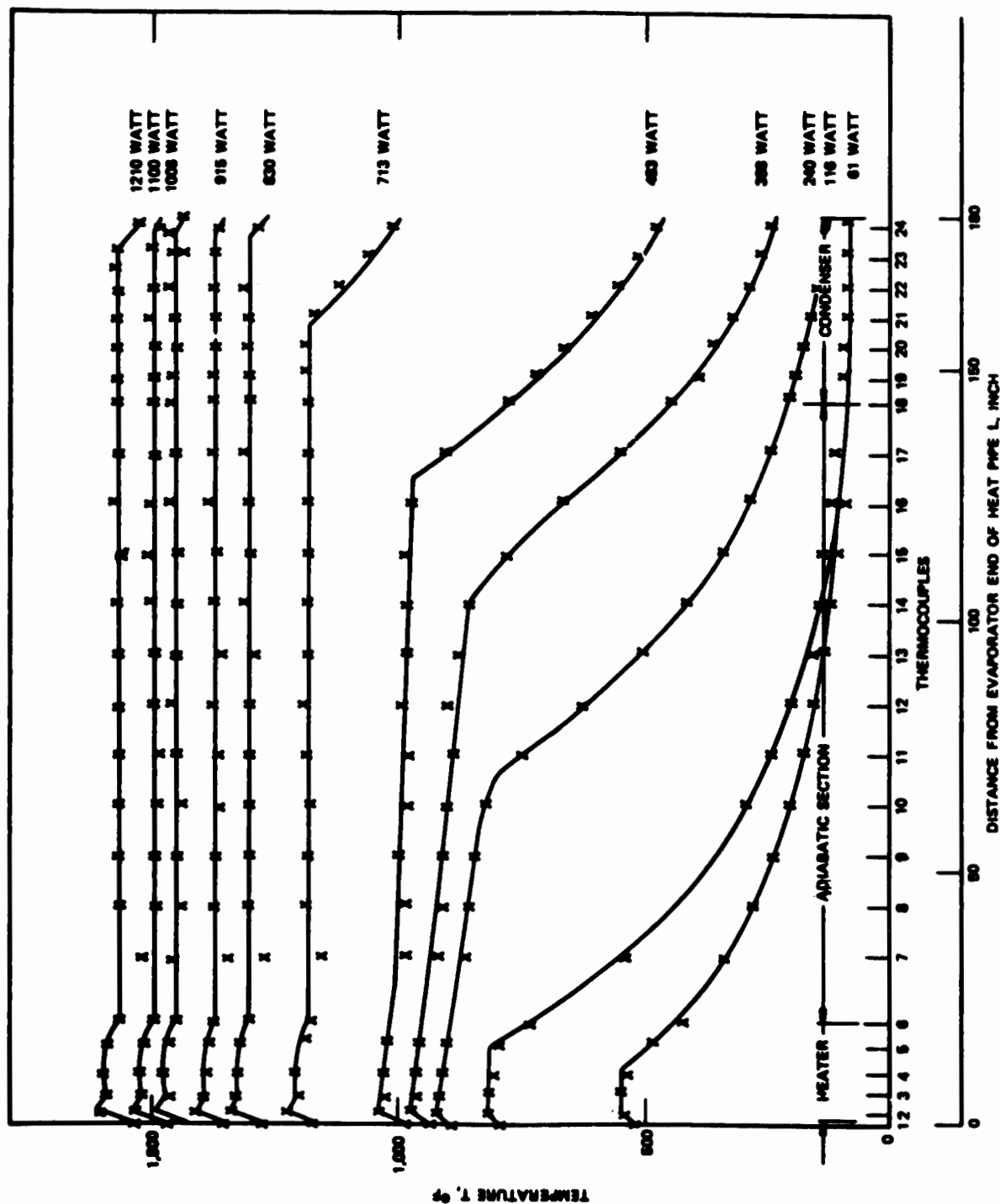


Figure 100. Steady-State Temperature Distribution Along Second Primary Heat Pipe

in Figures 66 and 67. All temperature distributions were taken after steady-state conditions had been achieved.

In Figure 101, the most pertinent temperatures along the heat pipe are correlated with the power input at the evaporator. It takes about 870 watt of power to raise the condenser section fully to the temperature of the adiabatic section. Furthermore, the adiabatic section has to have achieved a temperature of at least 1300°F to bring about uniform conditions for the entire heat pipe. The power and temperature required for constant temperature conditions appeared to be quite high. The test results are compared with the test results of the first primary heat pipe in Figure 102. The second primary heat pipe achieved full operation with a power input of 870 watt and a temperature of 1340°F. This compares with the first primary heat pipe which required a power input of 1240 watt and a temperature of 1450°F. The temperature and power correlation for both heat pipes is shown in Figure 103. The results indicated that the second primary heat pipe showed some improved performance in an area that had not been the primary cause of failure for the first heat pipe.

To permit the correct evaluation of data, the transient characteristic of the heat pipe was analyzed. The heat pipe characteristic can be taken from Table XIII where the heat capacity of the entire heat pipe alone and with a heat exchanger which was to be added, are presented. The steady-state measurements provided the confirmation of the heat losses which could be approximated by the correlation*

$$C_L = P_L / \Delta T \text{ watt/}^\circ\text{R}$$

where

$$P_L = \text{Power loss}$$

$$\Delta T = \text{Temperature difference between heat pipe and ambient temperature}$$

For the entire heat pipe, this loss value was found to be 0.821 watt/°R.

The differential equation for the heat pipe can be written as

$$C_{CT} \frac{d(\Delta T)}{dt} = P_{IN} - C_L \Delta T$$

which can be written in the integrated form, where P_{IN} = power input

$$\Delta T = (\Delta T_0 - P_{IN}/C_L) \exp(-C_L t/C_{CT}) + P_{IN}/C_L$$

*This correlation is valid only in a very restricted region and must be considered a linear approximation.

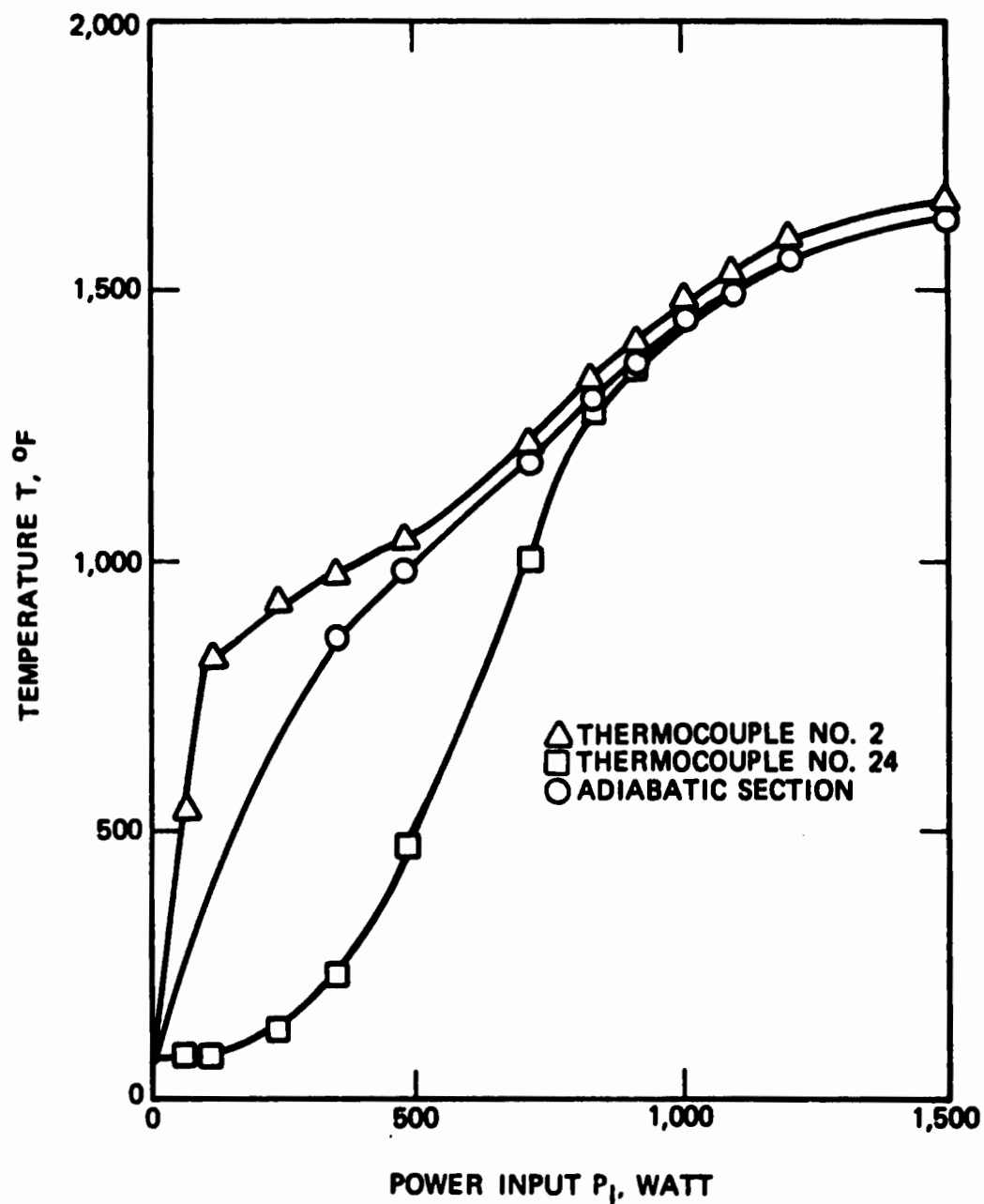


Figure 101. Temperatures along the 15-ft Heat Pipe as Function of Power Input at the Evaporator

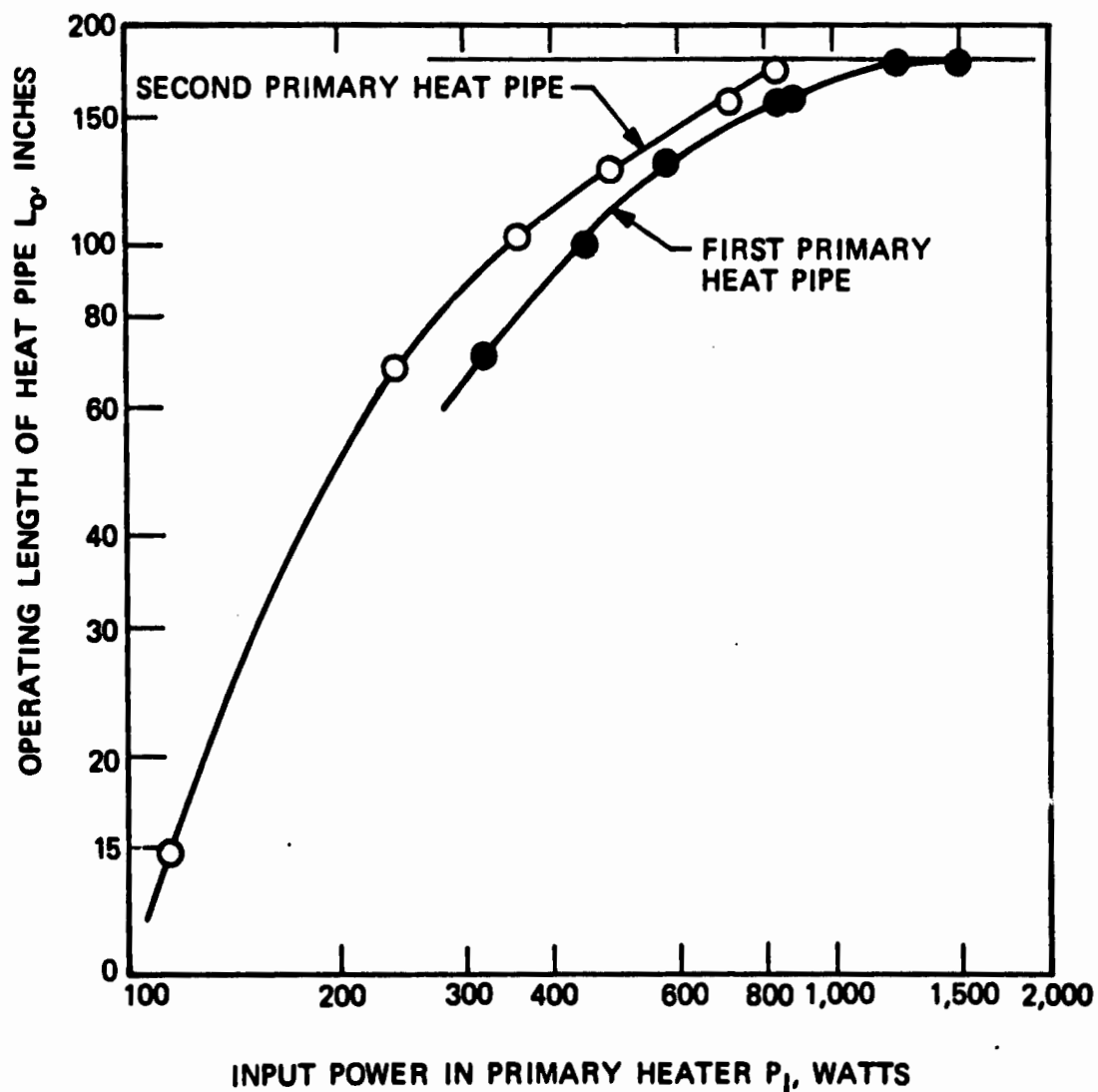


Figure 102. Operating Length of Primary Heat Pipe (Length of Uniform Temperature) (Second Primary Heat Pipe and First Primary Heat Pipe)

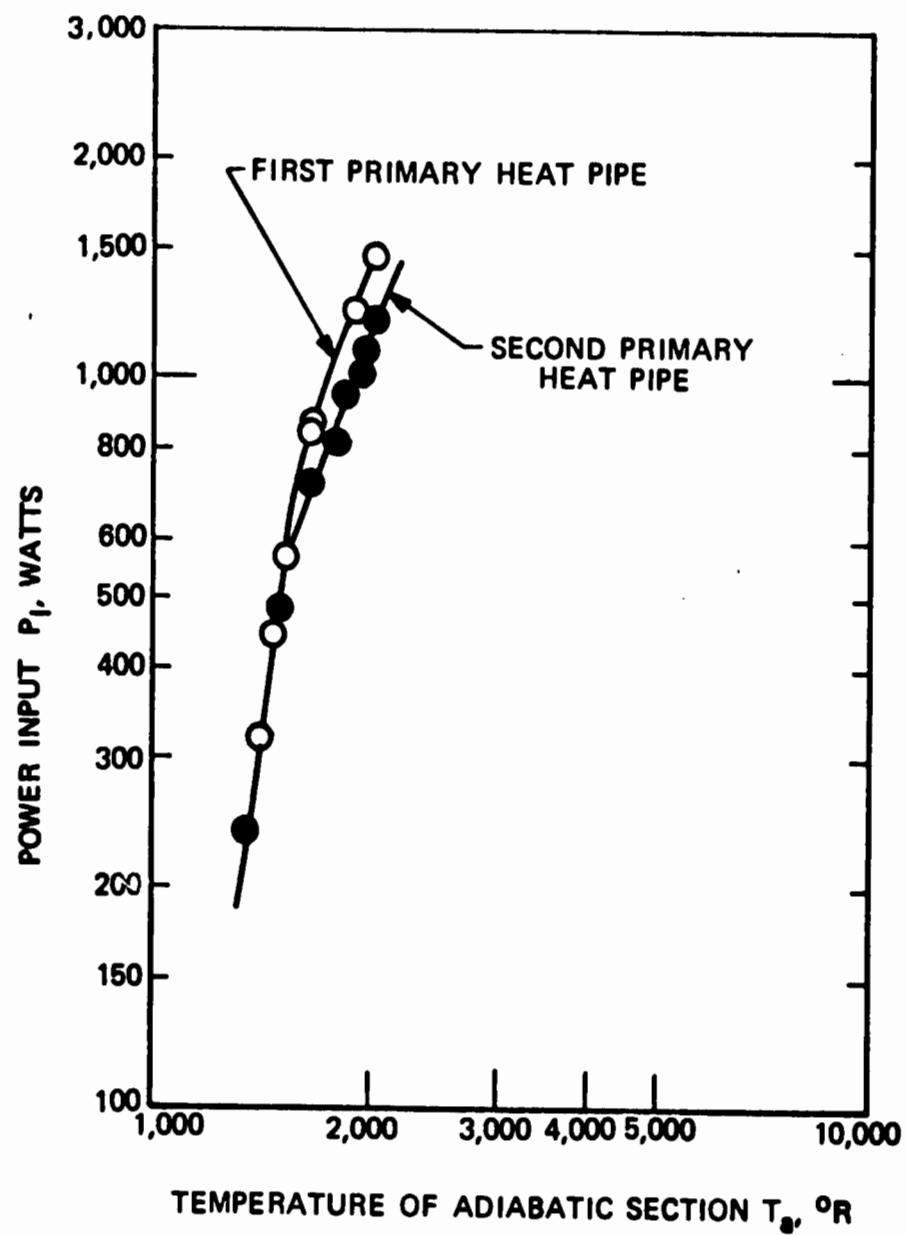


Figure 103. Temperature and Power Loss Correlation for the Two Primary Heat Pipes

TABLE XIII

HEAT PIPE CHARACTERISTICS

	Inconel 617	Wick Material	Sodium	Total	Heat Exchanger	Total w/Heat Exchanger
Total, C_{CT} watt-sec/ $^{\circ}F$	2,473.92	3,512.72	3,640.18	9,626.82	828.48	10,455.30
Unit Length, C_{CW} watt-sec/ $^{\circ}F$	13.56	19.51	20.25	53.32		
Condenser, C_{CC} watt-sec/ $^{\circ}F$	508.67	731.82	758.36	1,998.85	828.48	2,827.33

Thus, the value C_L/C_c is the time constant which determines the time it takes for the heat pipe to reach steady-state temperatures. A typical temperature history is presented in Table XV. The values presented show that after 20 hours, the heat pipe temperature was still 5 $^{\circ}F$ from the final temperature of 1561.99 $^{\circ}F$.

4.6.2 TESTING WITH POWER TRANSFER AT THE CONDENSER

The initial tests had established that at the operating temperature of 1558 $^{\circ}F$, the power losses from the entire heat pipe were 1210 watts. This indicated a loss of 6.722 watt/inch length and therefore, a loss of 958 watts (calculations shown in Figure 55 predicted a loss of 980 watt) from the adiabatic section and the evaporator section and 252 watts (270 watts calculated) from the condenser section. The losses from the evaporator section might have been slightly higher because of the higher temperature of the heater. The exact value would have been very difficult to establish and would have been outside of the accuracy of the testing.

The initial power transfer by the heat pipe beyond the losses through the insulation was to be achieved by removing successive layers of insulation from the condenser section. The expected power losses, as taken from Figures 55 and 104 are tabulated in Table XV.

These were the first test results which did not quite agree with predictions. The power losses from the heat pipe increased only to 2 kW vs. 2.2 kW predicted, while the temperatures at the condenser decreased and the temperature along the adiabatic section continued to increase and never achieved steady state. Pressure of time and the large time constant of the heat pipe did not permit further testing that would have been required for explaining the deviation from the predicted behavior.

TABLE XIV

TEMPERATURE HISTORY OF PRIMARY HEAT PIPE

TRANSIENT CONDENSER TEMPERATURE 28 MARCH 1974

70.0000 .8110 10455.3008
 70.0000 1210.0000 1800.0000 5.0000

POWER INPUT 1210.00 WATT
 FINAL TEMPERATURE 1561.99 DEGREE F

TIME CONSTANT 12891.9 SEC 214.9 MIN 3.581 H

TIME AFTER START	TEMPERATURE
SEC MIN HR	DEGREE F
0 .0 .00	70.00
1800 30.0 .20	264.43
3600 60.0 1.00	433.52
5400 90.0 1.50	580.57
7200 120.0 2.00	708.46
9000 150.0 2.50	819.69
10800 180.0 3.00	916.42
12600 210.0 3.50	1000.55
14400 240.0 4.00	1073.71
16200 270.0 4.50	1157.34
18000 300.0 5.00	1192.68
19800 330.0 5.50	1240.80
21600 360.0 6.00	1282.66
23400 390.0 6.50	1319.06
25200 420.0 7.00	1350.71
27000 450.0 7.50	1378.25
28800 480.0 8.00	1402.19
30600 510.0 8.50	1423.01
32400 540.0 9.00	1441.12
34200 570.0 9.50	1456.87
36000 600.0 10.00	1470.57
37800 630.0 10.50	1482.48
39600 660.0 11.00	1492.84
41400 690.0 11.50	1501.85
43200 720.0 12.00	1509.69
45000 750.0 12.50	1516.50
46800 780.0 13.00	1522.43
48600 810.0 13.50	1527.59
50400 840.0 14.00	1532.67
52200 870.0 14.50	1535.97
54000 900.0 15.00	1539.36
55800 930.0 15.50	1542.31
57600 960.0 16.00	1544.87
59400 990.0 16.50	1547.10
61200 1020.0 17.00	1549.04
63000 1050.0 17.50	1550.73
64800 1080.0 18.00	1552.19
66600 1110.0 18.50	1553.47
68400 1140.0 19.00	1554.28
70200 1170.0 19.50	1555.34
72000 1200.0 20.00	1556.38
73600 1230.0 20.50	1557.11

Reproduced from
 best available copy.

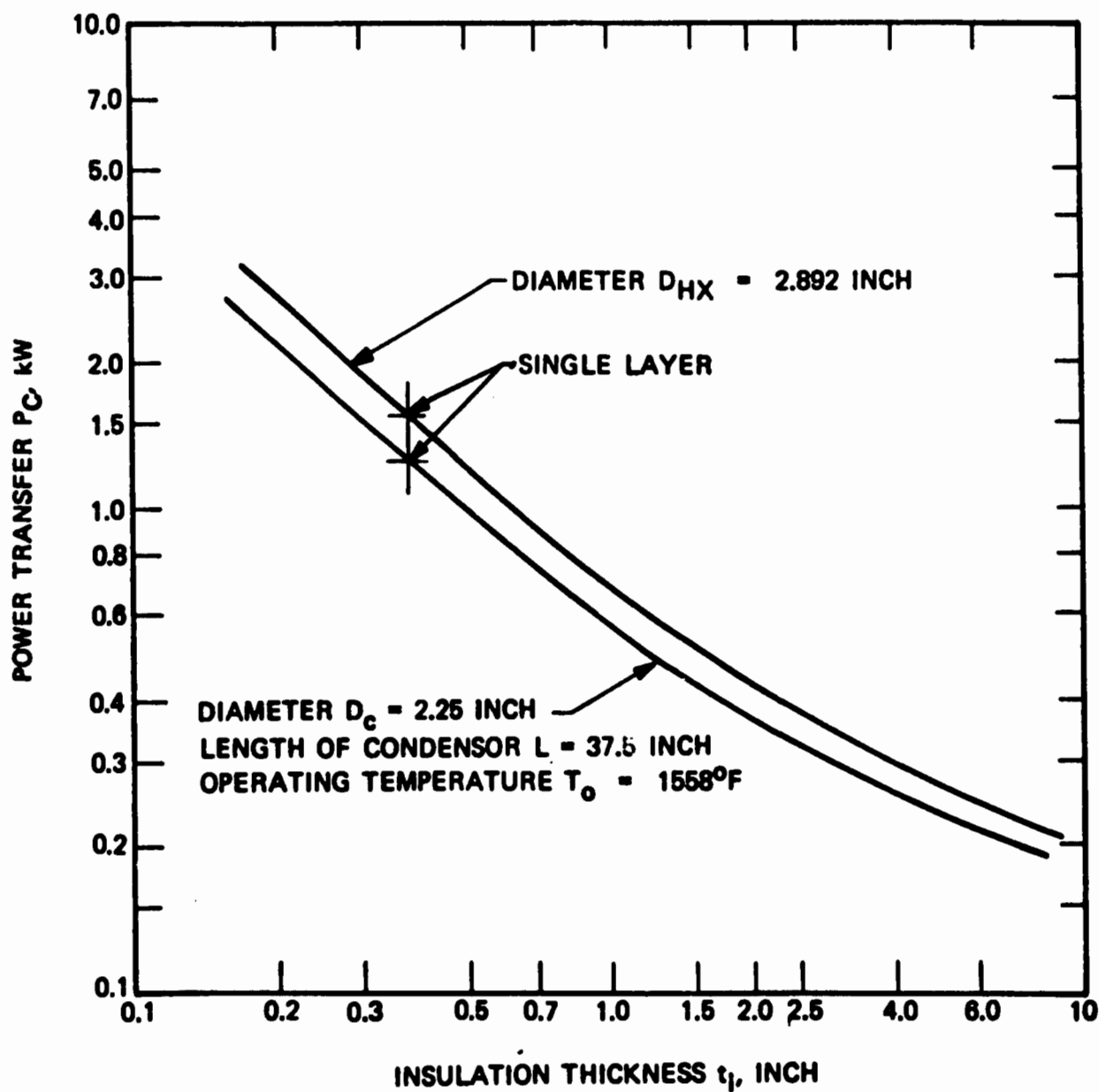


Figure 104. Power Transfer at Condenser of Primary Heat Pipe for Varying Insulation Thickness ($k_I = 0.5 \text{ B-inch/Ft}^2\text{-Hr-}^\circ\text{R}$)

TABLE XV
POWER LOSSES FROM PRIMARY HEAT PIPE

Number of Insulation Layers at Condenser	Power Loss (kW)	Difference in Loss (kW)	Total Loss From Heat Pipe (kW)
8	0.27		1.2
		0.022	
7	0.292		1.222
		0.03	
6	0.322		1.23
		0.043	
5	0.365		1.273
		0.067	
4	0.432		1.34
		0.093	
3	0.525		1.433
		0.19	
2	0.715		1.623
		0.535	
1	1.25		2.158

The last layer of insulation was removed from the condenser section and the tubular heat exchanger installed as shown in Figure 105. The heat exchanger was designed to be operated either with air or with steam. It was assumed that the heat exchange would occur by radiation and conduction. The expected radiation transfer is shown in Figure 106. At a power transfer of 5 kW (6 kW minus 1 kW loss from the evaporator and adiabatic sections of the heat pipe) by radiation alone, the heat exchanger temperature would be at least 1320° F. This would very well satisfy the requirement of maintaining the operating temperature of the condenser at the heat pipe temperature.

After installation of the heat exchanger over the condenser section and replacement of the insulation, testing for power losses was conducted to establish again the relation between power losses versus operating temperature. The results of these tests are shown in Figure 107. They can be compared with those shown in Figure 101. A considerable temperature differential between the last temperature of the condenser section and the adiabatic section was observed. This temperature differential could not be explained by the slightly lower insulation efficiency resulting from the increased effective diameter of the heat pipe due to the heat exchanger. After a considerable amount of investigation into the various reasons for that variation in the behavior of the heat

007124



Figure 105. Tubular Heat Exchanger at Condenser Section of Second Primary Heat Pipe

50826

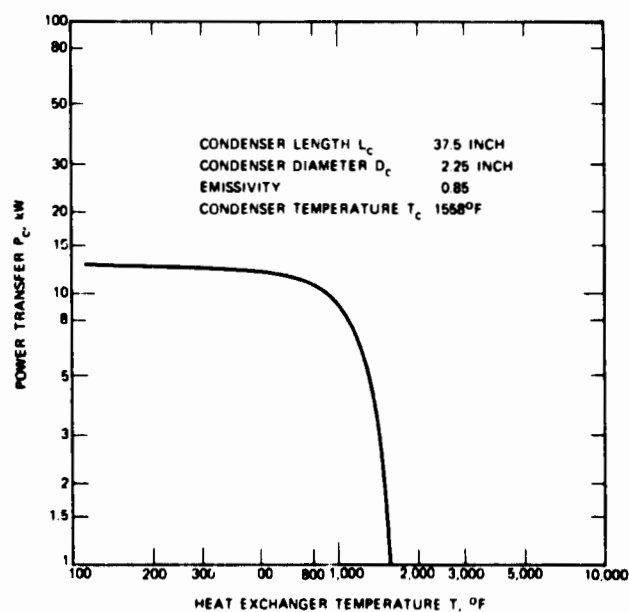


Figure 106. Power Transfer by Radiation from Condenser Section of Primary Heat Pipe to Heat Exchanger

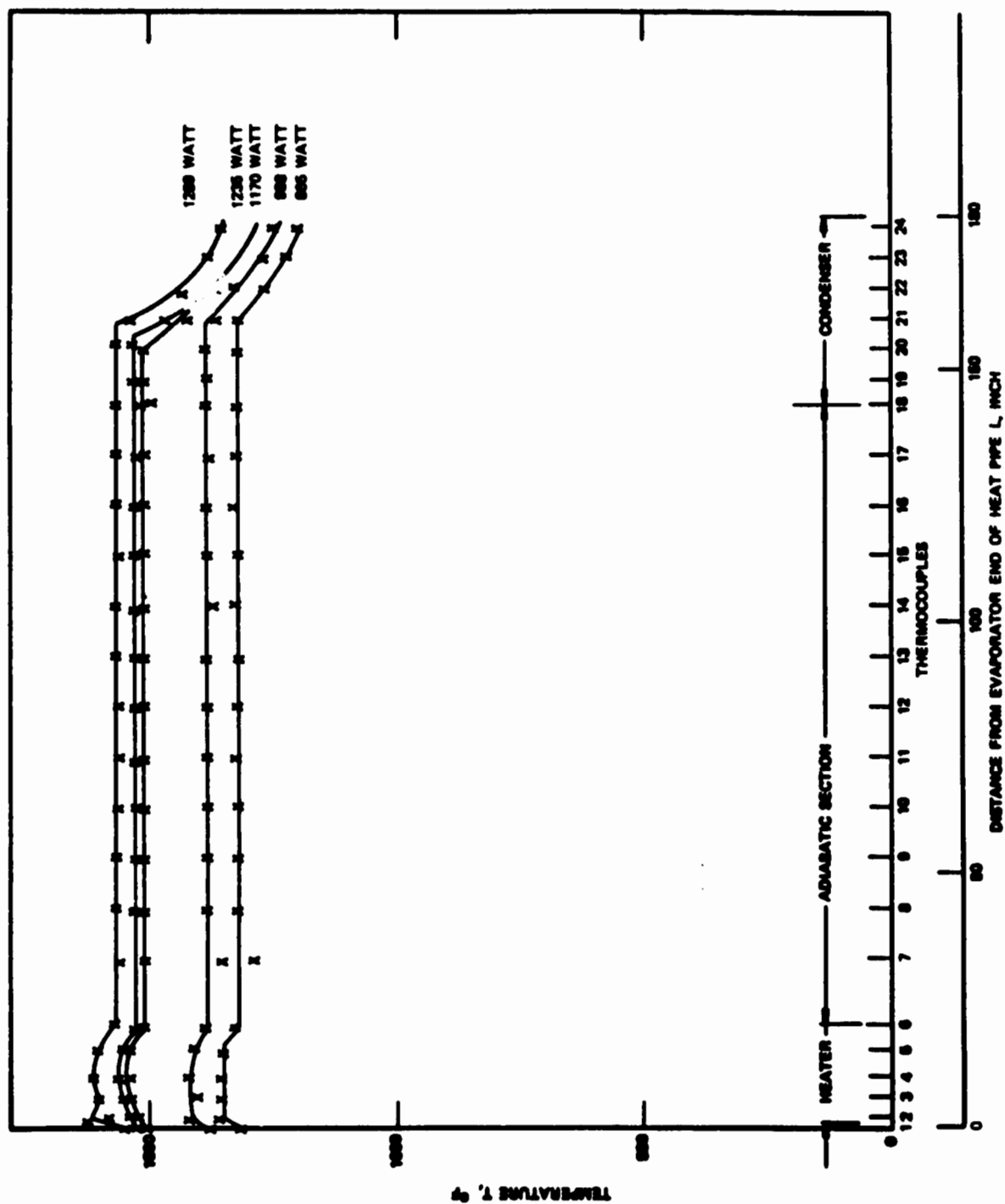


Figure 107. Temperature Distribution along 15-Ft Long Heat Pipe for Various Power Inputs into Second Primary Heat Pipe with Condenser 1-1/2 inch below Evaporator Elevation

pipe following the installation of the heat exchanger, it was finally realized that by an error the heat pipe had not been releveled and that the condenser section was 1-1/2 inches below the evaporator section. After releveled the heat pipe, the temperature distribution along the heat pipe was again that which had been measured prior to the installation of the heat exchanger. This confirmed that the heat exchanger itself should not have any effect on the operation of the heat pipe except for a slightly larger power loss when no power is being removed by the heat exchanger.

When power was removed through the heat exchanger, temperature differences between the adiabatic section and the condenser section increased by decreasing temperatures in the condenser section as well as by rising temperatures in the adiabatic and evaporator sections without reaching a steady-state condition. When this problem was analyzed it was established that this condition is brought about by an overfill of the heat pipe leading to blocking of the condenser section by excess working fluid.

The heat pipe had been filled with an amount of sodium sufficient to fully saturate the wick structure at the freezing temperature of sodium. This was done to assure that during start up of the heat pipe the evaporator wick would be fully saturated and no immediate dry out could occur. Under these conditions, however, an excess of 57.95 inch³ (949.63 cm³) will be in the heat pipe when the heat pipe reaches its operating condition at 1558°F. If all the excess sodium is transferred to the condenser section of the heat pipe, it would occupy 55.72 inches of the condenser. However, the entire condenser length of the primary heat pipe was only 37.5 inches long. In the 1-g gravitational field in which the heat pipe was tested, it would not have been possible to block the entire condenser section as some refluxing of the fluid had to occur, but still a considerable area of the condenser is blocked preventing heat transfer in the condenser and thus raising the temperature in the adiabatic section and the evaporator section. This was exactly what was observed. The test results clearly indicated that working fluid had to be removed. Since this had been expected, provisions for removal had been made.

It was decided to remove the excess sodium in steps of about 200 grams each. A 14 inch volume was attached to the fill tube of the heat pipe at the evaporator end and was instrumented with three thermocouples. The heat pipe was brought to the operating temperature while the volume temperature was raised only to the melting temperature of sodium. When these conditions were reached and the volume was fully evacuated, after several argon purges, the valve to the fill tube was opened. The influx of sodium into the volume was verified by the steep rise in the temperature of the volume as indicated by the attached thermocouples. This process was repeated three times. After the first venting, the volume

weight had increased by 224.2 grams. After the second and third time, the weight increase amounted to 195 grams and 185.9 grams respectively. Thus, the total amount of sodium that was withdrawn from the heat pipe was 605.1 grams. This compared to a possible surplus of sodium at the operating temperature of 710.33 grams.

Prior to the successful withdrawal of the sodium, a considerable amount of difficulties had been experienced. The reason for several unsuccessful attempts was finally found by accident to have been a fracture in a tube. This fracture was not evident during argon purge and evacuation of the volume because of sodium sealing it. After repair, the sodium withdrawal proceeded like clockwork in a fully predictable manner.

After withdrawal of sodium from the second primary heat pipe, the steady-state conditions without power transfer at the condenser section (except losses occurring through the insulation) were ascertained for two power settings as shown in Figure 108. The results were consistent with those measured prior to the withdrawal of sodium so that testing with power transfer at the condenser section of the heat pipe could be continued. First, the appropriate coolant flow rate for the heat exchanger was selected for a desired power transfer. The heater power was then raised to the desired power level. A temperature controller monitored the temperature of thermocouple #4 causing the power to the heaters to be turned off whenever its temperature would exceed 1800°F. The operation of the controller was timed and the effective power input was assumed to be the average power input during a cycle. For a typical test the heater would be on approximately 87 percent of the time and off only 13 percent of the time. The correlations which were obtained under these test conditions were very difficult to interpret. It appeared that the total average power input could not exceed 4.5 kW.

The test procedure was changed after observing that the temperature differential between thermocouples #1 and #2 was not a function of the power input alone, but also a function of the step increase in power input; the larger the step increase of the power, the larger was the temperature differential. When the power was increased from 3 kW to 4 kW after the heat pipe had operated for a considerable time at 3 kW and had reached steady-state conditions, the temperature difference between the adiabatic section of the heat pipe and the temperature measured by thermocouple #4 would be only about 140°F. When the power input, however, was raised from 1.2 kW to 4 kW, the temperature differential would advance to over 250°F despite the fact that the operating temperature of the heat pipe was the same. This behavior can now be explained by the inertia of the sodium in the wick.

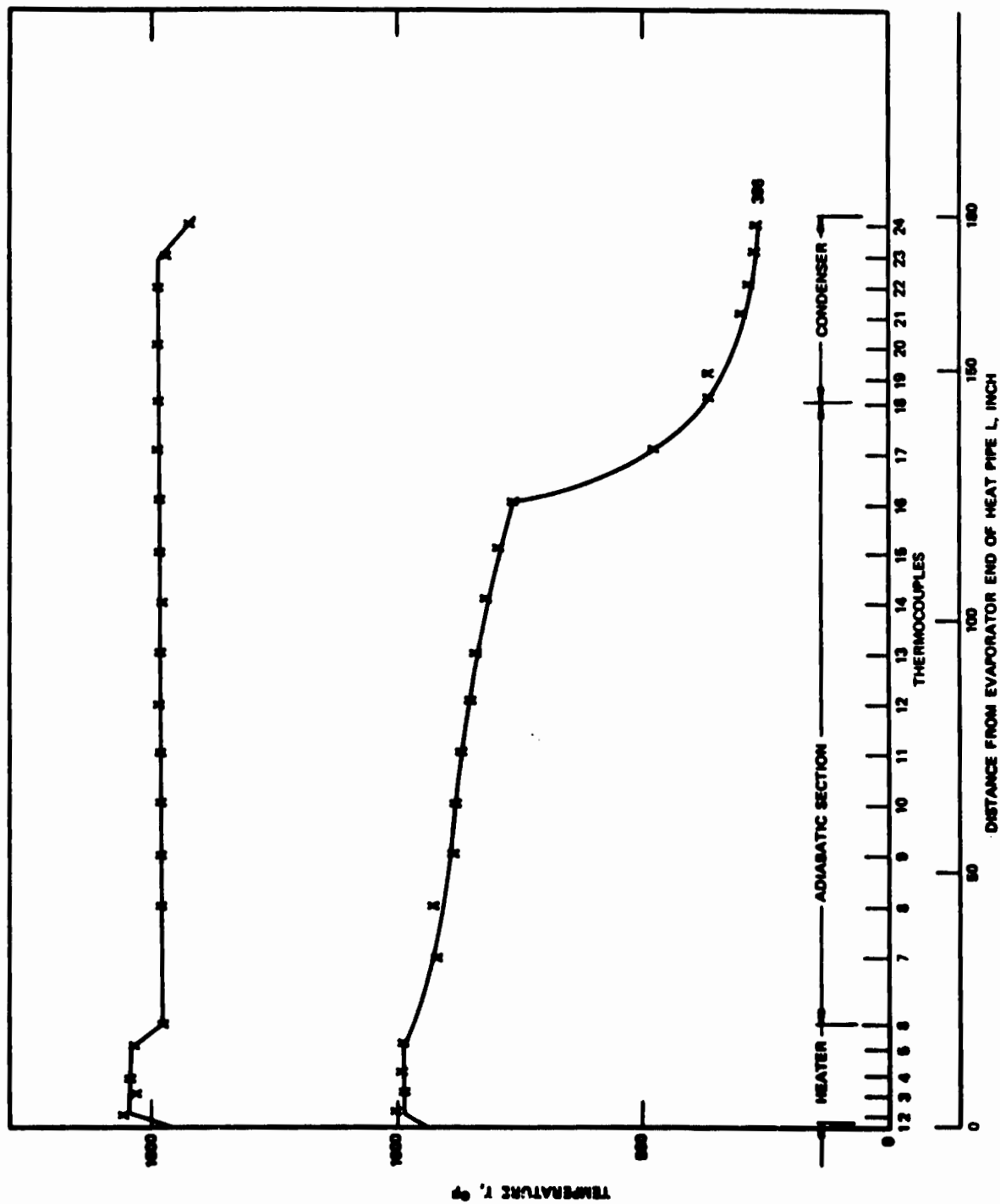


Figure 108. Temperature Distribution Along Primary Heat Pipe

After a better understanding of the behavior of the heat pipe had been obtained, the heat pipe was operated consistently with a total power input of slightly over 6 kW (6.11 kW). There was no indication that 6 kW was the upper power transfer limit for the heat pipe. Prudence, however, dictated the conclusion of the heat pipe tests at that power level. The temperatures along the heat pipe are shown in Figure 109. The steady-state conditions were near 1500°F. No effort was made to come to a power balance at exactly 1558°F, which would have been very time consuming with a heat pipe which has a large thermal inertia and time constant. It was surmised that operating the heat pipe at the design temperature would be considerably easier with the full thermal train when the thermal energy storage material would take over the temperature control. Figure 109 shows the temperatures along the heat pipe to be very constant. Thermocouples #19 through #24 measured a temperature between the heat exchanger and the heat pipe. Since the coolant is injected into the heat exchanger at the downstream end of the heat pipe, thermocouple #24 indicated the lowest temperature. This phenomenon is very similar to that which causes thermocouples #2 through #5 to measure temperatures somewhere between the heater and the heat pipe. The real temperature of the heat pipe at the evaporator was that indicated by thermocouple #1.

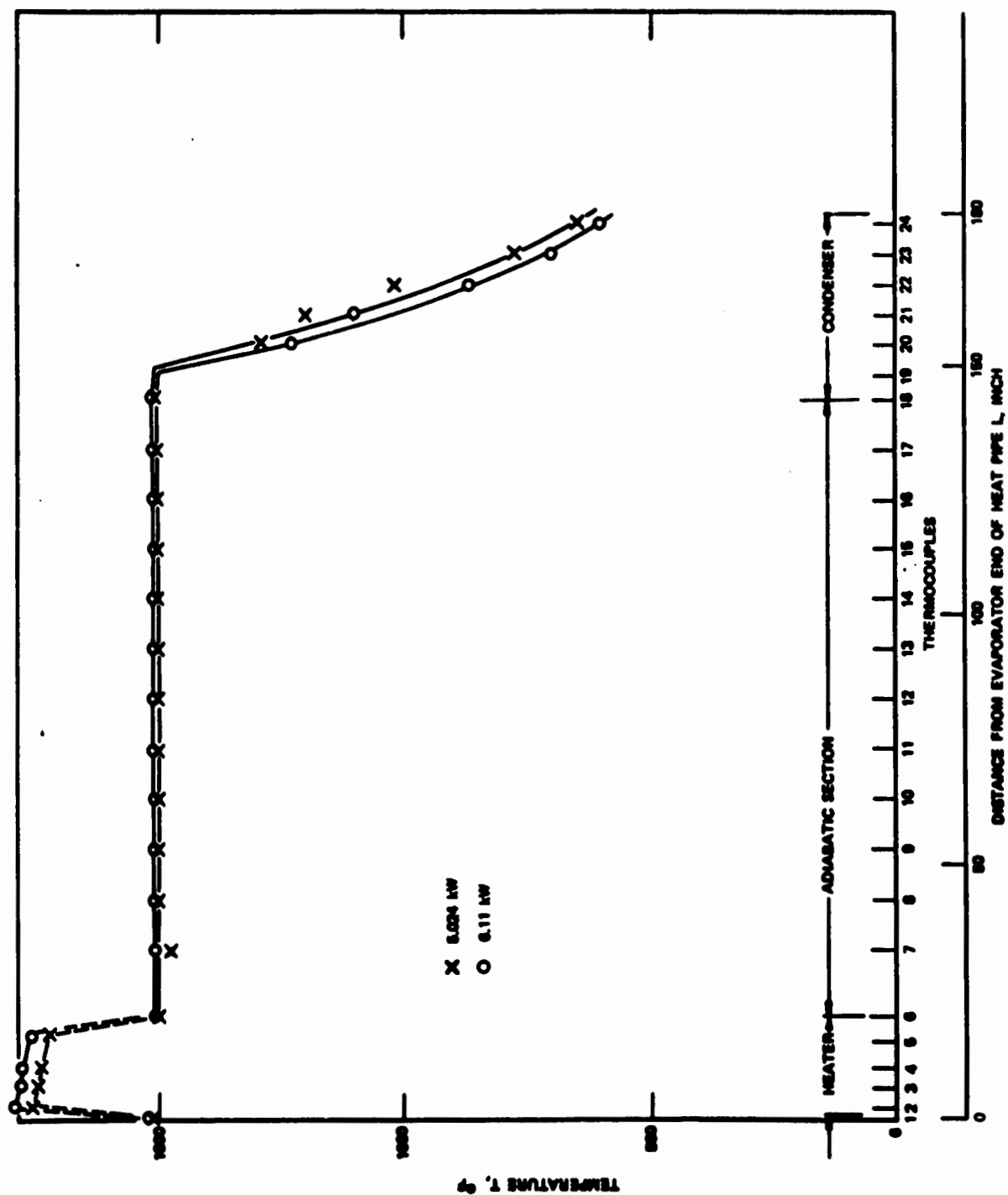


Figure 109. Temperature Distribution Along Primary Heat Pipe

SECTION 5

THERMAL TRAIN

5.1 INTRODUCTION

With all components of the thermal train tested and each one having been found to perform according to design, the second primary heat pipe, the secondary heat pipe with the thermal energy storage unit and the rotary radiation heat transfer joint were ready for integration.

5.2 INTEGRATION

For the integration of the thermal train, a sodium joint between the primary heat pipe and the secondary heat pipe was required. For filling the joint, a calibrated volume was built which could hold 18 in.³ of sodium. The net volume in the joint between the primary heat pipe and the secondary heat pipe was 24.58 in.³. When allowance was made for the sodium to expand by about 20 percent when raised to the operating temperature of 1558°F and for a void of 10 percent at the operating temperature, a volume of 17.22 in.³ of sodium at the fill temperature of about 320°F would have been called for.

The flange of the primary heat pipe (see Figure 17) was welded to the lip of the secondary heat pipe, shown in Figure 110, leaving a gap between the two heat pipes of about 0.025 inch. Spacers between the two heat pipes were not necessary. Because of minor distortions which had occurred during the testing of each of the two components, the two heat pipes made contact in several spots thereby supporting each other without spacers.

The filling of the joint with sodium proceeded without problems. The joint volume was not sealed permanently as had initially been intended, but was closed off with a valve to permit adjustment to the sodium fill at a later date if such should become desirable.

The rotary heat transfer joint was reworked by installing four new coils into the joint. To improve the cooling operation, the coils were supplied with coolant in a counter flow; i.e., coolant could be injected into two coils from the downstream side and into two from the upstream side of the thermal train. For improving the control of the cooling further, cooling could take place either with all four or with only two of the coils in operation.

In Figure 111, the complete full-scale thermal train of the solar collector thermal power system is shown, while in Figure 112, the condenser end of the secondary heat pipe with the rotary radiation heat transfer joint can be seen with the water lines and the pressure lines for measuring the upstream and downstream pressure at the metering orifice.

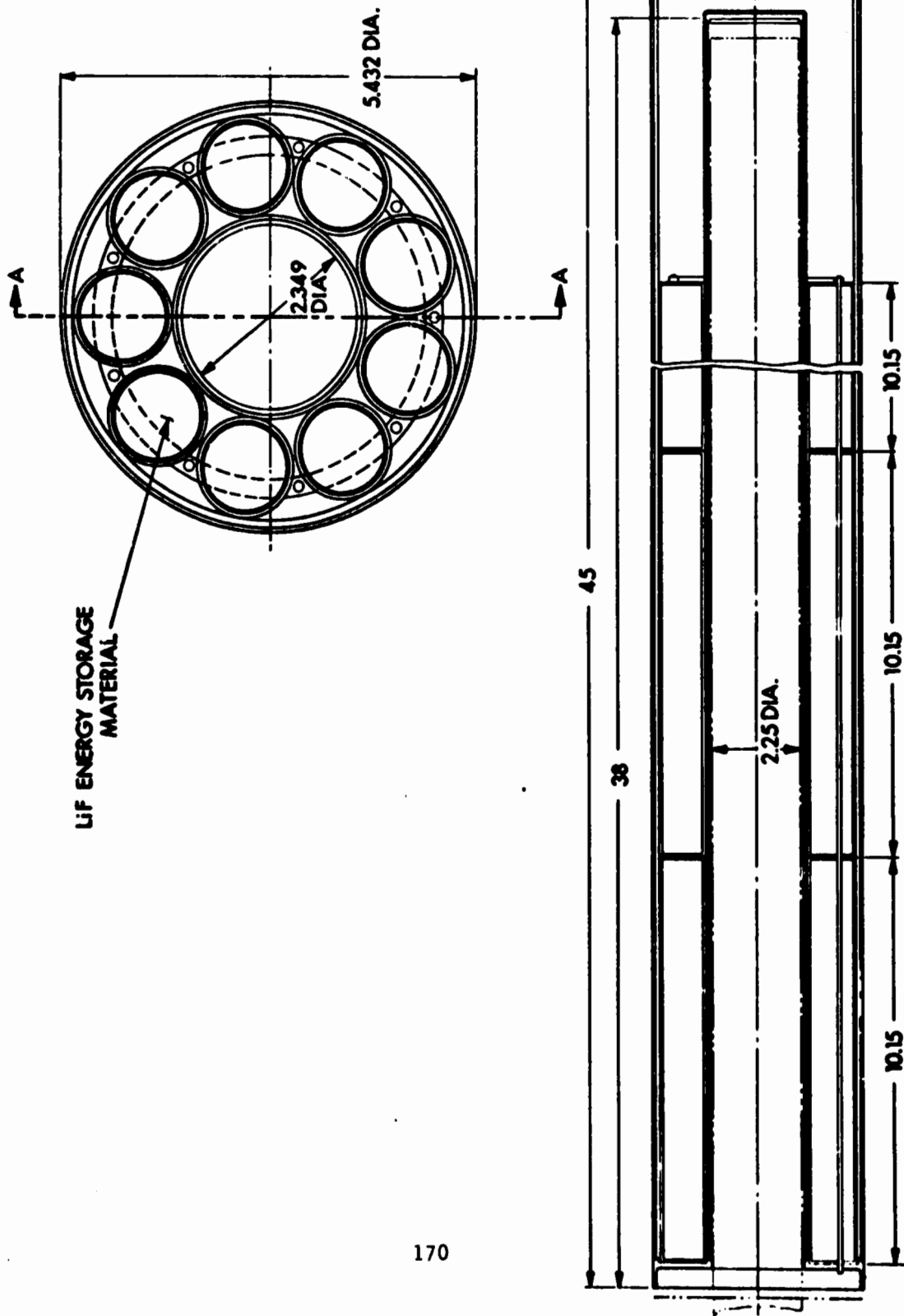


Figure 110. Secondary Heat Pipe with Thermal Energy Storage Unit



67462

Figure 111. Fully Assembled Full-Scale Thermal Train of
the Solar Collector Thermal Power System



Figure 112. Close-up View of Rotary Radiation Heat Transfer Joint and the Secondary Heat Pipe as Assembled in the Full-Scale Thermal Train of the Solar Collector Thermal Power System

67163

5.3 TEST SETUP

The basic test setup for testing the full-scale thermal train of the solar collector thermal power system is schematically shown in Figure 113. The primary heat pipe is inserted into the cavity of the secondary heat pipe which also encloses the thermal storage unit. The rotary radiation heat transfer joint was slipped over the condenser section of the secondary heat pipe. Approximately 20 inches of the evaporator section of the primary heat pipe was covered with the coils of the three electrical heaters which have a total electric power capacity of 9 kW. Thermocouples were placed along the entire thermal train as indicated in Figure 113. Thermocouples #2 through #5 were located directly under the primary heater. They measured temperatures considerably above the operating temperature of the heat pipe. Thermocouples #6 through #16 measured the temperatures along the adiabatic section of the primary heat pipe. Thermocouples #17 and #18 measured the temperature of the adiabatic section of the secondary heat pipe. Thermocouples #19 and #20 were placed on the condenser section of the secondary heat pipe while thermocouples #21 and #22 were located on the receiving surface of the rotary radiation heat transfer joint. Thermocouples #23 and #24 measured the temperatures of the cooling coil of the rotary radiation heat transfer joint.

5.4 TESTING

After checkout of the instrumentation, testing of the thermal train was initiated. First, the steady-state power losses for the entire train had to be ascertained. It was already shown that the time constant (which is the ratio between the thermal capacity and the power loss) for the primary heat pipe alone was such that the final steady-state temperature of the heat pipe was not achieved for 24 hours after adjusting the power input at the evaporator. Therefore, for each single test point at least a full day had to be allocated. Accuracy in the correlation between power loss and operating temperature was required for evaluating correctly the operation of the thermal train under conditions of charging and discharging of the thermal energy storage unit in the secondary heat pipe, and for the determination of the effective thermal mass of the thermal train.

The steady-state power loss data are presented in Figure 114. They could be approximated well by a straight line on double log paper and by the relation

$$P_{\text{loss}} = C \times T^n$$

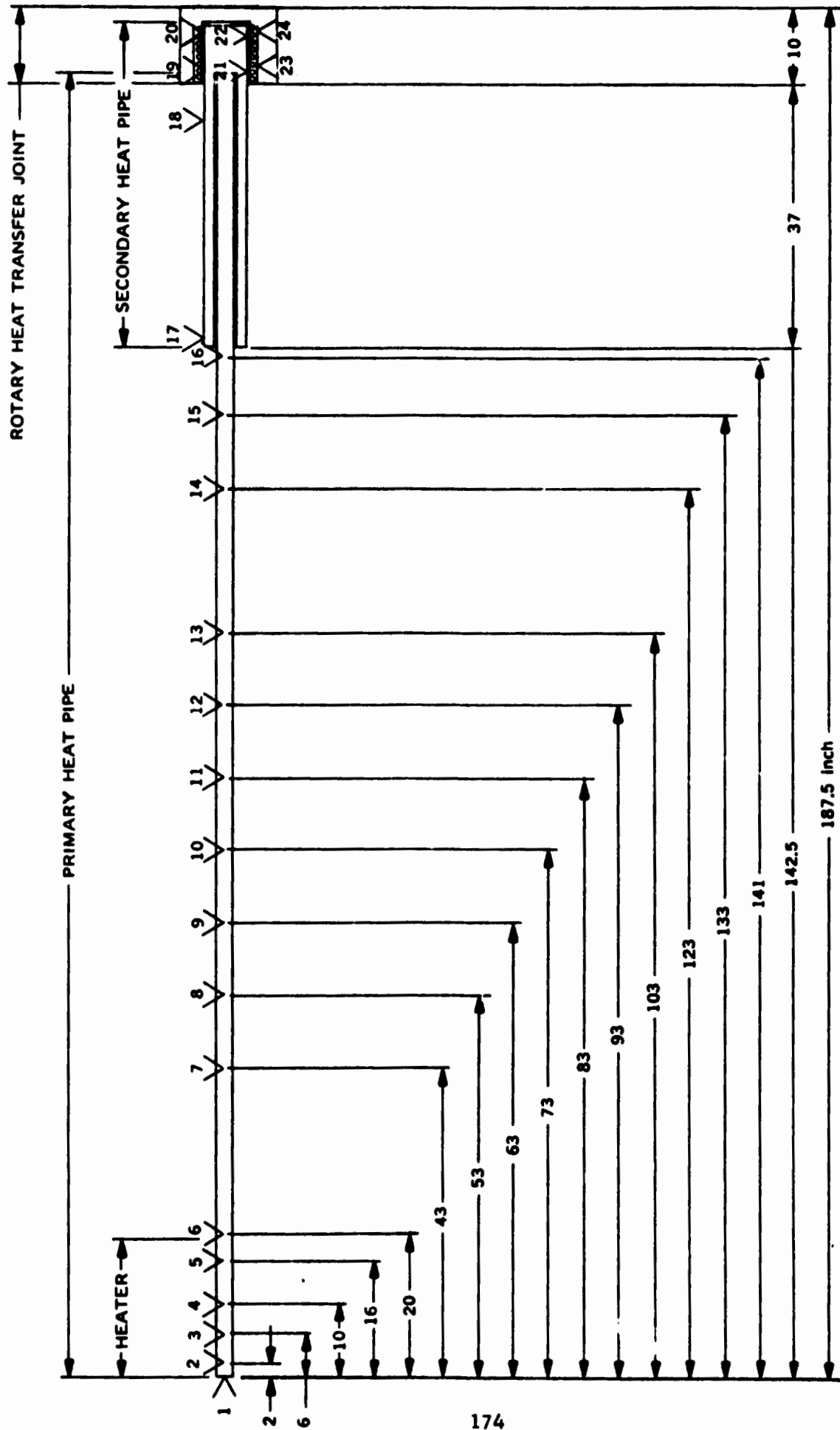


Figure 113. Thermocouple Arrangement for Testing of Full Scale Solar Collector Thermal Power System Thermal Train

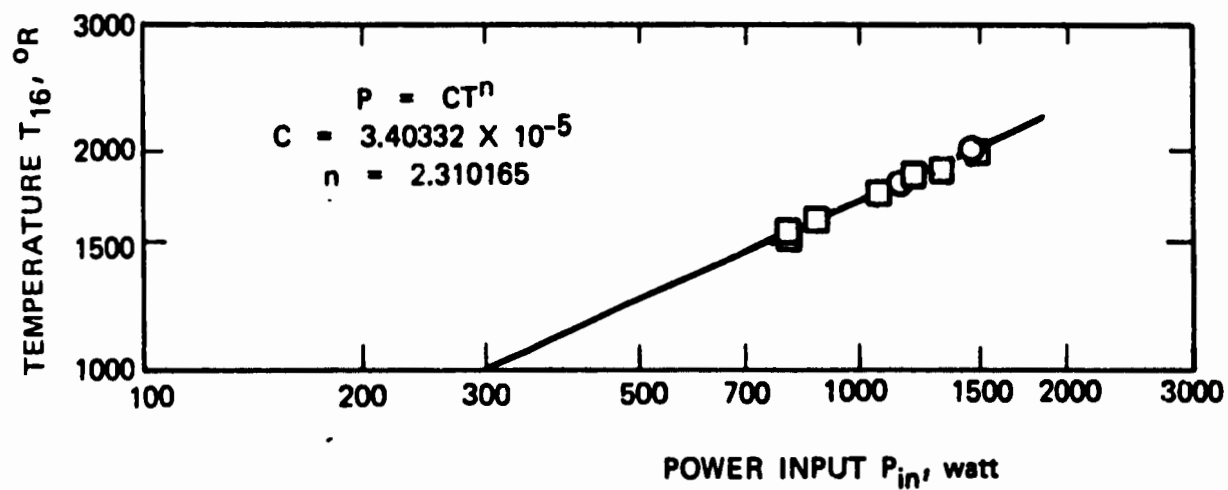


Figure 114. Power Losses of the Thermal Train (Primary Heat Pipe, Secondary Heat Pipe with Thermal Energy Storage Unit and Rotary Transfer Joint)

50790

where

- P_{loss} = Power loss, watts
 C = Constant, 3.40×10^{-5}
 T = Temperature, $^{\circ}\text{R}$
 n = Exponent, 2.310

With the steady-state power losses established, the thermal train was operated in the charging and discharging mode. Power was applied to the evaporator section of the primary heat pipe at different power levels while the thermal energy storage unit was charged. A typical temperature history for the thermal train is shown in Figure 115. The total power input into the evaporator is 4199.5 watts. From the data presented in Figure 116, the thermal train is losing about 1460 watts at the charging temperature of 1560°F . Thus, the total amount of power stored during the charging processes is about 2740 watts.

In Figures 116 through 118, the temperature distributions during charging at various power levels are presented. Thermocouples #2 through #5 were located directly under the heater, while thermocouples #1 and #6 were not exposed to the direct heat transfer by conduction and radiation from the heater. Thermocouple #1 was therefore the most important temperature indicator. If the evaporator should have become depleted of sodium, thermocouple #1 would have risen above the temperature of the adiabatic section of the primary heat pipe. The reason for this would have been that the end of the heat pipe would no longer have been cooled by evaporation of the working fluid.

During one test a divergent of the temperature indication of thermocouple #1 was observed. This occurred when the power at the heater was raised in a step from 1.2 kW to 6 kW while the thermal train was near the operating temperature of 1560°F . Fortunately, the malfunction was detected in time. The power to the evaporator was turned off and was not turned on again until all thermocouples of the primary heat pipe indicated the same temperature.

The interesting aspect of the above test was the realization that the working fluid has an inertia which has to be considered in the operation of the thermal train. During the steady-state condition, at which a power of less than 1500 watts is transferred at the evaporator section, the circulation of the working fluid in the heat pipe is accordingly low, i.e., the velocity of the working fluid in the wick is only one-fourth of the velocity when the heat pipe is operating at 6 kW. When the power input is increased, the fluid in the wick has to be accelerated.

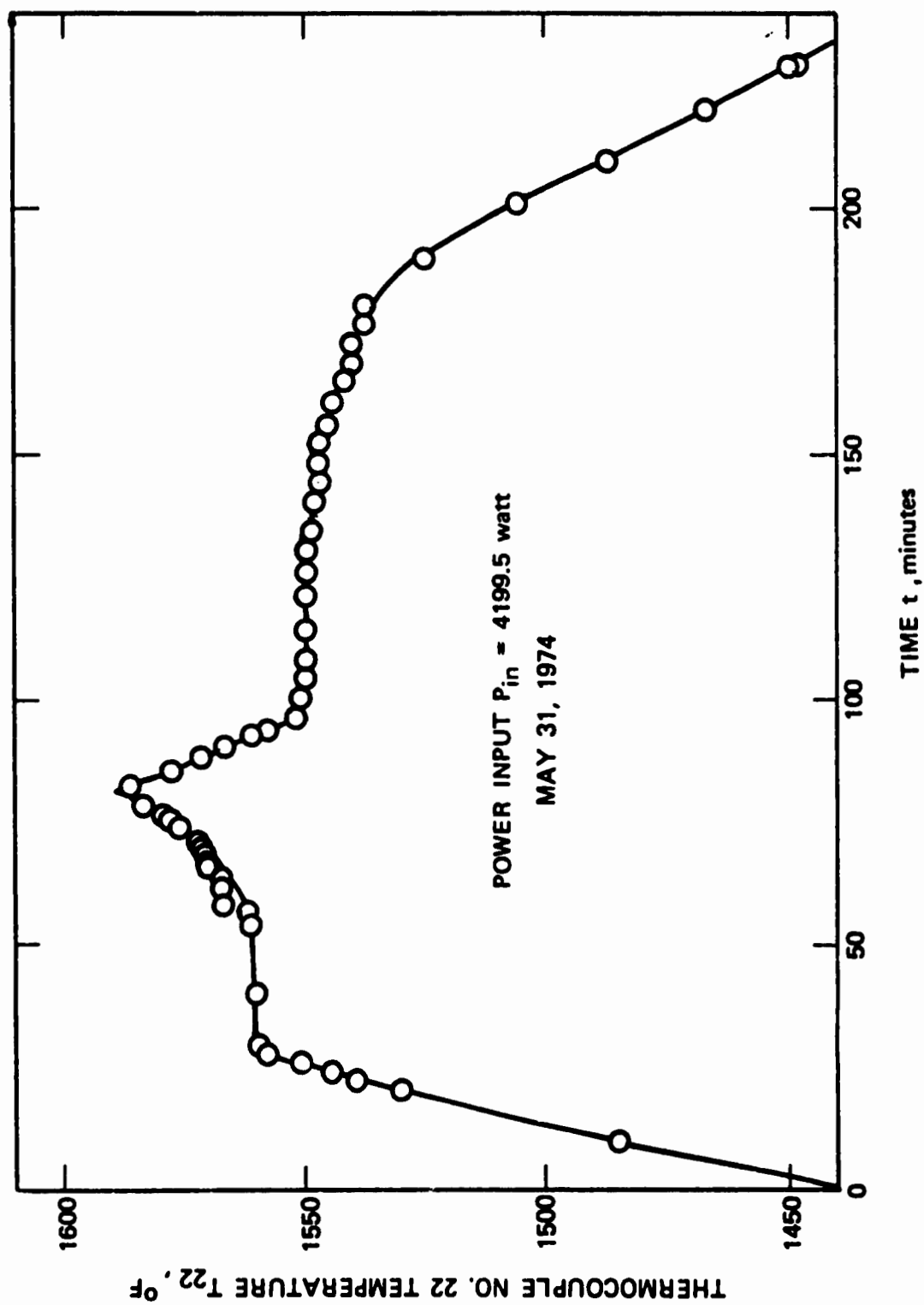
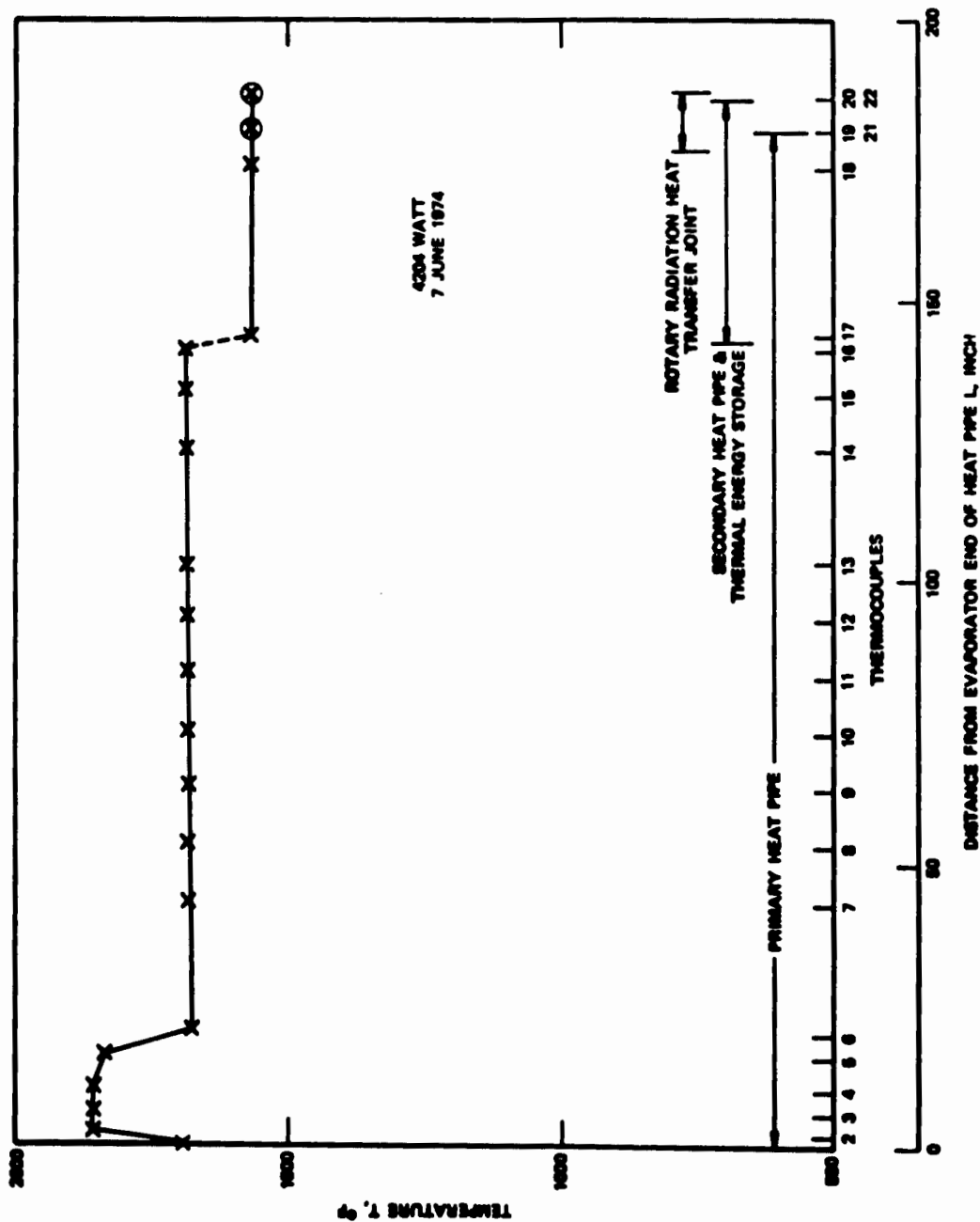


Figure 115. Temperature History of Full Scale Thermal Train (Primary Heat Pipe, Secondary Heat Pipe with Thermal Energy Storage Unit and Rotary Heat Transfer Joint)



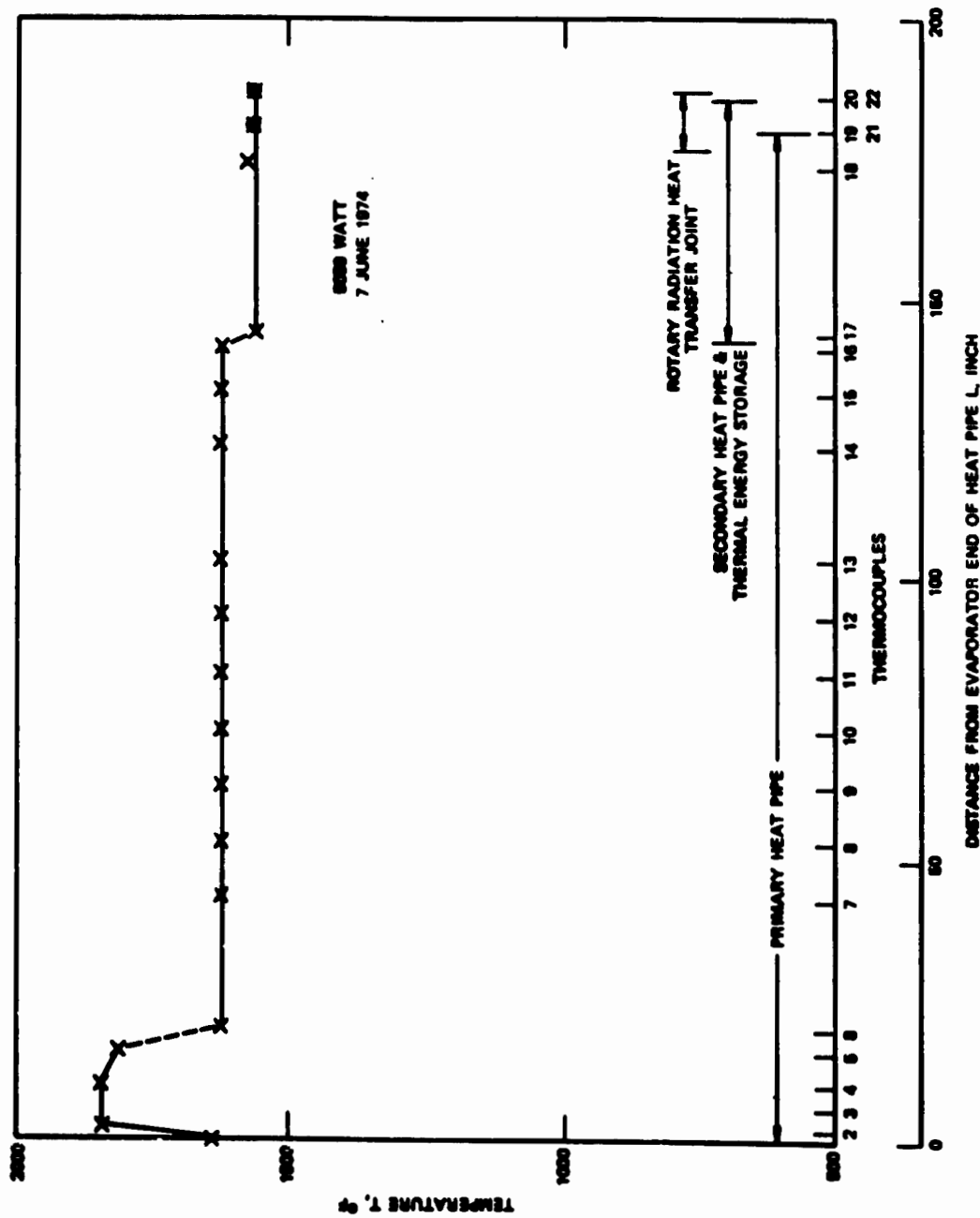


Figure 117. Temperature Distribution in the Thermal Train (5059 Watt Input)

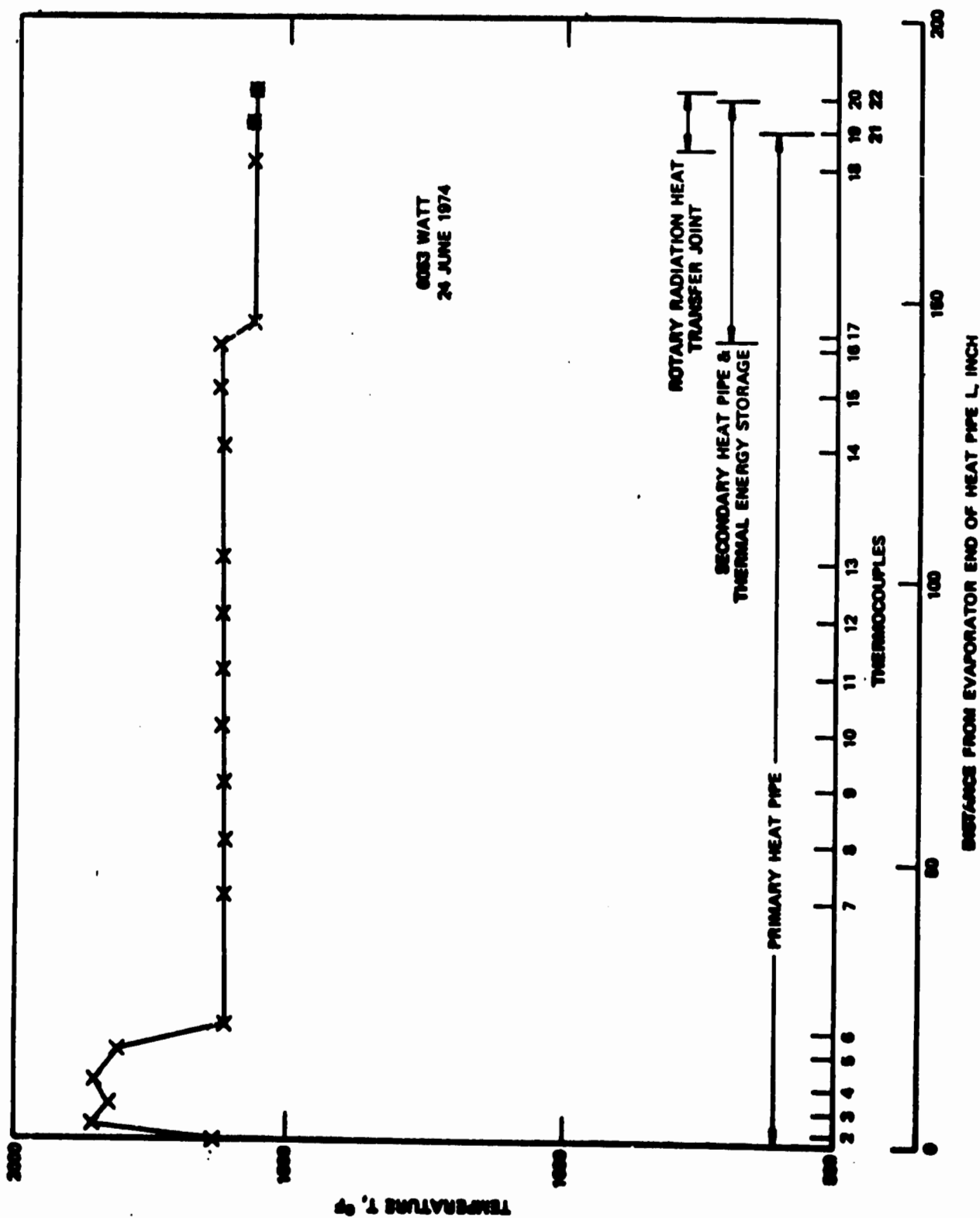


Figure 118. Temperature Distribution in the Thermal Train (6053 watt input)

To overcome the fluid inertia requires an additional suction pressure above and beyond the suction pressure needed to compensate for the flow resistance in the wick. As it was the case with the present heat pipe when operating in a 1-g gravitational field, available suction pressure was already limited and was just sufficient for steady-state operation. Thus severe transient condition could not be accommodated and dry-out at the evaporator occurred. This suggested that the heat pipe analysis needed further expansion and refinement to include the effect of transient conditions.

Figures 116 to 118 indicate relatively large temperature differentials between the thermocouples under the heater and the adiabatic section of the heat pipe. The temperature of thermocouple #1 clearly suggests that the indicated temperatures of thermocouples #2 to #5 were not the heat pipe temperatures but were temperatures between the heat pipe and the heater. A fairly good correlation could be established between a fictitious radiation heat transfer, P_r ,

$$P_r = \sigma \epsilon A_E (T_2^4 - T_a^4)$$

where:

P_r	radiation heat transfer
A_E	evaporator area
T_2	indicated temperature of thermocouple #2
T_a	temperature of the adiabatic section of the heat pipe
ϵ	emissivity (assumed unity)
σ	Boltzmann's constant

The correlation between the fictitious radiation heat transfer, P_r , and the heater power, P_{in} , are shown in Figure 119. This would indicate that the power transfer from the heater was very much influenced by radiation heat transfer and that the contact between the heater and the heat pipe was not maintained during operation as can be expected. Therefore large temperature differentials between the heater and the heat pipe had to be expected. This condition caused the operation of the heaters close to their maximum operating temperature.

Figures 115 through 118 show also relatively large temperature differences between the primary and the secondary heat pipe. This differential varies and depends on the time and power level. The differential

50792

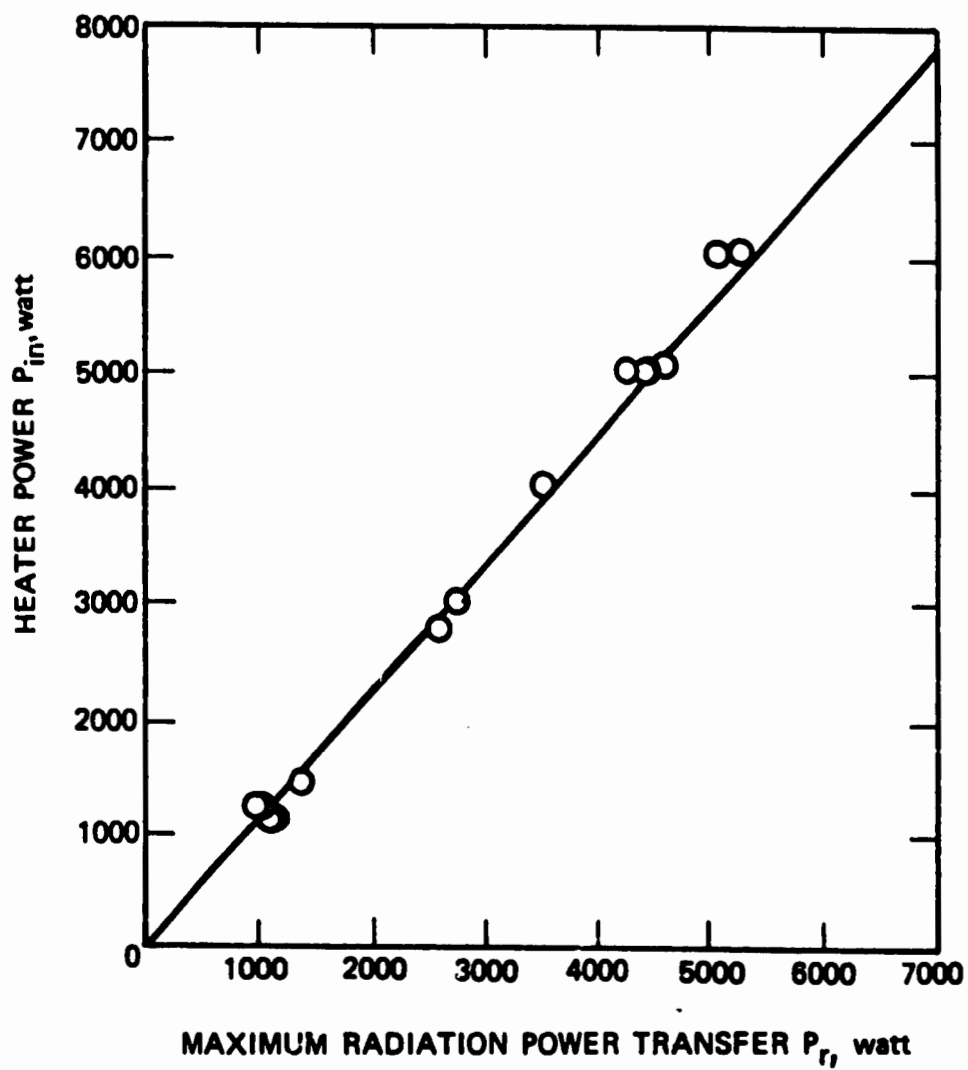


Figure 119. Correlation Between Maximum Possible Radiation Power Transfer and Heater Power at the Primary Heat Pipe Evaporator

was higher than had been anticipated and indicated that the thermal joint presented a larger thermal barrier than had been predicted. Several reasons for this discrepancy can be assumed. For achieving a relatively good conduction pass between the primary and secondary heat pipes, the gap between the two heat pipes was filled with sodium. Because of the relatively large thermal expansion of sodium, the gap had to be underfilled to prevent the expanding sodium from bursting the heat pipe joint. Probably the underfill was too large and considerable voids prevented a good heat transfer. The measured high temperature drop emphasizes the avoidance of joints in the thermal train.

In Figure 120 the operation of the thermal train with a power input of 6 kW and a power extraction of about 2.7 kW are presented. This is the most severe operating condition for which the entire thermal train was designed. Except for the larger than expected temperature difference between the primary heat pipe and the secondary heat pipe, the operation was fulfilling all design requirements at this operating condition. The thermal train was shut down on 28 June 1974 with the conclusion of the technical effort of the program.

All components of the thermal train had remained in full operating conditions. The thermal train appeared to perform well up to the design power level of 6 kW. The design power level was not exceeded to protect the components from damage. Testing of the thermal train can be initiated again at any time.

5.5 CONCLUSION

With the full power testing of the solar collector thermal power system thermal train, the basic feasibility of the Solar Collector Thermal Power System had been demonstrated. The thermal train performed according to most of the design goals, i.e., a total power input of 6 kW at the evaporator, an energy storage rate of 3 kW, a power transfer across the radiation heat transfer joint of 3 kW, and an energy extraction rate of 3 kW. The only discrepancy between design requirements and test results was experienced in the heat transfer from the primary heat pipe to the secondary heat pipe through the sodium joint. It is not quite clear where and why the temperature drop occurred. It is possible that the thermal coupling between the two heat pipes is impeded either by an underfill of the joint, by scaling of the two surfaces which were exposed to the atmosphere during testing of the components individually, although the surfaces were cleaned prior to integration, or by a temperature drop in the condenser of the primary heat pipe. Such a temperature drop was not measured in the subscale cavity heat pipe which is described in Volume III of this report.

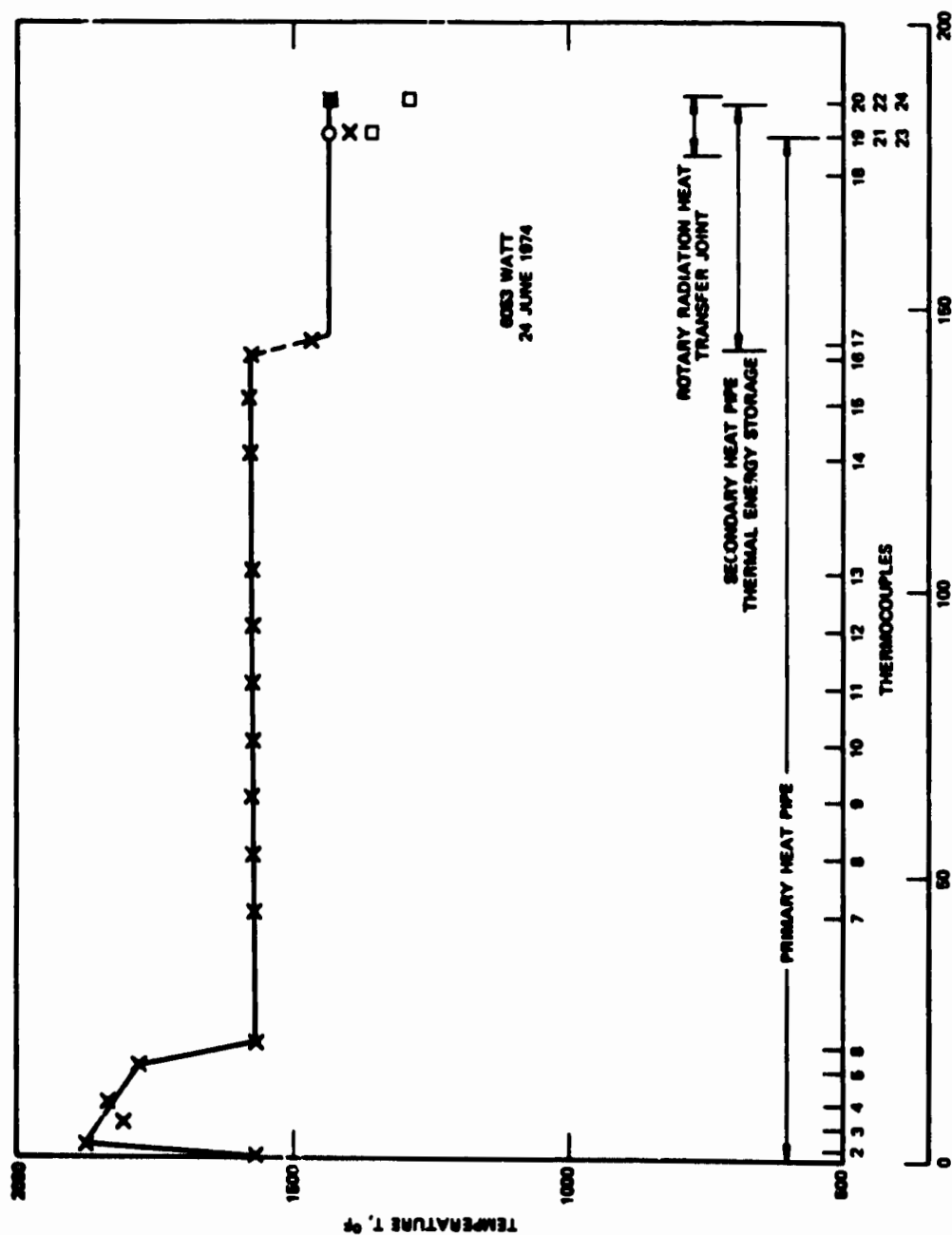


Figure 120. Temperature Distribution in the Thermal Train
(6053 Watt Input and 2700 Watt Output)

APPENDIX A

FLUID FLOW IN HEMISPHERICAL RECEIVER

When the hemispherical receiver is irradiated fluid is evaporating from the back surface of the receiver carrying the radiation energy away in the form of latent heat. The working fluid has to be resupplied by the flow in the wick which is governed by Darcey's law and by the law of capillary action. The analytical model for the fluid flow in the wick of a hemispherical receiver is shown in Figure 121.

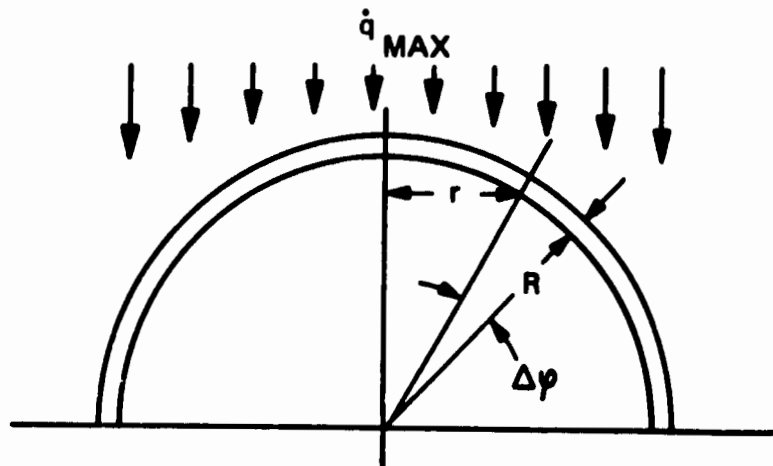


Figure 121. Geometric Relations

By Darcey's Law the volumetric flow rate \dot{V} is

$$\dot{V} = - \frac{K A_f}{\mu} \frac{\Delta p}{\Delta L} \quad (11)$$

where

- \dot{V} volumetric flow rate
- K permeability of wick structure
- A_f flow area perpendicular to flow direction
- Δp pressure drop
- ΔL distance along flow pass
- μ viscosity

The volumetric flow rate can be expressed by the density ρ and the mass flow rate \dot{W}

$$\dot{V} = \dot{W} / \rho \quad (12)$$

The flow area A_f and the distance along the flow pass ΔL are

$$A_f = 2 \pi R t \cos \varphi \quad (13)$$

$$\Delta L = R \Delta \varphi \quad (14)$$

Using relations 12, 13 and 14, Darcey's law can be expressed in differential form

$$dp = \frac{\dot{W}}{2 \pi K \rho t \cos \varphi} \frac{d\varphi}{\cos \varphi} \quad (15)$$

The change in the mass flow rate is equal to the amount of fluid evaporated

$$d\dot{W} = - \frac{\dot{q}(\varphi) dA_1}{H_{fg}} \quad (16)$$

where

A_1 irradiated receiver area

\dot{q} heat input per unit area

H_{fg} latent heat of evaporation of the working fluid

The incremental surface area is

$$dA_1 = 2 \pi R^2 \cos \varphi d\varphi \quad (17)$$

and the heat load is by the cosine law

$$\dot{q} = \dot{q}_{\max} \sin \varphi \quad (18)$$

where

\dot{q}_{\max} maximum heat load which occurs on the center of the hemisphere

Combining relations 16, 17 and 18 results in the differential equation for the mass flow rate

$$d\dot{W} = - \frac{2 \pi \dot{q}_{\max} R^2}{H_{fg}} \sin \varphi \cos \varphi d\varphi \quad (19)$$

Since

$$\dot{Q} = \dot{q}_{\max} R^2 \pi \quad (20)$$

where

$$\dot{Q} \quad \text{total power input}$$

and

$$\dot{W}_0 = \dot{Q}/H_{fg} \quad (21)$$

where

$$\dot{W}_0 \quad \text{total mass flow rate into the hemisphere}$$

relation (19) can be written

$$d\dot{W} = 2\dot{W}_0 \sin \varphi \cos \varphi d\varphi \quad (22)$$

The solution of equation 19 is

$$\dot{W} = \dot{W}_0 (1 - \sin^2 \varphi) \quad (23a)$$

$$\dot{W} = \dot{W}_0 \cos^2 \varphi \quad (23b)$$

When the mass flow rate \dot{W} of relation 23 is inserted into relation 15 the differential equation for the pressure along the hemispherical flow pass is found to be

$$\int_{p_1}^{p_2} dp = - \int_0^{\pi/2} \frac{\mu \dot{W}_0 \cos \varphi}{2 \pi K \rho t} d\varphi \quad (24)$$

Integration of the differential equation 23 and relation 21 results in the desired relation between the pressure drop and the total heat input.

$$\Delta p = - \frac{\mu \dot{Q}}{2 \pi \rho K t H_{fg}} \quad (25)$$

It is interesting to observe that the radius of the hemisphere does not enter into the relation. The pressure drop can then be equated with the available suction pressure produced by the capillary force as given by

$$\Delta p = \frac{2\gamma}{r_c}$$

where

γ surface tension

r_c effective pore radius

All values have to be in consistent units in the above relations.

REFERENCES

1. B. D. Marcus. "Theory and Design of Variable Conductance Heat Pipes: Hydrodynamics and Heat Transfer," Research Report No. 1, NASA Contract No. NAS 2-5503, April 1971.
2. O. W. Clausen, B. D. Marcus, et al., "Circumferential Heat Pipe System for Large Structures," Final Report NASA Contract No. NAS 9-10299, December 1970.
3. R. J. Roark, Formulas for Stress and Strain, McGraw-Hill Book Co., 3rd Edition.
4. Engineering Properties of Inconel Alloy 600, Huntington Alloy Products Division, The International Nickel Company, Inc., 1969.
5. B. D. Marcus, "Theory and Design of Variable Conductance Heat Pipes: Control Techniques," Research Report No. 2, NASA Contract No. NAS 2-5503, July 1971.
6. D. K. Edwards, G. L. Fleischman, B. D. Marcus, "User's Manual for the TRW Gaspipe Program," NASA CR-114306, April 1971.